Universidade do Minho
Escola de Medicina

Ana Cristina Nunes Gonçalves

New insights in (ab)normal fetal lung development:

predictive and mechanistic studies

outubro de 2021

New insights in (ab)normal fetal lung development:
predictive and mechanistic studies
Ana Cristina Nunes Gonçalves
UMinho | 2021

ICVS Life and Health Sciences Research Institute
Instituto de Investigação em Ciências da Vida e Saúde
JOSÉ DE MELLO SAÚDE
2CA Braga Centro Clínico Académico
NORTE2020 PROGRAMA OPERACIONAL REGIONAL DO NORTE
PORTUGAL 2020
FCT Fundação para a Ciência e a Tecnologia
Universidade do Minho
Escola de Medicina

Universidade do Minho
Escola de Medicina

Ana Cristina Nunes Gonçalves

New insights in (ab)normal fetal lung development:
predictive and mechanistic studies

Tese de Doutoramento em Ciências da Saúde

Trabalho efetuado sob a orientação da:
Doutora Cristina Isabel Nogueira Silva
Professora Auxiliar
Escola de Medicina
Universidade do Minho, Braga, Portugal
e do
Doutor Jorge Manuel Nunes Correia Pinto
Professor Catedrático
Escola de Medicina
Universidade do Minho, Braga, Portugal

outubro de 2021

DIREITOS DE AUTOR E CONDIÇÕES DE UTILIZAÇÃO DO TRABALHO POR TERCEIROS

Este é um trabalho académico que pode ser utilizado por terceiros desde que respeitadas as regras e boas práticas internacionalmente aceites, no que concerne aos direitos de autor e direitos conexos.

Assim, o presente trabalho pode ser utilizado nos termos previstos na licença abaixo indicada.

Caso o utilizador necessite de permissão para poder fazer um uso do trabalho em condições não previstas no licenciamento indicado, deverá contactar o autor, através do RepositóriUM da Universidade do Minho.

Licença concedida aos utilizadores deste trabalho

Atribuição
CC BY

https://creativecommons.org/licenses/by/4.0/

Acknowledgments/Agradecimentos

À Professora Doutora Cristina Nogueira-Silva, agradeço por ter acreditado e por me ter permitido chegar até aqui. Agradeço por tudo o que me ensinou, pela sinceridade, pela confiança e pela liberdade e autonomia que sempre depositou em mim. Obrigado por me possibilitar crescer, não só no trabalho, mas também como pessoa.

Ao Professor Doutor Jorge Correia-Pinto, Diretor do Instituto de Investigação em Ciências da Vida e Saúde, agradeço a orientação desta tese, disponibilidade, confiança e liberdade que foram fundamentais na realização deste trabalho.

Ao Professor Doutor Nuno Sousa, presidente da Escola de Medicina, e à Professora Fátima Baltazar, Coordenadora do Domínio de Investigação em Ciências Cirúrgicas, agradeço todas as condições proporcionadas para que este trabalho se realizasse da melhor forma possível.

To the reviewers of our published and unpublished papers, for their detailed analysis of our work, which helped us to improve and strengthen the manuscripts.

To Professor Graeme Polglase and the Perinatal transition group at Hudson Institute of Medical Research/Ritchie Centre, Australia, for accepting me in your laboratory, for the scientific sharing, and the "pub time".

A todos os membros do domínio de Investigação em Ciências Cirúrgicas, obrigada pela forma acolhedora como me receberam e pelas excelentes condições de trabalho que me proporcionaram.

Aos PhD-iHES, à Laura, Ana Bela, Cristina e Aurélie com quem partilhei estes quatro anos, agradeço a amizade, partilha, almoços, jantares e noites agradáveis em Braga.

À minha irmã, Diana Gonçalves, que hoje sabe mais sobre desenvolvimento pulmonar do que precisa, agradeço a paciência infinita e a ajuda imprescindível com todo o processo burocrático que envolve um PhD e uma viagem à Austrália. À minha família, Natália e José, que estiveram sempre presentes.

"If we knew what it was we were doing, it would not be called research, would it?"
(Albert Einstein)

Esta tese de doutoramento aqui apresentada foi desenvolvida no âmbito de financiamento pela Fundação para a Ciência e a Tecnologia (FCT) e pela empresa José de Mello Saúde – 2CA através de uma bolsa individual de doutoramento, com a referência: PD/BDE/127829/2016. Parte do trabalho aqui desenvolvido foi cofinanciado pela FCT (UIDB/50026/2020; POCI-01-0145-FEDER-030881), ICVS (PPBI-POCI-01-0145-FEDER-022122) e NORTE2020 (NORTE-01-0145-FEDER-000013; NORTE-01-0145-FEDER-000023).

STATEMENT OF INTEGRITY

I hereby declare having conducted this academic work with integrity. I confirm that I have not used plagiarism or any form of undue use of information or falsification of results along the process leading to its elaboration. I further declare that I have fully acknowledged the Code of Ethical Conduct of the University of Minho.

University of Minho, 20 October 2021

Full name: Ana Cristina Nunes Gonçalves

Signature:

Novas perspetivas no desenvolvimento pulmonar fetal (a)normal: estudos preditivos e mecanísticos

Resumo

O desenvolvimento pulmonar é um complexo e desafiante tópico de pesquisa uma vez que, compreende diferentes zonas funcionais que diferem entre si em termos de nichos celulares e vias de sinalização. Estas zonas contribuem para a regulação da respiração neonatal normal. A hipoplasia pulmonar fetal (HPF) é caracterizada por pulmões pouco ramificados nos estadios iniciais e um reduzido número de ductos alveolares no final da gestação. Esta doença constitui uma das mais comuns causas de falha respiratória neonatal, para a qual o diagnóstico e tratamento pré-natal permanecem pouco conhecidos. Métodos imagiológicos e oclusão traqueal fetal endoscópica (FETO) são atualmente as ferramentas mais favoráveis para predizer e tratar a HPF, respetivamente. Contudo, os controversos valores preditivos por método imagiológico e os efeitos secundários associados com o FETO limitam a sua aplicabilidade. Tendo a sua máxima severidade na hérnia diafragmática congénita (HDC), a HPF é muitas vezes estudada no modelo da HDC induzida pelo nitrofen, o qual mimetiza de forma razoável a HDC humana no que concerne às alterações morfológicas e moleculares.

No presente estudo pretendemos contribuir para o conhecimento do desenvolvimento pulmonar fetal. Para isso, exploramos o valor preditivo dos métodos imagiológicos na HPF letal; caracterizamos o pulmão hipoplásico fetal em termos de perfil epitelial celular da fase embriónica até à sacular e analisamos o papel funcional do Roundabout 1 (ROBO1) e ROBO2 na ramificação pulmonar e no perfil SRY-related HMG BOX (SOX2)/SOX9. Investigamos ainda os mecanismos desencadeados pelo fluido intraluminal que estimulam o crescimento pulmonar. Com esse intuito, avaliamos as culturas de explantes como modelo *ex vivo* para o estudo da composição do fluido intraluminal na ramificação pulmonar.

Ao longo deste trabalho descrevemos os ultrassons como importantes preditores de HPF letal e recomendamos estudos restritos por tipo de doença e grau de severidade. Nos pulmões CDH-induzidos, verificamos um comprometimento do padrão próximo-distal e da diferenciação das células ciliadas na fase sacular. Identificamos o ROBO2 como estimulador da ramificação pulmonar via SOX9 e, descrevemos o ROBO2 como desregulado nos pulmões hipoplásicos. Demonstramos o fluido intraluminal como manipulável nas culturas de explantes pulmonares *ex vivo* e, reportamos a concentração de cloro intraluminal como promotor de crescimento celular num mecanismo dependente de PIEZO1/PIEZO2, expressos nas células pulmonares neuroendócrinas/corpos neuroepiteliais.

Em conclusão, este trabalho contribui significativamente para o estado da arte do desenvolvimento pulmonar fetal e expõe novas perspetivas e possibilidades de investigação.

Palavras-chave: células epiteliais, hipoplasia pulmonar fetal, mecanotradução, morfogénese ramificada, ultrassom

New insights in (ab)normal fetal lung development: predictive and mechanistic studies

Abstract

Fetal lung development is a complex and challenging topic of research since comprise distinct functional zones with unique cell niches and pathways that work together to permit normal respiratory function at birth. Fetal lung hypoplasia (FLH) with underbranched lungs at early and reduced number of alveoli at later development stages, constitute one of the most common causes of neonatal respiratory failure, for which the prenatal prediction and treatment remains uncertain. Imagiological methods and fetoscopic endoluminal tracheal occlusion (FETO) are the current more favorable approaches to predict and treat FLH, respectively. Nevertheless, the controversial predictive values by imagiological method and the inherent secondary effects after FETO restrain their applicability. Reaching its maximum severity in congenital diaphragmatic hernia (CDH), FLH is preferable studied in nitrofen-induced CDH rat model since it reasonably mimics the human CDH in terms of morphological and molecular alterations.

In the present study, we intend to contribute to the body of knowledge in (ab)normal fetal lung development by exploring the predictive value of imagiological methods in lethal FLH estimation. In addition, we determine the epithelial cell profile from embryonic-to-saccular phases in induced-CDH lungs and evaluate the functional role of Roundabout 1 (ROBO1) and ROBO2 in branching morphogenesis and SRY-related HMG BOX (SOX2)/SOX9 profile. We then extend our studies to investigate the mechanisms triggered by intraluminal fluid in stimulation of fetal lung growth. For that, we evaluate the experimental relevance of the *ex vivo* lung explant cultures to study the intraluminal lung fluid composition in branching morphogenesis.

In this Ph.D. thesis, we describe ultrasounds as valuable predictor for lethal FLH and recommend restrict studies by disease type and severity degree. In induced-CDH lungs, we provide evidence that both proximodistal patterning and the differentiated profile of ciliated cells at saccular stage are impaired. We identify ROBO2 as promotor of SOX9 instead of SOX2 expression in branching morphogenesis and describe ROBO2 as dysregulated in hypoplastic lungs. Lastly, we demonstrate the intraluminal fluid able to be manipulated in *ex vivo* lung explant cultures, for which the intraluminal chloride concentration is modulator of *ex vivo* lung growth under a mechanism dependent on PIEZO1/PIEZO2, expressed in pulmonary neuroendocrine cells/neuroepithelial bodies.

In conclusion, this work significantly contributes to the state-of-the-art in (ab)normal fetal lung development and exposes new perspectives and possibilities for research.

Keywords: branching, epithelial cells, fetal lung hypoplasia, mechanotransduction, ultrasound.

Contents

List of figures

List of tables

List of abbreviations

+: positive

[Cl]: chloride concentration

2D-US: two-dimensional ultrasound

3D-US: three-dimensional ultrasound

Abca3: *ATP binding cassette subfamily A member 3*

ADRP: adipose differentiation-related protein

AFG: anterior foregut

AFV: amniotic fluid volume

Agr2: *anterior gradient 2*

AMFs: alveolar macrophages

ANO1: anoctamin-1

AQP5: aquaporin 5

Arp2/3: *actin-related protein 2/3 complex*

Ascl1: *achaete-scute homolog 1 (also known as Mash1)*

ASM: airway smooth muscle

AT1: type 1 angiotensin receptor

AT2: type 2 angiotensin receptor

ATP: adenosine triphosphate

BADJ: bronchioalveolar duct junction

BMP: bone morphogenetic protein

BMP4: bone morphogenetic protein 4

CA: chest area

CaCC: calcium-dependent chloride

cAMP: cyclic adenosine monophosphate

CaR: extracellular calcium receptor

CC10: clara cell-specific 10 kD protein

CCDC39: coiled-coil domain containing 39

CCSP: clara cell secretory protein

CDH: congenital diaphragmatic hernia

CFTR: cystic fibrosis transmembrane conductance regulator

cGMP: cyclic guanosine monophosphate

CGRP: calcitonin gene-related peptide

Cl: chloride

CIC2: voltage-sensitive chloride channel2

CNS: central nervous system

CO_2: carbon dioxide

CPAM: congenital pulmonary airway malformation

Cyp2f2: *cytochrome p450*

Cyr61: *cysteine-rich 61*

DBN1: drebin 1

DH: diaphragmatic hernia

DLK1: delta like non-canonical Notch ligand 1

Dll1: *Delta like canonical Notch ligand 1*

DNA: deoxyribonucleic acid

E: embryonic day

E2F4: *E2F transcription factor 4*

ECM: extracellular matrix

ECMO: extracorporeal membrane oxygenation

EFHC1: EF-hand domain containing protein 1

EGF: epidermal growth factor

Egr1: *early growth response 1*

ENKUR: enkurin

EXIT: ex-utero intrapartum therapy

FACs: focal adhesion complexes

FAK: focal adhesion kinase

FANK1: fibronectin type III and ankyrin repeat domains 1

FBMs: fetal breathing movements

FETO: fetoscopic endoluminal tracheal occlusion

FGF9: fibroblast growth factor 9

FGF10: fibroblast growth factor 10

FGFR: fibroblast growth factor receptor

FGFRL1: fibroblast growth factor receptor-like 1

FLB: lung volume to body weight ratio

FLH: fetal lung hypoplasia

FOX: forkhead box proteins

Foxa3: *forkhead box A3*

Foxf1: *forkhead box F1*

Foxj1: *forkhead box J1*

FoxP1: *forkhead box P1*

FoxP2: *forkhead box P2*

GABA: gamma-aminobutyric acid

GRP: gastrin-releasing peptide

HA: heart area

HDAC3: histone deacetylase 3

Hes1: *Hes family bHLH transcription factor 1*

HOX: homeobox

Hopx: *homeodomain-only protein homeobox*

ICM1: intercellular adhesion molecule 1

ID2: inhibitor of DNA binding 2

IGF1: insulin-like growth factors 1

IGF2: insulin-like growth factors 2

IGF1R: insulin-like growth factors 1 receptor

ILK: integrin-linked kinase

IP3: inositol trisphosphate

iPPROM: iatrogenic preterm premature rupture of membranes

iNO: inhaled nitric oxide

ITGA6: integrin alpha6

ITGB1: integrin beta1

KDR: kinase insert domain receptor

KO: knockout

LA: lung area

LHR: lung-to-head ratio

LIFs: lipofibroblasts

LRRC23: leucine rich repeat containing 23

LRRIQ1: leucine rich repeats and IQ motif containing 1

MAPK: mitogen-activated protein kinase

MHC: myosin heavy-chain

mINSC: inscuteable

MMP: matrix metalloproteins

mRNA: messenger ribonucleic acid

Muc5ac: Mucin 5AC

Myocd: *Myocardin*

Na^+: sodium

Na^+/K^+-ATPase: sodium-potassium adenosine triphosphatase

NANCI: Nkx2.1-associated noncoding intergenic RNA

NE: neuroendocrine

NEBs: neuroepithelial bodies

NKCC: sodium–potassium–chloride cotransporter

***Nkx2-1*:** *Nk2 homeobox 1*

O_2: oxygen

o/e-LHR: observed-to-expected lung-to-head ratio

P: postnatal day

PDE5: phosphodiesterase type 5

PDGRα: parathyroid hormone-related protein alpha

***Pdpn*:** *podoplanin*

PGE2: prostaglandin E2

PGP9.5: protein gene product 9.5

PINCH: particularly interesting new cysteine-histidine-rich protein

PKC: protein kinase C

PLIN2A: perilipin 2A

PLs: phospholipids

PNECs: pulmonary neuroendocrine cells

PPAP2B: phosphatidic acid phosphatase type 2B

PPARg: peroxisome proliferator activated receptor gamma

PPROM: preterm premature rupture of membranes

PTHrP: parathyroid hormone-related protein

PTHrR: parathyroid hormone-related receptor

RA: retinoic acid

RALDH2: retinal dehydrogenase 2

RALDH3: retinal dehydrogenase 3

Rarα: *retinoic acid receptor alpha*

Rarβ2: *retinoic acid receptor beta 2*

RBP: retinol-binding protein

Ref: reference

Rfx2: *regulatory factor X2*

ROBO1: roundabout 1

ROBO2: roundabout 2

ROCK: Rho-associated protein kinase

RxRα: retinoid X receptor alpha

SAGE: serial analysis of gene expression

Scgb1a1: *secretoglobin family 1A member 1*

Sftp: *surfactant-associated protein*

SHH: sonic hedgehog

sm22α: smooth muscle protein 22 alpha

Smooth: smoothened

SNAI1: transcription factor Snail

SP-C: surfactant protein-C

Spry1: *sprout 1*

Spry2: *sprout 2*

SOX: SRY-related HMG BOX

TBX4: T-box gene 4

TBX5: T-box gene 5

TGFβ: transforming growth factor beta

TGFβi: transforming growth factor beta induced

TβRI: TGF-beta type I receptor (or ALK5)

TIMP: tissue inhibitors of matrix metalloproteins

TNFα: tumor necrosis factor alpha

TO: tracheal occlusion

TRα1: thyroid hormone receptor alpha 1

TRβ1: thyroid hormone receptor and beta 1

Trop2: *trophoblast antigen 2*

Tsp1: *thrombospondin-1*

TTC18: tetratricopeptide repeat domain 18

TTF: tyroid transcription factor

Tubb4a: *tubulin beta 4A*

US: ultrasound

VDUP1: vitamin D3 up-regulated protein 1

VEGF: vascular endothelial growth factor

VEGFR: vascular endothelial growth factor receptor

WDR16: WD repeat-containing proteins

WNT2: wingless 2

WNT7b: wingless 7b

YAP: Yes-associated protein

Chapter 1 – General introduction

1.1. Normal fetal lung development

The transition from fetal to neonatal life is dependent upon major changes within the respiratory system that allow the infant to initiate the pulmonary gas exchange, a function that is performed by the placenta during fetal life. Traditionally, lung formation is divided into five distinct periods based on structure: embryonic, pseudoglandular, canalicular, saccular, and alveolar, which are shared among mammalian species. Nowadays, our understanding of fetal lung development and neonatal respiratory function results from studies that highlight the cellular and molecular mechanisms in the underlying morphologic alterations. As such, this introduction pretends to emphasize the current knowledge regarding the (ab)normal fetal lung development and support the key research topics that are relevant to the goals addressed in this project.

Development of the lung begins with the early specification of the germ layers as the ectoderm, mesoderm, and endoderm are formed. Therefore, sequential signals among mesenchymal and epithelial cells direct transcriptional programs to produce the foregut endoderm that gives rise to the thymus, lung, liver, and pancreas. For instance, the high levels of bone morphogenetic protein (BMP), retinoic acid (RA), and the expression of Wingless 2/2b (WNT2/2b) in the ventral mesenchyme induce the expression *of NK2 homeobox 1* (*Nkx2-1*, also known as *thyroid transcription factor 1* (*Ttf1*) or *T/EBP*) that distinguishes the future lung from the other foregut derivatives at the onset of **embryonic** phase [occurs between weeks 4 and 8 of human's gestation and embryonic day (E) 11 to E13 in rat] (reviewed in Jacobs et al 2012, Rankin et al 2016, Rock & Hogan 2010, Swarr & Morrisey 2015, Zhang et al 2017). In addition, RA activates paracrine networks dependent on Sonic Hedgehog (SHH) signaling from the endoderm to mesenchymal targets that include *glioma-associated oncogene family zinc finger* (*Gli*) 2/3, *Forkhead box F1* (*FoxF1*), and *T-box gene 4* (*Tbx4*) (Figure 1). The expression of *Bmp4* in the ventral mesoderm, and the Bmp antagonist, Noggin, expressed from the notochord on the dorsal side, establish the dorsal-ventral gradient of *Bmp* that is required to promote the proper placement of the lung along the proximodistal axis (reviewed in Arora et al 2012, Goss & Morrisey 2010, Hrycaj et al 2015, Jacobs et al 2012, Kimura et al 1996).

Pseudoglandular stage occurs between weeks 8 and 16 of gestation in humans, and E12.5 to E18.5 in rats, and it is characterized by the initial outgrowth of the lung bud, and consequent branching of the lung tips. Airway patterning starts from a single tube or cluster of cells that grows and undergoes rounds of budding and/or bifurcation that leads to the formation of the complex arborized network (Lovric et al 2017, Metzger et al 2008, Schittny 2017). The repetition of these bifurcations at defined angles (planar or orthogonal to the long axis of the parent tube) generates the stereotyped, hierarchically organized three-dimensional branched architecture of the lung (Lovric et al 2017, Metzger et al 2008). Interestingly, it is the mesenchymal expression of TBX family members, FOXF1, and odd-skipped related transcription factor 1

(OSR1) that produce the WNT, BMP, and fibroblast growth factor 10 (FGF10) gradients, expressed at high levels in the distal tips of the lung (reviewed in Arora et al 2012, Morrisey & Hogan 2010, Whitsett et al 2019). These gradients working with SHH, transcription growth factor-beta (TGFβ), and RA control the epithelial progenitor differentiation into SRY-related HMG BOX 2 (SOX2) versus SOX9 positive ($^+$) cells and identify the proximal and distal pattern, respectively, at branching morphogenesis (Bellusci et al 1997, Daniel et al 2020, Grindley et al 1997, Lü et al 2004, Serra & Moses 1995, Whitsett et al 2019). In fact, the expression of FGF10 that directly activates β-Catenin in the distal epithelial progenitors' cells induces the expression of BMP4 and SOX9. Conversely, as the epithelial tube grows towards these distal sources of FGF10 and BMP4, progeny from the distal multipotent epithelial progenitors are left behind in the epithelial stalk and once they are out of FGF10 and BMP4, they lose SOX9 expression and start expressing SOX2 (Figure 1) (Hashimoto et al 2012, Mucenski et al 2005, Mucenski et al 2003, Shu et al 2005, Volckaert et al 2013).

Transmural pressure of the chest cavity and smooth muscle contractions are also key regulators of branching morphogenesis (Goodwin et al 2019, Kim et al 2015, Lin et al 2017, Nelson et al 2017). For instance, the local transmural pressure alters the proximal smooth muscle contraction that tunes the airway branching. In fact, as transmural pressure increased, the time interval between peristaltic contractions of proximal smooth muscle decreased, which result in increased rates of branching (Nelson et al 2017). In addition, increasing smooth muscle differentiation suppresses branching initiation and extension, whereas their decrease leads to ectopic branching and alterations in branch positioning (Goodwin et al 2019, Kim et al 2015). Unfortunately, the exact identity of smooth muscle progenitors is unclear. However, the FGF9 secreted by the mesothelium surrounding the lungs maintains the progenitor status of mesenchymal cells (Weaver et al 2003, Yi et al 2009); *Fgf10*- and *Wilms tumor 1* (*WT1*)-expressing progenitors give rise to a minor fraction of smooth muscle cells at E15.5 and E18.5, whereas glioma-associated oncogene 1 (*Gli1*)- and *Axin2*expressing progenitors construct the majority of smooth muscle cells at E18.5 (Figure 1) (Moiseenko et al 2017).

The intrapulmonary arterial system starts to develop at pseudoglandular stage with the connection between the microcirculation of the peripheral lung and the larger pulmonary arteries and veins established (deMello et al 1997). Pulmonary vasculature is not required for initiation or branching of the embryonic lung buds but is essential for their survival and growth later in the development (reviewed in Tan & Lewandowski 2020).

Canalicular stage includes the period between 16- and 26-weeks in humans (E18.5 to E20 in rats). This stage comprises the expansion of the respiratory tree in diameter and length, the division of terminal

bronchioles, and the increase of capillaries number leaning against the epithelium that marks the beginning of the prospective gas-exchange region. In humans, terminal bronchioles divide into respiratory bronchioles and alveolar ducts, whereas there are no respiratory bronchioles in rodents (Pan et al 2019). The formation of respiratory bronchioles in humans and alveolar ducts in humans and rodents overlaps with the epithelial and mesenchymal differentiation and contributes to the morphological distinction between conducting and respiratory airways. In brief, epithelial cell differentiation implies the differentiation of bronchiolar and alveolar lineages from SOX2 and $SOX9^{+}$ cells, respectively. Proximal or bronchiolar progenitors, $SOX2^{+}$, give rise to pulmonary neuroendocrine cells (PNECs), clara or ciliated, whereas alveolar differentiation forms alveolar type I (AT1) and alveolar type II (AT2) cells in a mechanism dependent on Notch signaling (Figure 1) and detailed discusses in section 1.1.1. (Chang et al 2013, Gontan et al 2008, Rockich et al 2013, Tompkins et al 2011, Tompkins et al 2009). At the end of canalicular phase, the first future air–blood barriers are formed, and at least a minimal pulmonary surfactant is produced (Bohnhorst & Peter 2020, Schittny 2017). Indeed, the specification of AT1 cells that allow oxygen (O_2) and carbon dioxide (CO_2) diffusion, and the AT2 cells that produce the pulmonary surfactant support the first chance of a human fetus to survive. Surfactant is a complex mixture of about 90% phospholipids (PLs) and 10% proteins that decrease the surface tension at the alveolar air-liquid interface, reduce the work of breathing, and inhibit/inactivates the environmental pathogens (reviewed in Bernhard 2016).

Starting on week 26 and finishing on week 36 of gestation in humans (E21 to postnatal day (P) 4 in rats), the **saccular** stage represents an intermediate phase, when branching morphogenesis ceases and alveolarization has yet to start (Cardoso & Lu 2006, Morrisey et al 2013). This stage is categorized by the enlargement of the terminal clusters into transitory alveolar saccules and ducts with a marked reduction on surrounding mesenchymal tissue. The capillaries also grow rapidly in the mesenchyme surrounding the primary alveoli to form a complex double network. AT2 covers part of the primary septa surface and surfactant continuous to be produced (Morton & Brodsky 2016, reviewed in Schittny 2017). Regarding the underlying mechanisms, the mesenchymal cells differentiated into lipofibroblasts (LIFs) and myofibroblasts in a process mediated by FGF10 and TGFβ type I receptor (TβRI or ALK5), (El Agha & Bellusci 2014, Li et al 2016). Importantly, the function of AT2 cells is supported by LIFs via an intercellular crosstalk pathway-dependent of stretch, parathyroid hormone-related peptide (PTHRP), prostaglandin E2 (PGE2), and leptin, while myofibroblasts produce elastin and collagen that are compounds of extracellular matrix (ECM) (Figure 1). The deposition of elastin and collagen and the presence of alveolar myofibroblasts are decisive for secondary septation during alveolarization with platelet-derived growth factor (PDGF)-A signaling as major regulator (Figure 1) (Andrae et al 2014, Boström et al 2002, Boström et al 1996, Lindahl et al 1997). In

fact, PDGF-A knockout mice show severe failure on alveolar septation since damage the alveolar myofibroblasts maturation and lack the elastin deposition (Boström et al 2002, Boström et al 1996, Lau et al 2011, Lindahl et al 1997), whereas overexpression of PDGF-A causes perinatal lethality due to marked mesenchymal cell proliferation (Li & Hoyle 2001).

The transition from saccular to alveolar stages involves the LIF formation that is recognized by their abundant lipid droplets and expression of perilipin 2A (PLIN2A), PDGF receptor (PDGFR), and THY-1. Alveolarization represents a process during lung development that leads to the formation and maturation of the distal parts of the lung: the alveoli. The **alveolar** stage starts at 36 weeks of gestation in humans and continues through early childhood (P4 to P21 in rats). Albeit the formation of alveoli is essentially postnatal in rodents and humans (Amy et al 1977, Burri et al 1974, Hislop et al 1986, Langston et al 1984, Pan et al 2019, Zeltner et al 1987), maturation of peripheral alveoli is initiated before birth in the human lung, whereas the similar morphological issues are only visualized after birth in rodents (Burri 1984, Langston et al 1984, Pan et al 2019, Thurlbeck 1975).

Alveolarization is marked by a dramatic increase in gas exchange surface due to the subdivision of the primitive saccules by new interair-space walls resulting in new alveoli. In fact, restructuring of the terminal saccule into a true alveolus consists of lengthening and thinning of the secondary septa, reduction of septal interstitial tissue, and remodeling of the capillary bed by fusion of the two septal capillary networks into one (Burri 2006, Rodríguez-Castillo et al 2018). Alveolarization requires complex interactions among differentiating AT1 and AT2 epithelial cells and diverse mesenchymal progenitors that form the collagen and elastin-rich scaffold and define the alveolar structure (Li et al 2015). Secondary septa arrive at the place of elastin deposition, which is produced by alveolar myofibroblasts (Figure 1). In rodents, by P4, so-called secondary septa appear in the primary septa at sites of elastin deposition (Morrisey & Hogan 2010, Tschanz et al 2014). At the tip (secondary crest) of these still-immature secondary septa, alpha-smooth muscle actin (α-SMA)$^+$ myofibroblasts appear, and the expression of ECM components such as elastin further increases (Boström et al 1996, Chao et al 2015, Mižíková & Morty 2015, Morrisey & Hogan 2010). Signals like mechanical forces, PDGFRα, and TGFβ induce a myogenic phenotype (Torday & Rehan 2002, Torday et al 2002), whereas Thy-1 severely impairs the alveolarization since inhibits the TGFβ, leading to reduced myogenic phenotype (Nicola et al 2009). In conclusion, mature alveoli are lined by two main epithelial cell types, AT1 and AT2. AT1 cells constitute about 95% of the surface area and are located immediately adjacent to the capillaries, which allows the efficient O_2 and CO_2 diffusion, whereas AT2 cells secrete surfactants to prevent alveolar collapse (Barkauskas et al 2013, Desai et al 2014).

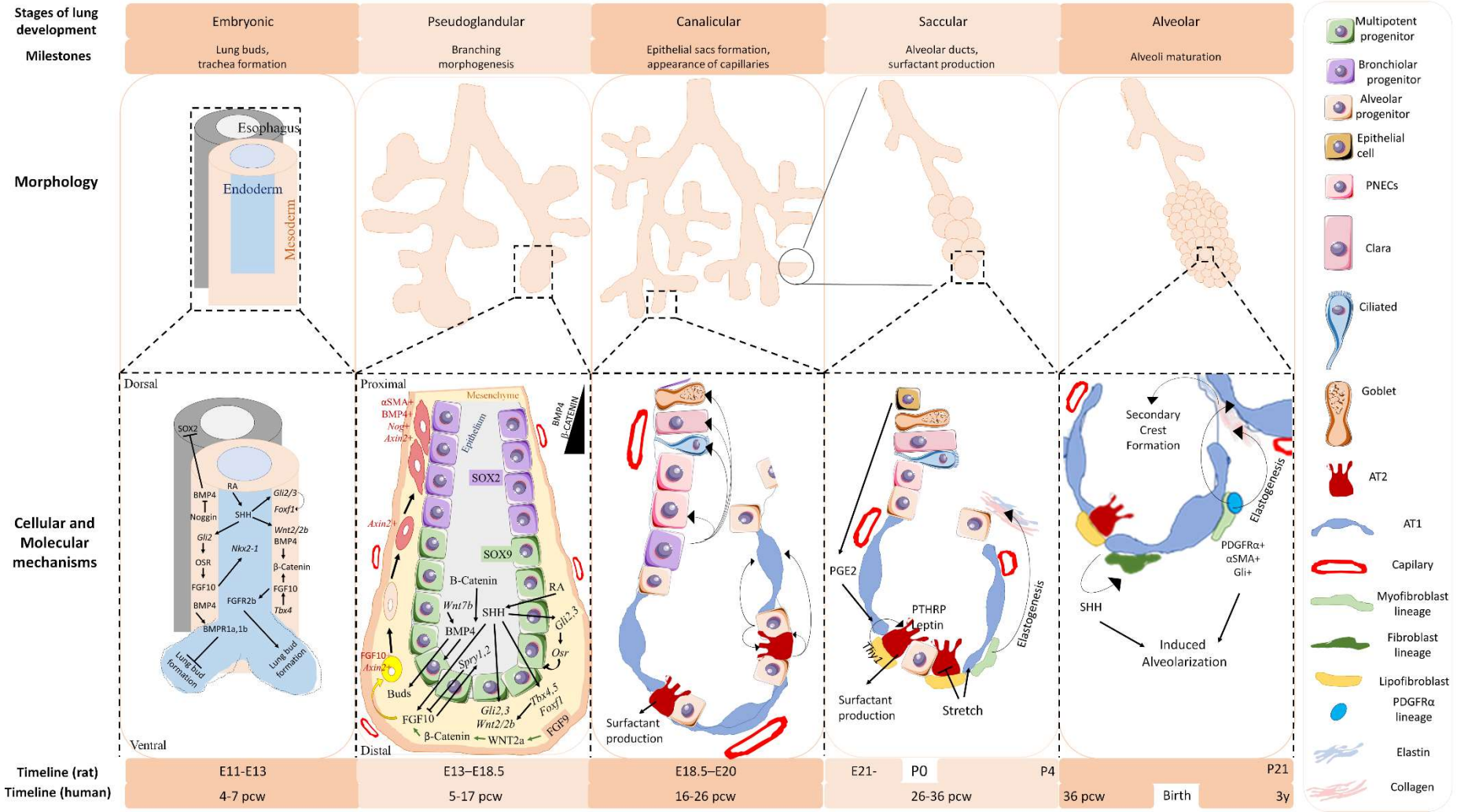

Figure 1 - Timeline of five stages of lung development in rats and humans with the underlying molecular and cellular mechanisms. The five milestones of lung development are embryonic (formation of lung buds), pseudoglandular (branching morphogenesis), canalicular (formation of epithelial *(continues in the next page)*

(continuation of the previous page) sacs and appearance of capillaries), saccular (production of alveolar ducts and surfactant protein), and alveolar (maturation of the alveoli). The principal signal pathways that control lung bud formation (embryonic), proximodistal patterning (pseudoglandular); epithelial cell differentiation (canalicular); and primary (saccular) and secondary (alveolar) septa formation are characterized in the lower panel. Rat stages are represented in embryonic (E) or postnatal (P) days and human stages are represented by post-conception weeks (pcw) and years (y). α-SMA: alpha-smooth muscle action; BMP4: bone morphogenetic protein; BMPR1a: bone morphogenetic protein receptor 1a; BMPR1b: bone morphogenetic protein receptor 1b; FGF9: fibroblast growth factor 9; FGF10: fibroblast growth factor 10; FGFR2b: fibroblast growth factor receptor 2b; *Foxf1*: *Forkhead box factor 1*; GLI: glioma-associated oncogene family zinc finger; *Gli2*: *glioma-associated oncogene family zinc finger 2*; *Gli3*: *glioma-associated oncogene family zinc finger 3*; *Nkx2-1*: *NK2 homeobox 1*; Nog: noggin; *Osr*: *odd-skipped related 1*; PGE: prostaglandin E2; PDGFRα: parathyroid hormone-related protein alpha; PTHrP: parathyroid hormone-related protein; RA: Retinoic acid; SHH: sonic hedgehog; SOX2: SRY-related HMG BOX 2; SOX9: SRY-related HMG BOX 9; *Spry1*: Sprouty 1; *Spry2*: Sprouty 2; *Tbx4*: T-box gene 4; *Tbx5*: *T-box gene 5*; *Wnt2a*: *wingless 2a*; *Wnt7b*: *wingless 7b*.

1.1.1. Specification of epithelial lineages

The complexity of lung morphogenesis is evident from the multiple cell types that constitute the lung, all present in appropriate numbers and sites to support the first respiration at birth (reviewed in Whitsett et al 2019). Lung identity is established during the embryonic phase when morphogens into the surrounding mesoderm induce the expression of *Nkx2-1* in the ventral anterior foregut endoderm. Then, reciprocal mesodermal-endodermal interactions support branching morphogenesis and the specification of multipotent progenitor cells into a proximal and distal fate. For instance, during branching morphogenesis, the distal tip of the developing lung contains a pool of multipotent *Sox9/Id2*+ epithelial progenitors able to give rise to bronchiolar and alveolar epithelium (Figure 2). These progenitor cells proliferate at pseudoglandular stage and form the proximodistal patterning. For that, the high levels of *Fgf10/ Fgfr2b*, *Wnt/β-Catenin*, and *Bmp4* in the distal tip of the lung promote the *Sox9* or distal profile (Abler et al 2009, Chang et al 2013, Cornett et al 2013, Mucenski et al 2003, Shu et al 2005), whereas the consecutive grow of the epithelial tubes towards these distal sources decrease the levels of *β-Catenin* and *Bmp4* and cells start expressing *Sox2* (Figure 2) (Eblaghie et al 2006, El Agha et al 2014, Gontan et al 2008, Hashimoto et al 2012, Park et al 1998, Rockich et al 2013, reviewed in Volckaert & De Langhe 2015, Weaver et al 2000, Weaver et al 1999).

Later, it is the SOX2 and SOX9^{+} cells that differentiated and form the conducting and respiratory airways, respectively, at canalicular and saccular stages.

The current model of bronchial and alveolar differentiation admits the bronchiolar lineages (SOX2^{+}), giving rise to clara, ciliated, goblet, or PNECs, whilst alveolar (SOX9^{+}) forms AT1 and AT2 cells (Figure 2). Molecularly, the bronchiolar differentiation implies a first molecular decision mediated by Notch via *Hes1*, a major Notch target gene, that establishes the pulmonary neuroendocrine (PNECs) and non-neuroendocrine profile. At this time, PNEC and non-neuroendocrine cells are distinguished by the expression of *achaete-scute homolog 1* (*Ascl1*) (also called *Mash1*) and *Scgb3a2*, respectively. Then, the non-neuroendocrine cells undergo a second Notch-mediated decision to commit the ciliated (*forkhead box J1*, *Foxj1*$^{+}$/β-tubulin^{+}) or clara cells [*secretoglobin family 1A member 1*, *Scgb1a1*, also called Clara cell-specific 10 kD protein (*CC10*) or Clara cell secretory protein (CCSP)] (Figure 2) (Borges et al 1997, Guha et al 2012, Guseh et al 2009, Ito et al 2000, Morimoto et al 2010, Morimoto et al 2012, Post et al 2000, Shan et al 2007, Stupnikov et al 2019, Tsao et al 2009, Zhang et al 2013). Inhibition of Notch signaling activates a regulatory gene network that includes *Gemc1* (also called *Gmnc*), *multicilin* (also called *Mcidas*), *E2F transcription factor 4* (*E2F4), regulatory factor X2 (Rfx2)*, and *FoxJ1* and supports the ciliated profile (Figure 2) (Arbi et al 2016, Campbell et al 2016, Didon et al 2013, Quigley & Kintner 2017, Stubbs et al 2012, Zhou et al 2017). *Mcidas* and *Foxj1* are key transcriptional regulators of multiciliogenesis (Marshall et al 2016, Nemajerova et al 2016).

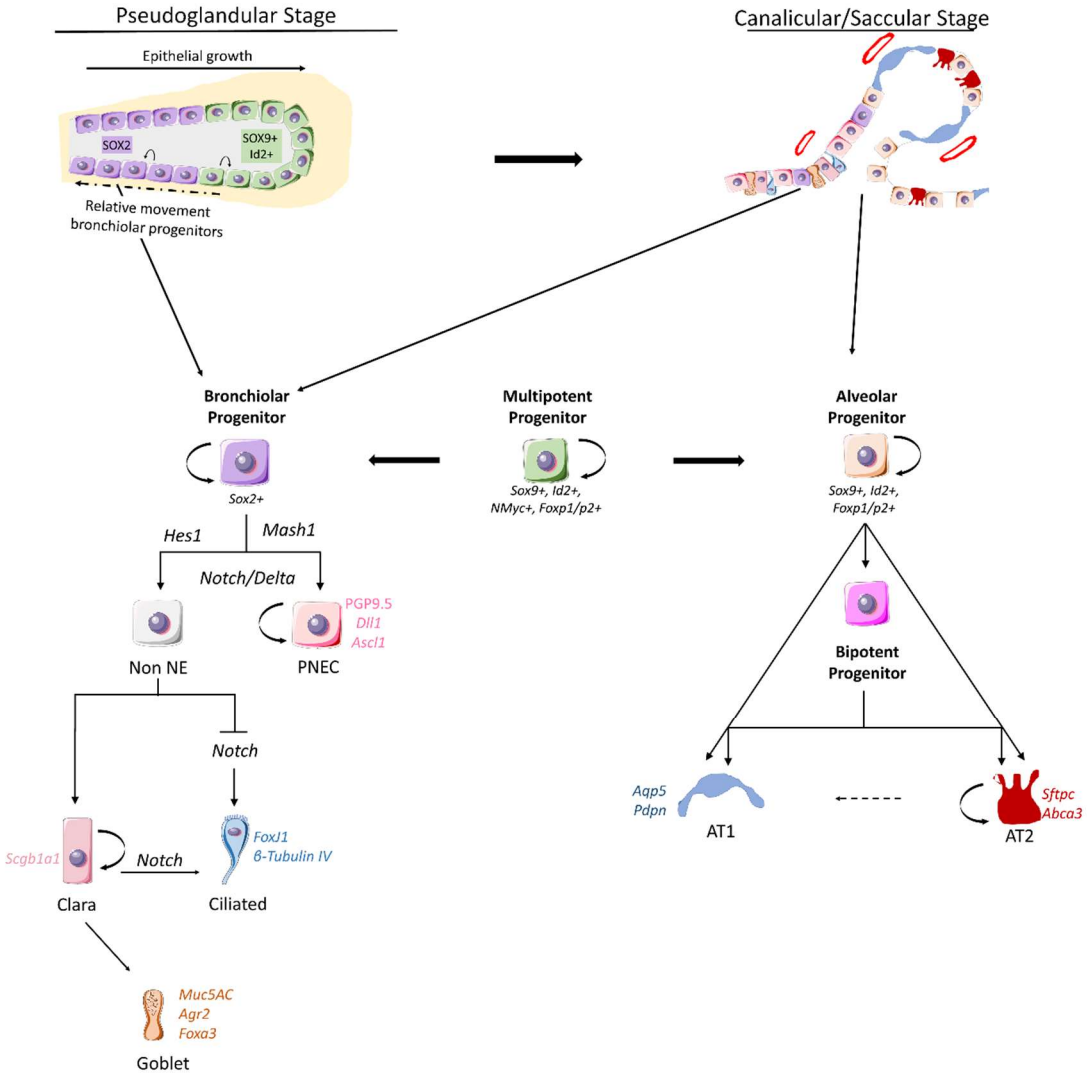

Figure 2 - Overview of bronchiolar and alveolar differentiation in the development of the lung – At the pseudoglandular stage, progenitor cells (SRY-related HMG BOX 9, $SOX9^+$, green) within the distal tip epithelium both self-renew and generate descendants ($SOX2^+$, violet) that exit the tip and populate the conducting airways. $SOX9^+$ cells persist to the canalicular stage when they generate alveolar progenitors (orange) that populate the future alveoli, whereas proximal progenitors (SOX2) give rise to bronchiolar lineage. It is not clear if this switch from the production of bronchiolar to alveolar descendants is intrinsic or imposed by extrinsic factors. Alveolar progenitors generate type 1 (AT1) and type 2 (AT2) alveolar epithelial cells, directly or indirectly through a bipotent progenitor. The proximal $SOX2^+$ progenitors form neuroendocrine (PNECs), clara, ciliated, and goblet cells. *Abca3: ATP binding cassette subfamily A member 3; Agr2: anterior gradient 2; Aqp5: aquaporin 5*; *Ascl1: achaete-scute homolog 1 (*also known as *Mash1); Dll1: Delta like canonical Notch ligand 1*; *Foxa3: forkhead box proteins; FoxJ1: forkhead boxJ1*; *FoxP1: forkhead box P1*; *FoxP2: forkhead box P2*; *Hes1*: *Hes family bHLH transcription factor 1*; *Id2: inhibitor of DNA binding 2; Muc5ac: Mucin 5AC;* NE: neuroendocrine; *(continues in the next page)*

(continuation of the previous page) Pdpn: podoplanin; PGP9.5: protein gene product 9.5; PNECs: pulmonary neuroendocrine cells; *Scgb1a1: secretoglobin family 1A member 1*; *Sftpc: surfactant- associated protein* (adapted from Rock & Hogan 2011).

Concerning alveolar lineage, transcriptional studies showed two origins for AT1 and AT2 cells (Chang et al 2013, Desai et al 2014, Frank et al 2019, Treutlein et al 2014). For instance, at early developmental stages, AT2 cells arise from highly proliferative $SOX9^{+}$ cells localized in the most distal tip, whereas AT1 emerges from a region just proximal to this in the stalk of the lung bud. This study also suggests the small number of bilineage AT1/AT2 cells observed between these two regions, representing residual undifferentiated progenitor cells, which progressively differentiate during development but do not contribute in a significant manner to mature alveolar epithelial lineages (Frank et al 2019). Conversely, at the later canalicular-saccular period, a common "bipotent" progenitor proliferates and gives rise to AT1 and AT2 cells (Figure 2). Authors also describe little epithelial proliferation during sacculation and for several weeks afterward, indicating that maturation of bipotent progenitors generates most or possibly all AT1 and AT2 cells in development (Desai et al 2014, Treutlein et al 2014).

More recently, other stimuli like tissue environment, mechanical forces, ECM, and intracellular factors are also identified in the regulation of alveolar cell differentiation. Indeed, reduced mechanical tension from fetal breathing by depletion of amniotic fluid or lowered stiffness of cell culture surface favors AT2 over AT1 cell differentiation (Li et al 2018). In addition, the canonical WNT and FGF signaling inhibit the AT1 cell differentiation (Desai et al 2014, Frank et al 2016, Li et al 2018, Wang et al 2016b), whereas the histone deacetylase 3 (HDAC3)-dependent TGFβ signaling is required for proper epithelium expansion and AT1 cell spacing (Wang et al 2016b, Wang et al 2016c).

1.1.2. Epithelial cell profile in fetal lung development

With comparable conducting, respiratory and vascular components, the rodent and human lungs are organized into a proximodistal patterning that controls the first breath at birth. At the cellular level, slight differences have been described, particularly at birth (Berend et al 1991, Boers et al 1999, Pan et al 2019, Plopper & Hyde 2015, Reynolds et al 2015). For instance, at the more proximal airways (bronchi), the human lung is composed of the basal, ciliated, clara, serous, mucus, and neuroendocrine cells, and exhibits abundant submucosal glands (Berend et al 1991, Boers et al 1999, Plopper & Hyde 2015, Reynolds et al 2015). In the mouse, the more proximal intrapulmonary conducting airways are composed primarily of ciliated and clara cells with clusters of PNECs largely located at airway branch points. In addition, the

respiratory bronchioles of the human lung are lined by cuboidal epithelia, alternating with thin-walled alveoli lined by squamous AT1 (Berend et al 1991, Boers et al 1999, Pan et al 2019, Plopper & Hyde 2015, Reynolds et al 2015), whereas the terminal bronchioles in mouse are lined by cuboidal epithelial cells with an abrupt transition (bronchioalveolar duct junction, BADJ) to the alveolar duct, which is lined by squamous AT1 (Boers et al 1999, Pan et al 2019, Suarez et al 2012). Besides these differences, the current knowledge demonstrates similar cellular functions during gestational life that allow the rodent model to be used in the study of human lung morphogenesis as followed described.

1.1.2.1. Pulmonary neuroendocrine epithelial cells (PNECs)

PNECs are the first specified cell type to appear in the respiratory epithelium, detectable at E12.5 in mice and 10 weeks in humans by the expression of bombesin. The cellular profile of neuroendocrine cells initiates as solitary with a salt-and-pepper patterning that later cluster into neuroepithelial bodies (NEBs). PNECs are rare, innervated airway epithelial cell types that account for <1% of the lung epithelium population and are enriched at airway branch point junctions (Table 1) (reviewed in Kuo & Krasnow 2015). Upon activation, PNECs release small neuropeptides [calcitonin gene-related peptide (CGRP), bombesin] and neurotransmitters [serotonin, gamma-aminobutyric acid (GABA), adenosine triphosphate (ATP)] (Brouns et al 2000, Cho et al 1989, Cutz et al 1993, Emanuel et al 1999, Garg et al 2019, Lauweryns et al 1973). These molecules may either act locally in an autocrine and paracrine manner or signal through neurons that innervate them. Importantly, the *in utero* injection or the treatment of the lung explant cultures with neuroendocrine products, ghrelin or bombesin, increase the surfactant protein-C (SP-C) content of AT2 cells, the deoxyribonucleic acid (DNA) content of mesenchymal cells, and the branching morphogenesis (Emanuel et al 1999, King et al 1995, Sunday et al 1990). These findings raised the possibility that PNECs act through their products to promote lung growth. (Noguchi et al 2015). In contrast, the absence of PNECs in *Ascl1* knockout mice*,* led to normal lungs in terms of branching pattern and size, with normal differentiated profile of the major epithelial cells, including clara, ciliated, AT1, and AT2 cells, indicating that PNECs are not required for primary aspects of lung development (Ito et al 2000).

Over the last years, PNECs/NEBs have been reported as sensors of hypoxia, hypercapnia, acidosis, and airway stretch (reviewed in Garg et al 2019) with, however, unclear value in fetal lung development. Indeed, a recent publication showed PIEZO2, a known mechanosensor (Coste et al 2010, Ranade et al 2014b, Woo et al 2014), expressed in NEBs at term with undetermined function since the regulation of fetal lung expansion and efficient neonatal respiration was attributed to PIEZO2 expressed in sensory neurons (Nonomura et al 2017).

Table 1 – Summary of the molecular markers, function, and other observations that characterize the differentiated epithelial cell types. AQP5: aquaporin 5; AT1: alveolar type 1 cell; AT2: alveolar type 2 cell; *Cgrp*: *calcitonin gene-related peptide*; *Cyp2f2*: *cytochrome p450*: *FoxJ1*: *forkhead box J1*; *Hopx*: *homeodomain-only protein homeobox*; ND: not defined; NEBs: neuroepithelial bodies; *Pdpn*: *podoplanin*; PNECs: pulmonary neuroendocrine cells; Ref: references; *Scgb1a1*: *secretoglobin family 1A member 1*; *Sftpc*: *surfactant- associated protein; Tubb4a*: *Tubulin Beta 4A*.

Stem or progenitor population	Marker Gene	Proliferative Capacity	Function	Other observations	Ref.
PNECs/ NEBs	*Cgrp*	ND	Airway sensor; required for appropriate innate immune inflammatory response	<1% of the lung epithelium	Garg 2019
Clara	*Scgb1a1; Cyp2f2*	Yes	Reparative cells for the airway epithelium; Barrier maintenance, secretion, and metabolism	Secretory cells	Reynolds 2010; Pan 2019
Ciliated	*FoxJ1; Tubb4a*	No	Critical for mucociliary clearance	Recognized by the multiple cilia	Rawlins 2007 Toskala 2005
AT1	*Pdpn; Aqp5; Hopx*	No	Allow the efficient O_2 and CO_2 diffusion	Cover 95% of the gas exchange surface	Yang 2016; Nguyen 2019
AT2	*Sftpc*	Yes	Produce pulmonary surfactant proteins; reduce alveolar surfactant tension	Maturation occurs later in gestation	Whitsett & Alenghat 2015; Bernhard 2016

1.1.2.2. Clara cells

Predominantly found in the intrapulmonary airway in human, the differentiation of clara cells starts at canalicular period and populate the trachea and conducting airway in mice (Pan et al 2019, Rawlins et al 2009). Clara is a secretory cell whose numbers vary among mammalian species, during development, and along the proximal-distal and dorsal-ventral axis of the airways (Ji et al 1995, Massaro et al 1994). In fact, distinct subsets of clara-secretory cells are in selective niches near NEBs, along the ducts of submucosal glands, and in the bronchoalveolar ductal regions. Within the normal lung, clara cells maintain the facultative progenitor cell pool (self-renewal) and restore terminally differentiated cells of the conducting airway epithelium (Table 1) (Reynolds & Malkinson 2010).

1.1.2.3. Ciliated cells

Critical for efficient mucociliary transport, a major defense system of the lung that removes pathogenic microbes and inhaled particles from the respiratory tract, ciliated cells are first visualized in trachea and mainstem bronchi at approximately E14.0 in mice and proceed into a proximal to distal patterning as the fetal lung morphogenesis progress (Table 1) (Rawlins et al 2007). During development, the differentiation of ciliated lineage is the default of the non-neuroendocrine proximal airway epithelial cells. In mice, the ciliated cells appear as single cells in all three airway generations. However, with increasing age, the more proximal airways (trachea and lobar bronchi) develop ciliated cells in rows of 3-4 cells, while ciliated cells in the terminal bronchioles remain as single or paired cells (Toskala et al 2005). After differentiation, ciliated cells are recognized by the multiple cilia that are present on their apical surfaces (Toskala et al 2005).

1.1.2.4. Alveolar type 1 (AT1) cells

AT1 cells cover 95% of the gas exchange surface and are responsible for the physiological function of the pulmonary gas exchange (Table 1). Indeed, it is the thick morphology of the AT1 cells, covering the multiple alveoli, that allows the close contact with the vasculature and the passive diffusion of O_2 into the bloodstream (Morrisey & Hogan 2010, Weibel 1971, Weibel 2015, Yang & Chen 2014, Yang et al 2016). Loss of AT1 cell type is related to fetal lung hypoplasia (FLH) with the simultaneous promotion of AT2 cellular profile (Flecknoe et al 2000, Nguyen et al 2019, Takayasu et al 2007c).

1.1.2.5. Alveolar type 2 (AT2) cells

The other major cell type of the alveolar epithelium, AT2 cells, is cuboidal and secretes surfactant to reduce surface tension (Table 1) (Morrisey & Hogan 2010, Weibel 2015). AT2 cells synthesize and recycle surfactant lipids, predominately palmitoyl-phosphatidylcholine, and surfactant proteins, SP-A, SP-B, SP-C, and SP-D, with each protein serving innate immune, biophysical and regulatory functions (Whitsett & Alenghat 2015, Whitsett et al 2015).

The AT2 cell maturation occurs relatively late in gestation with the preterm infants frequently suffering from lung disease caused by surfactant deficiency. In fact, exogenous surfactant replacement preparations are used to provide surfactant lipids and proteins (SP-B and SP-C) that support the infant until endogenous surfactant synthesis by AT2 cells to be sufficient to maintain ventilation after birth (Bernhard 2016, Olmeda et al 2017).

1.1.3. Regulation of normal lung development by mechanical stimuli

Physical forces in the form of fetal breathing movements (FBMs), transpulmonary pressures, or intraluminal lung fluid are critical regulators of lung architecture during development. In fact, the lung develops as a fluid-filled organ, in which the intraluminal fluid moved by contractions of the smooth muscle and breathing movements assure the basal degree of lung expansion. The degree to which the lung can expand, and grow is ultimately dependent on the available intrathoracic and intrauterine space (Figure 3) as detail discussed in followed section.

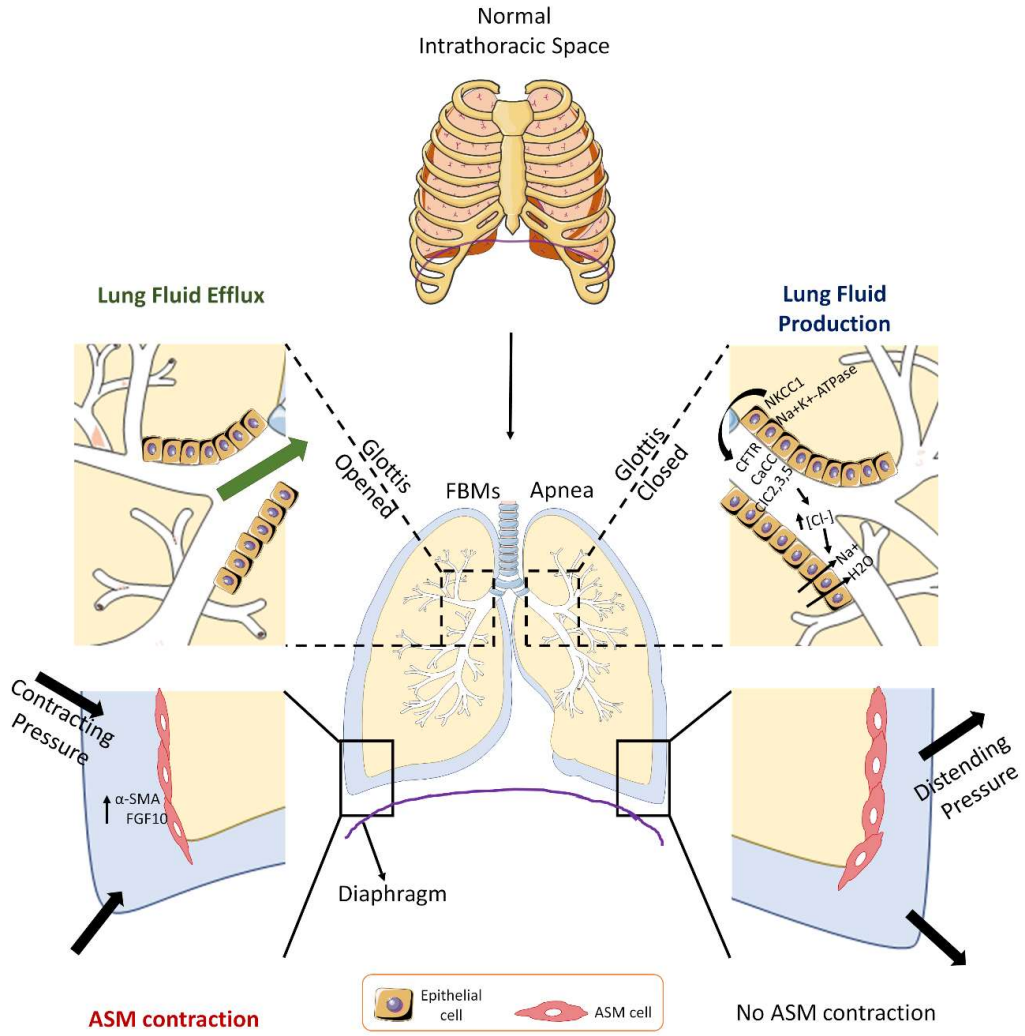

Figure 3 – The role of mechanical stimuli in the regulation of fetal lung expansion. Schematic diagram showing the function of mechanical stimuli in the regulation of lung liquid efflux during episodes of both fetal apnea and fetal breathing movements (FBMs). During apnea, the glottis is constricted, providing high resistance to the efflux of lung liquid. The production of lung fluid is dependent on the basolateral intake of sodium (Na^+), potassium (K^+), and chloride (Cl^-) through sodium-potassium adenosine triphosphatase (Na^+/K^+-ATPase) pumps and $Na^+/K^+/2$chloride (Cl^-, NKCC1) co-transporters *(continues in the next page)*

(continuation of the previous page) that in turn stimulate the apical Cl^- secretion via cystic fibrosis transmembrane conductance regulator (CFTR), calcium-dependent chloride (CaCC) or voltage-sensitive chloride channel 2,3,5 (ClC2,3,5). As such, the continued secretion of lung liquid, therefore, provides a distending force on the lung, raising intraluminal pressure 1–2 mmHg above the pressure in the amniotic sac. This pressure gradient is referred to as transpulmonary pressure gradient. During FBM, the glottis dilates, allowing lung liquid to flow along the trachea, following its pressure gradient, from the lung lumen to the mouth where it is either swallowed or it enters in the amniotic sac. α-SMA: alpha-smooth muscle action; ASM: airway smooth muscle cell; FGF10: fibroblast growth factor 10; H_2O: water.

1.1.3.1. Intrathoracic space

The synchronous development of the thoracic cage, diaphragm and pleural cavities is vital for the normal development of the lungs and postnatal functioning of the respiratory system. At its costal surface, the fetal lung is adjacent to the thoracic wall, while its basal surface, located adjacent to the diaphragmatic dome is shifted cranially by the growing liver (Yamamoto et al 2018). As such, the shape of the lung in fetuses, at least at its costal and basal aspects, is determined by the shape of the thoracic cavity, which needs to be firm enough to resist the pressure of the growing and expanding lungs (Figure 3). During pseudoglandular and canalicular phases, the lung surface is regulated by proliferation, branching, and outward growth of the bronchiolar system. Interestingly, in *ex vivo* microfluidic chest cavities, transmural pressure synchronizes the branching with airway smooth muscle contractions (Nelson et al 2017).

In humans, from the third fetal trimester onward, the lung surface develops an evenly smooth morphology to adapt to respiratory movements *in utero* and facilitate further development of the airway and diaphragm (Harper 1996, Yamamoto et al 2018). Indeed, the breathing movements observed in fetuses depend on the intact thoracic and abdominal cavities so that the diaphragm can descend towards the rigid pelvic bowl, pushing out the abdominal wall (Mantilla et al 2017).

1.1.3.2. Fetal breathing movements (FBMs)

FBMs are breathing-like movements that occur episodically in healthy mammalian fetuses. FBMs begins early in fetal life and progressively become organized into discrete episodes that are largely associated with a fetal behavioral state resembling rapid eye movement sleep (Dawes et al 1972). Breathing-like movements oscillate between FBMs and apnea periods. During FBM episode, the laryngeal abductor (dilator) muscles contract in phase with the diaphragm, and the intrathoracic pressure reduce with small oscillations of liquid flow within the fetal upper airways (Figure 3). The contraction of the diaphragm limits the loss of

fetal lung liquid and therefore maintains the basal lung expansion (Fewell & Johnson 1983, Harding & Hooper 1996). In contrast, apnea involves the accumulation of lung liquid within the lung since the glottis is constricted and provides high resistance to tracheal efflux (Figure 3) (Harding et al 1984).

Phrenic nerve section, thoracoplasty, or fetal paralysis are used to damage FMBs in the evaluation of subsequent morphological effects in *in vivo* fetal lung development. These studies demonstrated a significant decrease in fetal lung growth that suggests a direct consequence of FBMs in *in vivo* fetal lung development. However, a careful analysis regarding these experimental approaches seems to indicate an indirect effect of FBMs in the development of the lung. For instance, the section of phrenic nerve causes dystrophy of diaphragm muscle; thoracoplasty allows lung compression; and fetal paralysis abolishes laryngeal adductor activity, and may alter fetal posture that can separately explain the reduction in fetal lung growth by decreasing the pulmonary expansion (Harding et al 1993, Miller et al 1993). Indeed, the percent decrease in lung expansion is similar to the reduction in lung growth (Harding et al 1993, Miller et al 1993).

Given the difficulty that it is the restricted manipulation of *in vivo* FBMs, alternative methods have been the focus of research to disclose the underlying mechanisms. Fetal lung cells exposed to 5% phasic distension, either constantly at a rate of ~60 cycles/min or intermittently (e.g., 15 min/h), in 2- or 3-dimensional cultures are described as a potential alternative method to study mechanical stretch and FBMs, although the used stimulus (approximately 5% stretch) probably exceeds the stretch-induced by *in vivo* FBMs (Liu et al 1995a, Liu et al 1995c, Sanchez-Esteban et al 1998, Wang et al 2009). Molecularly, the applied 5% phasic distension in fetal lung cells increases lung epithelial cell proliferation (Liu et al 1995b, Liu et al 1994) and differentiation (Silbert et al 2008, Wang et al 2013, Wang et al 2006), whilst induces the expression of many growth factors, including PDGF, vascular endothelial growth factor (VEGF), epidermal growth factor (EGF), TGF (Liu et al 1995a, Muratore et al 2000, Wang et al 2013) and other components of intracellular signaling pathways, such as inositol trisphosphate (IP3), protein kinase C (PKC), calcium, cyclic adenosine monophosphate (cAMP), and mitogen-activated protein kinase (MAPK) (Liu et al 1996, Liu et al 1994, Sanchez-Esteban et al 2006, Wang et al 2006). Almost of these pathways are also reported in the regulation of normal fetal lung development, whilst are impaired in the congenital diaphragmatic hernia (CDH) (Dingemann et al 2010, Doi et al 2010, Friedmacher et al 2014b, Friedmacher et al 2014c, Gosemann et al 2012, Sanz-López et al 2013, Schmidt et al 2012).

1.1.3.3. Lung fluid

Lung develops as a fluid-filled organ that maintains the lung in a constantly distended state, stimulating their growth and maturation. Lung fluid is produced by the lung in a mechanism driven by active

Cl^- secretion from the adjacent epithelial cells. Indeed, it is the sodium-potassium adenosine triphosphatase (Na^+/K^+-ATPase) pumps and Na^+/K^+/2chloride (Cl^-) co-transporters, located on the basolateral surface of pulmonary epithelial cells, that allows the cellular intake of Cl^-, Na^+, and K^+ (Bardou et al 2009, Brennan et al 2013, Brennan et al 2016, Finney et al 2008, Gillie et al 2001). The intracellular increase of chloride concentration ([Cl^-]) stimulates their apical secretion via cystic fibrosis transmembrane conductance regulator (CFTR), calcium-dependent chloride (CaCC), and voltage-gated chloride channel 2, 3, or 5 (ClCs 2,3,5) into the lumen that favors the movement of Na^+ and water in the same direction, producing the intraluminal lung liquid (Figure 3) (Bardou et al 2009, Blaisdell et al 2004, Brennan et al 2013, Brennan et al 2016, Dickson & Harding 1987, Edmonds et al 2002, Finney et al 2008, Lamb et al 2001, Olver et al 1981, Olver & Strang 1974, Welsh 1983, Welsh et al 1982). After its secretion, the liquid exits the lung into the pharynx where it either contributes to the amniotic fluid or is swallowed and supports the normal fetal gastrointestinal contents. The volume of lung liquid within the future air space and its flux to and from the lower airways is influenced by fetal muscular activity, as well as by fetal posture and other factors that influence fetal transpulmonary pressure (reviewed in Wallace et al 2017).

Multiple studies concerning the intraluminal lung fluid function demonstrate the lug fluid as key modulator of fetal lung development, in which the constant increases on lung liquid volume accelerate both lung growth and maturation, while continued reductions retard fetal lung development (Harding & Hooper 1996, Hooper & Harding 1995). These alterations on intraluminal lung fluid volume also adjust FBMs, tracheal pressure, and tracheal efflux rate that sustain the tissue growth and cellular function (Figure 3). For instance, the continued drainage of fetal lung liquid reduces FBMs, tracheal pressure, and tracheal efflux rate that in turn damages the fetal lung growth (Figure 3) (Dickson & Harding 1987). Conversely, the increased lung liquid volume increase tracheal pressure and accelerate the tracheal efflux, with, however, no changes in liquid secretion rate and in the incidence and amplitude of fetal inspiratory muscle activity or in the activity of laryngeal adductor muscle (Dickson & Harding 1987). Finally, the alveolar wall and AT2 cells are enhanced in ligated and inhibited in drained lungs (Alcorn et al 1977).

1.1.3.4. Peristaltic airway contractions

Contractile cells start to perform spontaneous contractions pushing peristaltic waves of inter-bronchial fluid into the periphery that cause a rhythmic extension of the distal airways including the terminal buds. It was postulated that these movements stimulate branching morphogenesis and prevent an uncontrolled expansion of the airways as pulmonary fluid is secreted into the lung lumen (Schittny et al 2000, Sparrow et al 1994). Indeed, the movement of lung fluid from proximal to distal parts of the developing lung begins

when a layer of α-SMA$^+$ cells is formed around the most proximal airways at pseudoglandular or branching phase (Bokka et al 2015, Jesudason 2009, Jesudason et al 2006, Schittny 2017, Schittny et al 2000). The earlier expression of contractile protein α-SMA (Leslie et al 1990) and smooth muscle myosin heavy chain (MHC) filaments (Pandya et al 2006) in both proximal and distal lung mesenchyme (Mailleux et al 2005, Shan et al 2008) firstly recognize the airway smooth muscle (ASM) progenitor cells. The force generated by contraction of fetal ASM significantly stimulates fetal lung growth by inducing the expression of *Fgf10* (Figure 3) (Schittny et al 2000). FGF10 is produced by ASM precursor cells in the distal lung and drives their growth and entry into the smooth muscle cell lineage. This growth factor produces a dose-dependent proliferation of progenitor cells in early lung development, while in knockout mice lacking the *Fgf10* gene, the airways fail to extend beyond carina (Mailleux et al 2005). In separate studies with phasic contractions at a frequency of 0.5–1 min−1, the increase of FGF10 expression is associated with increased fetal lung growth (Jesudason et al 2005).

A recent publication conducted an *in vivo* study regarding the consequences of *Myocardin* (*Myocd*) inactivation in early-stage embryos. *Myocd* encodes a transcription factor necessary for ASM differentiation peristalsis. Authors showed that while airway smooth muscle is dispensable for epithelial branching, it is integral for building the tracheal architecture and promoting airway growth (Young et al 2020).

1.1.4. Mechanotransduction

The first demonstration that mechanical forces could directly activate/influence cellular function was the work by Hudspeth and Corey in 1979 (Corey & Hudspeth 1979). Authors argued that the activation of ionic currents in bullfrog auditory epithelial cells by mechanical stimulation was too fast (sub-millisecond range) to be compatible with a mechanism involving second messengers. As knowledge goes through, the specific role of mechanotransduction in embryo development and particularly in fetal lung development arise, improving our understanding of lung morphogenesis as dependent on physical forces. In fact, the lung is a mechanosensory organ, for which fetal lung expansion is regulator of lung growth and maturation in gestational life. As such, tracheal occlusion (TO) that increases the *in vivo* intraluminal volume and pressure is the preferable method to study the morphological and molecular features under the fetal lung expansion. Research comparing normal and TO lungs shows multiple up- and down-stream genes and pathways implied in cell proliferation and growth; reorganization of cytoskeleton-ECM; or alveolarization (Figure 4) (Boström et al 1996, Cock et al 2004, Filby et al 2006, Joyce et al 2003, Lindahl et al 1997, McDougall et al 2013, McDougall et al 2011, Riveline et al 2001, Schulze et al 2002, Seaborn et al 2008, Sozo et al 2007, Sozo et al 2006, Vuckovic et al 2013). More relevant, the crosstalk analysis of these genes indicates a functional

interdependency between pathways, suggesting a coordinate response in fetal lung expansion and alveolarization.

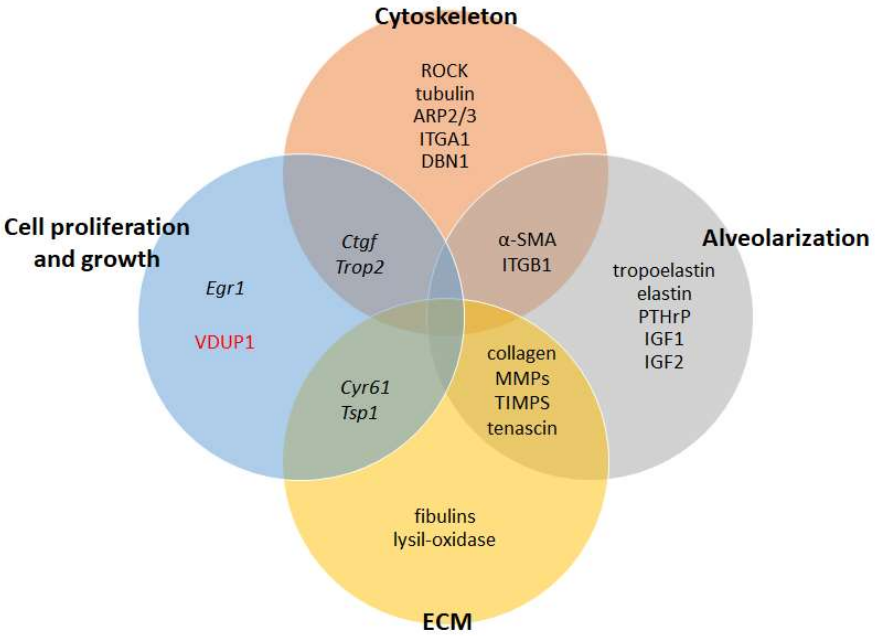

Figure 4 – Venn diagrams showing the overlap between genes up-and down-regulated after *in vivo* tracheal occlusion compared with normal lungs. Up-and downregulated genes are identified in black and red, respectively. ARP2/3: actin-related protein 2/3 complex; α-SMA: alpha-smooth muscle actin; *Ctgf*: ; *connective tissue growth factor*; *Cyr61*: *cysteine-rich 61*; DBN1: drebrin; ECM: extracellular matrix; *Egr1*: *early growth response 1*; IGF1: insulin-like growth factors 1; IGF2: insulin-like growth factors 2; ITGA1: integrin alpha-1; ITGB1: integrin beta1; MMPs: matrix metalloproteins; PTHrP: parathyroid hormone-related protein; ROCK: Rho-associated protein kinase; TIMPS: tissue inhibitors of MMPs; *Trop2*: *trophoblast antigen 2*; *Tsp1*: *thrombospondin-1*; VDUP1: vitamin D3 up-regulated protein 1.

Complementary studies regarding the above-mentioned pathways demonstrate stretch as an upstream target of ECM activation via integrins. Indeed, after activation, integrins triggers complex intracellular signaling that includes the focal adhesion kinase (FAK) through linker proteins [talin, vinculin, filamin, the integrin-linked kinase (ILK)-particularly interesting new cysteine-histidine-rich protein (PINCH)-parvin complex, and α-actinin], and finished on cytoskeleton-actin pathways activation (Copland & Post 2007, Wallace et al 2014, Whitsett et al 2019). In addition, the functional impairment of integrins induces critical morphological defects in fetal lungs that impair neonatal respiratory function. For instance, the *integrin α3-null* mice have abnormal branching morphogenesis (Kreidberg et al 1996); double *α3/α6 integrin null*-mice have a complete lack of the left lung and severe right lung hypoplasia (De Arcangelis et al

1999); the integrin *α8-null* mouse has large dilated airspaces with defects in secondary septation, abnormal elastin deposition, and fusion of the medial and caudal lobes of the right lung (Benjamin et al 2009). These defects appear due to the inability of the mesenchymal cells to form focal contacts and control cell migration (Benjamin et al 2009). In addition, the lung epithelial cell proliferation and differentiation require the β1−integrin signaling (Berger et al 2003), in which the blocking of β1, α3, and α6-integrins reduce the SP-C expression in induced (5% phasic stretch) cultures of fetal lung epithelial cells (Sanchez-Esteban et al 2006). Concomitant with these findings, the deletion of β1-integrin from E10.5 onwards using *Sftpc* promoter-driven Cre induce defects in both airways branching and alveolarization. For instance, the airway branching defects are associated with impaired epithelial cell adhesion and migration, whereas the disrupted secondary septation, abnormal alveolar epithelial cell differentiation with excessive collagen I and elastin deposition, identified the morphological defects related to alveolarization (Plosa et al 2014).

Concomitant with these findings, the overexpression of elastin, collagen, PTHrP, IGF1, and -2 in exposed-TO lungs evidenced the essential role of mechanical stretch in the improvement of alveolar septation (Figure 4) (Cilley et al 2000, Hooper et al 1993, Nobuhara et al 1998, Torday & Rehan 2002). In fact, elastin and collagen are decisive intermediators of secondary septation during alveolarization with the disorganized and immature profiles identifying a CDH lung. *Igf2* knockout mice delay lung development with decreased septation through inhibition of cell differentiation (Liu et al 1993, Silva et al 2006), whereas the lung-specific deletion of *Igf1* receptor (*Igf1r*) results in severely hypoplastic lungs with thickened mesenchyme, increased cell proliferation, and apoptosis, and delayed differentiation of epithelial and endothelial cells (Epaud et al 2012).

1.1.4.1. PIEZO1/PIEZO2

A novel ion channel family, the *Piezo* family was recently discovered by Coste et al (Coste et al 2010). PIEZOs proteins are pore-forming multimeric ion channels, with the resulting proteins, PIEZO1 and PIEZO2, able to respond to mechanical stimuli. Besides the similar structure, global and tissue-specific knockout mice have enriched our knowledge regarding the function of these ionic channels. Indeed, divergent functions as dependent on the expressed cell type arise in regulation of vasculogenesis, pulmonary function, control of red blood cell volume, detection of basal blood pressure, touch or proprioception (Alcaino et al 2018, Cahalan et al 2015, Coste et al 2012, Feng et al 2018, Maneshi et al 2018, Nonomura et al 2017, Ranade et al 2014b, Wang et al 2017, Woo et al 2014, Zeng et al 2018).

PIEZO1 is expressed predominantly in non-neuronal cell types, and it is essential in the transduction of external and internal applied forces in the plasma membrane. During embryogenesis, shear stress, that is, the frictional force generated from fluid flow over cells, initiates endothelial cell migration and alignment, which control the vessel formation and maturation. Shear stress also regulates vascular tone by releasing endothelial-cell-derived relaxing factors, such as nitric oxide, that modulate arterial diameter. When expressed in embryonic and mouse endothelial cells, PIEZO1 controls vasculogenesis under a mechanism calcium-dependent (Li et al 2014, Ranade et al 2014a). The diameter and wall thickness of small arteries are also regulated by PIEZO1 during hypertension, in which the stretch-induced PIEZO1 stimulates the calcium influx and activates the ECM crosslinking enzyme transglutaminase that controls the vascular inward remodeling (decreasing vessel diameter) (Retailleau et al 2015).

In adult mice, PIEZO1 activity is required to maintain basal blood pressure, where it mediates shear-stress-induced arterial dilation. In fact, PIEZO1-dependent calcium influx responds to shear stress and leads to endothelial ATP release. The release of ATP acts to initiate the purinergic P2Y2 receptor coupled to the G proteins, Gq and G11, in endothelial cells, that in turn phosphorylates the serine/threonine-protein kinase (AKT) and increase the nitric oxide production and release, which causes vasodilation (Wang et al 2016a). Furthermore, PIEZO1 expressed in red blood cells is required for their volume regulation with the activation of PIEZO1 causing the influx and activation of the calcium-activated potassium channel KCa3.1 that results in K^+ and water efflux and consequent dehydration (Cahalan et al 2015).

Regarding PIEZO2, their critical function in sensory processes, like detection of touch and proprioception, and in respiratory physiology, have been extensively reported. In fact, PIEZO2 expressed in Merkel cells regulates the sensation of touch through low-threshold mechanoreceptor fibers (Ikeda et al 2014, Maksimovic et al 2014, Ranade et al 2014b, Woo et al 2014), whereas their selective deletion in proprioceptive neurons in mice, strikingly abolishes the muscle stretch-induced firing of these neuronal fibers

and led to severe deficits in body coordination and limb position (Florez-Paz et al 2016, Woo et al 2015). Pulmonary function is also dependent on PIEZO2 expressed in nodose ganglion and dorsal root ganglion that in turn regulates lung expansion in newborns and adult mice. Specifically, PIEZO2 expressed in sensor neurons in the neural crest of the newborn mice is required for both proper lung expansion and efficient respiration with hypoventilation, decreased inspiratory activity, altered expiratory pattern, or unexpanded lungs observed under the functional impairment of PIEZO2 (Nonomura et al 2017). This study also described PIEZO2 expressed in NEBs at birth with, however, undefined functions. In adult mice, PIEZO2 expressed in nodose sensory neurons works as a sensor required for lung volume regulation and the Hering-Breuer reflex response (Nonomura et al 2017).

In light of all the above-described functions, it is easy to understand the gain and loss of function as responsible for multiple human diseases. In fact, mutations in the human *Piezo1* and *Piezo2* genes are linked to distinct hereditary human diseases, such as hereditary xerocytosis (also known as dehydrated stomatocytosis); or the autosomal recessive syndrome of muscular atrophy with perinatal respiratory distress, arthrogryposis, and scoliosis (reviewed in Alper 2017).

1.2. Hypoplastic fetal lung development

FLH affects 1.4 per 1000 births (Tisekar & Ak 2021) and can be either primary (or idiopathic) or secondary to other anomalies (Cotten 2017, Knox & Barson 1986, Moessinger et al 1983). Primary pulmonary hypoplasia includes congenital acinar dysplasia and genetic disorders like trisomy 13, trisomy 18, or trisomy 21 (Tisekar & Ak 2021). Anomalies affecting the intrathoracic cavity or amniotic fluid volume cause secondary pulmonary hypoplasia. CDH, congenital pulmonary airway malformation (CPAM), or chest wall deformities are examples of intrathoracic space-occupying lesions. These abnormalities cause a reduction in the volume of the thoracic cavity, which physically restricts the growth of the peripheral lung. Conversely, oligohydramnios secondary to preterm premature rupture of membranes (PPROM), lack of functional renal parenchyma, or urinary outflow tract abnormalities are examples of amniotic fluid decrease. As such, when the volume of amniotic fluid volume is reduced, the uterus compresses the fetus increasing flexion of the fetal body. The increase in fetal trunk flexion increases abdominal and intrathoracic pressures, which increases the transpulmonary pressure gradient, causing an increased efflux of lung liquid along the trachea and a reduction in lung expansion (Mehler et al 2011, Mileto et al 2018, Spiro et al 2015).

PPROM and CDH constitute the most common extra- and intrathoracic causes of FLH, respectively, with the timing of injury in relation to embryologic lung development determining the chance for neonatal survival (Thibeault & Haney 1998, Thurlbeck 1992, Tisekar & Ak 2021). In general, underdeveloped lungs with impaired branching morphogenesis and reduced number of alveoli identified a hypoplastic lung during gestational life. At birth, diagnosis comprises a spectrum of respiratory complications ranging from neonatal death to less severe manifestations, including chronic respiratory failure, pulmonary hemorrhage, bronchopulmonary dysplasia, or even transient respiratory distress that require high ventilatory support in the absence of obstruction or with abnormal radiologic findings (elevated diaphragm, bell-shaped chest) (Knox & Barson 1986, Laudy & Wladimiroff 2000, Lauria et al 1995, Moessinger et al 1989, Triebwasser & Treadwell 2017). Finally, decreases in lung weight:body weight ratio of less than 0.015 (De Paepe et al 2005) with reduced radial alveolar count or total DNA count, defines the postmortem diagnosis (Askenazi & Perlman 1979, Wigglesworth & Desai 1981).

1.2.1. Preterm premature rupture of membranes (PPROM)

1.2.1.1. Clinical aspects

PPROM is the rupture of gestational membranes before the onset of labor and before 37 weeks of gestation. PPROM prior to the limit of fetal viability i.e. 24 weeks of gestation is known as "previable PPROM" and complicates less than 1% of all pregnancies (Kiver et al 2018), whereas mid-trimester PPROM, defined as rupture of fetal membranes before 28 weeks of gestation, complicates approximately 0.4%–0.7% of all pregnancies (Tchirikov et al 2017). Previable and mid-trimester PPROM are associated with high neonatal mortality and long- and short-term severe morbidities (Kiver et al 2018, Tchirikov et al 2017). Infants with pulmonary hypoplasia exhibit abnormal lung function at birth with reduced tidal volume, increased respiratory rate, and reduced static lung compliance and functional residual capacity. The duration of latency between the timing of membrane rupture and delivery appears to be inversely related to the gestational age at PPROM. Neonates delivered following previable PPROM are at a significantly higher risk for a multitude of adverse outcomes during both the neonatal period and early childhood. These associations persist when controlled for confounders, including gestational age at delivery or infectious morbidity (Manuck & Varner 2014).

1.2.1.2. Experimental evidence

Studies regarding oligohydramnios secondary to lack of amniotic fluid volume in humans demonstrated a significant decrease in collagen expression (Chen et al 2008) and absence of elastic tissue (Haidar et al 1991, Nakamura et al 1990). In fetal rat lungs, the induction of oligohydramnios promotes a similar degradation of collagen deposition in interstitial spaces that was dependent on higher MMP levels. Furthermore, when oligohydramnios is caused at pseudoglandular stage, the developed lung has reduced elastin deposition; impaired alveolarization, and decreased expression of PDGF and its receptor (Chen et al 2007b).

1.2.2. Congenital diaphragmatic hernia (CDH)

1.2.2.1. Clinical aspects

CDH occurs when the diaphragm fails to close during embryonic development that permits the abdominal contents to enter into the thorax cavity. The reduced space available causes chronic lung collapse on the affected side that impairs the normal fetal lung development. In addition, as the diaphragmatic defect occurs early in the development, it usually results in severe lung hypoplasia, with major impairments on lung structure and function. CDH occurs in approximately 1-5 of every 10.000 live births and can be diagnosed at routine obstetric screening from 15 weeks of gestation (Chandrasekharan et al 2017, Shanmugam et al 2017, Yang et al 2006).

Ultrasonography has been the primary mode of prenatal imaging for CDH with an overall prenatal detection rate of about 50–60% at a mean gestational age of 24 weeks (Mesas Burgos et al 2016). Ultrasound is also used to assess the degree of severity of the CDH by estimating the lung size. However, ultrasound is user-dependent and has several limitations, thus many centers use magnetic resonance imaging (MRI) as an adjunct. MRI can better identify the type of hernia, provide an anatomical assessment of herniated organs and their effects on surrounding structures and determine specific lung volumes and liver herniation measurements (Mehollin-Ray et al 2012). After confirmation of the prenatal diagnosis of CDH is necessary to stratify the prognosis (reviewed in Doné et al 2008). The two prognostic factors that have obtained more consistent results in prenatal and postnatal outcomes are lung-to-head ratio (LHR; expressed as a function of what is expected in a gestational aged control, observed /expected LHR) (Alfaraj et al 2011, Jani et al 2006, Jani et al 2009, King et al 2016) and liver position (Burgos et al 2019, Coughlin et al 2016, Hedrick et al 2007, Ruano et al 2014, Ruano et al 2012a).

Based upon these parameters, CDH fetuses can be now prenatally stratified into low and high-risk groups. The low-risk fetuses should be managed expectantly during pregnancy (Burgos et al 2019, Coughlin et al 2016, Hedrick et al 2007, Ruano et al 2014, Ruano et al 2012a). In opposition, for the high-risk fetuses (i.e. fetuses which prognosis is predictably poor with postnatal treatment available), the consensus is that something needs to be done before the birth in order to total or partially revert the fetal lung hypoplasia. In fact, over the last decades have emerged *in vivo* and *ex vivo* studies that highlight the morphological, cellular, and molecular mechanisms under fetal lung development with, unfortunately, poor clinical relevance (Chiu 2014, Costlow & Manson 1981, Nakamura et al 2020). As such, the urgency of this topic permitted the development and validation of distinct animal models now available for the study not only the lung morphogenesis and mechanisms but also to test promising antenatal therapies.

1.2.2.2. Experimental evidence

1.2.2.2.1. Animal models

Performed in sheep and rabbits*, surgical* model is used to test promising antenatal therapies, whereas their applicability to study the earliest origins of CDH and FLH is limited since the diaphragmatic defect is created late in gestation. *Genetic* models are created under the experimental evidence of dysregulated genes in CDH are responsible for diaphragm formation (Nakamura et al 2020). This concept permits the description of *Roundabout 1/2 (Robo1/2)*, *retinoic acid receptor alpha* and *beta 2 (Raro* and *Rarb2)*, or *Sox7* transgenic mice all able to create the diaphragmatic defect observed in CDH fetuses (reviewed in Nakamura et al 2020). However, a minority of cases (18%) are associated with known genetic defects (reviewed in Wynn et al 2014). As so, these models do not reflect the true nature of human CDH (reviewed in Nakamura et al 2020, Wynn et al 2014). *Teratogenic* model uses the administration of a herbicide called nitrofen (2,4-dichlorophenyl-p-nitrophenyl ether) to a pregnant rat and consequent CDH and FLH is developed in a relatively high proportion of the progeny (Costlow & Manson 1981). Nitrofen induces a marked decrease in RA levels, most probably due to inhibition of retinal dehydrogenases (RALDH) function rather than expression since RALDH mRNA levels are normal (Mendelsohn et al 1994). The advantage of this model is that the defect is induced at the stage when the foregut has just separated into the esophagus and trachea, giving the opportunity to carefully study the developmental anatomy of the lungs and diaphragm in CDH (Kluth et al 1990, Montalva & Zani 2019, Montedonico et al 2008a, Tenbrinck et al 1990). In fact, the nitrofen administration during midgestation to pregnant dams causes developmental anomalies that reasonably replicate the major abnormalities and the pathophysiology described in human CDH (Montedonico et al 2008a, van Loenhout et al 2009).

Human and nitrofen-induced CDH lungs have reduced surface area for gas exchange due to hypoplasia with the lung parenchyma suffering from reduced distal branching and alveoli. Finally, the alveoli that do exist have thicker walls that impair the close association of the airspaces with the capillaries (Ameis et al 2017, Donahoe et al 2016). In this model, the specific location and extent of the diaphragmatic defects are very comparable, but also the similarities in the CDH-associated anomalies, including lung hypoplasia, pulmonary hypertension, cardiovascular and skeletal defects, are impressive too (Ameis et al 2017, Donahoe et al 2016, Tenbrinck et al 1990, van Loenhout et al 2009). Therefore, the nitrofen-induced CDH model is one of the best to investigate the etiology, pathogenesis, and therapeutic options in CDH.

1.2.2.2.1.1. ROBO/SLIT signaling

Roundabout (Robo) genes encode cell-surface receptors that respond to their secreted ligands, SLIT proteins, in a wide variety of cellular processes. Four *Robo* genes and three *Slit* have been identified in mammals (Brose et al 1999, Huminiecki et al 2002, Kidd et al 1998). First implicated in the regulation of axon pathfinding (Kidd et al 1999, Kidd et al 1998, Rothberg et al 1988), ROBO/SLIT signaling has since been demonstrated to play a role in processes such as neural crest cell migration and sensory ganglia morphogenesis (De Bellard et al 2003, Giovannone et al 2012, Shiau & Bronner-Fraser 2009), leukocyte chemotaxis (Ye et al 2010), epithelial adhesion (Macias et al 2011), or diaphragm and kidney formation (Grieshammer et al 2004, Liu et al 2003, Yuan et al 2003). Functionally, ROBO/SLIT signaling has been shown to transmit migratory cues by modulating cell adhesion and actin polymerization (Lundström et al 2004, Rhee et al 2007, Rhee et al 2002, Shiau & Bronner-Fraser 2009). More recently, ROBO/SLIT signaling is reported in regulation of progenitor cell profile during the development of the central nervous system (CNS) (Borrell et al 2012), mammary gland (Ballard et al 2015, Harburg et al 2014, Macias et al 2011), or pancreas (Blockus & Chédotal 2016, Escot et al 2018).

In fetal lungs, *Robo1/Robo2* knockout mice delayed the separation of foregut from the dorsal body wall, describing this as primary defect that precedes the organ misplacement and diaphragm malformation (Domyan et al 2013). In addition, Xian et al described that homozygous *Robo1/Dutt1* knockout mice almost die at birth due to respiratory failure with delayed lung maturation. Lungs from these mice have reduced air spaces and increased mesenchyme, features that are present some days before birth. Survivors acquire extensive bronchial hyperplasia (Xian et al 2001).

1.2.2.2.2. A CDH lung by developmental stage: what is known?

Studies regarding the morphological features in CDH lungs demonstrate important defects from early-to-later developmental stages. Indeed, the initial reduction in the number of terminal end buds expands to reduced air space with septa notably thicker as the hypoplastic lung development progress. Molecularly, the comparison between normal and induced-CDH lungs describes multiple dysregulated genes and pathways during branching or alveolar morphogenesis. For instance, the earlier pseudoglandular stage (E15.5) is marked by the decreased expression on FGF9, BMP4, T-box2,4,5, WNT7b, and WNT2a that evolve to decreased FGF (FGF2, FGF7, FGF10, FGF18) and BMP (BMP4, BMPR2, T-box2,4,5), increased RA [RARβ, RARα, retinoid X receptor alpha (RxRα), RALDH3] and unchanged WNT (WNT2, WNT7b) signaling at the time of arrested branching morphogenesis (Figure 5) (Doi & Puri 2009, Gosemann et al 2013, Makanga et al 2013, Takahashi et al 2013, Takahashi et al 2017, Takayasu et al 2007a).

Induced-CDH lungs also evidence the bronchiolar and alveolar differentiation as damaged, in which the initial decrease on neuroendocrine markers (*Mash1*, *Dll1,* and ghrelin) expression with the overexpression of *Hes1* and *Scgb1a1* (non-neuroendocrine markers) indicate a preferable bronchiolar differentiation to neuroendocrine instead of non-neuroendocrine cells (Pereira-Terra et al 2015, Santos et al 2006, Santos et al 2007). Regarding the alveolar differentiation, an opposite effect on the expression of AT1 and AT2 differentiated cell markers is also described in CDH lungs at term. In fact, markers of AT1 mature cells (AQP5, ICAM1, TRα1, and TRβ1) are downregulated in nitrofen-exposed CDH lungs, while the AT2 cell markers (SP-C, TNFα, and TTF1) are overexpressed (Losada et al 2000, Shima et al 1999, Takayasu et al 2007b, Takayasu et al 2007c, Teramoto et al 2001, Van Tuyl et al 2003). Interestingly, the decrease in surfactant production and secretion, evidenced by the low levels of phosphatidylcholine, and the factors involved in stimulating surfactant lipids maturation report unfunctional AT2 cells. In addition, the expression of PTHrP, adipose differentiation-related protein (ADRP), Thy1, peroxisome proliferator-activated receptor-gamma (PPARg), and RA are demonstrated to be downregulated, whereas the inhibitor of surfactant phospholipid synthesis, TNFα, is overexpressed (Figure 5) (Carroll et al 2002, Doi et al 2010, Friedmacher et al 2014a, Friedmacher et al 2014c, Gosemann et al 2012, Nakazawa et al 2007, Shima et al 1999). Finally, the overexpression of alveolar macrophages (AMFs)-specific markers, PDGFA/PDGFRα, collagen, α-SMA, and elastin in CDH lungs reinforce the idea of a damaged alveolarization since the defective expression of SHH and FGF10 signaling must explain the impairment on AMF migration and the resultant immature and disorganized elastin distribution and reduced secondary septation (Figure 5) (Boucherat et al 2007, Dingemann et al 2010, Fox et al 2018, Mychaliska et al 2004, Taira et al 1999). The current knowledge showed the differentiated alveolar epithelial cells, AT1 and AT2, as critical for gas exchange at birth that

must explain the neonatal respiratory failure in CDH (Alfanso et al 1996, Bohnhorst & Peter 2020, Lin et al 2007, North et al 1995, Utsuki et al 2001).

In human CDH lungs, similar morphological and molecular features are described, in which the deficient secondary septation, with decreased elastin deposition at the tips of growing septa, is associated with high levels of PDGF in amniocentesis and cord blood opening important questions regarding the therapeutic value of these molecules and pathways in CDH lungs (Boucherat et al 2007, Candilera et al 2016, Fleck et al 2013).

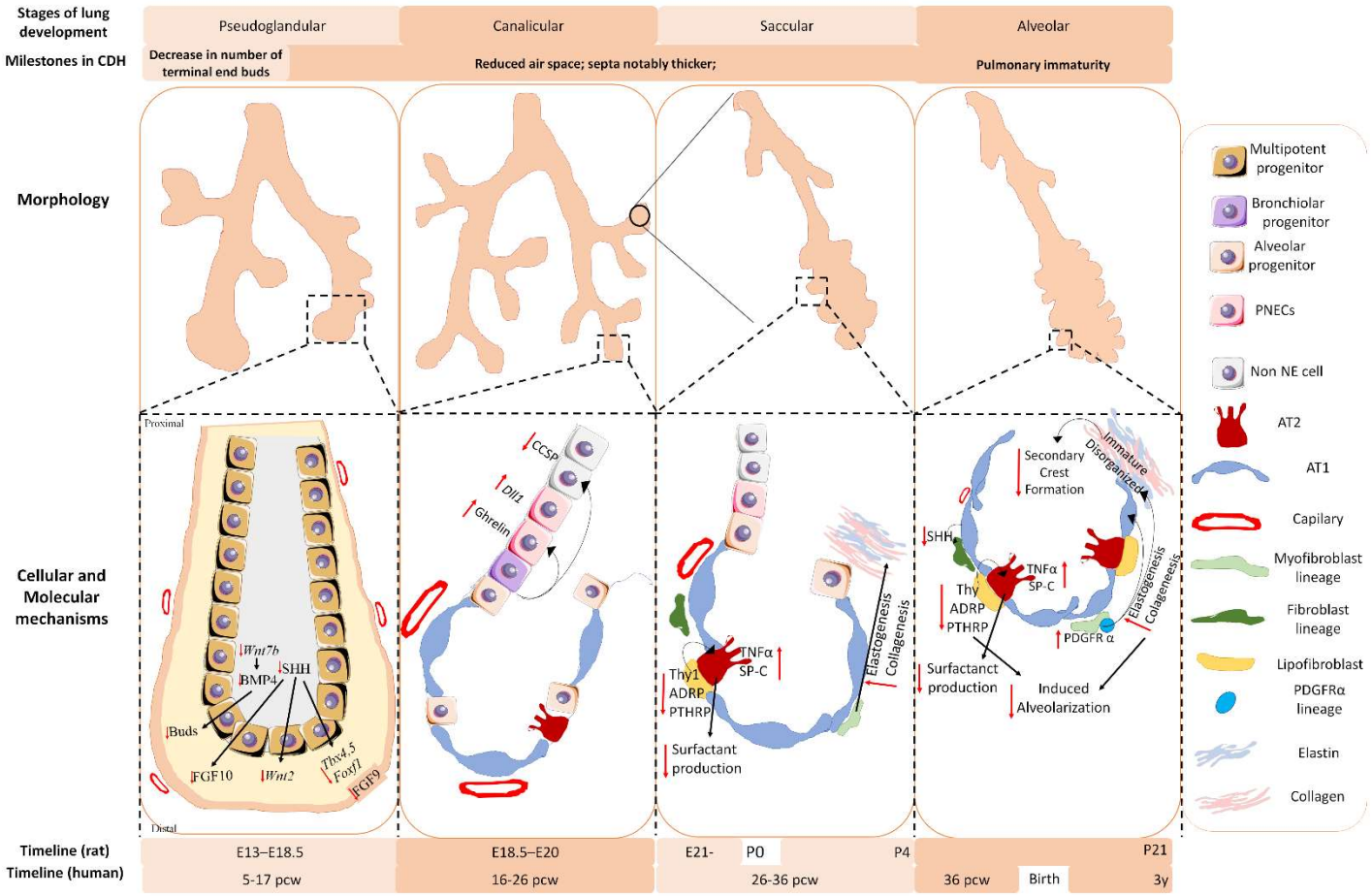

Figure 5 – Timeline of the fetal lung development in rats and humans with the indication of the more relevant morphological and molecular alterations observed in the experimental congenital diaphragmatic hernia (CDH) lungs. *(continues in the next page)*

(continuation of the previous page) ADRP: adipose differentiation-related protein; BMP4: bone morphogenetic protein 4; CDH: congenital diaphragmatic hernia; CCSP: clara cell secretory protein; Dll1: Delta like canonical Notch ligand 1; E: embryonic day; FGF9: fibroblast growth factor 9; FGF10: fibroblast growth factor 10; *Foxf1*: *Forkhead box factor 1*; NE: neuroendocrine; P: postnatal day; pcw: post-conception weeks; PDGFRα: parathyroid hormone-related protein alpha; PNECs: pulmonary neuroendocrine cells; PTHRP: parathyroid hormone-related protein; SHH: sonic hedgehog; SP-C: surfactant protein-C; *Tbx4*: *T-box gene 4*; *Tbx5*: *T-box gene 5*; TNFα: tumor necrosis factor alpha; y: year; *Wnt2*: *wingless 2*; *Wnt7b*: *wingless 7b*.

1.2.2.3. Antenatal therapies

Advances in prenatal diagnosis of CDH and the increased ability to stratify the risk for neonatal respiratory failure open a key "window of opportunity" for fetal intervention, whose antenatal therapies are the appealing approaches to improve fetal lung growth and neonatal survival in fetuses at high risk for the condition (Kovler & Jelin 2019). Currently, retinoids, corticosteroids, and sildenafil are the most promising non-surgical prenatal interventions to correct lung hypoplasia and pulmonary hypertension in CDH, whereas fetoscopic endoluminal tracheal occlusion (FETO) is the surgical therapy indicated for the more severe cases of FLH in CDH fetuses (reviewed in Kashyap et al 2018).

1.2.2.3.1. Retinoids

Decreased levels of vitamin A and RA have been shown to contribute to the pathogenesis of pulmonary hypertension and hypoplasia observed in human CDH and animal models (reviewed in Kashyap et al 2018). The retinoid signaling appears important in normal diaphragmatic and pulmonary development, and it is hypothesized that disruptions in this pathway may contribute to the pathogenesis of CDH (Chen et al 2007a, Chen et al 2013, Chen et al 2007c, Cho et al 2005, reviewed in Fernandes-Silva et al 2020, Fernandes-Silva et al 2017, Liebeskind et al 2000, McGowan et al 1995, Nakazawa et al 2007, Noble et al 2007, Pereira-Terra et al 2015, Rankin et al 2016). In fact, retinoid signaling is an important component of lung budding and branching early in development, and later influences septation and alveolarization. The retinoid signaling pathway also appears to play an important role in complete closure of the diaphragm. Diaphragmatic defects are present in the offspring of vitamin A–deficient rats and *retinoic acid receptor* double knockout mice, and infants with CDH have low levels of plasma retinol (reviewed in Kashyap et al 2018). As such, treatment with RA during gestation in animal models reduces the incidence of CDH and

improve lung hypoplasia, lung development, and vascular abnormalities (Baptista et al 2005, Gallot et al 2008, Lewis et al 2011, Montedonico et al 2008b, Oshiro et al 2005, Schmidt et al 2012, Thébaud et al 1999). Unfortunately, the teratogenic effect of RA establishes a clinical challenge in the application of this treatment in human CDH fetuses (Eastwood et al 2015).

1.2.2.3.2. Corticosteroids

Corticosteroid administration before anticipated preterm birth is one of the most important antenatal therapies available to improve newborn outcomes. Betamethasone and dexamethasone are the most widely studied corticosteroids, and they generally have been preferred for antenatal treatment to accelerate fetal lung maturation (Briceño-Pérez et al 2019, Wynne et al 2020). As such, a small human randomized controlled trial compares placebo to the administration of corticosteroids (betamethasone) to the pregnant woman and their unborn baby with CDH at 34 weeks of gestation. This study showed no difference in the improvement of perinatal mortality, in the number of days with mechanical ventilation, or in hospital admission between the two groups (Grivell et al 2015, Lally et al 2006). As such, the use of prenatal steroids in CDH fetuses is considered dispensable since do not improve neonatal outcomes (Kashyap et al 2018, Wynne et al 2020).

1.2.2.3.3. Sildenafil

Concomitant with FLH, pulmonary hypertension persists postnatally in CDH babies and adversely affects survival if not adequately treated. In many centers, inhaled nitric oxide (iNO) is used for pulmonary vasodilation. Molecular studies show the beneficial effects of iNO mediated by cyclic guanosine monophosphate (cGMP) pathway. Phosphodiesterase type 5 (PDE5) inactivates the cyclic GMP pathway, leading to a decrease in nitric oxide effects. Studies in animals showed that the prenatal administration of sildenafil (PDE5 inhibitor) significantly improves lung structure and pulmonary vessel density, reduces right ventricular hypertrophy, decreases pulmonary artery resistance, and improves oxygenation (Burgos et al 2016, Luong et al 2011, Mous et al 2016). Indeed, sildenafil is already used clinically in the postnatal management of persistent pulmonary hypertension in CDH neonates (Kashyap et al 2018). More recently, it was described that sildenafil can cross the placenta at a relatively high transfer rate, in which the fetal drug administration in combination with fetal tracheal occlusion restore the lung parenchyma, size, and vasculature to normal outcomes, making it a promising prenatal therapy for CDH under clinical investigation (Kashyap et al 2019, Russo et al 2019).

1.2.2.3.4. Fetoscopic endoluminal tracheal occlusion (FETO)

1.2.2.3.4.1. Clinical aspects

The first report of fetal tracheal occlusion for the treatment of CDH in humans was by Harrison et al (Harrison et al 1996), in which the placement of a foam plug inside the trachea was performed by open hysterotomy. The foam plug was then substituted for external tracheal clips placed after open tracheal exposure. In both cases, the clips or plugs were removed after birth via an ex-utero intrapartum therapy (EXIT) procedure. In the first report of eight human fetuses treated with fetal tracheal occlusion, there were no long-term survivors (Harrison et al 1996). However, several of the patients showed dramatic lung growth, and the deaths were all thought to be due to non-pulmonary causes. These sensational early cases led to the rapid refinement of the techniques for attaining tracheal occlusion in an effort to minimize the consequences of the hysterotomy and EXIT procedures (Flake et al 2000). As such, a detachable balloon was developed for deployment inside the trachea, avoiding the need for neck dissection and open hysterotomy by the introduction of fetal endoscopic surgery, called 'Fetendo' (Deprest et al 2004, Harrison et al 2001, Harrison et al 1998).

The rapid improvements achieved in the late 1990s and early 2000s led to a series of successful initial trials using the current technique of Fetal Endoscopic Tracheal Occlusion (FETO) (Harrison et al 2003, Harrison et al 1998). FETO uses continuous US guidance to insert a deflated balloon into the fetal mouth under local anesthesia. In brief, a 3mm cannula is placed percutaneously (i.e., through the maternal skin, abdominal wall, and uterus) and directed towards the fetal mouth. For that, the fetoscope is passed through the cannula into the amniotic fluid, and with a combination of ultrasound guidance and direct endoscopic visualization, the endoscope is guided into the fetal larynx and through the vocal cords. A detachable latex balloon is placed in the fetal trachea halfway between the carina and the vocal cords. The balloon is next inflated with 0.6mL of saline solution and the endoscope and cannula are removed (Perrone & Deprest 2021, Van der Veeken et al 2018). The balloon is typically placed between weeks 27-29 in severe and later (30-32 weeks) for moderate cases of FLH, secondary to CDH. The maternal is continuously monitored for potential deflation of the balloon and other complications, i.e., polyhydramnios, chorioamniotic membrane separation, PPROM, chorioamnionitis, or other signs of preterm labor (Van der Veeken et al 2018). Removal of the balloon is recommended at between 34 0/7 and 34 6/7 and can be performed via fetoscopic retrieval, percutaneous puncture using ultrasound-guidance, tracheoscopic removal on placental circulation during standard cesarean section or, at last option, in the immediate neonatal period (Jiménez et al 2017). The method of balloon removal depends upon the expertise at each center, the accessibility of the balloon for

an ultrasound-guided puncture, and the stability of the mother and fetus at the time of removal. Once the balloon is removed, the pregnancy can be managed expectantly, and women can deliver vaginally.

Concerning the therapeutic value of FETO, clinical research evaluating the improvement in fetal lung development describes a significant increase in lung size within 48 hours of balloon placement (Ruano et al 2013). This increase is dependent on initial o/e LHR and the timing of the occlusion and balloon removal (Nawapun et al 2015, Peralta et al 2008). Regarding the most commonly reported neonatal outcomes: survival and gestational age at delivery, comparative studies consistently report earlier gestational age at delivery for FETO and mixed results around survival, fluctuating from no differences between control and intervention to significant improvement after FETO (Deprest et al 2004, Deprest et al 2006, Harrison et al 2003, Ruano et al 2011, Ruano et al 2012b). Few studies also report rates of extracorporeal membrane oxygenation (ECMO) utilization and severe pulmonary hypertension and that neonate who received FETO have lower rates of both (Dhillon et al 2018, Ruano et al 2011, Ruano et al 2012b, Style et al 2019). Collectively, these findings motivate a randomized standard multicenter international trial to evaluate the therapeutic value of FETO in pulmonary hypoplasia secondary to CDH (NCT01240057 and NCT00763737). As such, the Tracheal Occlusion to Accelerate Lung growth (TOTAL) trial was initiated in 2011 in Europe and has begun recruitment from several centers in the United States (www.totaltrial.eu). The trial has two strata for randomization comparing the outcome to expectant management, a moderate and severe isolated left-sided CDH. At this time, the TOTAL trial is completed, and the results are expected in the near future (Perrone & Deprest 2021).

1.2.2.3.4.2. Experimental evidence

Experiments in animal models reveal distinct capacities for fetal lung growth and maturation depending on the time and duration of the tracheal occlusion (TO) (De Paepe et al 1999, De Paepe et al 1998, Keramidaris et al 1996, Maltais et al 2003, Probyn et al 2000). In fact, the *in vivo* experiments in the sheep model demonstrates a higher effect of TO when applied at early than later developmental stages. This discrepancy in fetal lung growth is probably explained by the compliance of the rib cage that imposes less restriction on lung expansion at early than later stages (De Paepe et al 1998, Probyn et al 2000). As such, TO applied at late pseudoglandular/ early canalicular stage induces slow onset of lung growth that quick and progressively increase as fetal lung development advance. Conversely, when applied at early alveolar stage, the fetal lung growth increases linearly between 2 and 7 days after TO, reaching a maximum on day 7 (Hooper et al 1993, Keramidaris et al 1996, Nardo et al 1998, Wallace et al 2014). However, the total number of alveoli and the lung weight observed on day 4 of TO remain unchanged until day10, indicating a

limited capacity for pulmonary expansion and alveoli formation in *in vivo* lungs (Lines et al 1999, Nardo et al 1998, Nardo et al 2000).

In this context, it is easy to understand the following studies that further evaluate the morphological, cellular, and molecular effects of TO in fetuses with CDH. In nitrofen-induced CDH rats, TO increases lung weight, DNA and protein content, lung volume, and surface area. The increased distension on CDH lungs (i.e., CDH+TO) reverse pulmonary hypoplasia, promote maturation of AT1 cells and reduce the expression of SP-C and TTF-1 observed in induced-CDH lung (Chapin et al 2005, Yoshizawa et al 2003). TO-applied CDH fetuses also reverse the increased pulmonary arterial medial and adventitial thickness associated with CDH. In fetal rabbits, the applied short and long-duration TO in fetuses with a diaphragmatic hernia (DH) showed the longer able to induce fetal lung growth and correct the pulmonary vascular anomalies (Bratu et al 2001, Kanai et al 2001, Luks et al 2000), whereas the surfactant production and the number of AT2 cells decrease (Benachi et al 1998, Benachi et al 1999, Bratu et al 2001). Conversely, the short-duration TO does not affect lung growth, whereas reverse the pulmonary vascular anomalies and AT2 cell numbers (Luks et al 2000, Papadakis et al 1998, Wild et al 2000, Wu et al 2002).

More recently, transcriptomic studies regarding the molecular profile in DH versus DH+TO lungs establish TO able to stimulate alveolar formation through an increase in the number of secondary crests in both intact and hypoplastic lungs. This effect is related to the overexpression of genes evolved in ECM function and alveolarization. Those genes include molecules expressed in the growing secondary septa, like *elastin*, *tropoelastin*, *fibulin-5*, or involved in interactions between cells (*α6-integrin*, *tenascin-C*) and extracellular environment. Unexpectedly, TO also induce changes in the expression of other genes like *β1-integrin*, *lysyl oxidase*, and *drebrin* that are not affected by lung hypoplasia, raising the question of TO-inducing disturbances in alveolar remodeling (Vuckovic et al 2013).

At the cellular level, Engels et al (Engels et al 2016) display confused expression profiles for several of the epithelial cell markers. For instance, the molecular markers for clara cells demonstrate *phosphatidic acid phosphatase type 2B* (*PPAP2B)* and *kinase insert domain receptor* (*KDR*) upregulated in DH and downregulated after TO, whereas *Scgb1a1* was unchanged in DH, and overexpressed in DH-TO. Regarding AT2 cell markers, *CD36* was downregulated in DH and upregulated by TO, while *delta like non-canonical Notch ligand 1* (*DLK1)* was overexpressed in DH and downregulated by TO. An opposite profile was also visualized for ciliated cell markers with *FOXJ1*, coiled-coil domain containing 39 (*CCDC39)*, *leucine rich repeats and IQ motif containing 1* (*LRRIQ1)*, *EF-hand domain containing protein 1* (*EFHC1),* and *tetratricopeptide repeat domain 18 (TTC18)* upregulated in DH and downregulated in DH+TO, whereas *CCDC19*, *leucine rich repeat containing 23* (*LRRC23)*, *WD repeat-containing proteins* (*WDR16*), *fibronectin*

type III and ankyrin repeat domains 1 (*FANK1)*, *enkurin* (*ENKUR)* and *CCDC113* were downregulated in DH+TO and unchanged in DH.

Aims

Despite sophisticated prenatal and postnatal clinical interventions applied in severe cases of pulmonary hypoplasia, the mortality rate remains unacceptably high. Pulmonary hypoplasia is a developmental problem, and the emerging consensus is that the prenatal period is the preferrable therapeutic window of opportunity to improve morphological defects and future neonatal respiratory function. As such, research regarding diagnosis and the pathophysiology of FLH has arisen over the last decades with, however, limited clinical relevance. In fact, albeit imagiological methods that allow the *in vivo* examination and measurement of fetal lungs have been described as valuable in FLH prediction in fetuses at high risk for the condition, the controversial predictive values by method difficult their applicability (Fong et al 1988, Gerards et al 2007, Gerards et al 2008, Kilbride et al 1996, Peralta et al 2006, van Teeffelen et al 2010, van Teeffelen et al 2012, Vergani et al 2010).

Regarding the FLH pathophysiology, punctual molecular and cellular interactions have highlighted our understanding of the morphological defects in branching and alveolar formation. Indeed, the transcriptome and genome-wide studies in human and induced-CDH lungs report high priority genes and pathways, such as ROBO/SLIT signaling, to treat FLH or CDH. ROBO/SLIT pathway is regulator of epithelial progenitor cell profile in the development of pancreas, mammary gland, or CNS. In fetal lung development, ROBO/SLIT signaling is essential for diaphragm formation, whereas SOX2 and $SOX9^{+}$ cells are the epithelial progenitor cells that give rise to the proximodistal patterning and later differentiate into bronchiolar and alveolar lineages. Surprisingly, the molecular function of ROBO1 and ROBO2 in branching morphogenesis and in the epithelial progenitor cell profile was never topic of research in normal or hypoplastic fetal lungs.

In FLH, recovering the fetal lung growth or maturation to improve neonatal respiratory function are inescapable areas of research. FETO is the therapy recommended for the more severe cases of FLH in CDH with verified advancements in fetal lung growth, maturation, and neonatal respiratory function (reviewed in Kovler & Jelin 2019, Tsao & Johnson 2020). Unfortunately, the increased risk for iatrogenic PPROM after FETO simultaneously limits their clinical relevance and enhances the research interest on the underlying mechanisms (Engels et al 2016, Nelson et al 2005, Vuckovic et al 2013). As such, since to predict or treat, we need to understand first, this Ph.D. thesis aims to **i)** evaluate the imagiological methods to predict lethal FLH; **ii)** characterize the epithelial cell profile in induced-CDH lungs; **iii)** understand the molecular function of ROBO1/2 in branching morphogenesis and SOX2/SOX9 profile; and **iv)** reveals the molecular/cellular mechanisms triggered by intraluminal fluid in the stimulation of branching morphogenesis.

To achieve our general research aims, the work was divided into the following specific aims:

- Investigate the effectiveness of the available imagiological methods in the prediction of lethal pulmonary hypoplasia;
- Characterize an induced-CDH lung in terms of proximodistal patterning and epithelial cell profile;
- Study the presence and functional relevance of ROBO1/ROBO2 in epithelial progenitor cell profile and branching morphogenesis;
- Describe an *ex vivo* model that allows the study of lung fluid composition in fetal lung growth;
- Reveal the mechanical relevance of PIEZO1/PIEZO2 in branching morphogenesis.

Thesis layout

The present Ph.D. thesis is organized into eight chapters:

In **Chapter 1**, just before Aims and Thesis layout, a General introduction to the thesis theme has been presented, including a review of the literature focused on the signal pathways that control fetal lung development. Aiming to the direct work developed in the present thesis, special attention is also dedicated to the mechanical stimuli in the regulation of (ab)normal fetal lung morphogenesis.

Chapter 2 includes a published systematic review focused on noninvasive ultrasound methods and their value to predict fetal lung hypoplasia in general diseases, premature rupture of membranes, and congenital diaphragmatic hernia.

Chapter 3 comprises a published research manuscript entitled "*ROBO2 signaling in lung development regulates SOX2/SOX9 balance, branching morphogenesis and is dysregulated in nitrofen-induced congenital diaphragmatic hernia*". This chapter reports both the relative expression levels and spatiotemporal distribution of epithelial progenitor cell markers (SOX2 and SOX9), and membrane receptors (ROBO1 and ROBO2) during *in vivo* normal and hypoplastic fetal lung development. The biological role of ROBO1 and ROBO2 in the SOX2 and SOX9 molecular profile is also explored in *ex vivo* branching morphogenesis.

Chapter 4 includes a study entitled *"Distinct epithelial cell signatures during normal and hypoplastic fetal lung development*". This exploratory research describes the expression profile of CCSP, FOXJ1, CGRP, and SP-C from pseudoglandular-to-saccular stages in nitrofen induced-CDH rat model.

Chapter 5 presents the article "*Intraluminal chloride regulates lung branching morphogenesis: involvement of PIEZO1/PIEZO2*" that is submitted in a peer-reviewed journal. In this work, lung explant cultures are reported as *ex vivo* models useful to study the lung fluid composition effects in branching morphogenesis. The increase of intraluminal chloride concentration is also described as a stimulator of fetal branching morphogenesis through PIEZO1/PIEZO2.

Chapter 6 contains a general discussion of the most relevant results of this thesis.

Chapter 7 includes a compendium of the major conclusions drawn from this work as well as the future perspectives.

In the end of the thesis, in **Chapter 8**, all the references from the entire write-up are presented in alphabetical order.

Chapter 2 – Ultrasound for lethal prenatal pulmonary hypoplasia prediction

The results presented in this chapter are:

i) Published in an international peer-reviewed journal:

Gonçalves AN, Correia-Pinto J, Nogueira-Silva C. Imagiological methods for prediction of fetal pulmonary hypoplasia: a systematic review. J Matern Fetal Neonatal Med. 2021 May;34(9):1459-1468. doi: 10.1080/14767058.2019.1636029. Epub 2019 Jul 3. PMID: 31269833. *(the integral reproduction was authorized by Taylor & Francis Group, Annex A)*

2.1. Chapter overview

2.1.1. Rationale

Secondary to multiple disorders with intra or extrathoracic causes, FLH is one of the most common cause of neonatal respiratory failure. Interestingly, the prediction of FLH in fetuses at high risk for the condition determines the familiar counseling, the specialized neonatal assistance, and improve neonatal survival. As such, the study of the more predictive method that correlates FLH with neonatal respiratory function is an inevitable topic of research.

US and MRI are the only available methods that noninvasively allowed the examination and measurement of the *in vivo* fetal lungs being reasonable in their use to detect FLH. However, the controversial predictive values by method have limited their clinical relevance. Interestingly, PROM and CDH are the most common extra- and intrathoracic causes of FLH, respectively, for which FLH is estimated by o/e-LHR, when secondary to CDH, while remains unpredictable if secondary to PPROM (Araujo Júnior et al 2010, Barros et al 2016, Milks et al 2017, Oluyomi-Obi et al 2017, Snoek et al 2017, Vergani et al 2010, Weaver et al 2014). As such, in this chapter we pretend to **i)** detect general gaps regarding the clinical experimental design; and **ii)** describe the more predictive method for lethal FLH in general diseases, PPROM, and CDH.

2.1.2. Major Findings

The major findings from this chapter are described below:

- 3 dimensional-fetal lung volume to body weight ratio (3D-FLB) and 2 dimensional-lung area (2D-LA) predict lethal FLH in general diseases;
- 2D- chest area (CA)-head area (HA)x100/CA estimate lethal FLH in PPROM;
- MRI-observed-to-expect fetal lung volume predict FLH in CDH;
- 2D and 3D-US have equal predictive values in groups with 0% survival;
- Restrict studies for disease groups and severity degrees are recommended.

THE JOURNAL OF MATERNAL-FETAL & NEONATAL MEDICINE
https://doi.org/10.1080/14767058.2019.1636029

Taylor & Francis
Taylor & Francis Group

REVIEW ARTICLE

Imagiological methods for prediction of fetal pulmonary hypoplasia: a systematic review

Ana N. Gonçalves[a,b], Jorge Correia-Pinto[a,b,c] and Cristina Nogueira-Silva[a,b,d]

[a]Life and Health Sciences Research Institute, School of Medicine, University of Minho, Braga, Portugal; [b]Life and Health Sciences Research Institute /3B's - PT Government Associate Laboratory, Braga, Portugal; [c]Department of Paediatric Surgery, Hospital de Braga, Braga, Portugal; [d]Department of Obstetrics and Gynaecology, Hospital de Braga, Braga, Portugal

ABSTRACT

Objective: To compare the different imagiological methods for prediction of fetal pulmonary hypoplasia (PH) in general diseases and associated with preterm rupture of membranes (PROM), and congenital diaphragmatic hernia (CDH).

Methods: According to PRISMA guidelines, all the literature on PH from 1988 to 2018 was reviewed. Twenty-nine articles were selected and analyzed for two- and three- dimensional-ultrasounds (2D and 3D-US) as predictors for the lethal outcome.

Results: Overall, the results identify a general gap correlating prenatal pulmonary measurements and survival at birth; discrepant predictive values for the same imagiological methods are explained by the group heterogeneity in terms of diseases and degree of severity, with the 2D measurements being more affected than 3D; 2D and 3D-US present equally predictive values for groups with 0% of survival. Regarding PROM, results demonstrate comparable accuracies for similar survival rates suggesting a useful predictive value of 2D-US in outcome estimation; they also identify ultrasonographic methods as a more accurate prognostic factor than gestational age at rupture, latency or amniotic fluid index. In CDH, consistent with previous studies, our review shows magnetic resonance imaging as a better survival predictor followed by the 3D and 2D methods, while 2D-LHR was the more precise prognosticator correlating prenatal PH, survival at birth, and the need for neonatal respiratory support.

Conclusion: Ultrasonographic methods can be valuable predictors for lethal PH and should be validated for a broad set of diseases (e.g. PROM). For that, restricted studies for disease groups and correlating fetal PH with the needed of neonatal support, and survival at birth is critically recommended.

ARTICLE HISTORY
Received 1 May 2019
Revised 4 June 2019
Accepted 21 June 2019

KEYWORDS
CDH; PROM; pulmonary hypoplasia; systematic review; ultrasonography

Introduction

Normal lung development depends on an intricate and finely regulated network of multiple mechanical and biochemical factors [1]. In fact, restriction or compression of developing lungs associated with space-occupying lesions, thoracic musculoskeletal abnormalities or lack of amniotic fluid is closely related to pulmonary hypoplasia (PH) [2].

PH is described as incomplete lung development the severity of which reflects the time of the insult in relation to the stage of embryonic development. Clinically, it presents as neonatal respiratory failure strictly associated with the degree of reduction in lung size or in the number of lung cells, airways and alveoli [3].

Although it is a relatively rare condition affecting 9–11 per 10,000 live births and 14 per 10,000 births, it's high mortality and morbidity rates make the prenatal PH prediction critical for improvement in familial counseling and neonatal assistance [4,5]. Previous reports have established the respiratory function at birth is dependent upon a sufficiently sized area of the gas-exchanging epithelium. Additionally, a correlation between fetal lung volume and the overall alveolar surface was also demonstrated with the prenatal examination of fetal lung volumes being reasonable to detect macroscopic hypoplastic lungs. The 2- (2D-US) and 3-dimensional ultrasounds (3D-US) and magnetic resonance imaging (MRI) are the only available methods to noninvasively examine the fetal lungs *in vivo*. Consequently, significant efforts have been made to improve the credibility and prognostic ability of prenatal imaging in PH determination [6–8].

CONTACT Cristina Nogueira-Silva cristinasilva@med.uminho.pt Life and Health Sciences Research Institute, School of Medicine, University of Minho, Campus de Gualtar, Gualtar, Braga 4710-057, Portugal

Nonetheless, controversial studies regarding the efficiency of ultrasounds (US) as predictive tools for PH and survival at birth have arisen [9–11]. Thus, to determine the accuracy of imagiological methods in prediction of lethal PH, we compared the 2D and 3D-US and MRI in all reported patients with general diseases and those related to premature rupture of membranes (PROM) and congenital diaphragmatic hernia (CDH).

Materials and methods

Search strategy and selection criteria

The review was performed according to the PRISMA guidelines. An electronic search of PubMed, Web of Science and Scopus (inception to 04/2018) without any language restrictions was carried out and reference lists, reviews, and primary articles were checked to identify cited articles not captured by the electronic search. One hundred and thirty-five studies were found by the online search after removing duplicates. Twenty-nine articles from a total of 973 normal and 1300 PH fetuses were included in our study, which represents 170 PH fetuses for general diseases, 200 for PROM and 930 for CDH.

Study selection and data extraction

To be included, studies must report the 2D or 3D-US or MRI method used and quantitative data, allowing the calculation of the area under the curve (AUC) or sensitivity, specificity, positive and negative predicted value (PPV and NPV). Exclusion criteria were: omitting at least one inclusion criteria, and data reported in graph or percentage form rather than proportional rates.

Lethal hypoplasia was defined as hypoplasia resulting in the death of the fetus or neonate due to PH. Fetuses with autopsy-proven lung hypoplasia after early pregnancy termination were also included in the lethal group. Any form of hypoplasia was defined as the sum of lethal and nonlethal hypoplasia.

Statistical analysis

Outcomes were defined as rates of lethal PH prediction. For each imagiological (2D, 3D, and MRI) method, the AUC, sensitivity, specificity, PPV, and NPV were calculated.

Results

Prenatal PH generally occurs as a secondary problem to another health condition that limits lung development. Thus, our systematic review evaluated imagiological methods as predictive tools for lethal PH in three distinct groups that were indicated as an extensive set of disorders: general diseases and, as the more common extra- and intrathoracic causes of neonatal respiratory failure, PROM and CDH, respectively.

In this context, according to PRISMA guidelines, a total of 135 articles was found: 65 were excluded by means of the abstracts and 41 after full reading. Lethal PH was predicted in 29 articles, representing: 6 for general diseases [12–17], 6 for PROM [18–21], and 17 for CDH [8,22–38] (Figure 1).

In the literature, different indices have been used to diagnose PH. For 2D and 3D-US methods, the indices most commonly evaluated to define PH are thoracic circumference (TC); TC/abdominal circumference (AC) ratio; thoracic area/heart area (TA/HA); lung length (LL); lung volume (LV) and fetal lung volume/body weight (FLB) [10–13,15,18–20,39]. All these indices define PH when they are equal to or lower than the fifth percentile of normal reference (Tables 1 and 2) [10–13,15,18–20, 40,41].

On the other hand, as specific diagnostic indices for 2D-US, Yoshimura et al. [16] define PH when the measurements are 2 standard deviations below, while Ruano et al. [17] consider the FLB of less than 0.012 when gestational age (GA) was 28 weeks or more, and less than 0.015 when GA was less than 28 weeks [42,43] (Table 1). In addition, Jozan et al. [21] used quantitative lung index (QLI, calculated by dividing the lung area by the square of the head circumference) and observed-to-expected lung-to-head ratio (o/e LHR, calculated by dividing fetal lung area to head circumference ratio) as gestational age-independent measurements, and interpret the QLI < 0.6, and o/e LHR < 25 as pathologic lung development [44,45] (Table 2).

Finally, postnatal diagnosis of PH was assessed by clinical, radiologic and/or pathologic parameters in all included studies.

General diseases

Comprising a wide set of disorders, general diseases were assessed in a total of 339 fetuses – 169 without and 170 with PH reported in six articles (Table 1).

Lethal PH was first predicted by Yoshimura et al., demonstrating useful statistical values for 2D methods with lung area (LA, sensitivity 0.81; specificity 1.00;

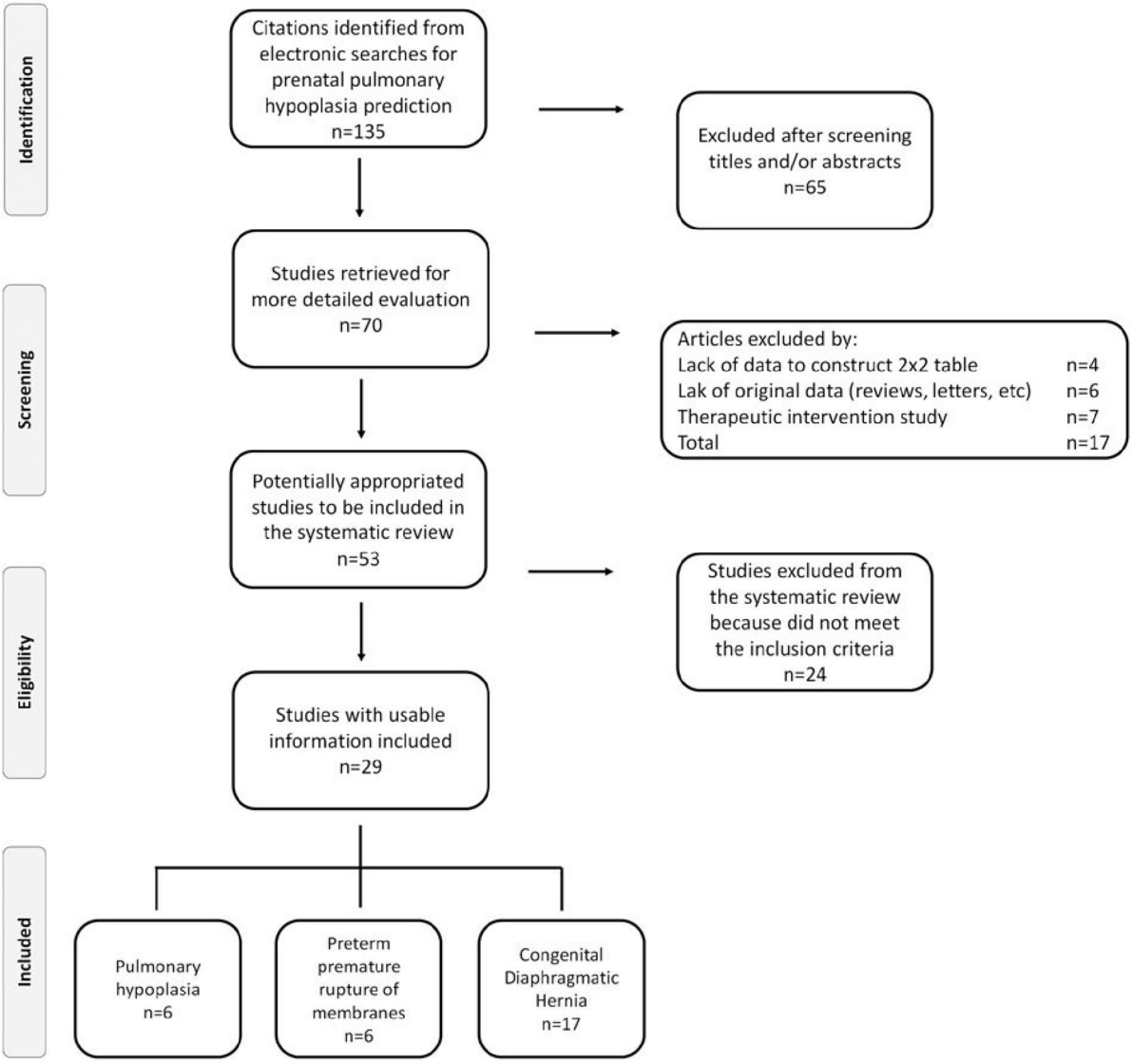

Figure 1. Flow diagram of included studies.

PPV 1.00; NPV 0.91; accuracy 0.94) and LA/TA (sensitivity 0.31; specificity 1.00; PPV 1.00; NPV 0.73; accuracy 0.76) as greater and lesser valuable predictors, respectively [16].

More recently, studies have analysed distinct 2D- and 3D- methods as advantageous outcome estimators, showing 3D to be more valuable predictors than 2D-US. Specifically, 3D-LV (sensitivity 0.94; specificity 0.82; PPV 0.83; NPV 0.93, and sensitivity 0.92; specificity 0.84; PPV 0.80; NPV 0.94), and 3D-FLB (AUC 0.93) were consistently defined as better prognostic indices than 2D-TC (sensitivity 0.63; specificity 0.47; PPV 0.53; NPV 0.57); 2D-TC/AC (sensitivity 0.46; specificity 0.74; PPV 0.55; NPV 0.77); and 2D-o/e TC (AUC 0.61) [12,13,15]. Additionally, 3D-o/e fetal lung volume (FLV) and 2D-o/e TA/HA were demonstrated to be poorer prognostic indices [15] (Table 1).

Furthermore, to determine the sensitivity of imagiological methods as lethal PH predictor, we calculated neonatal survival rates as an indirect measurement of group heterogeneity. Our review detected four survival rates, 0, 26, 41–43 and 52%, suggesting important differences in terms of degrees of severity between studies [12,13,15–17,19]. Interestingly, our findings demonstrate 3D (FLB, accuracy 0.91) and 2D (LA, accuracy 0.94) as having similar predictive capacities in groups with 0% survival [16,17]. In addition, comparable predictive values for 2D and 3D methods were also detected for 41 and 52% of neonatal survival, whereas 3D-LV (sensitivity 0.94; specificity 0.82; PPV 0.83; NPV 0.93) and 2D-TC/AC (sensitivity 0.81; specificity 0.59; PPV 0.65; NPV 0.77) for 52% were more useful predictors, reinforcing the robustness of these imagiological methods in outcome estimation

Table 1. Statistical analysis for comparison of the different imagiological methods in prenatal pulmonary hypoplasia (PH) prediction related to general diseases.

					Prenatal PH prediction								
Author, Year [ref]	Diseases	PH type	n (PH/ total fetuses)	GA (weeks)	Method	Normal Refernce Curves	Cut-off	AUC	Sensitivity	Specificity	PPV	NPV	Accuracy	Survival (%)
Gerards, 2008 [13]	Renal hypoplasia ($n=4$); Renal agenesis ($n=4$); multicystic ($n=2$); Polycystic kidney disease ($n=1$); Thanatophoric dwarfism ($n=3$); Osteogenesis imperfecta ($n=1$); Ellis-van Creveld syndrome ($n=2$); Pena Shokeir syndrome ($n=2$); Congenital cystic adenamoid malformation ($n=1$); Lung tumour ($n=1$); Hydrops fetalis ($n=3$); Gastroschisis ($n=1$)	Lethal	33/33	18-36	3D – LV 3D – FLB 2D – TC/AC 2D – TA/HA 2D – TC 2D – TC/FL	Gerards, 2006 [39] Laudy, 2002 [19] Vintzileos, 1989 [20] Fong, 1988 [10]	≤5th percentile		0.94 0.62 0.81 0.94 0.63 0.25	0.82 1.00 0.59 0.47 0.47 1.00	0.83 1.00 0.65 0.63 0.53 1.00	0.93 0.74 0.77 0.89 0.57 0.59		17/33 (52)
de Castro Rezende, 2013 [15]	Renal/ urinary tract anomalies ($n=20$); Skeletal malformations ($n=14$); Congenital diaphragmatic hernia ($n=8$); Adenomatoid cystic malformation ($n=4$); Preterm premature rupture of membranes ($n=1$)	Lethal	47/47	20-32	3D – FLB 3D – o/e – FLV 2D – o/e AFI 2D – o/e – TC 2D – o/e TC/AC 2D – o/eTA/HA	Rua no, 2006 [17]; Ruano, 2008 [41] Moore, 1990 [40] Laudy, 2002 [19] Vintzileos, 1989 [20]	≤5th percentile	0.93 0.86 0.71 0.69 0.55 0.46						12/47 (26)
Ruano, 2006 [17]	Congenital diaphragmatic hernia ($n=9$); Severe heart malformations ($n=8$); Severe brain abnormalities ($n=7$); Aneuploidies ($n=3$); Fetal akinesia sequence ($n=2$); Multiple malformations syndrome ($n=2$); Osteochondrodysplasia ($n=1$); Bruneville tuberous sclerosis ($n=1$); Pierre-Robin syndrome ($n=1$); Amniotic band syndrome ($n=1$)	Lethal	35/35	15-38	3D – FLB	Bland, 1999 [42]; Bland, 2003 [43]	≥28 weeks - <0.012; <28weeks - <0.015		0.84	0.95	0.84	0.91	0.91	0/35 (0)

(*continued*)

Table 1. Continued.

Author, Year [ref]	Diseases	PH type	n (PH/ total fetuses)	GA (weeks)	Prenatal PH prediction									Survival (%)
					Method	Normal Refernce Curves	Cut-off	AUC	Sensitivity	Specificity	PPV	NPV	Accuracy	
Vergani, 2010 [12]	Preterm premature rupture of membranes ($n = 14$); Osteogenesis imperfecta ($n = 3$); Arthrogryposis ($n = 1$); Hypophosphatasia ($n = 1$); Achondrogenesis ($n = 1$); Camptomelic Dysplasia ($n = 1$); Bilateral renal dyslasia or Potter II ($n = 4$); Hydrothorax ($n = 7$)	Lethal	13/32	19-24	3D – LV	Gerards, 2006 [39]	≤5th percentile		0.92	0.84	0.80	0.94		13/32 (41)
					3D – FLB				0.85	0.95	0.92	0.90		
					2D – TC/AC	Laudy, 2002 [19]			0.46	0.74	0.55	0.77		
					2D – TA/HA	Vintizileos, 1989 [20]			0.23	0.95	0.75	0.64		
					2D – TC	Fong 1988 [10]			0.23	0.89	0.60	0.63		
					2D – TC/FL				0.23	0.89	0.60	0.63		
Yoshimura, 1996 [16]	Bilateral renal agenesis ($n = 5$); Infantile polycystic kidney ($n = 2$); Unilateral renal agenesis and contralateral multicystic kidney ($n = 6$); Preterm premature rupture of membranes ($n = 2$); Thanatophoric dwarfism ($n = 6$)	Lethal	21/150	18-40	2D – LA	Yoshimura, 1996 [16]	<2 Standard Desviations		0.81	1.00	1.00	0.91	0.94	0/21 (0)
					2D – TA				1.00	0.87	0.84	1.00	0.92	
					2D – TA – HA				1.00	0.87	0.80	1.00	0.91	
					2D – TC				1.00	0.83	0.81	1.00	0.90	
					2D – TC/AC				0.91	0.90	0.86	0.93	0.90	
					2D – TC/HA				0.69	1.00	1.00	0.86	0.89	
					2D – (TA – HA)/ TA				0.69	0.97	0.92	0.85	0.87	
					2D – LA/TA				0.31	1.00	1.00	0.73	0.76	

Abbreviations: AC: abdominal circumference; AUC: area under the curve; FL: femur length; FLB: fetal lung volume to body weight ratio; GA: gestational age; HA: heart area; LA: lung area; LV: lung volume; NPV: negative predicted value; o/e-AFI: observed-to-expected amniotic fluid index; o/e-FLV: observed-to-expected fetal lung volume; PPV: positive predicted value; TA: thoracic area; TC: thoracic circumference; 2D: two-dimensional ultrasonography; 3D: three-dimensional ultrasonography.

Table 2. Evaluation of the different two- or three-dimensional methods for prenatal pulmonary hypoplasia (PH) prediction in premature rupture of membranes (PROM).

				Prenatal PH Prediction								
Author, Year [ref]	PH type	n (PROM/ total fetuses)	GA (weeks)	Method	Normal Reference Curves	Cut-off	AUC	Sensitivity	Specificity	PPV	NPV	Accuracy	Survival (%)
Fong, 1988 [10]	Lethal	17/17	21–39	2D – CC/AC	Fong, 1988 [10]	≤0.75		0.6	1.00	1.00	0.25	0.65	9/17 (53)
Jozan, 2018 [21]	Lethal	34/34	24–40	2D – tot o/e LHR (LDM)	Jani, 2007 [45]	<25	0.84						
				2D – tot o/e LHR (TM)			0.83						
				2D – QLI	Quintero, 2011 [44]	<0.6	0.85						
Kilbride, 1996 [9]	Lethal	71/71	22–34	2D – TC/AC	Kilbride, 1996 [9]	<0.89		0.68	0.48	0.63	0.54		40/71 (56)
Laudy, 2002 [19]	Lethal	31/42	20–36	2D – TC/AC	Laudy, 2002 [19]	≤5th percentile		0.63	0.73	0.45	0.84	0.70	9/31 (29)
				2D – TC				1.00	0.36	0.39	1.00	0.55	
				2D – CC/TC				0.78	0.50	0.39	0.85	0.58	
Roberts, 1990 [18]	Lethal	14/20	12–40	2D – LL	Roberts, 1990 [18]	≤26		0.83	0.93	0.83	0.93	0.90	6/20 (30)
Vintzileos, 1989 [20]	Lethal	13/194	16–40	2D – (CA – HA) × 100/CA	Vintzileos, 1989 [20]	≤5th percentile		0.85	0.85	0.83	0.85	0.85	6/13 (54)
				2D – CA/HA				0.66	0.85	0.80	0.75	0.77	
				2D – CA – HA				0.50	0.71	0.60	0.62	0.62	
				2D – CC × 100/AC				0.33	0.85	0.66	0.60	0.62	
				2D – CA				0.33	0.71	0.50	0.55	0.54	
				2D – CC				0.33	0.57	0.40	0.50	0.46	

Abbreviations: AC: abdominal circumference; CA: chest area; CC: chest circumference; GA: gestational age; HA: heart area; LDM: longest diameter method; LL: lung length; NPV: negative predicted value; o/e-LHR: observed-to-expected lung-to-head ratio; PPV: positive predicted value; TA: thoracic area; TC: thoracic circumference; TM: trace methods; 2D: two-dimensional ultrasonography.

(Tabl 1) [12,13]. Finally, our analysis also discloses a constant improvement in outcome estimation by 2D methods related to a decrease in group heterogeneity, corroborating the valuable capacity of US tools as neonatal survival estimators.

In this context, the usefulness of imagiological tools as lethal PH predictors were also assessed for PROM, and CDH.

PROM

Our review detected six studies that analyze distinct 2D-US methods in a total of 708 fetuses (508 healthy and 200 PH) [9–11,18–21,46].

Our results indicated (chest area (CA) − HA)/CA × 100/CA (accuracy 0.85), QLI (AUC 0.85), and total o/e LHR (AUC 0.84) as better predictors than TC (accuracy 0.55), CA (accuracy 0.54) or chest circumference (CC, accuracy 0.46) for outcome estimators (Table 2) [19–21]. In addition, survival at birth was also predicted by Kilbride et al. and Roberts et al. demonstrating 2D − TC/AC ≥ 0.89 (sensitivity 0.68; specificity 0.48; PPV 0.63; NPV 0.54), and LL ≥ 26 (sensitivity 0.83; specificity 0.93; PPV 0.83; NPV 0.93, accuracy 0.90) as advantageous estimators (Table 2) [9,18].

Furthermore, in order to determine the degree of severity by group, neonatal survival rates were also calculated and the distinct 2D-US tools analysed. Our results revealed similar statistical values for (CA − HA) × 100/CA (accuracy 0.85), CA/HA (accuracy 0.77) and TC/AC (accuracy 0.70) related to 53–57% of survival, whereas QLI (AUC 0.85) and total o/e-LHR (0.84) were the principal prognostic indices for 44%, and LL (sensitivity 1.00; specificity 0.75; PPV 0.86; NPV 1.00) for 30% (Table 2) [18,20,21,34].

Lastly, as for general diseases, a comparable improvement in outcome estimation was observed with the progressive decrease of group heterogeneity, suggesting a useful value of US as predictive tools of lethal prenatal PH (Table 2).

CDH

Regarding CDH, our research found 17 articles comprising 930 fetuses and 4 US methods – LHR, FLV, percentage of predicted lung volume (PPLV) or total fetal lung volume (TFLV) as estimators of neonatal survival [22,23,26–34,47,48].

Comparing three independent studies assessing PPLV, observed-to-expected TFLV or o/e LHR as survival predictors, our analysis showed PPLV < 15 (sensitivity 0.82; specificity 1.00; PPV 1.00; NPV 0.60) as more

predictive tool than o/e TFLV < 35 (sensitivity 0.75; specificity 0.89; PPV 0.75; NPV 0.89) and o/e LHR < 25 (sensitivity 0.36; specificity 0.94; PPV 0.75; NPV 0.73) [23,26–28]. More recently, these methods were simultaneously investigated by Ruano et al. demonstrating o/e TFLV < 32 (measured by MRI, AUC 0.78; sensitivity 0.78; specificity 0.74) and PPLV < 10.3 (measured by MRI, AUC 0.74; sensitivity 0.77; specificity 0.74) as better predictors than o/e LHR < 0.41 (2D-ultrassound method, AUC 0.72; sensitivity 0.68; specificity 0.69), or LHR < 1.40 (AUC 0.70; sensitivity 0.65; specificity 0.71) [47]. Finally, Alfaraj et al. and Akinkuotu et al. similarly revealed o/e TFLV < 35 (sensitivity 0.56; specificity 0.90; PPV 0.94; NPV 0.44; sensitivity 0.70; specificity 0.88; PPV 0.78; NPV 0.82) as better prognosticators than LHR < 1.40 (sensitivity 0.67; specificity 0.68; PPV 0.86; NPV 0.42; sensitivity 0.36; specificity 0.94; PPV 0.75; NPV 0.73) [23,24].

Although o/e-TFLV and PPLV were demonstrated to be better survival predictors than LHR, a critical link between prenatal PH prediction, the need for neonatal respiratory support and survival at birth were consistently described for LHR [19,24,29–31,35]. Indeed, LHR < 0.6 was established for 0% survival (sensitivity 1.00; specificity 0.29; PPV 0.64; NPV 1.00), while > 1 and > 1.4 were defined for 75% (sensitivity 0.88; specificity 0.49; PPV 0.75; NPV 0.70) and 86% survival (sensitivity 0.80; specificity 0.75; PPV 0.65; NPV 0.86), respectively, suggesting a pivotal predicted value of this parameter for CDH risk-stratification [22,29,31,45].

Discussion

Despite the different underlying pathologies related to PH, distinct combinations of clinical, ultrasound, and MRI parameters have been evaluated as potential predictors of prenatal PH. Unfortunately, at least for now, there is no single or combined test commonly accepted as a predictor for neonatal survival. In this context, to determine the potential capacity of the imagiological methods for lethal PH prediction, we compare the 2D, 3D and MRI methods as prognostic indic s for an extensive set of disorders, PROM and CDH.

Overall, our study detects interesting statistical values for the 2D and 3D-US for general diseases, PROM and CDH, in which FLB ≤ 5th percentile and LA < 2 standard deviations are the best prognostic indices for general diseases, 2D − (CA − HA) × 100/CA ≤ 5th percentile for PROM, with o/e TFLV < 35 and o/e LHR < 25 for neonatal survival in CDH (Table 3).

Surprisingly, our study discerned discrepant statistical values for similar US methods. A careful analysis of the distinct reports reveals four main reasons for this divergence as follows:

1. differences in measurements from distinct medical centers that are included in the same study;
2. absence of data normalization for uncomplicated pregnancies;
3. differences in the study population, ie the inclusion of fetuses with diverse types of diseases and/or associated with distinct severities;
4. variances regarding the endpoint of the prediction.

Indeed, a constant improvement in outcome prediction seems to be associated with data normalization for uncomplicated pregnancies and medical centers. Specifically, two distinct studies estimating lethal PH by 3D and 2D-US methods demonstrate comparable accuracies for 3D-FLB (accuracy 0.91), 2D-LA (accuracy 0.94) and 2D-TA (accuracy 0.92) approaches [16,17]. Importantly, Ruano et al. use 3D-FLB estimated lethal PH based on [42,43], whereas Yoshimura et al. establish nomograms in a cross-sectional manner for uncomplicated pregnancies and assess the efficacy of each parameter by studying patients with PROM not at risk for PH [16,17]. In effect, comparing the six articles that assess both 2D and 3D methods, our findings reveal 2D-US reported by Yoshimura et al. as the more valuable outcome predictors [16].

Our research also indicated that although the need for neonatal respiratory support and survival at birth

Table 3. Predictive indices for imagiological methods in prenatal lethal hypoplasia estimation.

	Lethal PH prediction		
	Method	Normal reference curves	Cut-off
General diseases	3D-FLB	Ruano, 2006 [17]; Ruano, 2008 [41]	≤5th percentile
	2D-LA	Yoshimura, 1996 [16]	<2 standard deviations
PROM	2D−(CA − HA)×100/CA	Vintzileos, 1989 [20]	≤5th percentile
CDH	MRI-o/e TFLV	Ruano, 2009 [26]	<35
	2D-o/e LHR	Jani, 2007 [45]	<25
	2D-LHR	Mektus, 1996 [31], Lipshutz 1997 [30]; Laudy, 2003 [34]; Peralta, 2006 [6]	<0.6

Abbreviations: CDH: congenital diaphragmatic hernia; FLB: fetal lung volume to body weight ratio; LA: lung area; LHR: lung-to-head ratio; MRI: magnetic resonance imaging; o/e-LHR: observed-to-expected lung-to-head ratio; o/e-TFLV: observed-to-expected total fetal lung volume; PROM: premature rupture of membranes; 2D: two-dimensiona ul rasonography; 3D: three-dimensional ultrasonography.

are usually described by the authors, a general gap correlating prenatal pulmonary measurements and neonatal survival is detected by our study. Thus, we calculated the survival rates as an indirect measurement of groups heterogeneity. Our study demonstrates comparable prenatal PH prediction for 3D-FLB and 2D-LA related to 0% survival [16,17]. Oppositely, an increase in group heterogeneity leads to an unchanged 3D-US accuracy, with a progressive decrease of 2D-US capacity in outcome estimation. Specifically, 3D-FLB and 3D-LV equally predict PH in groups with 26, 41, and 52% survival whereas a constant reduction in outcome estimation by 2D-TC/AC; 2D-TA/HA; 2D-o/e-TC is related to an increase in survival rate [12,13,15].

Our findings also suggest aetiology as another important variable that influences the predictive capacity of the US. Particularly, the general accuracies reported by 3D-LV (sensitivity 0.94; specificity 0.82; PPV 0.83; NPV 0.93) and 2D-TC/AC (sensitivity 0.81; specificity 0.59; PPV 0.65; NPV 0.77) for overall disorders (52% survival) are converted into sensitivity 0.88; specificity 1.00; PPV 1.00; NPV 0.75 for 3D-LV, and sensitivity 0.75; specificity 0.67; PPV 0.86; NPV 0.50 for 2D-TC/AC in renal anomalies (64% survival); and sensitivity 1.00; specificity 1.00; PPV 1.00; NPV 1.00 for 3D-LV, and sensitivity 0.80; specificity 0.33; PPV 0.67; NPV 0.50 for 2D-TC/AC in skeletal and neuromuscular malformations (0% neonatal survival) [13]. Together, similar improvement in 2D and 3D accuracies after disease segregation according with their aetiology seems to support the sensitivity/utility of the imagiological methods as prenatal PH prediction.

These observations urged us to investigate the 2D-US, as outcome predictors for the more common extra- and intrathoracic causes of prenatal respiratory failure, PROM and CDH, respectively.

Concerning PROM, a total of six studies ranging from 30–60% survival were analyzed and comparable accuracies were detected to similar survival rates. Specifically, TC/AC, TC, and CC/TC for 57% and $[(CA-HA)\times 100/CA]$, CA/HA, $CA-HA$; $CC\times 100/AC$ for 54% survival equally predicted the outcome [20,34]. In addition, Jozan et al. show interesting AUC values detection of lethal (QLI 0.85 and o/e LHR 0.84), and severe (QLI 0.70; total o/e LHR 0.69) PH [21]. Collectively, these results seem to corroborate the useful value of US methods as outcome prognostic indices.

Finally, distinct methods (gestational age at rupture, latency or amniotic fluid index (AFI)) have been reported as PH predic ors in PROM [49,50]. Inter stingly, our statistical analysis identified 3D-LV, 2D-TA/HA, or 2D-o/e LHR as better prenatal PH prognostic indices than gestational age at rupture, latency or AFI [11,21,49,50].

Regarding CDH, in agreement with previous studies, our review shows MRI (o/e-TFLV or PPLV) as a better neonatal survival predictor followed by 3D-FLV and 2D-LHR, while LHR is consistently defined as the most accurate prognostic index correlating survival at birth, and the need for neonatal respiratory support [23,28]. In fact, a useful risk-stratification of LHR <0.6, >1, and >1.4 related to 0, 75 and 86% of neonatal survival, respectively, is already accepted [22,24,29,30,32,33,35,47]. Consequently, our results demonstrate distinct sonographic tools for prenatal PH prediction, neonatal survival estimation and the need for respiratory support.

In conclusion, our systematic review indicates $2D-LA<2$ standard deviations and $3D-FLB\leq$ 5th percentile as predictive methods for general diseases; $(CA-HA)\times 100/CA\leq$ 5th percentile for PROM; and $3D-o/e-TFLV<35$ or $2D-LHR<0.6$ for CDH in lethal PH estimation. Restricted studies for particular disease groups/severities and correlating prenatal PH, survival at birth, and the need for neonatal respiratory support are critically recommended.

Disclosure statement

The authors report no conflict of interest.

Funding

This work was supported by the European Regional Development Fund (ERDF), through the Operational Programme for Competitiveness and Internationalisation (COMPETE 2020), under Portugal 2020, and by Fundação para a Ciência e a Tecnologia (FCT) through national funds, under de project POCI-01–0145-FEDER-030881; Northern Portugal Regional Operational Programme (NORTE 2020), under the Portugal 2020 Partnership Agreement, through the European Regional Development Fund (FEDER) under the scope of the project NORTE-01–0246-FEDER-000012; Gonçalves was supported by FCT (reference PD/BDE/127829/2016).

References

[1] Schittny JC. Development of the lung. Cell Tissue Res. 2017;367:427–444.

[2] Sadler TW, Langman J. Langman's medical embryology. Philadelphia, PA: Wolters Kluwer Health/Lippincott Williams & Wilkins; 2012.

[3] Lauria MR, Gonik B, Romero R. Pulmonary hypoplasia: pathogenesis, diagnosis, and antenatal prediction. Obstet Gynecol. 1995;86:466–475.
[4] Moessinger AC, Santiago A, Paneth NS, et al. Time-trends in necropsy prevalence and birth prevalence of lung hypoplasia. Paediatr Perinat Epidemiol. 1989; 3:421–431.
[5] Laudy JA, Wladimiroff JW. The fetal lung. 2: Pulmonary hypoplasia. Ultrasound Obstet Gynecol. 2000;16:482–494.
[6] Peralta CF, Kazan-Tannus JF, Bunduki V, et al. Evaluation of the agreement between 3-dimensional ultrasonography and magnetic resonance imaging for fetal lung volume measurement. J Ultrasound Med. 2006;25:461–467.
[7] van Teeffelen AS, Van Der Heijden J, Oei SG, et al. Accuracy of imaging parameters in the prediction of lethal pulmonary hypoplasia secondary to mid-trimester prelabor rupture of fetal membranes: a systematic review and meta-analysis. Ultrasound Obstet Gynecol. 2012;39:495–499.
[8] Britto IS, Araujo Júnior E, Sangi-Haghpeykar H, et al. Reference ranges for 2-dimensional sonographic lung measurements in healthy fetuses a longitudinal study. J Ultrasound Med. 2014;33:1917–1923.
[9] Kilbride HW, Yeast J, Thibeault DW. Defining limits of survival: lethal pulmonary hypoplasia after mid-trimester premature rupture of membranes. Am J Obstet Gynecol. 1996;175:675–681.
[10] Fong K, Ohlsson A, Zalev A. Fetal thoracic circumference: a prospective cross-sectional study with real-time ultrasound. Am J Obstet Gynecol. 1988;158: 1154–1160.
[11] Gerards FA, Twisk JW, Fetter WP, et al. Two- or three-dimensional ultrasonography to predict pulmonary hypoplasia in pregnancies complicated by preterm premature rupture of the membranes. Prenat Diagn. 2007;27:216–221.
[12] Vergani P, Andreani M, Greco M, et al. Two- or three-dimensional ultrasonography: which is the best predictor of pulmonary hypoplasia? Prenat Diagn. 2010; 30:834–838.
[13] Gerards FA, Twisk JW, Fetter WP, et al. Predicting pulmonary hypoplasia with 2- or 3-dimensional ultrasonography in complicated pregnancies. Am J Obstet Gynecol. 2008;198:140.e1–140.e6.
[14] Tanigaki S, Miyakoshi K, Tanaka M, et al. Pulmonary hypoplasia: prediction with use of ratio of MR imaging-measured fetal lung volume to US-estimated fetal body weight. Radiology 2004;232:767–772.
[15] de Castro Rezende G, Pereira AK, Araujo Júnior E, et al. Prediction of lethal pulmonary hypoplasia among high-risk fetuses *via* 2D and 3D ultrasonography. Int J Gynecol Obstet. 2013;123:42–45.
[16] Yoshimura S, Masuzaki H, Gotoh H, et al. Ultrasonographic prediction of lethal pulmonary hypoplasia: comparison of eight different ultrasonographic parameters. Am J Obstet Gynecol. 1996;175: 477–483.
[17] Ruano R, Martinovic J, Aubry MC, et al. Predicting pulmonary hypoplasia using the sonographic fetal lung volume to body weigh ratio – how precise and accurate is it? Ultrasound Obstet Gynecol. 2006;28: 958–962.
[18] Roberts AB, Mitchell JM. Direct ultrasonographic measurement of fetal lung length in normal pregnancies and pregnancies complicated by prolonged rupture of membranes. Am J Obstet Gynecol. 1990;163: 1560–1566.
[19] Laudy JA, Tibboel D, Robben SG, et al. Prenatal prediction of pulmonary hypoplasia: clinical, biometric, and Doppler velocity correlates. Pediatrics 2002;109: 250–258.
[20] Vintzileos AM, Campbell WA, Rodis JF, et al. Comparison of six different ultrasonographic methods for predicting lethal fetal pulmonary hypoplasia. Am J Obstet Gynecol. 1989;161:606–612.
[21] Jozan C, Huissoud C, Labaune JM, et al. Contribution of ultrasound pulmonary ratio in pre-viable premature ruptures of membranes. Gynecol Obstet Fertil Senol. 2018;46:78–85.
[22] Ruano R, Takashi E, da Silva MM, et al. Prediction and probability of neonatal outcome in isolated congenital diaphragmatic hernia using multiple ultrasound parameters. Ultrasound Obstet Gynecol. 2012;39: 42–49.
[23] Alfaraj MA, Shah PS, Bohn D, et al. Congenital diaphragmatic hernia: lung-to-head ratio and lung volume for prediction of outcome. Am J Obstet Gynecol. 2011;205:43.e1–43.e8.
[24] Akinkuotu AC, Cruz SM, Abbas PI, et al. Risk-stratification of severity for infants with CDH: prenatal versus postnatal predictors of outcome. J Pediatr Surg. 2016; 51:44–48.
[25] Kastenholz KE, Weis M, Hagelstein C, et al. Correlation of observed-to-expected MRI fetal lung volume and ultrasound lung-to–head ratio at different gestational times in fetuses with congenital diaphragmatic hernia. AJR Am J Roentgenol. 2016;206:856–866.
[26] Ruano R, Aubry MC, Barthe B, et al. Three-dimensional ultrasonographic measurements of the fetal lungs for prediction of perinatal outcome in isolated congenital diaphragmatic hernia. J Obstet Gynaecol Res. 2009;35: 1031–1041.
[27] Barnewolt CE, Kunisaki SM, Fauza DO, et al. Percent predicted lung volumes as measured on fetal magnetic resonance imaging: a useful biometric parameter for risk stratification in congenital diaphragmatic hernia. J Pediatr Surg. 2007;42:193–197.
[28] Mahieu-Caputo D, Sonigo P, Dommergues M, et al. Fetal lung volume measurement by magnetic resonance imaging in congenital diaphragmatic hernia. Bjog. 2001;108:863–868.
[29] Heling KS, Wauer RR, Hammer H, et al. Reliability of the lung-to-head ratio in predicting outcome and neonatal ventilation parameters in fetuses with congenital diaphragmatic hernia. Ultrasound Obstet Gynecol. 2005;25:112–118.
[30] Lipshutz GS, Albanese CT, Feldstein VA, et al. Prospective analysis of lung-to-head ratio predicts survival for patients with prenatally diagnosed congenital diaphragmatic hernia. J Pediatr Surg. 1997;32: 1634–1636.

[31] Metkus AP, Filly RA, Stringer MD, et al. Sonographic predictors of survival in fetal diaphragmatic hernia. J Pediatr Surg. 1996;31:148–152.
[32] Yoshimura S, Masuzaki H, Hiraki K, et al. Congenital diaphragmatic hernia: an evaluation of the prognostic value of the lung-to-head ratio. J Med Ultrasonics. 2005;32:115–119.
[33] Hedrick HL, Danzer E, Merchant AM, et al. Liver position and lung-to-head ratio for prediction of extracorporeal membrane oxygenation and survival in isolated left congenital diaphragmatic hernia. Am J Obstet Gynecol. 2007;197:422.e1–422.e4.
[34] Laudy JA, Van Gucht M, Van Dooren MF, et al. Congenital diaphragmatic hernia: an evaluation of the prognostic value of the lung-to-head ratio and other prenatal parameters. Prenat Diagn. 2003;23:634–639.
[35] Aspelund G, Fisher JC, Simpson LL, et al. Prenatal lung–head ratio: threshold to predict outcome for congenital diaphragmatic hernia. J Matern Fetal Neonatal Med. 2012;25:1011–1016.
[36] Kehl S, Siemer J, Brunnemer S, et al. Prediction of postnatal outcomes in fetuses with isolated congenital diaphragmatic hernias using different lung-to-head ratio measurements. J Ultrasound Med. 2014;33:759–767.
[37] Kido S, Hidaka N, Sato Y, et al. Re-evaluation of lung to thorax transverse area ratio immediately before birth in predicting postnatal short-term outcomes of fetuses with isolated left-sided congenital diaphragmatic hernia: a single center analysis. Congenit Anom. 2018;58:87–92.
[38] Snoek KG, Peters NCJ, van Rosmalen J, et al. The validity of the observed-to-expected lung-to-head ratio in congenital diaphragmatic hernia in an era of standardized neonatal treatment; a multicenter study. Prenat Diagn. 2017;37:658–665.
[39] Gerards FA, Engels MA, Twisk JW, et al. Normal fetal lung volume measured with three-dimensional ultrasound. Ultrasound Obstet Gynecol. 2006;27:134–144.
[40] Moore TR, Cayle JE. The amniotic fluid index in normal human pregnancy. Am J Obstet Gynecol. 1990;162:1168–1173.
[41] Ruano R, Aubry MC, Barthe B, et al. Three-dimensional sonographic measurement of contralateral lung volume in fetuses with isolated congenital diaphragmatic hernia. J Clin Ultrasound. 2008;36:273–278.
[42] Bland JM, Altman DG. Measuring agreement in method comparison studies. Stat Methods Med Res. 1999;8:135–160.
[43] Bland JM, Altman DG. Applying the right statistics: analyses of measurement studies. Ultrasound Obstet Gynecol. 2003;22:85–93.
[44] Quintero RA, Quintero LF, Chmait R, et al. The quantitative lung index (QLI): a gestational age-independent sonographic predictor of fetal lung growth. Am J Obstet Gynecol. 2011;205:544.e1–544.e8.
[45] Jani J, Nicolaides KH, Keller RL, et al. Observed to expected lung area to head circumference ratio in the prediction of survival in fetuses with isolated diaphragmatic hernia. Ultrasound Obstet Gynecol. 2007;30:67–71.
[46] Harstad TW, Twickler DM, Leveno KJ, et al. Antepartum prediction of pulmonary hypoplasia: an elusive goal? Amer J Perinatol. 1993;10:8–11.
[47] Ruano R, Lazar DA, Cass DL, et al. Fetal lung volume and quantification of liver herniation by magnetic resonance imaging in isolated congenital diaphragmatic hernia. Ultrasound Obstet Gynecol. 2014;43:662–669.
[48] Kilian AK, Büsing KA, Schuetz EM, et al. Fetal MR lung volumetry in congenital diaphragmatic hernia (CDH): prediction of clinical outcome and the need for extracorporeal membrane oxygenation (ECMO). Klin Padiatr. 2009;221:295–301.
[49] Rossi AC, Prefumo F. Perinatal outcomes of isolated oligohydramnios at term and post-term pregnancy: a systematic review of literature with meta-analysis. Eur J Obstet Gynecol Reprod Biol. 2013;169:149–154.
[50] van Teeffelen AS, van der Ham DP, Oei SG, et al. The accuracy of clinical parameters in the prediction of perinatal pulmonary hypoplasia secondary to midtrimester prelabour rupture of fetal membranes: a meta-analysis. Eur J Obstet Gynecol Reprod Biol. 2010;148:3–12.

Chapter 3 – Epithelial progenitor cells and ROBO signaling in both branching morphogenesis and nitrofen-induced CDH rat model

The results presented in this chapter are:

i) Published in an international peer-reviewed journal:

Gonçalves AN, Correia-Pinto J, Nogueira-Silva C. ROBO2 signaling in lung development regulates SOX2/SOX9 balance, branching morphogenesis and is dysregulated in the nitrofen-induced congenital diaphragmatic hernia. Respir Res. 2020 Nov 18;21(1):302. doi: 10.1186/s12931-020-01568-w. PMID: 33208157.

(the integral reproduction was authorized by Springer Nature, Annex B)

3.1. Chapter overview

3.1.1. Rationale

Identified by a diaphragmatic defect that allows the herniation of abdominal organs into the thorax cavity, CDH affects 1-5 in 10.000 live births. Hypoplastic lungs with decreased branching morphogenesis at early and reduced number of alveoli with septa notably thicker a later developmental stages characterize the pulmonary immaturity and respiratory failure at birth. Transcriptome and genome-wide studies have demonstrated multiple up- and downregulated genes and pathways, like ROBO/SLIT signaling, in induced-CDH lungs that highlight our understating of the morphological defects by developmental stage (reviewed in Montalva & Zani 2019, Longoni et al 2014, Russell et al 2012).

Robo1/2 knockout mice delay the separation of foregut from the body wall (Domyan et al 2013), whereas the *Robo1/Dutt1* functional impairment damage the neonatal respiratory function at birth (Xian et al 2001). More recently, ROBO/SLIT signaling was described as regulator of epithelial progenitor cell profile in the development of CNS, mammary gland, and pancreas (Ballard et al 2015, Blockus & Chédotal 2016, Borrell et al 2012, Escot et al 2018, Harburg et al 2014, Macias et al 2011). In fetal lungs, SOX2 and SOX9 identified the epithelial progenitor cells that define the proximodistal patterning at branching morphogenesis, whereas the *Sox2* or *Sox9* knockout mice have impaired epithelial cell differentiation with abnormal fetal lung development (Gontan et al 2008, Rockich et al 2013, Tompkins et al 2011, Tompkins et al 2009). Indeed, the primordial capacity of SOX2 and $SOX9^{+}$ cells to give rise to bronchial and alveolar lineages, respectively, is almost established at the time of conducting and respiratory airways formation (Eblaghie et al 2006, El Agha et al 2014, Gontan et al 2008, Hashimoto et al 2012, Park et al 1998, Rockich et al 2013, reviewed in Volckaert & De Langhe 2015, Weaver et al 2000, Weaver et al 1999).

Since the potential function of ROBO1/2 in branching morphogenesis and in SOX2/SOX9 profile were never described, this chapter aimed to **i)** identify the spatiotemporal distribution of proximodistal markers (SOX2, SOX9) and receptors (ROBO1, ROBO2) from embryonic-to-saccular stages in nitrofen induced-CDH rat model; and **ii)** elucidate the functional role of ROBO1 and ROBO2 in both branching morphogenesis and SOX2/SOX9 profile.

3.1.2. Major Findings

The major findings from this chapter are described below:

- Proximodistal patterning is impaired from pseudoglandular-to-saccular stages in nitrofen-induced CDH rat model;

- Spatiotemporal distribution and relative expression levels of ROBO1 and ROBO2 are altered after CDH-induction;
- Distinct or balanced functions for ROBO1 and ROBO2 receptors in branching morphogenesis;
- Inhibition of ROBO2 stimulates pulmonary branching morphogenesis through overexpression of BMP4 and β-Catenin that promote SOX9 instead of SOX2 expression.

Respiratory Research 13

RESEARCH Open Access

ROBO2 signaling in lung development regulates SOX2/SOX9 balance, branching morphogenesis and is dysregulated in nitrofen-induced congenital diaphragmatic hernia

Ana N. Gonçalves[1,2], Jorge Correia-Pinto[1,2,3] and Cristina Nogueira-Silva[1,2,4*]

Abstract

Background: Characterized by abnormal lung growth or maturation, congenital diaphragmatic hernia (CDH) affects 1:3000 live births. Cellular studies report proximal ($SOX2^+$) and distal ($SOX9^+$) progenitor cells as key modulators of branching morphogenesis and epithelial differentiation, whereas transcriptome studies demonstrate ROBO/SLIT as potential therapeutic targets for diaphragm defect repair in CDH. In this study, we tested the hypothesis that (a) experimental-CDH could changes the expression profile of ROBO1, ROBO2, SOX2 and SOX9; and (b) ROBO1 or ROBO2 receptors are regulators of branching morphogenesis and SOX2/SOX9 balance.

Methods: The expression profile for receptors and epithelial progenitor markers were assessed by Western blot and immunohistochemistry in a nitrofen-induced CDH rat model. Immunohistochemistry signals by pulmonary structure were also quantified from embryonic-to-saccular stages in normal and hypoplastic lungs. Ex vivo lung explant cultures were harvested at E13.5, cultures during 4 days and treated with increasing doses of recombinant rat ROBO1 or human ROBO2 Fc Chimera proteins for ROBO1 and ROBO2 inhibition, respectively. The lung explants were analyzed morphometrically and ROBO1, ROBO2, SOX2, SOX9, BMP4, and β-Catenin were quantified by Western blot.

Results: Experimental-CDH induces distinct expression profiles by pulmonary structure and developmental stage for both receptors (ROBO1 and ROBO2) and epithelial progenitor markers (SOX2 and SOX9) that provide evidence of the impairment of proximodistal patterning in experimental-CDH. Ex vivo functional studies showed unchanged branching morphogenesis after ROBO1 inhibition; increased fetal lung growth after ROBO2 inhibition in a mechanism-dependent on SOX2 depletion and overexpression of SOX9, non-phospho β-Catenin, and BMP4.

Conclusions: These studies provided evidence of receptors and epithelial progenitor cells which are severely affected by CDH-induction from embryonic-to-saccular stages and established the ROBO2 inhibition as promoter of branching morphogenesis through SOX2/SOX9 balance.

Keywords: Branching, CDH, Epithelial progenitors, ROBO, SOX

Background

Respiratory function depends on proximal or conducting airways that allow the continuous passageway of air and the distal or respiratory airways, where the gas exchange takes place [1, 2]. Interestingly, a family of transcription

*Correspondence: cristinasilva@med.uminho.pt
[1] Life and Health Sciences Research Institute (ICVS), School of Medicine, University of Minho, Campus de Gualtar, 4710-057 Gualtar, Braga, Portugal
Full list of author information is available at the end of the article

factors, SRY-related high-mobility-group, HMG, box (SOX) proteins, that bind DNA in a sequence-specific manner defined the proximal and distal arrangement during fetal life. Indeed, the fetal lung development starts from a multipotent stem cell population (SOX9 positive) that forms the most, if not all, conducting airways in a mechanism dependent on Wntless (Wnt), bone morphogenetic protein (BMP), and fibroblast growth factor (FGF) signaling ([3–10], reviewed in [11]). In brief, FGF10 directly activates β-Catenin in the distal epithelial progenitors, and induces BMP4 and SOX9 expression, to maintain and keep cells from differentiating into the SOX2 conducting airway epithelium. As the epithelial tube grows towards the distal source of FGF10, progeny from the distal multipotent epithelial progenitor are left behind in the epithelial stalk and once they are out of FGF reach they lose SOX9, β-Catenin and BMP4, start expressing SOX2, and differentiate into conducting airway epithelium ([3–10], reviewed in [11]). Finally, it is the separate capacity of SOX2 versus SOX9 cells to be differentiated in bronchiolar and alveolar lineages, respectively, that allows the morphological distinction between conducting and respiratory airways at the end of canalicular stage and pulmonary maturation at saccular phase in preparation for the first breath at birth [3, 4, 12–14].

Neonatal respiratory failure is common in moderate-to-severe cases of congenital diaphragmatic hernia (CDH). CDH is defined by a diaphragmatic defect that allows the herniation of abdominal organs into the thorax and consequently lung hypoplasia, affecting 1 in 3000 live-births [15, 16]. These hypoplastic lungs, strictly associated with high rates of mortality and morbidity, demonstrate a reduced number of terminal buds at early developmental stages (embryonic/pseudoglandular); reduced surface areas; and a decrease in distal branching and alveoli (saccular/alveolar) that impaired the efficient gas exchanges [17, 18]. Molecularly, the study of the underlying mechanisms demonstrated stage-dependent dynamics for BMP, WNT, or FGF pathways in experimental-CDH ([19–23], reviewed in [24]) with unexplored SOX2 or SOX9 profiles.

Genome-wide and transcriptome studies in CDH versus normal lungs in humans and rodents described high priority genes and pathways, such as ROBO/SLIT, as potential therapeutic target for the diaphragmatic defect repair [25, 26]. *Roundabout* (*Robo*) genes encode cell-surface receptors that respond to their secreted ligands, SLIT proteins, in a wide variety of cellular processes. In the lung, ROBO/SLIT knockout is inductor of diaphragm defect, delayed separation of foregut from the body wall [27], poor lung inflation and lethality at birth [27, 28]. On the other hand, ROBO/SLIT signaling is described in regulation of cell proliferation or progenitor cell profile in the development of mammary gland [29, 30], a branching organ-like lung, and in the central nervous system [31]. These intriguing functions as regulator of progenitor cell profile in development of mammary gland and central nervous system and inductor of the morphological defects in fetal lung development allowed us to hypothesize the ROBO1/2 as regulators of SOX2/SOX9 balance in fetal lung development, particularly in branching morphogenesis.

In this context, considering the intricate morphological, cellular and molecular dynamics during fetal lung development that determine the complex architecture of the lung at birth, the purpose of our investigation was determine the spatiotemporal distribution for receptors (ROBO1 and ROBO2) and epithelial progenitor markers (SOX2 and SOX9) from embryonic-to-saccular developmental stages in nitrofen-induced CDH rat model; and to identify the molecular effect of ROBO1 and ROBO2 inhibition in both ex vivo branching morphogenesis and SOX2/SOX9 profiles.

Methods

Animal model and experimental design

This study was carried out in strict accordance with FELASA guidelines [32] and with European (European Union Directive 86/609/EEC) regulation. The protocol was approved by the Direção Geral de Alimentação e Veterinária (DGAV 021328).

Female Sprague–Dawley rats (225 g; Charles-River; Spain) were maintained in appropriate cages under controlled conditions and fed with commercial solid food. The rats were mated and checked daily for vaginal plug. The day of plugging was defined as embryonic day (E) 0.5 for time dating purposes. According to the nitrofen-induced CDH rat model [33, 34], at E9.5, randomly selected pregnant rats were exposed to 100 mg of nitrofen (2,4-dichlorophenyl-*p*-nitrophenylether). At different time points (E13.5, E15.5, E17.5, E19.5, and E21.5), fetuses were harvested by cesarean section. After fetal decapitation, a thoracic-laparotomy was performed under a binocular surgical microscope (Leica, Wild M651.MSD, Switzerland) to inspect the diaphragm and harvest the organs.

The fetuses were divided into two groups: a control group (control) with fetuses exposed to olive oil alone, and hypoplastic group (hypoplastic) with those exposed to nitrofen. Regarding this experimental design, the assessment of diaphragmatic defects by surgical inspection at E13.5 and E15.5 is impractical. Therefore, for early gestational age, the hypoplastic group refers to the fetuses exposed to nitrofen (independently of CDH development), while at later gestational ages (E17.5, E19.5, and E21.5), the hypoplastic group refers to fetuses exposed to

nitrofen which developed CDH. Lungs were either snap-frozen in liquid nitrogen for protein extraction or fixed in 4% paraformaldehyde for immunohistochemistry. Lungs of fetuses at 13.5 days post-conception were also dissected to perform fetal lung explants cultures and posterior Western blot analysis. GPower 3.1.9.4 (Franz Faul, Universitat Kiel, Germany) was used for sample size calculation. In total, 18 dams and 165 embryonic rats were used in this study.

Immunohistochemistry

Normal and hypoplastic lungs of different gestational ages (E13.5–21.5) were fixed in 4% paraformaldehyde and embedded in paraffin as previously described [35]. 4 µm sections were placed onto glass microscope slides. Heat-induced antigen retrieval was performed with a citrate buffer. Sample sections were blocked with 4% fetal bovine serum for 1 h at room temperature and incubated with primary antibodies [ROBO1 (Cat No. sc25672) and ROBO2 (Cat No. sc16615), 1:200, overnight (ON), 4 °C, Santa Cruz Biotechnology Inc, USA; SOX2 (Cat No. AF2018) and SOX9 (Cat No. AF3075), 1:100, ON, 4 °C, R&D systems, USA] diluted in phosphate-buffered saline (PBS1x). Negative control reactions included omission of the primary antibody for which the immunoreactive staining was not observed. Tissue sections for negative control, ROBO1, SOX2, and SOX9 were labeled with a streptavidin–biotin immunoenzymatic antigen detection system (Cat No. TL-125-QHD, Thermo Scientific, USA) according to the manufacturer's instructions and visualized with a diaminobenzidine tetrahydrochloride solution (Cat No. TA-125-QHDX, Thermo Scientific, USA) [36]. Tissues sections for ROBO2 and respective negative control were labeled with biotinylated anti-goat IgG (Cat No. BA-9500, Vector Laboratories, UK) followed by streptavidin–horseradish peroxidase incubation and visualized with a diaminobenzidine tetrahydrochloride solution (DAB, Cat No. TA-125-QHDX, Thermo Scientific, USA). Sections with and without primary antibodies were simultaneously processed and analyzed. The time expended in DAB solution was variable according to the developmental stage, but equally matched between control and hypoplastic sections, allowing the quantification of immunohistochemical signals. The percentage of stained cells per microscopic field was scored in four independent areas per section (four sections per each experimental group) by two blinded observers. Scoring was as follows: 0, 0–1% cells/pulmonary structure; 1, 1–25% cells/pulmonary structure; 2, 25–50% cells/pulmonary structure; 3, 50–75% cells/pulmonary structure; 4, 75–100% cells/pulmonary structure in accordance with [37]. At least three independent experiments were performed for each antibody tested. In each experiment, a different set of slides comprising the whole range of gestational ages was used. Different and unrepeated animal samples were selected for each group (gestational age). Six different animals were examined for each group per studied antibody. All sections were scanned with Olympus BX61 Upright Microscope (Olympus corporation, Japan) and independently evaluated by two investigators.

Western blot analysis

Normal and hypoplastic lungs from different gestational ages (E13.5–E21.5) were processed for Western blot analysis in accordance with previously described methods [38, 39]. Briefly, 15 µg of protein were loaded onto 10% acrylamide mini gels, electrophoresed at 100 V at room temperature, and then transferred to nitrocellulose membranes (HybondTM-C Extra, GE Healthcare Life Sciences, UK). Blots were blocked in 5% bovine serum albumin and probed with primary antibodies to ROBO1 (1:500, ON, 4 °C; Cat No. sc25672, Santa Cruz Biotechnology Inc., USA), ROBO2 (1:250, ON, 4 °C; Cat No. sc16615, Santa Cruz Biotechnology Inc. USA), SOX2 (1:250, ON, 4 °C; Cat No. AF2018, R&D system, USA), SOX9 (1:250, ON, 4 °C; Cat No. AF3075, R&D system, USA), non-phospho (Active) β-Catenin (Ser33/37/Thr41) (1:5000; Cat No. #4270, Cell Signaling Technology Inc., USA), total β-Catenin (1:30,000; Cat No. #NBP1-54,467, NOVUS Biologicals, USA), and BMP4 (1:250, ON, 4 °C; Cat No. sc-6896, Santa Cruz Biotechnology Inc., USA) according to the manufacturer's instructions. For loading control, blots were probed with β-Tubulin (1:150.000; Cat No. ab15568, Abcam, USA). After this, membranes were incubated with a secondary horseradish peroxidase conjugate, developed with Clarity West ECL substrate (Cat No. 1705060, Bio-Rad, USA) and the chemiluminescent signal was captured using the Chemidoc XRS (Bio-Rad, USA) [36].

Quantitative analysis was performed with Quantity One 4.6.5 1-D Analysis Software (Bio-Rad, USA). Three independent experiments were performed (n = 3). In total, nine animals were used in each group (gestational age/condition) per antibody.

Fetal lung explants

Harvesting and dissection of E13.5 lungs were made in PBS under a dissection microscope (Leica MZFLIII, Switzerland). The lungs were transferred to nucleopore membranes (Cat No. TETP01300, Whatman, USA), previously presoaked in Dulbecco's modified Eagle´s medium (DMEM) low glucose (Cat. No SH30021.01, Thermo Scientific, USA) for 1 h, and incubated in a 24-well culture plate (Nunc, Denmark). Floating cultures of the explants were incubated in a complete medium [50% DMEM, 50% nutrient mixture F-12

(Gibco, USA) supplemented with 100 µg/mL glutamine (Cat. No 25030081, Gibco, USA), 100 units/mL penicillin–streptomycin, (Cat. No 15140122, Gibco, USA), 0.25 mg/mL L-ascorbic acid (Cat No. A4403, Sigma-Aldrich, USA) and 10% fetal bovine serum (FBS) (Cat No. 26140079, Gibco, USA)].

The fetal lung explants were incubated in a 5% CO_2 incubator at 37 °C for 96 h, and the medium was replaced every 48 h. The branching morphogenesis was monitored daily by photographing the explants. At day 0 (D0: 0 h) and day 4 (D4: 96 h) of culture, the total number of peripheral airway buds (branching) of all lung explants was determined by counting the number of peripheral airway epithelial buds of the developing respiratory tree [37, 40].

ROBO1 and ROBO2 inhibitory studies

Ex vivo cultures of normal lung explants were complemented daily with distinct doses of recombinant rat ROBO1 Fc Chimera (0.04, 0.4, 4 and 40 ng/mL, R&D system; Cat No. 1749-RB-050), recombinant human ROBO2 Fc Chimera (0.04, 0.4, 4 and 40 ng/mL, R&D system; Cat No. 3147-RB-050), or recombinant human IgG1 Fc (used as control at higher dose, R&D; Cat No. 110-HG-100). These doses were selected according to the literature [41, 42]. Lung explants were obtained in three independent experiments ($n \geq 9$ for each dose tested). After 4 days in culture, control, ROBO1 and ROBO2 inhibited lung explants were analyzed for branching morphogenesis in terms of area, external and internal epithelial perimeter, and the number of peripheral airway buds. In addition, SOX2, SOX9, BMP4, total and non-phospho (active) β-Catenin were quantified by Western blot at day 4 in all experimental groups.

Statistical analysis

All quantitative data are presented as mean ± standard error of the mean (SEM). The statistical analysis was performed by two-way ANOVA for lung condition (normal and hypoplastic) and embryonic day (E13.5, E15.5, E17.5, E19.5, and E21.5) on protein expression level. One-way ANOVA was performed for the number of peripheral airway buds and protein expression levels on recombinant rat ROBO1 Fc Chimera (0.04, 0.4, 4, 40 ng/mL), and recombinant human ROBO2 Fc Chimera (0.04, 0.4, 4, 40 ng/mL). The parametric test assumptions were previously verified, and an additional LSD test was used for post-test analysis. Statistical analysis was performed using the statistical software IBM SPSS Statistics 24.0. Statistical significance was confirmed at $p < 0.05$.

Results

Experimental CDH alters the relative expression levels of ROBO1, ROBO2, SOX2, and SOX9 in fetal lung development

To determine the molecular changes for ROBO1, ROBO2, SOX2 and SOX9 in experimental-CDH, the relative expression levels of each protein were analyzed by Western blot at the distinct gestational ages: E13.5, E15.5, E17.5, E19.5, and E21.5. Subsequent analysis revealed distinct molecular profiles for receptors (Fig. 1a–c) and epithelial progenitor markers (Fig. 1d and e), in normal and hypoplastic fetal lung development. Specifically, the progress of normal fetal lung development was defined by unchanged ROBO1 (Fig. 1b) and SOX2 (Fig. 1d) expression levels at E13.5, E15.5, E17.5 and E21.5, with E19.5 as the only affected stage in which the overexpression of ROBO1 (Fig. 1b) and SOX2 (Fig. 1d) was visible. In contrast, separate molecular profiles for ROBO1 (Fig. 1b) and SOX2 (Fig. 1d) were visualized in the experimental-CDH. While on the one hand, the ROBO1 (Fig. 1b) was decreased at E19.5 and overexpressed at E21.5, the SOX2 (Fig. 1d) was revealed to be downregulated at E15.5 and overexpressed at later gestational ages (E17.5-, E19.5-, and E21.5-hypoplastic versus control).

Regarding the relative expression levels of ROBO2 (Fig. 1c) and SOX9 (Fig. 1e), Western blot analysis identified an opposite effect on ROBO2 and SOX9 at later (E17.5, E19.5 and E21.5) versus early (E13.5, E15.5) developmental stages, in which the significant overexpression of ROBO2 and SOX9 depletion marked the normal lungs. In contrast, after experimental-CDH induction, ROBO2 (Fig. 1c) was significantly increased at E13.5 and E15.5 and downregulated at E17.5, while SOX9 (Fig. 1e) showed an important decrease at E15.5 and was overexpressed at E17.5 and E19.5 in experimental-CDH versus normal lungs.

To further explore these molecular profiles across hypoplastic versus normal fetal lung development, in vivo spatiotemporal distributions for ROBO1, ROBO2, SOX2, and SOX9 were analyzed by immunohistochemistry and quantified by pulmonary structure.

Distinct ROBO1 and ROBO2 spatiotemporal dynamics during normal and hypoplastic fetal lung development

Our results showed ROBO1 first expressed in mesenchymal and epithelial cells defining the undifferentiated tissues at E13.5 (Fig. 2aA) and E15.5 (Fig. 2aB). ROBO1+ was next expressed in bronchi and primordia of bronchiole (Fig. 2aC and aD) at E17.5, characterizing the first differentiated pulmonary structures in normal lungs. As lung development progressed, ROBO1 was observed in bronchi, terminal bronchiole, and bronchioalveolar junction (BADJ) at E19.5 (Fig. 2aE and aF) and E21.5 (Fig. 2aG

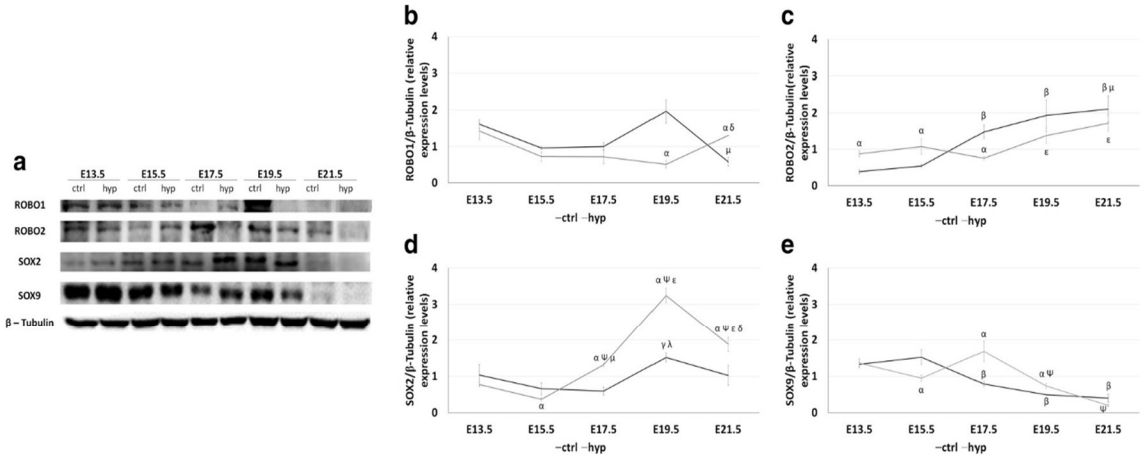

Fig. 1 Distinct expression profiles for receptors and epithelial progenitors in normal and hypoplastic lungs. **a** Examples of representative blots are shown for each protein analyzed. Western blot analysis of **b** ROBO1; **c** ROBO2; **d** SOX2; and **e** SOX9 relative expression levels in normal (ctrl) and hypoplastic (hyp) lungs at selected gestational ages from E13.5-to-E21.5. Each lane represents a pooled-tissue sample, and relative expression was determined against β-Tubulin. Semi-quantitative analysis of three independent experiments for each protein is plotted ($n \geq 9$ per timepoint and experimental groups, respectively). Results are presented as mean ± SEM. Symbols indicate the main effects and non-redundant interactions of the two-way ANOVA. $p < 0.05$: $^{\alpha}$vs. ctrl; $^{\beta}$vs. E13.5- and 15.5-ctrl; $^{\Psi}$vs E13.5- and E15.5-hyp; $^{\gamma}$vs E15.5-ctrl; $^{\mu}$vs E15.5-hyp; $^{\lambda}$vs E17.5-ctrl; $^{\varepsilon}$vs E17.5-hyp; $^{\delta}$vs E19.5-hyp

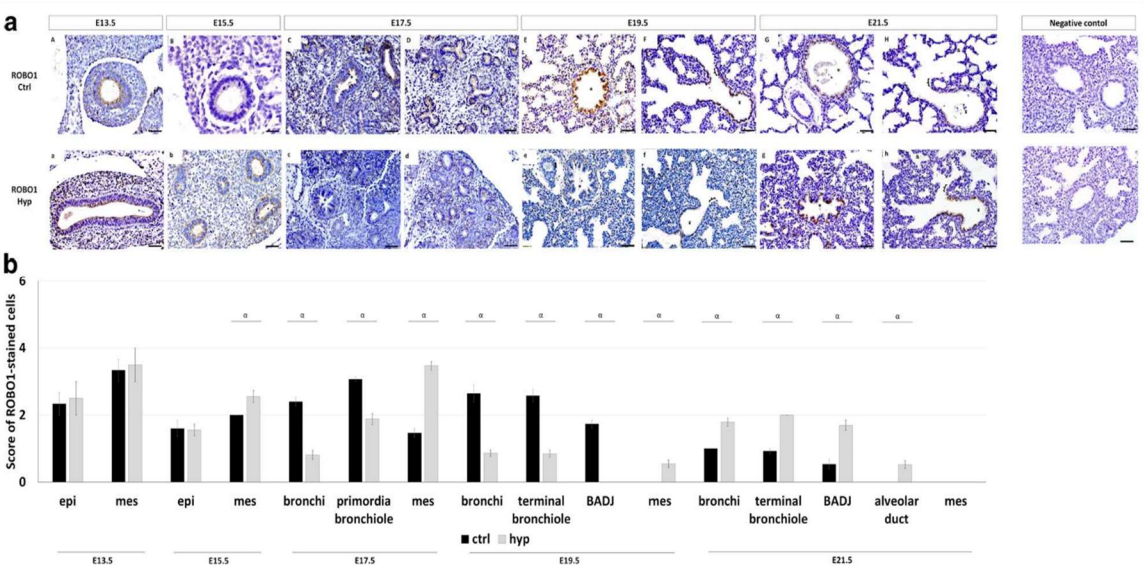

Fig. 2 ROBO1 expression profile in normal and hypoplastic lungs. **a** representative immunohistochemical evidence for the presence of ROBO1 during normal (**aA–aH**) and hypoplastic (hyp, **aa–ah**) fetal lung development at the distinct gestational ages. Symbols in each figure identify the distinct pulmonary structures: *bronchi; ¤primordia of bronchiole; ¥terminal bronchiole; {bronchioalveolar duct junction; &alveolar duct. Data is representative of $n \geq 3$ independent experiments per stage/protein. **b** ROBO1 stained cells quantified by pulmonary structure and developmental stage. Results are presented as mean ± SEM. Symbols indicate the main effects and non-redundant interactions of one-way ANOVA. $^{\alpha}p < 0.05$. Scale bar 50 μm

and aH), with important gain-or-loss expression after experimental-CDH induction (Fig. 2aa–ah). Indeed, quantification of immunohistochemistry signals demonstrated the decrease of ROBO1 expression in bronchi at E17.5 and E19.5; primordia of bronchiole at E17.5; and terminal bronchiole at E19.5 (Fig. 2b). Conversely, the overexpression of ROBO1 was visualized in bronchi, terminal bronchiole, and BADJ at E21.5 in experimental-CDH versus normal lungs (Fig. 2b). Finally, unexpected new ROBO1+ cells were observed in the alveolar duct at

E21.5 after induction of experimental-CDH (Figs. 2ag–ah and 2b).

Regarding ROBO2, the immunohistochemistry assay demonstrated restricted epithelial ROBO2 expression in undifferentiated tissues, with ROBO2+ cells staining all pulmonary structures in normal (Fig. 3aA–aH) and hypoplastic (Fig. 3aa–ah) fetal lungs. Interestingly, compared to normal lungs, the quantification of stained cells indicated ROBO2 overexpressed in epithelium at E13.5 and E15.5; bronchi and primordia of bronchiole at E17.5; and in the alveolar duct and mesenchyme at E21.5 (Fig. 3b) in the nitrofen-induced CDH rat model. In contrast, a significant decrease in ROBO2 was observed in bronchi at E19.5; terminal bronchiole and BADJ at E19.5 and E21.5 (Fig. 3b) after experimental-CDH induction. New ROBO2+ cells were observed in mesenchyme at E13.5, E15.5, and E17.5 in experimental-CDH versus normal lungs.

Damage of proximodistal patterning in experimental-CDH lungs

To define the cellular profile of proximal and distal epithelial progenitors, the spatiotemporal distribution for SOX2 and SOX9, respectively, were analyzed across the distinct gestational ages (from E13.5 to E21.5) in normal and hypoplastic lungs. Immunohistochemistry revealed initial SOX2 (Fig. 4aA and aB; and Fig. 4aa and ab) expression in undifferentiated epithelial cells that progressively populate the proximal pulmonary structures in normal fetal lung development. Specifically, SOX2 was visualized in bronchi at E17.5 (Fig. 4aC and aD), E19.5 (Fig. 4aE and aF) and E21.5 (Fig. 4aG and aH); primordia of bronchiole at E17.5; terminal bronchiole and BADJ at E19.5 and E21.5 across normal fetal lung development. Regarding experimental-CDH, overexpression of SOX2 (Fig. 4b) was detected in the undifferentiated epithelium at E13.5 (Fig. 4aa) and E15.5 (Fig. 4ab); terminal bronchiole at E19.5 (Fig. 4ae and af) and E21.5 (Fig. 4ag and ah); and bronchi at E21.5. Interestingly, no SOX2+ cells were observed in primordia of bronchiole at E17.5 in experimental-CDH, whereas significant SOX2 loss characterized the BADJ at E19.5 and E21.5 (Fig. 4b).

Concerning SOX9, the immunohistochemistry assay identified an initial SOX9 expression in epithelium at E13.5 and E15.5 and mesenchyme at E15.5 that give rise to wide staining in all pulmonary structures in normal (Fig. 5aA–aH) and hypoplastic lungs (Fig. 5aa–ah). Indeed, SOX9 was detected in bronchi at E17.5, E19.5, and E21.5; primordia of bronchiole at E17.5; terminal bronchiole and BADJ at E19.5 and E21.5; and in alveolar duct at E21.5 in normal (Fig. 5aC–aH), and hypoplastic lungs (Fig. 5ac–ah) for which the more significant differences were observed after quantification of immunohistochemical signals (Fig. 5b). Particularly in experimental-CDH, SOX9 was downregulated in

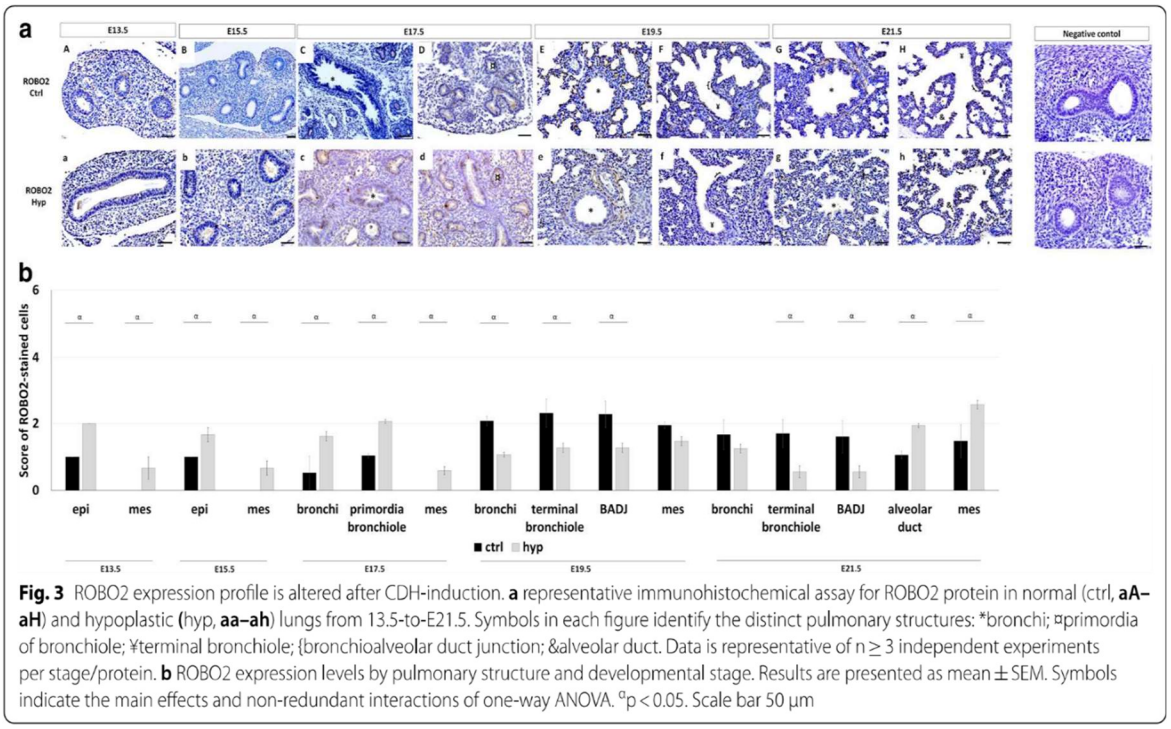

Fig. 3 ROBO2 expression profile is altered after CDH-induction. **a** representative immunohistochemical assay for ROBO2 protein in normal (ctrl, **aA–aH**) and hypoplastic (hyp, **aa–ah**) lungs from 13.5-to-E21.5. Symbols in each figure identify the distinct pulmonary structures: *bronchi; ¤primordia of bronchiole; ¥terminal bronchiole; {bronchioalveolar duct junction; &alveolar duct. Data is representative of n ≥ 3 independent experiments per stage/protein. **b** ROBO2 expression levels by pulmonary structure and developmental stage. Results are presented as mean ± SEM. Symbols indicate the main effects and non-redundant interactions of one-way ANOVA. °p < 0.05. Scale bar 50 μm

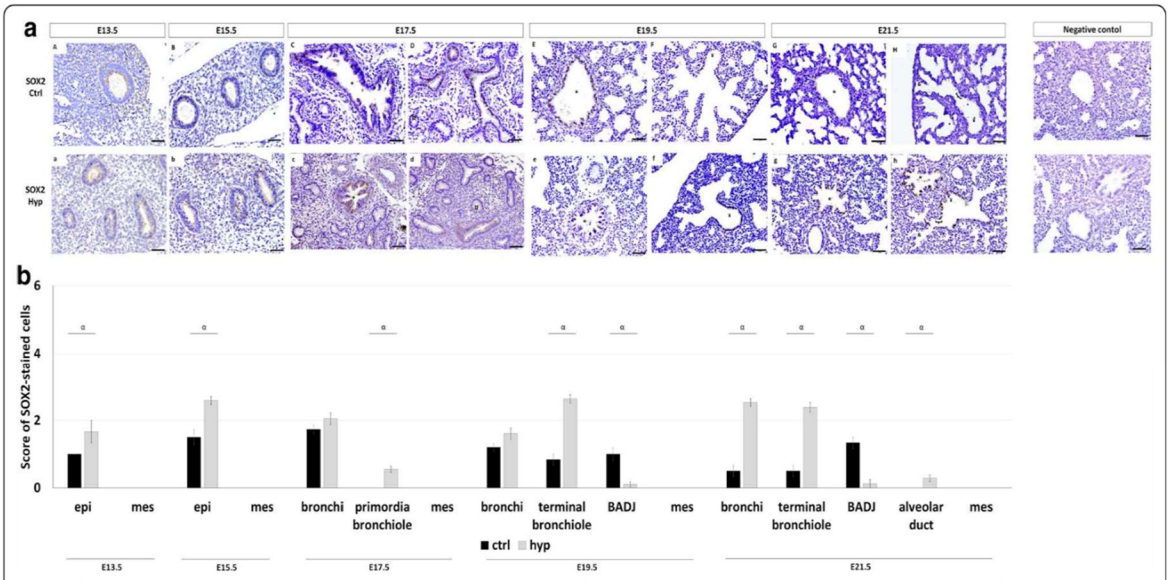

Fig. 4 Experimental CDH alters SOX2 expression profile in fetal lung development. **a** representative immunohistochemistry at the distinct analyzed gestational ages in normal (ctrl, **aA–aH**) and hypoplastic (hyp, **aa–ah**) lungs. Symbols in each figure identify the distinct pulmonary structures: *bronchi; ¤primordia of bronchiole; ¥terminal bronchiole; {bronchioalveolar duct junction; &alveolar duct. Data is representative of $n \geq 3$ independent experiments per stage/protein. **b** $SOX2^+$ positive cells were quantified by pulmonary structure and developmental stage. Results are presented as mean ± SEM. Symbols indicate the main effects and non-redundant interactions of one-way ANOVA. $^{\alpha}p < 0.05$. Scale bar 50 μm

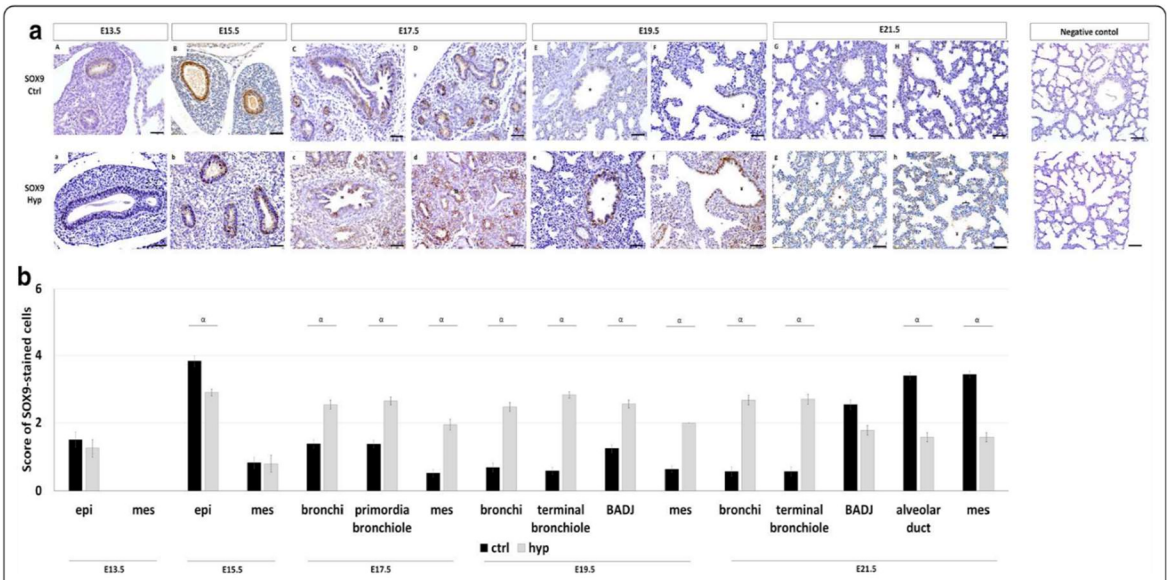

Fig. 5 SOX9 spatiotemporal distribution in normal and hypoplastic lungs. **a** Representative immunohistochemical evidence SOX9 expression along the normal (ctrl, **aA–aH**); and hypoplastic (hyp, **aa–ah**) fetal lung development, from E13.5-to-E21.5. Symbols in each figure identify the distinct pulmonary structures: *bronchi; ¤primordia of bronchiole; ¥terminal bronchiole; {bronchioalveolar duct junction; &alveolar duct. Data is representative of $n \geq 3$ independent experiments per stage/protein. **b** SOX9 stained cells quantified by pulmonary structure and developmental stage. Results are presented as mean ± SEM. Symbols indicate the main effects and non-redundant interactions of one-way ANOVA. $^{\alpha}p < 0.05$. Scale bar 50 μm

epithelium at E15.5 and in alveolar duct and mesenchyme at E21.5, whereas their overexpression was simultaneously observed in bronchi at E17.5, E19.5, and E21.5; primordia of bronchiole at E17.5; terminal bronchiole at E19.5 and E21.5; BADJ at E19.5; and mesenchyme at E17.5 and E19.5 (Fig. 5b).

These new findings urged us to explore the function of ROBO1 and ROBO2 in fetal lung development, particularly in branching morphogenesis and in SOX2/SOX9 expression profiles. For that, lung explant cultures at E13.5, previous reported as comparable to the in vivo lung both in structure and function, were selected as a model, in which restricted inhibition of ROBO1 or ROBO2 was performed followed by branching morphogenesis analysis and SOX2, SOX9, total and non-phospho (active) β-Catenin and BMP4 quantification at day 4.

ROBO2 inhibition promotes branching morphogenesis

Ex vivo fetal lung explant cultures, at E13.5, were supplemented with IgG; recombinant ROBO1, or ROBO2 chimera proteins. When added to the culture medium, ROBO1 and ROBO2 chimera proteins selectively inhibit ROBO1 and ROBO2 function [41, 42]. In addition, apart from the ROBO1 and ROBO2 quantification, Western blot analysis was also performed for SOX2, SOX9, total, and non-phospho (active) β-Catenin and BMP4 at day4.

Our results showed inhibition of ROBO2 as stimulator of branching morphogenesis from 0.04-to-40 ng/mL (Fig. 6a, b), while no significant differences in terms of number of peripheral airway buds were observed after ROBO1 inhibition (Fig. 6a, b). Molecular analysis showed significant ROBO1 and ROBO2 downregulation after supplementing the medium with recombinant rat ROBO1 Fc Chimera and recombinant human ROBO2 Fc Chimera, respectively, both versus recombinant human IgG Fc used as control (Fig. 6c, d). In addition, the overexpression of SOX2 (Fig. 6e) and total β-Catenin (Fig. 6g) with downregulation of BMP4 (Fig. 6i) and unchanged non-phospho (active) β-Catenin (Fig. 6h) and SOX9 (Fig. 6f) was identified after ROBO1 inhibition contrast, with a significative decrease in both SOX2 (Fig. 6e) and BMP4 (Fig. 6i); overexpression of SOX9 (Fig. 6f), non-phospho (active) (Fig. 6h) and total β-Catenin (Fig. 6g) observed after ROBO2 inhibition in promotion of fetal lung branching morphogenesis.

Discussion

Despite the various distinct models used for the study of CDH, the nitrofen-induced CDH rat model is the most extensively used, particularly for the study of cellular and molecular mechanisms at early developmental stages since it produces diaphragmatic hernias and abnormal lungs. In fact, the nitrofen administration to pregnant dams midgestation causes developmental anomalies that reasonably replicate the major abnormalities and the pathophysiology described in human CDH, namely the specific location and extent of the diaphragmatic defects, lung hypoplasia, pulmonary hypertension, cardiovascular and skeletal defects (reviewed in [24], reviewed in [43]). On the other hand, the surgical model is employed to test promising antenatal therapies since it better mimics the later human developmental stage, alveolarization, and the cardiopulmonary transition at birth (reviewed in [24], reviewed in [43]). Our research aimed to determine the cellular/molecular alterations in CDH context at early developmental stages, embryonic-to-saccular, and thus the nitrofen-induced CDH rat model was the selected strategy.

Our findings demonstrated changes in spatiotemporal distribution and relative expression levels for both receptors (ROBO1 and ROBO2) and epithelial progenitor markers (SOX2 and SOX9) in experimental-CDH versus normal lungs, according to pulmonary structure and developmental stage. In brief, the overexpression of ROBO2 and SOX2 in epithelium and the new ROBO2+ cells in mesenchyme defined the undifferentiated tissues in CDH. In contrast, at the time the first pulmonary structures are formed, distinct molecular profiles for ROBO1, ROBO2, SOX2 and SOX9 were visualized in epithelial cells (Fig. 7a), evidencing distinct capacities to react to molecular and environment signals in a hypoplastic lung.

Morphologic defects, such as decreased number of terminal buds at early and reduced air space and thicker septa at later developmental stages, characterize a CDH

(See figure on next page.)

Fig. 6 Effect of ROBO1 or ROBO2 functional impairment in branching morphogenesis. **a** The upper panel is representative of untreated lung explants (0 ng/mL) at D0; the bottom panel represents lung explants treated with recombinant IgG protein (0 ng/mL) and several doses of recombinant ROBO1 or ROBO2 proteins at day 4 (D4). **b** Morphometric analysis of the number of peripheral airway buds of fetal rat lung explants treated with increasing concentrations of recombinant ROBO1 (black) and ROBO2 (gray) proteins. Results are expressed as the D4/D0 ratio. **c** Examples of representative blots are showed for each analysed protein. Protein expression levels of **d** ROBO; **e** SOX2; **f** SOX9; **g** total β-Catenin; **h** non-phospho (active) β-Catenin; and **i** BMP4 in normal explant cultures treated with recombinant rat ROBO1 Fc Chimera for ROBO1 inhibition (black line) or recombinant human ROBO2 Fc Chimera for ROBO2 functional impairment (gray line). Recombinant human IgG Fc was used as control (IgG). $n \geq 9$ per protein/condition. Each lane represents a pooled-tissue sample, and relative expression was determined against β-Tubulin and IgG. The data are presented as means ± SEM. $p < 0.05$: $^{\alpha}$vs. IgG

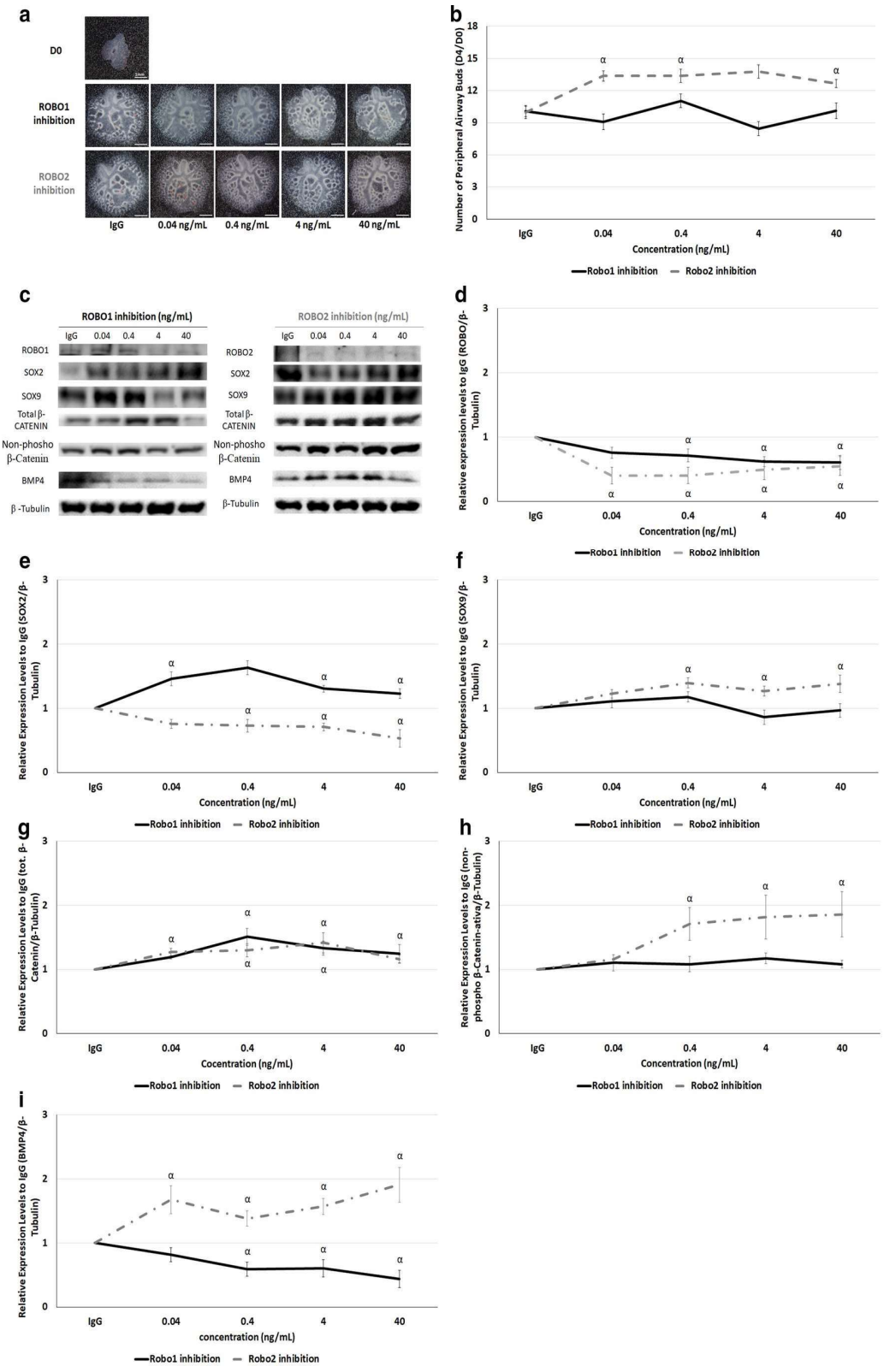
a
D0
ROBO1 inhibition
ROBO2 inhibition
IgG
0.04 ng/mL
0.4 ng/mL
4 ng/mL
40 ng/mL
b
Number of Peripheral Airway Buds (D4/D0)
Concentration (ng/mL)
Robo1 inhibition
Robo2 inhibition
c
ROBO1 inhibition (ng/mL)
ROBO2 inhibition (ng/mL)
ROBO1
ROBO2
SOX2
SOX9
Total β-CATENIN
Non-phosho β-Catenin
BMP4
β -Tubulin
d
Relative expression levels to IgG (ROBO/β-Tubulin)
e
Relative Expression Levels to IgG (SOX2/β-Tubulin)
f
Relative Expression Levels to IgG (SOX9/β-Tubulin)
g
Relative Expression Levels to IgG (tot. β-Catenin/β-Tubulin)
Cocentration (ng/mL)
h
Relative Expression Levels to IgG (non-phospho β-Catenin-ativa/β-Tubulin)
i
Relative Expression Levels to IgG (BMP4/β-Tubulin)
concentration (ng/mL)

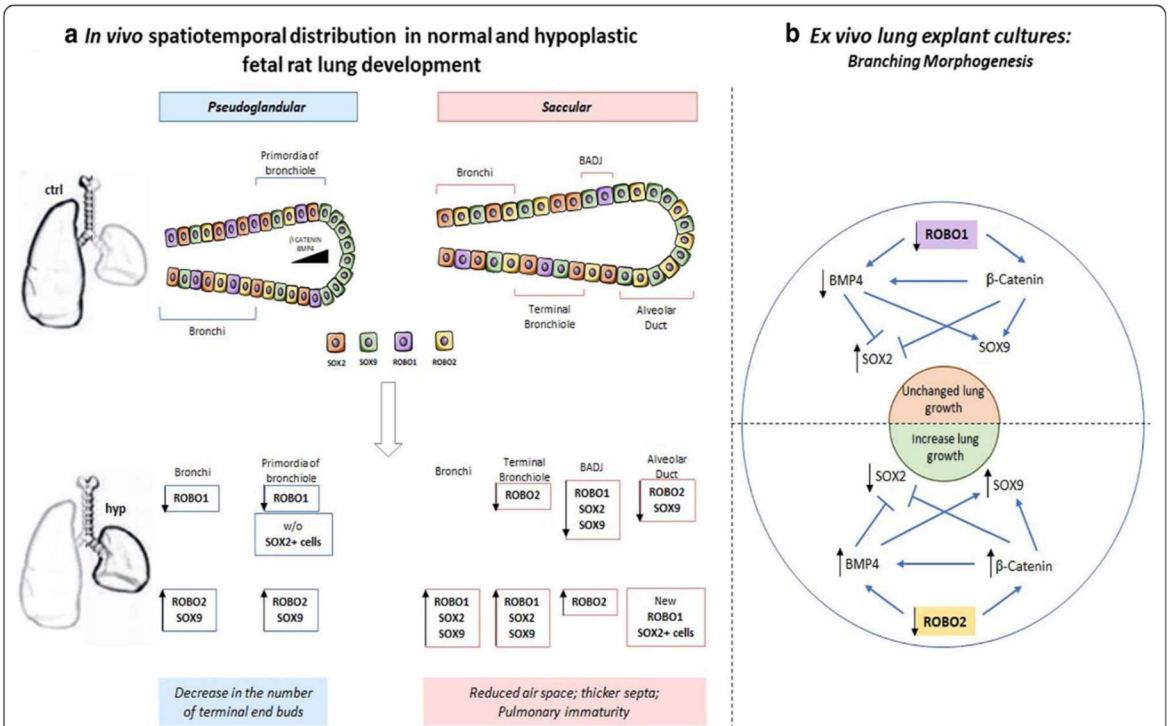

Fig. 7 **a** Overview of the main changes in spatiotemporal distribution of ROBO1, ROBO2, SOX2 and SOX9 at pseudoglandular (E17.5) and saccular stages (E21.5) in hypoplastic (hyp) fetal lungs (lower panel). w/o without **b** A proposed model of ROBO regulation of ex vivo branching morphogenesis through BMP4, β-Catenin, SOX2 and SOX9

lung in both human infant and animal models. Underlying these morphological anomalies, our in vivo data demonstrated the impairment of proximodistal patterning from pseudoglandular-to-saccular stages (Fig. 7a), contributing to a better understanding of CDH pathogenesis. Indeed, the previous studies showed the proximodistal patterning formed at pseudoglandular stage building the functional units, i.e. the conducting airways, and respiratory airways at canalicular and saccular phases in preparation for the first breath at birth [3, 4, 12–14]. In addition, severe defects in branching morphogenesis and epithelial cell differentiation were observed after SOX2 [4, 13] or SOX9 [3] knockout. Our results also exposed distinct expression profiles suggesting three independent zones (bronchi and terminal bronchiole; BADJ; and alveolar duct) in a hypoplastic lung, able to distinctly react to molecular or environmental signals at E21.5. This study is the first to present SOX2/SOX9 analysis by pulmonary structure. In the adjacent literature, the molecular regulators of SOX2/SOX9 profiles (WNT, FGF, or BMP) have been confusedly reported in a separate studies with undefined conclusions ([19–23], reviewed in [24]), because of the limited information that can be taken from the protein quantification in the whole lung. Indeed, when we are looking for formation of the conducting and respiratory airways defined by proximodistal patterns, molecular and cellular analysis by pulmonary structure could be relevant, particularly in pathologic scenarios, since distinct mechanisms can be at work.

Therefore, our investigation provides novel observations concerning the impairment of SOX2 versus SOX9 profiles and the morphological defects in experimental-CDH. In this context, research revealing the mechanisms underlying SOX2/SOX9 expression in fetal lung development is of paramount importance since it allows the manipulation of branching morphogenesis and later the formation of conducting and respiratory airways. Using ex vivo lung explants cultures, we detected the ROBO2 inhibition as stimulator of fetal lung growth through activation of β-Catenin and BMP4 that promote SOX9 instead of SOX2 profiles. In contrast, the decrease of BMP4 and SOX2 increase visible after ROBO1 inhibition determines unaffected branching morphogenesis (Fig. 7b). Importantly, lung explant cultures are described as a useful method in the study of branching morphogenesis since they maintain the native physiological interaction between cells in the developing lung. Simultaneously, molecular analysis of the proximal and distal network in terms of SOX2, SOX9, BMP4 and active β-Catenin (target of Wnt pathway) (reviewed in

[11]) allowed us to validate our ex vivo results regarding the molecular effects of ROBO2 inhibition in fetal lung growth and SOX9/SOX2 balance, since the proximodistal patterning is dependent on BMP4 and β-Catenin working in gradient in the distal tip of the lung (Fig. 7a).

Our in vivo observations also showed the overexpression of ROBO2 in lung hypoplasia, whereas the significant decrease of ROBO2 promotes the ex vivo branching morphogenesis, indicating a concordant role for ROBO2 in in vivo and ex vivo branching morphogenesis, respectively. In addition, there is similar inhibition of ROBO1 and overexpression of ROBO2 and SOX9 in bronchi and primordia of bronchiole with loss of SOX2+ cells only in primordia of bronchiole in experimental-CDH (Fig. 7a). This contrasts with the consistent opposite effect on SOX2 and SOX9 expression triggered by ROBO2 inhibition in ex vivo branching morphogenesis (Fig. 7b), providing evidence of the complexity of the in vivo model. Finally, genetic studies showing the impairment of SOX2 [44] and ROBO/SLIT signaling [25, 26] in human patients with CDH further validate the investigation of these targets in fetal lung development and particularly in CDH.

The literature has demonstrated a close relationship between epithelial and vascular development during fetal lung morphogenesis. Indeed, the downregulation of BMP, Wnt or transforming growth factor beta (TGFβ) signaling was previously associated not only with lung hypoplasia but also with pulmonary vascular remodeling, responsible for the development of persistent pulmonary hypertension at birth in a nitrofen-induced CDH rat model (reviewed in [21, 24, 45–48]). These observations are particularly relevant for in vivo studies since the development of the fetal lung and cardiovascular system cannot be separated when they divide the same molecular regulators, like BMP4. Our results showed that ROBO2 inhibition increases BMP4 expression and also branching morphogenesis. Thus, it is acceptable to suppose a simultaneous molecular effect of ROBO2 inhibition on epithelial and vascular branching, and consequent reversion of pulmonary hypoplasia and pulmonary hypertension in an experimental CDH context. In addition, the literature showed another SOX family member, SOX7, deleted in human infants with CDH [44] with functions in diaphragm formation [49], cardiovascular development [50] and in regulation of lineage decisions in cardiovascular progenitor cells [51] These functions are also identified for ROBO/SLIT signaling in fetal lung development, suggesting a potential association between SOX7 and ROBO/SLIT pathways.

Despite all the new findings reported here, we cannot ignore the limitations of our study regarding the in vivo applicability of this target and the challenge of treating a fetus patient, where several dysfunction pathways can be simultaneously targeted with one single treatment. Indeed, the careful analysis of our results suggests a limited applicability of ROBO2 in CDH. Although our observations report an upstream target that forms SOX9 instead of SOX2 progenitor cells at pseudoglandular stage, the literature showed distal and proximal progenitors giving rise to alveolar and bronchiolar lineages, respectively, in the next developmental stages in a mechanism dependent on both molecular and environment signals. In this context, the differentiated profile of the epithelial progenitor cells become unpredictable in a pathologic scenario, like CDH. Indeed, previous studies reported dysregulated factors involved in differentiation of airway epithelium in a nitrofen-induced CDH rat model (reviewed in [49]). Now, we describe cellular problems regarding the major coordinators of bronchiolar and alveolar differentiation, reinforcing the unanswered question: is the CDH pathogenesis a problem of differentiated or undifferentiated tissues?

Conclusion

Our data provide the first evidence that receptors (ROBO1 and ROBO2) and epithelial progenitor markers (SOX2 and SOX9) are affected in experimental-CDH from embryonic-to-saccular stages and identified the ROBO2 inhibition as stimulator of branching morphogenesis and regulator of SOX2/SOX9 profiles through β-Catenin and BMP4 that could play important roles not only in stimulating in vivo lung growth, but also proximodistal patterning. Although ROBO2 inhibitors could be a promising therapeutic strategy for treatment of pulmonary hypoplasia related to CDH, more studies are necessary to carefully evaluate the differentiated capacity of these epithelial progenitor cells in the in vivo CDH context and the potential improvement in both lung morphological defects and neonatal respiratory function.

Abbreviations

BADJ: Bronchioalveolar junction; BMP: Bone morphogenetic protein; CDH: Congenital diaphragmatic hernia; DAB: Diaminobenzidine tetrahydrochloride; DMEM: Dulbecco's modified Eagle medium; E: Embryonic day; FGF: Fibroblast growth factor; HMG: High-mobility-group; PBS: Phosphate-buffered saline; ROBO: Roundabout; SOX: SRY-related high-mobility-group box; Wnt: Wntless.

Acknowledgements

We are indebted to Goreti Pinto, Magda Carlos and Alice Miranda for expert technical assistance.

Authors' contributions

ANG performed the research, analyzed the data and wrote the paper; JCP designed the research and analyzed the data; CNS designed the research, analyzed the data and wrote the paper. All authors read and approved the final manuscript.

Funding
This work has been funded by National funds, through the Foundation for Science and Technology (FCT)—project UIDB/50026/2020; by the projects NORTE-01-0145-FEDER-000013 and NORTE-01-0145-FEDER-000023, supported by Norte Portugal Regional Operational Programme (NORTE 2020), under the PORTUGAL 2020 Partnership Agreement, through the European Regional Development Fund (ERDF); and by ICVS Scientific Microscopy Platform, member of the national infrastructure PPBI—Portuguese Platform of Bioimaging (PPBI-POCI-01-0145-FEDER-022122); This work was also funded by POCI-01-0145-FEDER-030881, financed by Fundos Europeus Estruturais e de Investimento (FEEI) and FCT. ANG was supported by FCT and the company José de Mello Saúde S.A.—2CA Braga (reference PD/BDE/127829/2016). The funders had no role in study design, data collection, and analysis, decision to publish, or preparation of the manuscript.

Availability of data and materials
Data sharing is not applicable to this article as no datasets were generated or analyzed during the current studies.

Ethics approval and consent to participate
All experiments using pregnant female Sprague–Dawley rats and their fetuses were carried out in strict accordance with FELASA guidelines and European (European Union Directive 86/609/EEC) regulation. The protocol was approved by Direção Geral de Alimentação e Veterinária (DGAV 021328).

Consent for publication
Not applicable.

Competing interests
The authors declare that they have no competing interests.

Author details
[1] Life and Health Sciences Research Institute (ICVS), School of Medicine, University of Minho, Campus de Gualtar, 4710-057 Gualtar, Braga, Portugal. [2] ICVS/3B's - PT Government Associate Laboratory, Braga/Guimarães, Portugal. [3] Department of Pediatric Surgery, Hospital de Braga, Braga, Portugal. [4] Department of Obstetrics and Gynecology, Hospital de Braga, Braga, Portugal.

Received: 4 August 2020 Accepted: 9 November 2020
Published online: 18 November 2020

References

1. Davis RP, Mychaliska GB. Neonatal pulmonary physiology. Semin Pediatr Surg. 2013;22:179–84.
2. Morton SU, Brodsky D. Fetal physiology and the transition to extrauterine life. Clin Perinatol. 2016;43:395–407.
3. Rockich BE, Hrycaj SM, Shih HP, Nagy MS, Ferguson MA, Kopp JL, Sander M, Wellik DM, Spence JR. Sox9 plays multiple roles in the lung epithelium during branching morphogenesis. Proc Natl Acad Sci USA. 2013;110:E4456-4464.
4. Gontan C, de Munck A, Vermeij M, Grosveld F, Tibboel D, Rottier R. Sox2 is important for two crucial processes in lung development: branching morphogenesis and epithelial cell differentiation. Dev Biol. 2008;317:296–309.
5. Hashimoto S, Chen H, Que J, Brockway BL, Drake JA, Snyder JC, Randell SH, Stripp BR. β-Catenin-SOX2 signaling regulates the fate of developing airway epithelium. J Cell Sci. 2012;125:932–42.
6. Park WY, Miranda B, Lebeche D, Hashimoto G, Cardoso WV. FGF-10 is a chemotactic factor for distal epithelial buds during lung development. Dev Biol. 1998;201:125–34.
7. El Agha E, Herold S, Al Alam D, Quantius J, MacKenzie B, Carraro G, Moiseenko A, Chao CM, Minoo P, Seeger W, Bellusci S. Fgf10-positive cells represent a progenitor cell population during lung development and postnatally. Development. 2014;141:296–306.
8. Weaver M, Dunn NR, Hogan BL. Bmp4 and Fgf10 play opposing roles during lung bud morphogenesis. Development. 2000;127:2695–704.
9. Weaver M, Yingling JM, Dunn NR, Bellusci S, Hogan BL. Bmp signaling regulates proximal-distal differentiation of endoderm in mouse lung development. Development. 1999;126:4005–15.
10. Eblaghie MC, Reedy M, Oliver T, Mishina Y, Hogan BL. Evidence that autocrine signaling through Bmpr1a regulates the proliferation, survival and morphogenetic behavior of distal lung epithelial cells. Dev Biol. 2006;291:67–82.
11. Volckaert T, De Langhe SP. Wnt and FGF mediated epithelial–mesenchymal crosstalk during lung development. Dev Dyn. 2015;244:342–66.
12. Chang DR, Martinez Alanis D, Miller RK, Ji H, Akiyama H, McCrea PD, Chen J. Lung epithelial branching program antagonizes alveolar differentiation. Proc Natl Acad Sci USA. 2013;110:18042–51.
13. Tompkins DH, Besnard V, Lange AW, Wert SE, Keiser AR, Smith AN, Lang R, Whitsett JA. Sox2 is required for maintenance and differentiation of bronchiolar Clara, ciliated, and goblet cells. PLoS ONE. 2009;4:e8248.
14. Tompkins DH, Besnard V, Lange AW, Keiser AR, Wert SE, Bruno MD, Whitsett JA. Sox2 activates cell proliferation and differentiation in the respiratory epithelium. Am J Respir Cell Mol Biol. 2011;45:101–10.
15. Cotten CM. Pulmonary hypoplasia. Semin Fetal Neonatal Med. 2017;22:250–5.
16. Goncalves AN, Correia-Pinto J, Nogueira-Silva C. Imagiological methods for prediction of fetal pulmonary hypoplasia: a systematic review. J Matern Fetal Neonatal Med. 2019. https://doi.org/10.1080/14767058.2019.1636029.
17. Coughlin MA, Werner NL, Gajarski R, Gadepalli S, Hirschl R, Barks J, Treadwell MC, Ladino-Torres M, Kreutzman J, Mychaliska GB. Prenatally diagnosed severe CDH: mortality and morbidity remain high. J Pediatr Surg. 2016;51:1091–5.
18. Kluth D, Tenbrinck R, von Ekesparre M, Kangah R, Reich P, Brandsma A, Tibboel D, Lambrecht W. The natural history of congenital diaphragmatic hernia and pulmonary hypoplasia in the embryo. J Pediatr Surg. 1993;28:456–62; discussion 462–453.
19. Takayasu H, Nakazawa N, Montedonico S, Puri P. Down-regulation of Wnt signal pathway in nitrofen-induced hypoplastic lung. J Pediatr Surg. 2007;42:426–30.
20. Gosemann JH, Friedmacher F, Fujiwara N, Alvarez LA, Corcionivoschi N, Puri P. Disruption of the bone morphogenetic protein receptor 2 pathway in nitrofen-induced congenital diaphragmatic hernia. Birth Defects Res B. 2013;98:304–9.
21. Makanga M, Dewachter C, Maruyama H, Vuckovic A, Rondelet B, Naeije R, Dewachter L. Downregulated bone morphogenetic protein signaling in nitrofen-induced congenital diaphragmatic hernia. Pediatr Surg Int. 2013;29:823–34.
22. Takahashi H, Friedmacher F, Fujiwara N, Hofmann A, Kutasy B, Gosemann JH, Puri P. Pulmonary FGF-18 gene expression is downregulated during the canalicular-saccular stages in nitrofen-induced hypoplastic lungs. Pediatr Surg Int. 2013;29:1199–203.
23. Takayasu H, Nakazawa N, Montedonico S, Sugimoto K, Sato H, Puri P. Impaired alveolar epithelial cell differentiation in the hypoplastic lung in nitrofen-induced congenital diaphragmatic hernia. Pediatr Surg Int. 2007;23:405–10.
24. Montalva L, Zani A. Assessment of the nitrofen model of congenital diaphragmatic hernia and of the dysregulated factors involved in pulmonary hypoplasia. Pediatr Surg Int. 2019;35:41–61.
25. Russell MK, Longoni M, Wells J, Maalouf FI, Tracy AA, Loscertales M, Ackerman KG, Pober BR, Lage K, Bult CJ, Donahoe PK. Congenital diaphragmatic hernia candidate genes derived from embryonic transcriptomes. Proc Natl Acad Sci USA. 2012;109:2978–83.
26. Longoni M, High FA, Russell MK, Kashani A, Tracy AA, Coletti CM, Hila R, Shamia A, Wells J, Ackerman KG, et al. Molecular pathogenesis of congenital diaphragmatic hernia revealed by exome sequencing, developmental data, and bioinformatics. Proc Natl Acad Sci USA. 2014;111:12450–5.
27. Domyan ET, Branchfield K, Gibson DA, Naiche LA, Lewandoski M, Tessier-Lavigne M, Ma L, Sun X. Roundabout receptors are critical for foregut separation from the body wall. Dev Cell. 2013;24:52–63.
28. Xian J, Clark KJ, Fordham R, Pannell R, Rabbitts TH, Rabbitts PH. Inadequate lung development and bronchial hyperplasia in mice with a targeted deletion in the Dutt1/Robo1 gene. Proc Natl Acad Sci USA. 2001;98:15062–6.

29. Ballard MS, Zhu A, Iwai N, Stensrud M, Mapps A, Postiglione MP, Knoblich JA, Hinck L. Mammary stem cell self-renewal is regulated by Slit2/Robo1 signaling through SNAI1 and mINSC. Cell Rep. 2015;13:290–301.
30. Harburg G, Compton J, Liu W, Iwai N, Zada S, Marlow R, Strickland P, Zeng YA, Hinck L. SLIT/ROBO2 signaling promotes mammary stem cell senescence by inhibiting Wnt signaling. Stem Cell Rep. 2014;3:385–93.
31. Borrell V, Cardenas A, Ciceri G, Galceran J, Flames N, Pla R, Nobrega-Pereira S, Garcia-Frigola C, Peregrin S, Zhao Z, et al. Slit/Robo signaling modulates the proliferation of central nervous system progenitors. Neuron. 2012;76:338–52.
32. Benavides F, Rulicke T, Prins JB, Bussell J, Scavizzi F, Cinelli P, Herault Y, Wedekind D. Genetic quality assurance and genetic monitoring of laboratory mice and rats: FELASA Working Group Report. Lab Anim. 2019;54(2):135–48.
33. Tenbrinck R, Tibboel D, Gaillard JL, Kluth D, Bos AP, Lachmann B, Molenaar JC. Experimentally induced congenital diaphragmatic hernia in rats. J Pediatr Surg. 1990;25:426–9.
34. Nogueira-Silva C, Piairo P, Carvalho-Dias E, Veiga C, Moura RS, Correia-Pinto J. The role of glycoprotein 130 family of cytokines in fetal rat lung development. PLoS ONE. 2013;8:e67607.
35. Nogueira-Silva C, Piairo P, Carvalho-Dias E, Peixoto FO, Moura RS, Correia-Pinto J. Leukemia inhibitory factor in rat fetal lung development: expression and functional studies. PLoS ONE. 2012;7:e30517.
36. Peixoto FO, Pereira-Terra P, Moura RS, Carvalho-Dias E, Correia-Pinto J, Nogueira-Silva C. The role of ephrins-B1 and -B2 during fetal rat lung development. Cell Physiol Biochem. 2015;35:104–15.
37. Nogueira-Silva C, Moura RS, Esteves N, Gonzaga S, Correia-Pinto J. Intrinsic catch-up growth of hypoplastic fetal lungs is mediated by interleukin-6. Pediatr Pulmonol. 2008;43:680–9.
38. Kling DE, Lorenzo HK, Trbovich AM, Kinane TB, Donahoe PK, Schnitzer JJ. MEK-1/2 inhibition reduces branching morphogenesis and causes mesenchymal cell apoptosis in fetal rat lungs. Am J Physiol Lung Cell Mol Physiol. 2002;282:L370-378.
39. Nogueira-Silva C, Carvalho-Dias E, Piairo P, Nunes S, Baptista MJ, Moura RS, Correia-Pinto J. Local fetal lung renin-angiotensin system as a target to treat congenital diaphragmatic hernia. Mol Med. 2012;18:231–43.
40. Massoud EA, Sekhon HS, Rotschild A, Puterman ML, Matsui R, Thurlbeck WM. In vitro branching morphogenesis of the fetal rat lung. Pediatr Pulmonol. 1993;15:89–97.
41. Ricano-Cornejo I, Altick AL, Garcia-Pena CM, Nural HF, Echevarria D, Miquelajauregui A, Mastick GS, Varela-Echavarria A. Slit-Robo signals regulate pioneer axon pathfinding of the tract of the postoptic commissure in the mammalian forebrain. J Neurosci Res. 2011;89:1531–41.
42. Garcia-Pena CM, Kim M, Frade-Perez D, Avila-Gonzalez D, Tellez E, Mastick GS, Tamariz E, Varela-Echavarria A. Ascending midbrain dopaminergic axons require descending GAD65 axon fascicles for normal pathfinding. Front Neuroanat. 2014;8:43.
43. Montalva L, Antounians L, Zani A. Pulmonary hypertension secondary to congenital diaphragmatic hernia: factors and pathways involved in pulmonary vascular remodeling. Pediatr Res. 2019;85:754–68.
44. Wat MJ, Veenma D, Hogue J, Holder AM, Yu Z, Wat JJ, Hanchard N, Shchelochkov OA, Fernandes CJ, Johnson A, et al. Genomic alterations that contribute to the development of isolated and non-isolated congenital diaphragmatic hernia. J Med Genet. 2011;48:299–307.
45. Burgos CM, Uggla AR, Fagerström-Billai F, Eklöf AC, Frenckner B, Nord M. Gene expression analysis in hypoplastic lungs in the nitrofen model of congenital diaphragmatic hernia. J Pediatr Surg. 2010;45:1445–54.
46. Makanga M, Maruyama H, Dewachter C, Da Costa AM, Hupkens E, de Medina G, Naeije R, Dewachter L. Prevention of pulmonary hypoplasia and pulmonary vascular remodeling by antenatal simvastatin treatment in nitrofen-induced congenital diaphragmatic hernia. Am J Physiol Lung Cell Mol Physiol. 2015;308:L672-682.
47. Pardali E, Ten Dijke P. TGFβ signaling and cardiovascular diseases. Int J Biol Sci. 2012;8:195–213.
48. Southwood M, Jeffery TK, Yang X, Upton PD, Hall SM, Atkinson C, Haworth SG, Stewart S, Reynolds PN, Long L, et al. Regulation of bone morphogenetic protein signalling in human pulmonary vascular development. J Pathol. 2008;214:85–95.
49. Wat MJ, Beck TF, Hernández-García A, Yu Z, Veenma D, Garcia M, Holder AM, Wat JJ, Chen Y, Mohila CA, et al. Mouse model reveals the role of SOX7 in the development of congenital diaphragmatic hernia associated with recurrent deletions of 8p23.1. Hum Mol Genet. 2012;21:4115–25.
50. Wat JJ, Wat MJ. Sox7 in vascular development: review, insights and potential mechanisms. Int J Dev Biol. 2014;58:1–8.
51. Doyle MJ, Magli A, Estharabadi N, Amundsen D, Mills LJ, Martin CM. Sox7 regulates lineage decisions in cardiovascular progenitor cells. Stem Cells Dev. 2019;28:1089–103.

Publisher's Note

Chapter 4 – Epithelial cell profile in the nitrofen-induced congenital diaphragmatic hernia rat model

The results presented in this chapter are:

i) Submitted for publication in an international peer-reviewed journal:

Gonçalves AN, Correia-Pinto J, Nogueira-Silva C. Distinct epithelial cell signatures during normal and hypoplastic fetal lung development. *submitted*.

4.1. Chapter overview

4.1.1. Rationale

Single-cell RNA sequencing and lineage-tracing studies demonstrate important cell niches in a proximodistal patterning during the development of the lung (Du et al 2015, Du et al 2017, Guo et al 2017, Guo et al 2019, Guo et al 2015, Guo & Xu 2018). In light of the results obtained in Chapter 3, where the proximodistal patterning was found to be impaired in nitrofen induced-CDH rat model, we intend to go further and investigate the epithelial cell profile of clara, PNECs, ciliated, and AT2 cells in induced-CDH lungs.

4.1.2. Major Findings

The major findings from this chapter are described below:

- CGRP is overexpressed in bronchi and terminal bronchiole in induced-CDH lungs;
- SP-C is overexpressed in bronchi, terminal bronchiole, and bronchioalveolar duct junction (BADJ) at E19.5, and in BADJ and alveolar duct at E21.5 in exposed-nitrofen CDH lungs;
- CCSP is decreased in bronchi at E19.5 and overexpressed in BADJ at E19.5 and E21.5, and in bronchi at E21.5 after CDH-induction;
- Contrary to normal lungs, FOXJ1 is expressed in BADJ at canalicular and saccular stages in induced-CDH lungs;
- In CDH lungs, the multi cilia that identify the differentiated profile of ciliated cells are almost absent in bronchi at E21.5.

Distinct epithelial cell signatures during normal and hypoplastic fetal lung development

Ana N Gonçalves (M.Sc.)[1,2], Jorge Correia-Pinto (M.D., Ph.D.)[1,2,3], Cristina Nogueira-Silva (M.D., Ph.D.)*[1,2,4]

[1]Life and Health Sciences Research Institute (ICVS), School of Medicine, University of Minho, Braga, Portugal; [2]ICVS/3B's - PT Government Associate Laboratory, Braga/ Guimarães, Portugal; [3]Department of Pediatric Surgery, Hospital de Braga, Braga, Portugal; [4]Department of Obstetrics and Gynecology, Hospital de Braga, Braga, Portugal

Abstract

Recent studies identified a great diversity of cell types in precise number and position to create the architectural features of the lung that ventilation and respiration at birth depend on. With damaged respiratory function at birth, congenital diaphragmatic hernia (CDH) is the more severe cause of fetal lung hypoplasia with unspecified cellular dynamics. As such, to characterize the epithelial cell tissue in hypoplastic lungs, a careful analysis regarding pulmonary morphology and epithelial cell profile was conducted from pseudoglandular-to-saccular phases in normal versus nitrofen-induced CDH rat lungs. Our analysis equally comprises the whole lung by quantification of the relative expression levels (western blot) and the specific pulmonary structures that were evaluated in terms of spatiotemporal distribution (immunohistochemistry). Surfactant protein-C (SP-C), calcitonin gene-related peptide (CGRP), clara cell secretory protein (CCSP), and forkhead box J1 (FOXJ1) were the used molecular markers for alveolar type II, pulmonary neuroendocrine, clara, and ciliated cell profiles, respectively.

Generally, we identified an aberrant expression of SP-C, CGRP, CCSP, and FOXJ1 in induced-CDH lungs. For instance, the overexpression of FOXJ1 and CGRP in bronchi and primordia of bronchiole defined the pseudoglandular stage, whereas the increased expression of CGRP in bronchi; FOXJ1 and CGRP in terminal bronchiole; and CCSP and SP-C in BADJ classified the canalicular and saccular hypoplastic stages. Our findings also describe unexpected FOXJ1 positive cells in BADJ at canalicular and saccular stages, whereas the multi cilia observed in bronchi were notably absent at embryonic day 21.5 in nitrofen-induced CDH lungs.

In conclusion, the recognized alterations in the epithelial cell profile contribute to a better understanding of neonatal respiratory insufficiency in induced-CDH lungs and indicate a problem in the epithelial cell differentiation in hypoplastic lungs.

Short Title: Epithelial signatures in CDH

Key Words: alveolar type II · CDH · ciliated · Clara · PNECs

Introduction

Respiratory function is dependent on lung architecture, created and maintained by interactions of myriad cells along with the gestational life (Schittny 2017a). Importantly, the traditional view of fetal lung development subdivides the lung morphogenesis into five distinct periods based on structure: embryonic, pseudoglandular, canalicular, saccular, and alveolar periods, which are shared among mammalian species (reviewed in Schittny 2017b, Warburton et al 2010). At the molecular level, it is the expression of *Nkx2-1* in the endoderm of the ventral wall of the anterior foregut that first identified the lung at the embryonic stage (Minoo et al 1999). Afterward, mesodermal-endodermal interactions support branching morphogenesis and the specification of multipotent progenitor cells into proximal (SOX2) versus distal (SOX9) profiles (Eblaghie et al 2006, El Agha et al 2014, Gontan et al 2008, Hashimoto et al 2012, Park et al 1998, Rockich et al 2013, reviewed in Volckaert & De Langhe 2015, Weaver et al 2000, Weaver et al 1999). Interestingly, the differentiation of proximodistal patterning at the time of conducting and respiratory airways formation control the neonatal respiratory function. More relevant, the current knowledge of epithelial cell differentiation admits distinct models for bronchiolar ($SOX2^+$) versus alveolar ($SOX9^+$) lineages, in which the bronchiolar differentiation gives rise to goblet, clara, ciliated, and neuroendocrine cells under mechanisms dependent on Notch signaling (Liu & Hogan 2002, Perl et al 2005, Post et al 2000, Rawlins et al 2009a, Tsao et al 2008, Wuenschell et al 1996), whereas SOX9 or a region just proximal to the $SOX9^+$ cells at early and a bipotent progenitor at later developmental stage form AT1 and AT2 cells (Frank et al 2019, Desai et al 2014, Treutlein et al 2014). AT1 cells constitute about 95% of the surface area and are located immediately adjacent to the capillaries, which allows the efficient O_2 and CO_2 diffusion, while AT2 cells secrete surfactants to prevent alveolar collapse (Barkauskas et al 2013, Desai et al 2014).

Reaching its maximum severity in the congenital diaphragmatic hernia (CDH), fetal lung hypoplasia remains one of the most common causes of morbidity and mortality for neonates. CDH is defined as a diaphragmatic defect that allows the herniation of abdominal organs into the thorax that impairs the normal fetal lung development (Cotten 2017, Gonçalves et al 2021, Nogueira-Silva et al 2008). Hypoplastic lungs have reduced surface area for gas exchange, with a decrease in distal branching and alveoli. The alveoli that do exist have thicker walls, impairing the close association of the airspaces to the capillaries (Coughlin et al 2016, Kluth et al 1993, Nogueira-Silva et al 2012). A recent publication has shown the proximodistal patterning impaired in induced-CDH lungs from pseudoglandular-to-saccular stages (Gonçalves et al 2020), whereas the epithelial cell dynamics that result from these differentiations continues uncertain. In this

context, taking advantage of the nitrofen-induced CDH rat model that mimics the *in vivo* human CDH in terms of the disrupted signal pathways in branching morphogenesis and alveolar differentiation (Montalva & Zani 2019), we performed a careful analysis regarding the pulmonary morphology and the epithelial cell profiles during normal versus hypoplastic pulmonary development.

Material and Methods

This study was carried out in strict accordance with FELASA guidelines (Benavides et al 2019) and European regulations (European Union Directive 86/609/EEC). All animal experiments were approved by the Life and Health Sciences Research Institute (ICVS), University of Minho, and by the Direção Geral de Alimentação e Veterinária (approval No. DGAV 021328).

Animal model and experimental design

Sprague-Dawley female rats (225 g; Charles-River, Spain) were maintained in appropriate cages under temperature-controlled room (22–23°C) on 12 hours' light: 12 hours' dark cycle, with commercial solid food and water *ad libitum*. The rats were mated and checked daily for vaginal plug. The day of plugging was defined as embryonic day (E) 0.5 for time dating purposes. According to the nitrofen-induced CDH rat model (Nogueira-Silva et al 2013, Tenbrinck et al 1990), at E9.5, randomly selected pregnant rats were exposed to 100 mg nitrofen (2,4- dichlorophenyl-p-nitrophenylether). At different time points (E17.5, E19.5, and E21.5), fetuses were harvested by cesarean section. After fetal decapitation, a thoracic laparotomy was performed under a binocular surgical microscope (Leica, Wild M651.MSD, Switzerland) to inspect the diaphragm and harvest the organs. Fetuses were divided into two groups, namely the control group (Ctrl), fetuses exposed to olive oil alone; and CDH group, fetuses exposed to nitrofen with the diaphragmatic defect. Lungs were either fixed in 4% paraformaldehyde for immunohistochemistry or snap-frozen in liquid nitrogen for protein extraction. GPower 3.1.9.4 (Franz Faul, Universitat Kiel, Germany) was used for sample size calculation. In total, 12 dams and 106 embryonic rats were used in this study.

Immunohistochemistry

Normal and induced-CDH lungs at different gestational ages (E17.5-21.5) were fixed in 4% paraformaldehyde and embedded in paraffin as previously described (Peixoto et al 2015). Primary antibodies for alveolar type II (AT2, Anti-Prosurfactant Protein C, Cat No. AB3786, Merck Millipore, Germany); Clara (Anti-Clara Cell Secretory Protein, Cat No. 07-623, Merck Millipore, Germany); ciliated (FOXJ1, Cat No. PA5-36210, ThermoFisher Scientific, USA); pulmonary neuroendocrine cells/

neuroepithelial bodies (PNECs/NEBs; CGRP, Cat No. ab91007, abcam, USA) were used. Negative control reactions included omission of primary antibody, in which immunoreactivity was not observed. Tissue sections were incubated with a streptavidin-biotin immunoenzymatic antigen detection system (Cat No. TL-125-QHD, Thermo Scientific, USA) according to the manufacturer's instructions and visualized with a diaminobenzidine tetrahydrochloride solution (Cat No. TA-125-QHDX, Thermo Scientific, USA) (Peixoto et al 2015). The time expended in DAB solution was dependent on the developmental stage, but equally between normal and CDH slides, allowing the quantification of immunohistochemical signals. The percentage of stained cells per microscopic field was scored in a single-blinded fashion in four independent peripheral areas per section (four sections per experimental group). Scoring was as follows: 0, 0-1% cells/pulmonary structure; 1, 1–25% cells/pulmonary structure; 2, 25–50% cells/pulmonary structure; 3, 50–75% cells/pulmonary structure; 4, 75–100% cells/pulmonary structure in accordance with (Nogueira-Silva et al 2008). At least three independent experiments were performed for each antibody tested. In each experiment, a different set of slides comprising the whole range of gestational ages was used. Different and unrepeated animal samples were selected for each group (gestational age). Six different animals were examined for each group per studied antibody. All sections were scanned with Olympus BX61 Upright Microscope (Olympus Corporation, Japan) and independently evaluated by two investigators.

Western Blot analysis

Normal and nitrofen-exposed CDH lungs from different gestational ages (E17.5 – E21.5) were processed for western blot analysis according to (Piairo et al 2018). Briefly, 15 µg of protein were loaded onto 10% acrylamide mini gels, electrophoresed at 100 V at room temperature, and then transferred to nitrocellulose membranes (HybondTM -C Extra, GE Healthcare Life Sciences, UK). Blots were blocked in 5% bovine serum albumin and probed with primary antibodies for AT2 (surfactant protein-C, SP-C, Cat No. AB3786); clara (clara cell secretory protein, CCSP, Cat No. 07-623); ciliated (FoxJ1, Cat No. PA5-36210); PNECs/NEBs (CGRP, Cat No. ab91007) were used according to the manufacturer's instructions. For loading control, blots were probed with β-tubulin (Cat No. ab15568 abcam, USA). Afterward, membranes were incubated with a secondary horseradish peroxidase conjugate, developed with Clarity West ECL subtract, and the chemiluminescent signal was captured using the Chemidoc XRS. Quantitative analysis was performed with Quantity One 4.6.5 1-D Analysis Software. Three independent experiments were performed (n=3). In total, nine animals were used in each group (gestational age/condition) per antibody.

Statistical analysis

All quantitative data are presented as the mean ± standard deviation (SD). The statistical analysis was performed by two-way ANOVA for lung condition (normal and CDH) and embryonic day (E17.5, E19.5, and E21.5) in protein expression level. The parametric test assumptions were previously verified, and an additional Fisher´s Least Significant Difference (LSD) test was used for post-test analysis. Statistical analysis was performed using the statistical software IBM SPSS Statistics 24.0. Statistical significance was set at *p< 0.05.

Results

To reveal the epithelial cell profile in hypoplastic lungs, CDH was induced by the nitrofen-induced CDH rat model, and the followed molecular markers: $CCSP^+$, $FOXJ1^+$, $CGRP^+$, and $SP\text{-}C^+$ identified the distinct epithelial cell types. The relative expression levels and the spatiotemporal distribution were revealed by western blot and immunohistochemistry (IHC), respectively, from E17.5-to-E21.5. Immunohistochemical signals were then quantified by pulmonary structure and developmental stage.

Experimental-CDH change the relative expression levels of bronchiolar and alveolar markers

In the whole lung, the quantification of the relative expression levels reveals a consistent increase in CCSP, FOXJ1, and SP-C expression as the development of the normal lung progress (Fig. 1A-E). After CDH-induction, a significant increase in FOXJ1 (Fig. 1C) and CGRP (Fig 1D) expression were observed, whereas the expression of CCSP (Fig. 1B) and SP-C (Fig. 1E) remains exchanged at pseudoglandular stage. In contrast, all makers were revealed as increased at canalicular phase. Finally, the depletion of SP-C with the overexpression of FOXJ1 and CGRP identified the saccular stage in induced-CDH lungs (Fig. 1A-E).

These molecular changes were further explored in terms of spatiotemporal distribution in CDH versus normal lungs. Concomitant with the developmental stage, this analysis also reveals the expression profile by pulmonary structure.

Similar spatiotemporal distribution for CCSP in normal and hypoplastic fetal lungs

CCSP was expressed in all pulmonary structures from pseudoglandular-to-saccular stages in normal and hypoplastic fetal lungs (Fig 2AA-AF and Aa-Af). In fact, CCSP was observed in bronchi and primordia of bronchiole at E17.5 (Fig 2AA-AB and Aa-Ab); and bronchi, terminal bronchiole, and bronchioalveolar duct junction (BADJ) at canalicular (Fig 2AC-AD and Ac-Ad) and saccular stages of normal and nitrofen-exposed lungs. Finally, CCSP+ cells were detected at E21.5 in alveolar duct (Fig 2AE-AF and Ae-Af).

Quantification of IHC signals by pulmonary structure and developmental stage demonstrated CCSP to be overexpressed in BADJ at E19.5 and E21.5, and in bronchi at E21.5 after CDH-Induction (Fig. 2B).

FOXJ1 expressed in BADJ at canalicular and saccular stages after CDH induction

FOXJ1 was used to distinguish the ciliated profile in normal and hypoplastic fetal lungs. In normal lungs, FOXJ1 was expressed in bronchi (Fig. 3AA-AF) at all gestational ages; in primordia of bronchiole at E17.5 (Fig. 3AA-AB); and terminal bronchiole at E19.5 (Fig. 3AC-AD) and E21.5 (Fig. 3AE-AF). Conversely, in induced-CDH lungs, FOXJ1 was observed in BADJ at E19.5 (Fig. 3Ac-Ad) and E21.5 (Fig. 3Ae-Af), whereas the multi cilia that characterize the differentiated profile of ciliated cells in bronchi were (near) absent at E21.5 (Fig. 3AG-Ag).

Quantification of IHC signals established FOXJ1 overexpressed in bronchi at E17.5, E19.5, and E21.5; in primordia of bronchiole at E17.5; and terminal bronchiole at E19.5 and E21.5 after CDH-induction (Fig. 3B).

Increased size of neuroepithelial bodies (NEBs) at canalicular and saccular stages in induced-CDH lungs

Punctual (PNECs) or aggregated (NEBs) expression of CGRP characterize the neuroendocrine profile in the developing lung. Immunohistochemistry analysis showed CGRP expressed in bronchi at E17.5-to-E21.5; primordia of bronchiole at E17.5 (Fig. 4AA-AB); and terminal bronchiole at E19.5 (Fig. 4AC-AD) and E21.5 (Fig. 4AE-AF) in normal and hypoplastic fetal lungs.

Apart from the CGRP overexpression in bronchi and terminal bronchiole at canalicular and saccular stages that close on larger NEBs, no significant differences were observed in normal versus CDH lungs (Fig. 4B).

Experimental CDH induce the expression of SP-C in bronchi and BADJ

The spatiotemporal profile of AT2 cells was detected by SP-C. In normal and nitrofen-exposed lungs, SP-C was expressed in bronchi at E17.5-to-E21.5 (Fig. 5AA-AF and Aa-Af); in primordia of bronchiole at E17.5 (Fig. 5AA-AB and Aa-Ab); in terminal bronchiole and BADJ at E19.5 (Fig. 5AC-AD and Ac-Ad) and E21.5 (Fig. 5AE-AF and Ae-Af); and in alveolar duct at E21.5 (Fig. 5AE-AF and Ae-Af).

Semi-quantitative analysis of SP-C expression in induced-CDH versus normal lungs showed the SP-C overexpressed in bronchi from pseudoglandular-to-canalicular stages; in terminal bronchiole at E19.5; in BADJ at E19.5 and E21.5; and in the alveolar duct at E21.5 (Fig. 5B).

Discussion

Single-cell transcriptomics and tracing-linage studies allowed the observation of precise numbers and positions for the distinct pulmonary cell types, their lineages, and differentiation (Guo et al 2017, Guo et al 2019, Guo et al 2015, H et al 1998). CDH fetuses with decreased distal branching and alveoli manifest reduced respiratory function at birth (Ameis et al 2017, Donahoe et al 2016). Recently, we describe the proximodistal patterning to be impaired in nitrofen-induced CDH lungs from pseudoglandular-to-saccular stages (Gonçalves et al 2020). As such, we intend to go further and determine the relative expression levels and the temporospatial distribution for CCSP, CGRP, FOXJ1, and SP-C proteins in hypoplastic (in nitrofen-induced CDH rat model) *versus* normal fetal lungs from pseudoglandular-to-saccular stages. The selected molecular markers: CCSP, CGRP, FOXJ1, and SP-C identified clara, PNECs/NEBs, ciliated and AT2 cells, respectively, when expressed in differentiated epithelial tissues. Conversely, when detected in undifferentiated epithelial tissues, they distinguish the cellular capacity to give rise to the above-mentioned epithelial cell types. At the pseudoglandular stage, our findings demonstrated FOXJ1 and CGRP overexpressed in bronchi and primordia of bronchiole after CDH-induction. As the epithelial cell differentiation goes through, we identified a general overexpression of CGRP in bronchi; FOXJ1, and CGRP in terminal bronchiole; and CCSP and SP-C in BADJ at both canalicular and saccular stages in induced CDH-lungs.

Discussing these results, it must be knowledge the distinct contribution of the epithelial progenitors and specialized epithelial cells that populate conducting and respiratory airways. In fact, several studies tried to describe the function of the distinct epithelial cell types during the development of the lung and at birth, when the first breath takes place. PNECs/NEBs are described as airway sensors required for appropriate innate immune inflammatory response and fetal lung growth. Subsequently, we and others demonstrate PNECs/NEBs overexpressed in *in vivo* CDH lungs, whereas the exogenous administration of neuroendocrine products, like bombesin or ghrelin, stimulate fetal lung growth (Asabe et al 1999, H et al 1998, Nunes et al 2008, Pereira-Terra et al 2015, Sakai et al 2014, Santos et al 2006, Sunday et al 1990). Clara is a secretory cell essential for airway epithelium reparation (Pan et al 2019, Reynolds & Malkinson 2010), that it is now described as overexpressed in bronchi and BADJ at canalicular and saccular stages in induced-CDH versus normal lungs. Ciliated cells are reported as terminally differentiated epithelial cells (Rawlins & Hogan 2008) working in mucociliary clearance at birth and thereafter (Bustamante-Marin & Ostrowski 2017). Now, in nitrofen-exposed CDH lungs, we detected FOXJ1 expressed in BADJ at E19.5 and E21.5 in opposition to the observed in normal lungs. More relevant, BADJ is formed and easily detected at the canalicular stage (Barre et al 2016, Barre et al 2014) that demarcates airway-fated epithelial cells from alveolar-fated epithelial cells

and works as stem cell niche in adult lung regeneration (Kuo & Krasnow 2015, Liu et al 2019). Indeed, BADJ represents the entrance of the small gas exchanging airways, with critical roles in the formation of both conducting and respiratory airways after injury (Kuo & Krasnow 2015, Liu et al 2019). We also described the multi cilia on the plasma membrane that characterize a normal bronchus at E21.5 as decrease in induced-CDH lungs. FOXJ1 is a master regulator of basal body docking, cilia formation, and motility (Vladar & Mitchell 2016, You et al 2004), whereas the multi cilia on the plasma membrane unequivocally identified their differentiated profile. As such, our observations describe a diffuse transition from conducting to respiratory airways in induced-CDH lungs and suggest an undifferentiated epithelium in hypoplastic lungs.

AT2 cells produce pulmonary surfactant proteins and reduce the alveolar surfactant tension that in turn facilitate the first breath at birth. In nitrofen-exposed lungs, the impairment on surfactant production and secretion is evidenced by the low levels of phosphatidylcholine, the lipid component of surfactant, and the factors involved in stimulating the maturation of surfactant lipids, such as PTHrP, adipose differentiation-related protein (ADRP), Thy1 and RA, whereas the inhibitor of surfactant phospholipid synthesis, TNFα, is overexpressed (Carroll et al 2002, Doi et al 2010, Friedmacher et al 2014a, Friedmacher et al 2014c, Gosemann et al 2012, Nakazawa et al 2007, Shima et al 1999). After CDH-induction, our results showed a general upregulation of SP-C expression in bronchi at pseudoglandular and canalicular stage; in terminal bronchiole at canalicular; in BADJ at canalicular and saccular; and in the alveolar duct at saccular. In addition, previous publications demonstrated an altered ratio of alveolar epithelial cells in CDH-associated lung hypoplasia, which was related to the dedifferentiation of AT2 into AT1 cells (Chapin et al 2005, Takayasu et al 2007c). More recently, Nguyen et al report a decrease in the number of AT1 in CDH lungs, while the AT2 population remains unchanged in mice at E17.5 (Nguyen et al 2019). These findings are probably due to the impossibility to distinguish the differentiated versus undifferentiated AT2 cell profile in these models.

Collectively, the described cellular changes by gestational age certainly contribute to a better understanding of the epithelial profile in CDH fetuses and suggest a more careful analysis regarding the differentiated versus undifferentiated epithelial cell profiles in hypoplasia.

Acknowledgments

We are indebted to Goretti Pinto, Magda Carlos, and Alice Miranda for expert technical assistance.

Funding information

This article has been developed under the scope of the projects NORTE-01-0145-FEDER-000013 and NORTE-01-0246-FEDER-000012, supported by the Northern Portugal Regional Operational Programme

(NORTE 2020), under the Portugal 2020 Partnership Agreement, through the European Regional Development Fund (FEDER); and by ICVS Scientific Microscopy Platform, member of the national infrastructure PPBI - Portuguese Platform of Bioimaging (PPBI-POCI-01-0145-FEDER-022122; by National funds, through the Foundation for Science and Technology, I.P. (FCT) - project UIDB/50026/2020 and UIDP/50026/2020. This work was also funded by POCI-01-0145-FEDER-030881, financed by Fundos Europeus Estruturais e de Investimento (FEEI) and FCT. ANG was supported by FCT (reference PD/BDE/127829/2016). The funders had no role in study design, data collection, and analysis, decision to publish, or preparation of the manuscript.

Compliance with Ethical Statements

Conflict of interest The authors declare that they have no conflict of interest.

Use of animals All applicable international, national, and/or institutional guidelines for the care and use of animals were followed. All animal experiments were approved by the Life and Health Sciences Research Institute (ICVS), University of Minho, and by the Direção Geral de Alimentação e Veterinária (approval No. DGAV 021328).

References

Abler LL, Mansour SL, Sun X (2009) Conditional gene inactivation reveals roles for Fgf10 and Fgfr2 in establishing a normal pattern of epithelial branching in the mouse lung. Dev Dyn 238 (8):1999-2013. doi:10.1002/dvdy.22032

Ameis D, Khoshgoo N, Keijzer R (2017) Abnormal lung development in congenital diaphragmatic hernia. Semin Pediatr Surg 26 (3):123-128. doi:10.1053/j.sempedsurg.2017.04.011

Asabe K, Tsuji K, Handa N, Kajiwara M, Suita S (1999) Immunohistochemical distribution of bombesin-positive pulmonary neuroendocrine cells in a congenital diaphragmatic hernia. Surg Today 29 (5):407-412. doi:10.1007/bf02483031

Barre SF, Haberthur D, Cremona TP, Stampanoni M, Schittny JC (2016) The total number of acini remains constant throughout postnatal rat lung development. Am J Physiol Lung Cell Mol Physiol 311 (6):L1082-l1089. doi:10.1152/ajplung.00325.2016

Barre SF, Haberthur D, Stampanoni M, Schittny JC (2014) Efficient estimation of the total number of acini in adult rat lung. Physiol Rep 2 (7). doi:10.14814/phy2.12063

Benavides F, Rulicke T, Prins JB, Bussell J, Scavizzi F, Cinelli P, Herault Y, Wedekind D (2019) Genetic quality assurance and genetic monitoring of laboratory mice and rats: FELASA Working Group Report. Lab Anim:23677219867719. doi:10.1177/0023677219867719

Bustamante-Marin XM, Ostrowski LE (2017) Cilia and Mucociliary Clearance. Cold Spring Harb Perspect Biol 9 (4). doi:10.1101/cshperspect.a028241

Carroll JL, Jr., McCoy DM, McGowan SE, Salome RG, Ryan AJ, Mallampalli RK (2002) Pulmonary-specific expression of tumor necrosis factor-alpha alters surfactant lipid metabolism. Am J Physiol Lung Cell Mol Physiol 282 (4):L735-742. doi:10.1152/ajplung.00120.2001

Chang DR, Martinez Alanis D, Miller RK, Ji H, Akiyama H, McCrea PD, Chen J (2013) Lung epithelial branching program antagonizes alveolar differentiation. Proc Natl Acad Sci U S A 110 (45):18042-18051. doi:10.1073/pnas.1311760110

Chapin CJ, Ertsey R, Yoshizawa J, Hara A, Sbragia L, Greer JJ, Kitterman JA (2005) Congenital diaphragmatic hernia, tracheal occlusion, thyroid transcription factor-1, and fetal pulmonary epithelial maturation. American Journal of Physiology-Lung Cellular and Molecular Physiology 289 (1):L44-L52. doi:10.1152/ajplung.00342.2004

Cornett B, Snowball J, Varisco BM, Lang R, Whitsett J, Sinner D (2013) Wntless is required for peripheral lung differentiation and pulmonary vascular development. Dev Biol 379 (1):38-52. doi:10.1016/j.ydbio.2013.03.010

Cotten CM (2017) Pulmonary hypoplasia. Semin Fetal Neonatal Med 22 (4):250-255. doi:10.1016/j.siny.2017.06.004

Coughlin MA, Werner NL, Gajarski R, Gadepalli S, Hirschl R, Barks J, Treadwell MC, Ladino-Torres M, Kreutzman J, Mychaliska GB (2016) Prenatally diagnosed severe CDH: mortality and morbidity remain high. J Pediatr Surg 51 (7):1091-1095. doi:10.1016/j.jpedsurg.2015.10.082

Desai TJ, Brownfield DG, Krasnow MA (2014) Alveolar progenitor and stem cells in lung development, renewal and cancer. Nature 507 (7491):190-194. doi:10.1038/nature12930

Doi T, Lukosiūte A, Ruttenstock E, Dingemann J, Puri P (2010) Disturbance of parathyroid hormone-related protein signaling in the nitrofen-induced hypoplastic lung. Pediatr Surg Int 26 (1):45-50. doi:10.1007/s00383-009-2506-8

Donahoe PK, Longoni M, High FA (2016) Polygenic Causes of Congenital Diaphragmatic Hernia Produce Common Lung Pathologies. Am J Pathol 186 (10):2532-2543. doi:10.1016/j.ajpath.2016.07.006

Eblaghie MC, Reedy M, Oliver T, Mishina Y, Hogan BL (2006) Evidence that autocrine signaling through Bmpr1a regulates the proliferation, survival and morphogenetic behavior of distal lung epithelial cells. Dev Biol 291 (1):67-82. doi:10.1016/j.ydbio.2005.12.006

El Agha E, Herold S, Al Alam D, Quantius J, MacKenzie B, Carraro G, Moiseenko A, Chao CM, Minoo P, Seeger W, Bellusci S (2014) Fgf10-positive cells represent a progenitor cell population during lung development and postnatally. Development 141 (2):296-306. doi:10.1242/dev.099747

Frank DB, Penkala IJ, Zepp JA, Sivakumar A, Linares-Saldana R, Zacharias WJ, Stolz KG, Pankin J, Lu M, Wang Q, Babu A, Li L, Zhou S, Morley MP, Jain R, Morrisey EE (2019) Early lineage specification defines alveolar epithelial ontogeny in the murine lung. Proc Natl Acad Sci U S A 116 (10):4362-4371. doi:10.1073/pnas.1813952116

Friedmacher F, Fujiwara N, Hofmann AD, Takahashi H, Alvarez LA, Gosemann JH, Puri P (2014a) Prenatal retinoic acid increases lipofibroblast expression in hypoplastic rat lungs with experimental congenital diaphragmatic hernia. J Pediatr Surg 49 (6):876-881; discussion 881. doi:10.1016/j.jpedsurg.2014.01.017

Friedmacher F, Hofmann AD, Takahashi H, Takahashi T, Gosemann JH, Puri P (2014b) Disruption of THY-1 signaling in alveolar lipofibroblasts in experimentally induced congenital diaphragmatic hernia. Pediatr Surg Int 30 (2):129-135. doi:10.1007/s00383-013-3444-z

Goncalves AN, Correia-Pinto J, Nogueira-Silva C (2019) Imagiological methods for prediction of fetal pulmonary hypoplasia: a systematic review. J Matern Fetal Neonatal Med:1-10. doi:10.1080/14767058.2019.1636029

Gontan C, de Munck A, Vermeij M, Grosveld F, Tibboel D, Rottier R (2008) Sox2 is important for two crucial processes in lung development: branching morphogenesis and epithelial cell differentiation. Dev Biol 317 (1):296-309. doi:10.1016/j.ydbio.2008.02.035

Gonçalves AN, Correia-Pinto J, Nogueira-Silva C (2020) ROBO2 signaling in lung development regulates SOX2/SOX9 balance, branching morphogenesis and is dysregulated in nitrofen-induced congenital diaphragmatic hernia. Respiratory Research 21 (1):302. doi:10.1186/s12931-020-01568-w

Gosemann JH, Doi T, Kutasy B, Friedmacher F, Dingemann J, Puri P (2012) Alterations of peroxisome proliferator-activated receptor γ and monocyte chemoattractant protein 1 gene expression in the nitrofen-induced hypoplastic lung. J Pediatr Surg 47 (5):847-851. doi:10.1016/j.jpedsurg.2012.01.038

Guo M, Bao EL, Wagner M, Whitsett JA, Xu Y (2017) SLICE: determining cell differentiation and lineage based on single cell entropy. Nucleic Acids Res 45 (7):e54. doi:10.1093/nar/gkw1278

Guo M, Du Y, Gokey JJ, Ray S, Bell SM, Adam M, Sudha P, Perl AK, Deshmukh H, Potter SS, Whitsett JA, Xu Y (2019) Single cell RNA analysis identifies cellular heterogeneity and adaptive responses of the lung at birth. Nat Commun 10 (1):37. doi:10.1038/s41467-018-07770-1

Guo M, Wang H, Potter SS, Whitsett JA, Xu Y (2015) SINCERA: A Pipeline for Single-Cell RNA-Seq Profiling Analysis. PLoS Comput Biol 11 (11):e1004575. doi:10.1371/journal.pcbi.1004575

H IJ, Hung N, de Jongste JC, Tibboel D, Cutz E (1998) Calcitonin gene-related peptide expression is altered in pulmonary neuroendocrine cells in developing lungs of rats with congenital diaphragmatic hernia. Am J Respir Cell Mol Biol 19 (2):278-285. doi:10.1165/ajrcmb.19.2.2853

Hashimoto S, Chen H, Que J, Brockway BL, Drake JA, Snyder JC, Randell SH, Stripp BR (2012) β-Catenin-SOX2 signaling regulates the fate of developing airway epithelium. J Cell Sci 125 (Pt 4):932-942. doi:10.1242/jcs.092734

Kluth D, Tenbrinck R, von Ekesparre M, Kangah R, Reich P, Brandsma A, Tibboel D, Lambrecht W (1993) The natural history of congenital diaphragmatic hernia and pulmonary hypoplasia in the embryo. J Pediatr Surg 28 (3):456-462; discussion 462-453

Kuo CS, Krasnow MA (2015) Formation of a Neurosensory Organ by Epithelial Cell Slithering. Cell 163 (2):394-405. doi:10.1016/j.cell.2015.09.021

Liu Q, Liu K, Cui G, Huang X, Yao S, Guo W, Qin Z, Li Y, Yang R, Pu W, Zhang L, He L, Zhao H, Yu W, Tang M, Tian X, Cai D, Nie Y, Hu S, Ren T, Qiao Z, Huang H, Zeng YA, Jing N, Peng G, Ji H, Zhou B (2019) Lung regeneration by multipotent stem cells residing at the bronchioalveolar-duct junction. Nat Genet 51 (4):728-738. doi:10.1038/s41588-019-0346-6

Liu Y, Hogan BL (2002) Differential gene expression in the distal tip endoderm of the embryonic mouse lung. Gene Expr Patterns 2 (3-4):229-233

Minoo P, Su G, Drum H, Bringas P, Kimura S (1999) Defects in tracheoesophageal and lung morphogenesis in Nkx2.1(-/-) mouse embryos. Dev Biol 209 (1):60-71. doi:10.1006/dbio.1999.9234

Montalva L, Zani A (2019) Assessment of the nitrofen model of congenital diaphragmatic hernia and of the dysregulated factors involved in pulmonary hypoplasia. Pediatr Surg Int 35 (1):41-61. doi:10.1007/s00383-018-4375-5

Mucenski ML, Wert SE, Nation JM, Loudy DE, Huelsken J, Birchmeier W, Morrisey EE, Whitsett JA (2003) beta-Catenin is required for specification of proximal/distal cell fate during lung morphogenesis. J Biol Chem 278 (41):40231-40238. doi:10.1074/jbc.M305892200

Nakazawa N, Montedonico S, Takayasu H, Paradisi F, Puri P (2007) Disturbance of retinol transportation causes nitrofen-induced hypoplastic lung. J Pediatr Surg 42 (2):345-349. doi:10.1016/j.jpedsurg.2006.10.028

Nguyen TM, Jimenez J, Rendin LE, Müller C, Westergren-Thorsson G, Deprest J, Toelen J (2019) The proportion of alveolar type 1 cells decreases in murine hypoplastic congenital diaphragmatic hernia lungs. PLoS One 14 (4):e0214793. doi:10.1371/journal.pone.0214793

Nogueira-Silva C, Carvalho-Dias E, Piairo P, Nunes S, Baptista MJ, Moura RS, Correia-Pinto J (2012) Local fetal lung renin-angiotensin system as a target to treat congenital diaphragmatic hernia. Mol Med 18:231-243. doi:10.2119/molmed.2011.00210

Nogueira-Silva C, Moura RS, Esteves N, Gonzaga S, Correia-Pinto J (2008) Intrinsic catch-up growth of hypoplastic fetal lungs is mediated by interleukin-6. Pediatr Pulmonol 43 (7):680-689. doi:10.1002/ppul.20840

Nogueira-Silva C, Piairo P, Carvalho-Dias E, Veiga C, Moura RS, Correia-Pinto J (2013) The role of glycoprotein 130 family of cytokines in fetal rat lung development. PLoS One 8 (6):e67607. doi:10.1371/journal.pone.0067607

Nunes S, Nogueira-Silva C, Dias E, Moura RS, Correia-Pinto J (2008) Ghrelin and obestatin: different role in fetal lung development? Peptides 29 (12):2150-2158. doi:10.1016/j.peptides.2008.08.012

Pan H, Deutsch GH, Wert SE (2019) Comprehensive anatomic ontologies for lung development: A comparison of alveolar formation and maturation within mouse and human lung. J Biomed Semantics 10 (1):18. doi:10.1186/s13326-019-0209-1

Park WY, Miranda B, Lebeche D, Hashimoto G, Cardoso WV (1998) FGF-10 is a chemotactic factor for distal epithelial buds during lung development. Dev Biol 201 (2):125-134. doi:10.1006/dbio.1998.8994

Peixoto FO, Pereira-Terra P, Moura RS, Carvalho-Dias E, Correia-Pinto J, Nogueira-Silva C (2015) The role of ephrins-B1 and -B2 during fetal rat lung development. Cell Physiol Biochem 35 (1):104-115. doi:10.1159/000369679

Pereira-Terra P, Moura RS, Nogueira-Silva C, Correia-Pinto J (2015) Neuroendocrine factors regulate retinoic acid receptors in normal and hypoplastic lung development. J Physiol 593 (15):3301-3311. doi:10.1113/jp270477

Perl AK, Kist R, Shan Z, Scherer G, Whitsett JA (2005) Normal lung development and function after Sox9 inactivation in the respiratory epithelium. Genesis 41 (1):23-32. doi:10.1002/gene.20093

Piairo P, Moura RS, Baptista MJ, Correia-Pinto J, Nogueira-Silva C (2018) STATs in Lung Development: Distinct Early and Late Expression, Growth Modulation and Signaling Dysregulation in Congenital Diaphragmatic Hernia. Cell Physiol Biochem 45 (1):1-14. doi:10.1159/000486218

Post LC, Ternet M, Hogan BL (2000) Notch/Delta expression in the developing mouse lung. Mech Dev 98 (1-2):95-98. doi:10.1016/s0925-4773(00)00432-9

Rawlins EL, Clark CP, Xue Y, Hogan BL (2009) The Id2+ distal tip lung epithelium contains individual multipotent embryonic progenitor cells. Development 136 (22):3741-3745. doi:10.1242/dev.037317

Rawlins EL, Hogan BL (2008) Ciliated epithelial cell lifespan in the mouse trachea and lung. Am J Physiol Lung Cell Mol Physiol 295 (1):L231-234. doi:10.1152/ajplung.90209.2008

Reynolds SD, Malkinson AM (2010) Clara cell: progenitor for the bronchiolar epithelium. Int J Biochem Cell Biol 42 (1):1-4. doi:10.1016/j.biocel.2009.09.002

Rockich BE, Hrycaj SM, Shih HP, Nagy MS, Ferguson MA, Kopp JL, Sander M, Wellik DM, Spence JR (2013) Sox9 plays multiple roles in the lung epithelium during branching morphogenesis. Proc Natl Acad Sci U S A 110 (47):E4456-4464. doi:10.1073/pnas.1311847110

Sakai K, Kimura O, Furukawa T, Fumino S, Higuchi K, Wakao J, Kimura K, Aoi S, Masumoto K, Tajiri T (2014) Prenatal administration of neuropeptide bombesin promotes lung development in a rat model of nitrofen-induced congenital diaphragmatic hernia. J Pediatr Surg 49 (12):1749-1752. doi:10.1016/j.jpedsurg.2014.09.015

Santos M, Bastos P, Gonzaga S, Roriz JM, Baptista MJ, Nogueira-Silva C, Melo-Rocha G, Henriques-Coelho T, Roncon-Albuquerque R, Jr., Leite-Moreira AF, De Krijger RR, Tibboel D, Rottier R, Correia-Pinto J (2006) Ghrelin expression in human and rat fetal lungs and the effect of ghrelin administration in nitrofen-induced congenital diaphragmatic hernia. Pediatr Res 59 (4 Pt 1):531-537. doi:10.1203/01.pdr.0000202748.66359.a9

Schittny JC (2017a) Development of the lung. Cell Tissue Res 367 (3):427-444. doi:10.1007/s00441-016-2545-0

Schittny JC (2017b) Development of the lung. Cell and Tissue Research 367 (3):427-444. doi:10.1007/s00441-016-2545-0

Shima H, Ohshiro K, Taira Y, Miyazaki E, Oue T, Puri P (1999) Antenatal dexamethasone suppresses tumor necrosis factor-alpha expression in hypoplastic lung in nitrofen-induced diaphragmatic hernia in rats. Pediatr Res 46 (5):633-637. doi:10.1203/00006450-199911000-00023

Shu W, Guttentag S, Wang Z, Andl T, Ballard P, Lu MM, Piccolo S, Birchmeier W, Whitsett JA, Millar SE, Morrisey EE (2005) Wnt/beta-catenin signaling acts upstream of N-myc, BMP4, and FGF signaling to regulate proximal-distal patterning in the lung. Dev Biol 283 (1):226-239. doi:10.1016/j.ydbio.2005.04.014

Sunday ME, Hua J, Dai HB, Nusrat A, Torday JS (1990) Bombesin increases fetal lung growth and maturation in utero and in organ culture. Am J Respir Cell Mol Biol 3 (3):199-205. doi:10.1165/ajrcmb/3.3.199

Takayasu H, Nakazawa N, Montedonico S, Sugimoto K, Sato H, Puri P (2007) Impaired alveolar epithelial cell differentiation in the hypoplastic lung in nitrofen-induced congenital diaphragmatic hernia. Pediatr Surg Int 23 (5):405-410. doi:10.1007/s00383-006-1853-y

Tenbrinck R, Tibboel D, Gaillard JL, Kluth D, Bos AP, Lachmann B, Molenaar JC (1990) Experimentally induced congenital diaphragmatic hernia in rats. J Pediatr Surg 25 (4):426-429

Treutlein B, Brownfield DG, Wu AR, Neff NF, Mantalas GL, Espinoza FH, Desai TJ, Krasnow MA, Quake SR (2014) Reconstructing lineage hierarchies of the distal lung epithelium using single-cell RNA-seq. Nature 509 (7500):371-375. doi:10.1038/nature13173

Tsao PN, Chen F, Izvolsky KI, Walker J, Kukuruzinska MA, Lu J, Cardoso WV (2008) Gamma-secretase activation of notch signaling regulates the balance of proximal and distal fates in progenitor cells of the developing lung. J Biol Chem 283 (43):29532-29544. doi:10.1074/jbc.M801565200

Vladar EK, Mitchell BJ (2016) It's a family act: the geminin triplets take center stage in motile ciliogenesis. Embo j 35 (9):904-906. doi:10.15252/embj.201694206

Volckaert T, De Langhe SP (2015) Wnt and FGF mediated epithelial-mesenchymal crosstalk during lung development. Dev Dyn 244 (3):342-366. doi:10.1002/dvdy.24234

Warburton D, El-Hashash A, Carraro G, Tiozzo C, Sala F, Rogers O, De Langhe S, Kemp PJ, Riccardi D, Torday J, Bellusci S, Shi W, Lubkin SR, Jesudason E (2010) Lung organogenesis. Curr Top Dev Biol 90:73-158. doi:10.1016/s0070-2153(10)90003-3

Weaver M, Dunn NR, Hogan BL (2000) Bmp4 and Fgf10 play opposing roles during lung bud morphogenesis. Development 127 (12):2695-2704

Weaver M, Yingling JM, Dunn NR, Bellusci S, Hogan BL (1999) Bmp signaling regulates proximal-distal differentiation of endoderm in mouse lung development. Development 126 (18):4005-4015

Wuenschell CW, Sunday ME, Singh G, Minoo P, Slavkin HC, Warburton D (1996) Embryonic mouse lung epithelial progenitor cells co-express immunohistochemical markers of diverse mature cell lineages. J Histochem Cytochem 44 (2):113-123. doi:10.1177/44.2.8609367

You Y, Huang T, Richer EJ, Schmidt JE, Zabner J, Borok Z, Brody SL (2004) Role of f-box factor foxj1 in differentiation of ciliated airway epithelial cells. Am J Physiol Lung Cell Mol Physiol 286 (4):L650-657. doi:10.1152/ajplung.00170.2003

Figure Legends

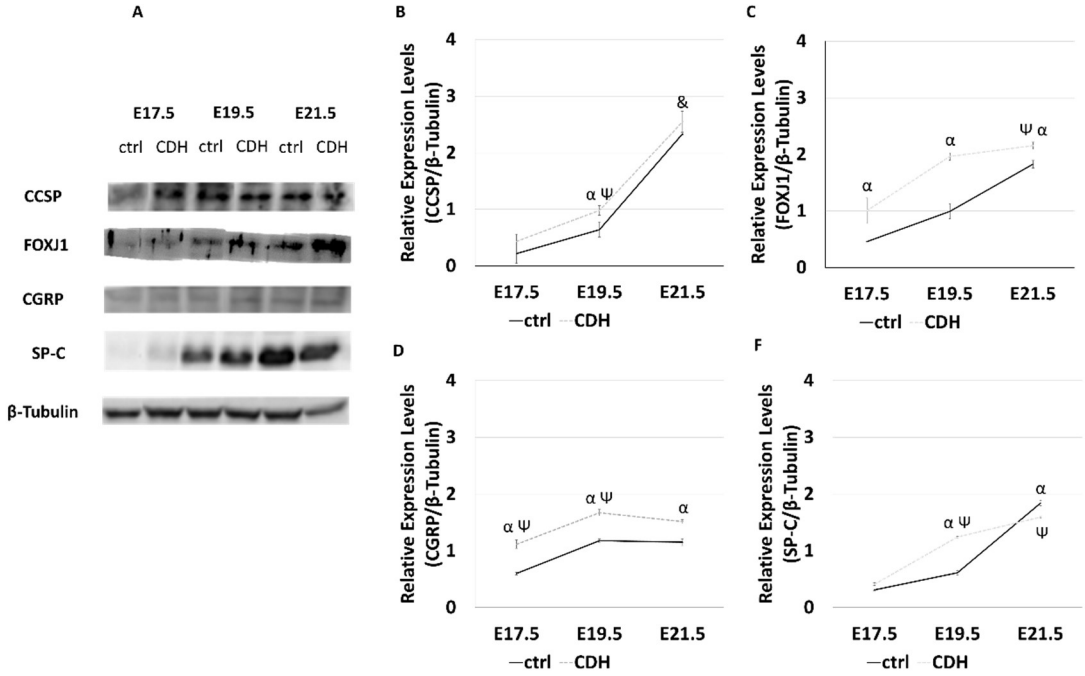

Figure 1 - Altered relative expression levels for clara cell secretory protein (CCSP), forkhead transcription factor 1 (FOXJ1), calcitonin gene-related peptide (CGRP), and surfactant protein-C (SP-C) after congenital diaphragmatic hernia (CDH)-induction. Western blot analysis for CCSP; FOXJ1; CGRP; and SP-C protein levels in normal (ctrl) and CDH lungs at embryonic day (E)17.5-to-E21.5. (A) Representative immunoblots are shown. Each lane represents a pooled tissue sample, and relative expression was determined against β-tubulin. Semi-quantitative analysis of three independent experiments is plotted (n≥9 per timepoint and experimental groups, respectively). Protein expression levels of (B) CCSP; (C) FOXJ1 and (D) CGRP, and (E) SP-C are shown at the distinct developmental stages of normal and CDH fetal lungs. Results are presented as mean±SD. Symbols indicate the main effects and non-redundant interactions of the two-way ANOVA. $p < 0.05$: $^{\alpha}$vs ctrl; $^{\Psi}$vs E17.5-ctrl; $^{\&}$vs E17.5-CDH and E19.5-CDH.

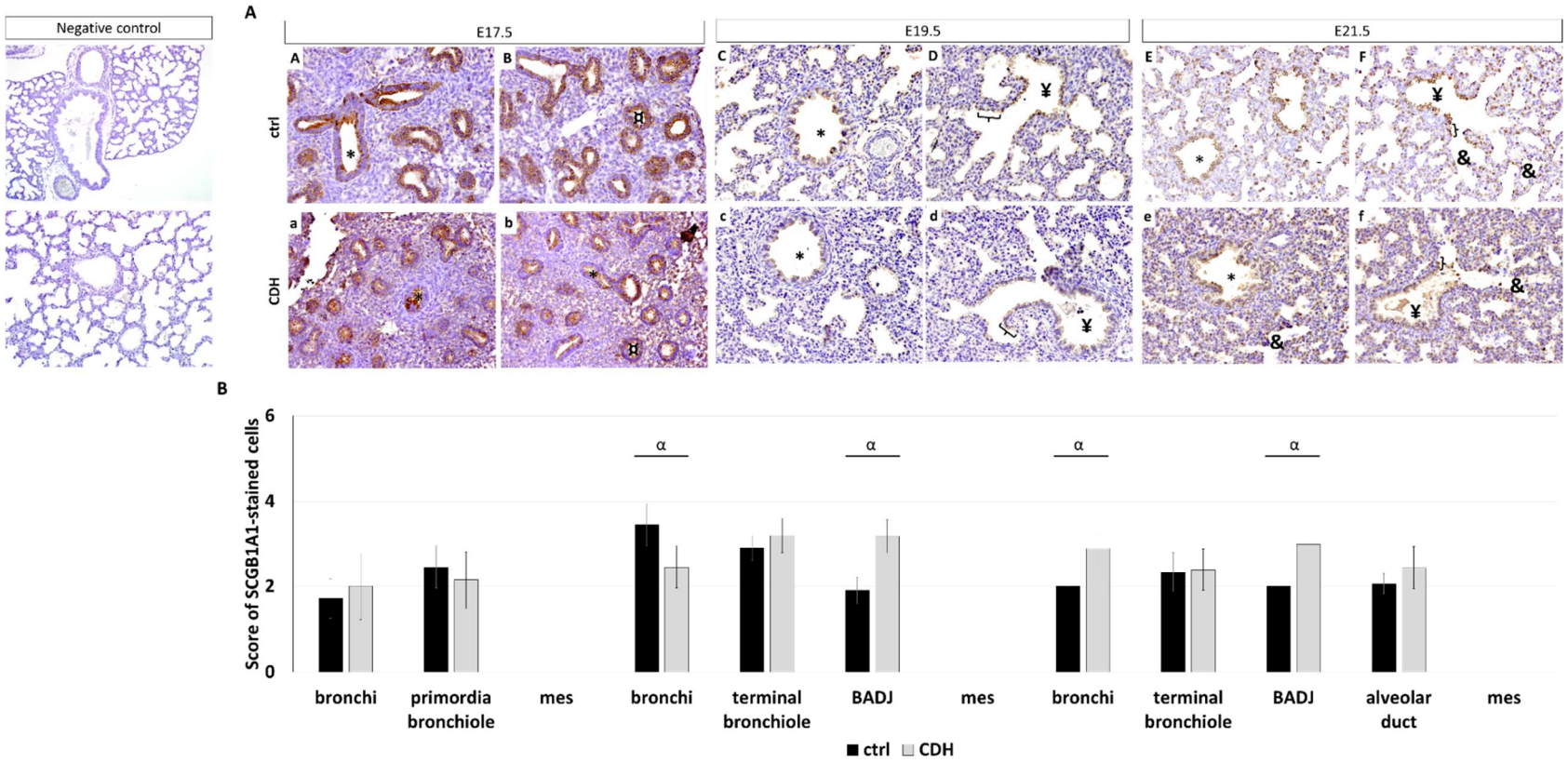

Figure 2 - Clara cell secretory protein (CCSP) expression pattern during normal and hypoplastic fetal lung development. Representative immunohistochemical evidence for CCSP expression at (AA-AB and Aa-Ab) pseudoglandular, (AC-AD and Ac-Ad) canalicular, and (AE-AF and Ae-Af) saccular stages in normal (ctrl) and congenital diaphragmatic hernia (CDH) lungs, respectively. *bronchiole; ¤primordia of bronchiole; ¥terminal bronchiole; [bronchioalveolar duct junction; &alveolar duct. Original magnification x200. (B) semi-quantitative analysis of CCSP expression from embryonic day (E)17.5-to-E21.5 in normal and CDH lungs. Data are presented as mean±SD. Symbols indicate the main effects and non-redundant interactions of one-way ANOVA. $^{\alpha}p<0.05$.

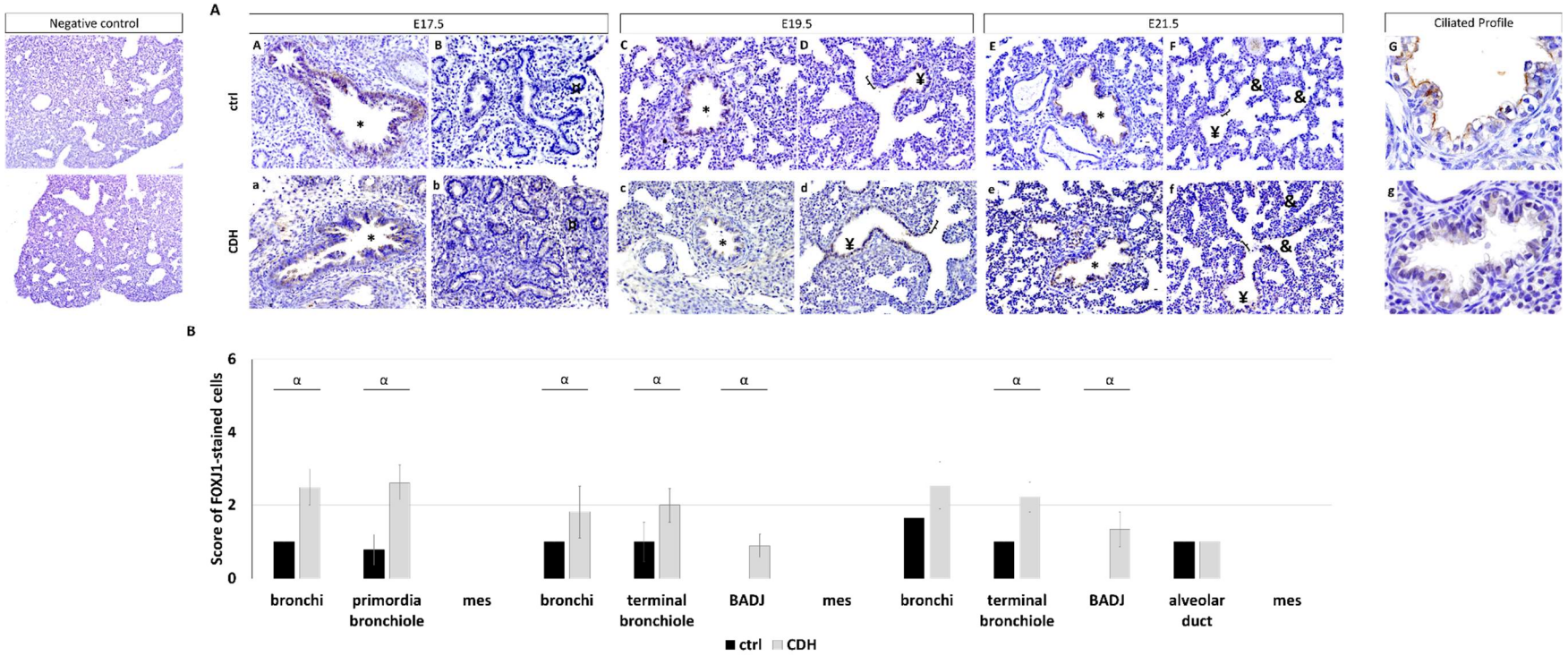

Figure 3 - Spatiotemporal distribution of FOXJ1 in normal and induced-congenital diaphragmatic hernia (CDH) rat model at pseudoglandular, canalicular and saccular stages. Representative immunohistochemical evidence for FOXJ1 expression at (AA-AB and Aa-Ab) embryonic day (E)17.5, (AC-AD and Ac-Ad) E19.5, and (AE-AF and Ae-Af) E21.5 in normal (ctrl) and induced-congenital diaphragmatic hernia rat model (CDH) fetal rat lungs, respectively. *bronchiole; ¤primordia of bronchiole; ¥terminal bronchiole; [bronchioalveolar duct junction; &alveolar duct. Original magnification x200. (B) semi-quantitative analysis of FOXJ1 expression from pseudoglandular-to-saccular stages in normal (ctrl) and CDH lungs. Results are presented as mean±SD. Symbols indicate the main effects and non-redundant interactions of one-way ANOVA. $^{\alpha}p<0.05$. (C) Representative immunohistochemical evidence for the absence of multi cilia on the plasma membrane of ciliated cells in bronchi at E21.5. Original magnification x600.

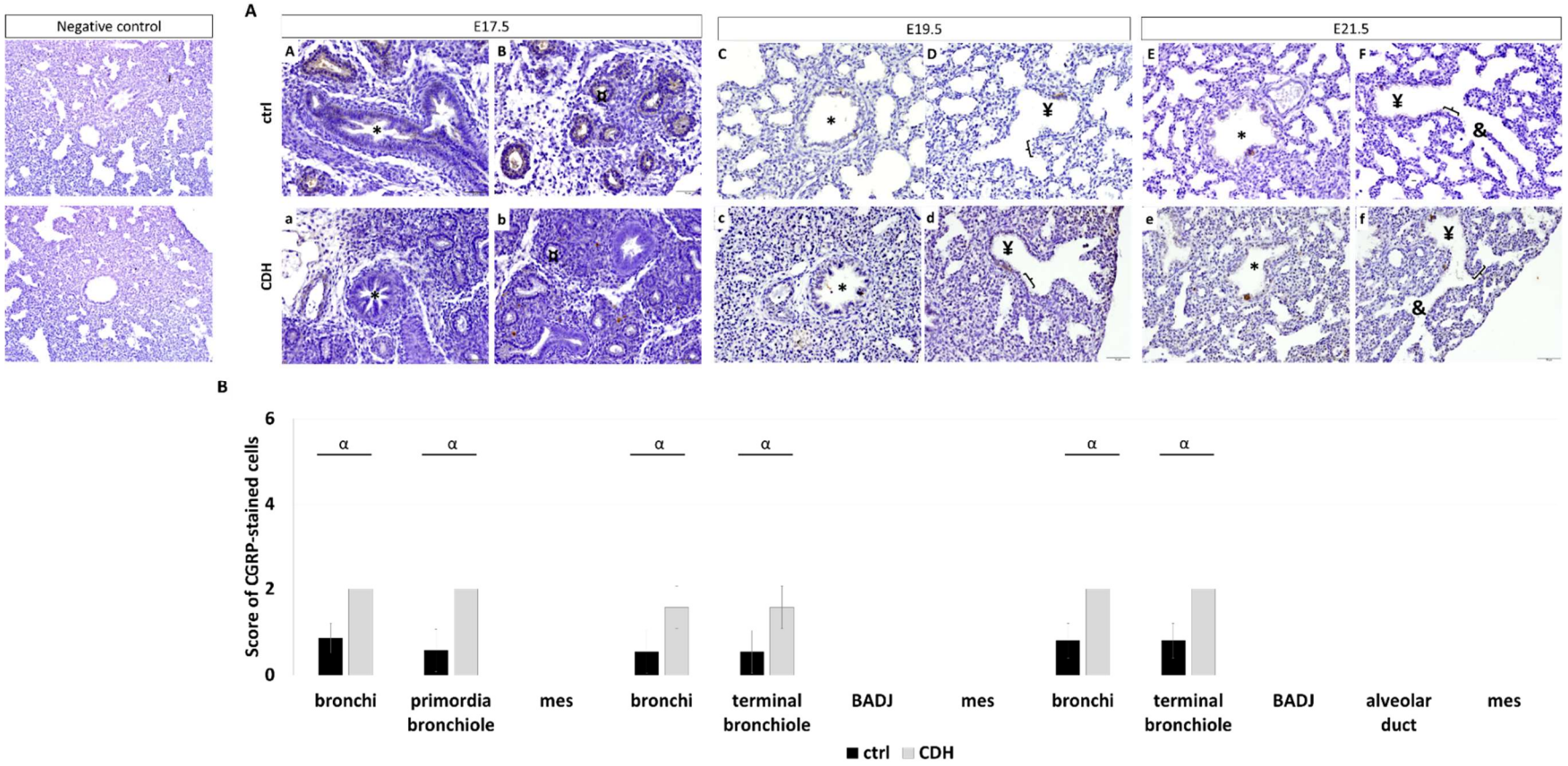

Figure 4 - Protein expression pattern of CGRP in nitrofen-exposed rat lungs at embryonic day (E)17.5-to-E21.5. Representative immunohistochemical evidence for CGRP expression at (AA-AB and Aa-Ab) pseudoglandular, (AC-AD and Ac-Ad) canalicular, and (AE-AF and Ae-Af) saccular stages in normal (ctrl) and nitrofen-exposed (CDH) rat lungs, respectively. Original magnification x200. (B) semi-quantitative analysis of CGRP expression from E17.5-to-E21.5 in normal (ctrl) and CDH lungs. Results are presented as mean±SD. Symbol indicates main effect and non-redundant interaction of one-way ANOVA. $^{\alpha}p<0.05$.

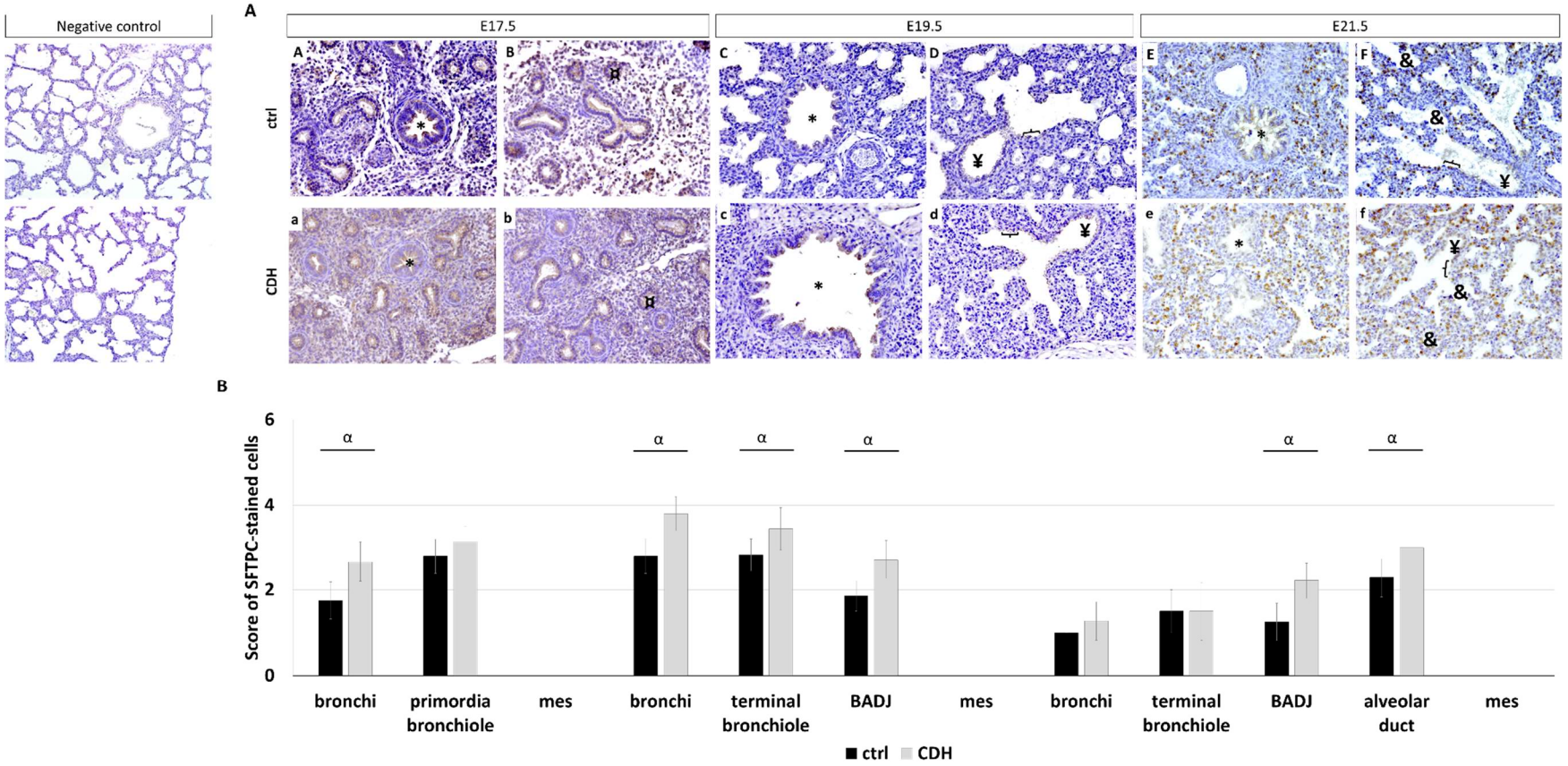

Figure 5 - Expression profile of surfactant protein-C (SP-C) in the normal and induced congenital diaphragmatic hernia (CDH) rat model. Representative immunohistochemical evidence for SP-C expression at (AA-AB and Aa-Ab) embryonic day (E)17.5, (AC-AD and Ac-Ad) E19.5, and (AE-AF and Ae-Af) E21.5 of normal and CDH phenotypes, respectively. *bronchiole; ¤primordia of bronchiole; ¥terminal bronchiole; [bronchioalveolar duct junction; &alveolar duct. Original magnification x200. (B) semi-quantitative analysis of SP-C expression from pseudoglandular-to-saccular stages in normal (ctrl) and CDH lungs. Results are presented as mean±SD. Symbols indicate the main effects and non-redundant interactions of one-way ANOVA. $^{\alpha}p<0.05$.

Chapter 5 – Intraluminal chloride in branching morphogenesis

The results presented in this chapter are:

i) Submitted for publication in an international peer-reviewed journal:

Gonçalves AN, Correia-Pinto J, Nogueira-Silva C. Intraluminal chloride regulates lung branching morphogenesis: involvement of PIEZO1/PIEZO2. *in revision*

5.1. Chapter overview

5.1.1. Rationale

Experimental evidence showed the intraluminal lung fluid as a modulator of *in vivo* fetal lung growth that permits the development of FETO. FETO consists in *in utero* insertion of a balloon into the trachea that prevents the pulmonary fluid egress. The block of the tracheal efflux increase stretches on lung parenchymal cells and promotes lung growth, maturation, and remodeling of the pulmonary vasculature. FETO is under clinical investigation to be applied at 30-32 weeks in moderate and at 27 to 29 weeks in severe cases of human FLH, secondary to CDH. However, in extremely severe CDH cases, defined as > 30% liver herniation with o/e LHR < 25% (LHR < 0.71), early intervention should be considered, possibly as early as 22 weeks of gestation to better improve the neonatal outcome. Unfortunately, when applied, the fetoscopic procedures increase the risk for iatrogenic PPROM that complicate their therapeutic value (reviewed in Beck et al 2012, Tsao & Johnson 2020).

Analysis of CDH and CDH+TO lungs in human and animal models demonstrated TO able to reverse several of the morphological defects associated with CDH. For instance, a hypoplastic-CDH lung has arrested branching morphogenesis with reduced alveolar space and alveoli. TO significant increase branching morphogenesis, alveolarization, and secondary crest formation in the improvement of the neonatal respiratory function. As such, multiple studies comparing the molecular profile of CDH and CDH+TO lungs have been performed and describe disorganized molecular networks that occasionally do not match in CDH and CDH+TO lungs (Engels et al 2016, Nelson et al 2005, Vuckovic et al 2013). In our interpretation, these observations indicate an additional challenge for our understanding of (ab)normal fetal lung morphogenesis since the molecular distinction between cause and consequences by morphological defect is dependent on the revealed basic mechanisms. Nevertheless, the difficulty that it is mimic or recapitulate in the lab the morphological aspects triggered by intraluminal lung fluid in fetal pulmonary growth further impairs the molecular/cellular studies.

In this context, given the urgency of this research topic, we aimed to **i)** establish an *ex vivo* model for the study of lung fluid in fetal lung growth; and **ii)** reveal the mechanisms triggered by intraluminal fluid in fetal branching morphogenesis.

5.1.2. Major Findings

The major findings from this chapter are described below:

- Effective intraluminal injection at day0 (D0) and D2 in *ex vivo* lung explant cultures with dynamic intraluminal movements at D4;

- Intraluminal chloride concentration ($[Cl^-]$) modulates fetal branching morphogenesis;
- PIEZO1/PIEZO2 expressed in PNECs/NEBs are activated by intraluminal $[Cl^-]$ that stimulates fetal lung growth;
- Pharmacological inhibition of PIEZO1/PIEZO2 expression decreases the *ex vivo* branching morphogenesis under a mechanism independent of intraluminal $[Cl^-]$.

Intraluminal chloride regulates lung branching morphogenesis: involvement of PIEZO1/PIEZO2

Ana N Gonçalves (M.Sc.)[1,2], Jorge Correia-Pinto (M.D., Ph.D.)[1,2,3], Cristina Nogueira-Silva (M.D., Ph.D.)*[1,2,4]

[1]Life and Health Sciences Research Institute (ICVS), School of Medicine, University of Minho, Braga, Portugal; [2]ICVS/3B's - PT Government Associate Laboratory, Braga/ Guimarães, Portugal; [3]Department of Pediatric Surgery, Hospital de Braga, Braga, Portugal; [4]Department of Obstetrics and Gynecology, Hospital de Braga, Braga, Portugal

Abstract

Clinical and experimental evidence showed the lung fluid volume as a modulator of fetal lung growth with important value in the treatment of fetal lung hypoplasia. Unfortunately, the molecular/ cellular mechanisms underlying these morphological dynamics remain almost undetermined. Here, we describe effective intraluminal injections at day0 (D0) and D2 and demonstrate the existence of dynamic intraluminal movements at D4 of the *ex vivo* lung explant cultures. Chloride concentration ($[Cl^-]$) is used as a modulator of sodium and water movements in the production of fetal lung fluid in the model. Distinct $[Cl^-]$ and Cl^- channel inhibitors are injected into the lumen followed by the morphological and molecular analysis at D4. Immunofluorescence assay in *in vivo* and *ex vivo* branching morphogenesis showed the colocalization of PGP9.5 (a neuroendocrine marker) with PIEZO1 and PIEZO2 mechanosensors. In addition, the increase of intraluminal $[Cl^-]$, 715mM Cl^-, promotes fetal lung growth through the overexpression of PIEZO1, PIEZO2, ghrelin, bombesin, myosin light chain 2 (MLC2), and alpha-smooth muscle actin (α-SMA). Oppositely, the depletion of cystic fibrosis transmembrane conductance regulator (CFTR) or calcium-dependent Cl^- channel (CaCC) by CFTR inhibitor172 or CaCC inhibitorA01, respectively, equally decreases the fetal lung growth as well as the expression of PIEZO1, PIEZO2, ghrelin, bombesin, MLC2, and α-SMA. Finally, the inhibition of PIEZO1/PIEZO2 by GsMTx4 decreases the branching morphogenesis and the expression of ghrelin, bombesin, MLC2, and α-SMA in an intraluminal injection independent-manner. Our results identify a potential mechanism by which the intraluminal lung fluid composition modulates the fetal branching morphogenesis.

Running Title: Intraluminal chloride in branching morphogenesis

Keywords: chloride; branching; lung development; lung fluid; mechanotransduction

Key points

- Intraluminal injections in *ex vivo* lung explant cultures are useful for the study of lung fluid composition in fetal branching morphogenesis;
- PIEZO1 and PIEZO2 are expressed in pulmonary neuroendocrine cells/ neuroepithelial bodies in *in vivo* and *ex vivo* branching morphogenesis;
- Intraluminal chloride concentration is a modulator of fetal branching morphogenesis through PIEZO1/PIEZO2 mechanosensors.

Introduction

Physical forces exerted on the developing fetal lung, namely by intraluminal lung fluid and peristaltic airway contractions, are important regulators of fetal lung branching morphogenesis. Concerning lung fluid and it is in utero intraluminal hydraulic pressure, lung fluid is secreted by the epithelial cells into the airway lumen, which are osmotically driven by active chloride (Cl^-) secretion, through Cl^- channels. This gives rise to a continuous forward flow of lung liquid that drains into the amniotic fluid. This physiological circulation of lung fluid filling the air spaces is critical to lung development. In fact, if it is disturbed lung growth and maturation are impaired. For instance, excess fluid drainage during fetal life or decrease of fluid pressure, due to premature rupture of the membranes or oligohydramnios, are associated with lung hypoplasia with underbranched lungs, which is a major cause of respiratory insufficiency and mortality in newborns (Moessinger *et al.*, 1986; Harding *et al.*, 1990; Copland & Post, 2004; Shi *et al.*, 2007; Wilson *et al.*, 2007; Jani *et al.*, 2009; Jani & Nicolaides, 2012; Gonçalves *et al.*, 2021). In opposition, experimental evidence shows the increase of lung fluid volume as a promotor of fetal lung growth (Dickson & Harding, 1987; Harding *et al.*, 1990). In fact, prenatal tracheal occlusion increases lung fluid volume, luminal pressure, and expansion and, consequently, enhances the rate of branching (Fletcher *et al.*, 2000; Khan *et al.*, 2007; Wilson *et al.*, 2007; Unbekandt *et al.*, 2008; Jiménez *et al.*, 2017). This evidence allowed the development of fetoscopic endoluminal tracheal occlusion (FETO) as a treatment for the more severe cases of pulmonary hypoplasia, in the context of congenital diaphragmatic hernia (CDH) (Ruano *et al.*, 2013; Ali *et al.*, 2016; Jiménez *et al.*, 2017; Khoshgoo *et al.*, 2019).

Molecular studies have been performed to determine the mechanisms underlying lung fluid production and pulmonary expansion. In brief, the lung fluid is produced by a mechanism dependent on sodium-potassium adenosine triphosphatase (Na^+/K^+-ATPase) pumps and Na^+/K^+2chloride (Cl^-) co-transporters, located on the basolateral surface of pulmonary epithelial cells (Gillie *et al.*, 2001; Finney *et al.*, 2008; Bardou *et al.*, 2009; Brennan *et al.*, 2013, 2016), that stimulate the apical Cl^- secretion via cystic

fibrosis transmembrane conductance regulator (CFTR) or calcium-dependent chloride (CaCC) (Olver & Strang, 1974; Olver *et al.*, 1981; Welsh *et al.*, 1982; Welsh, 1983; Finney *et al.*, 2008; Bardou *et al.*, 2009; Brennan *et al.*, 2013, 2016). Finally, it is the increase of intraluminal Cl^- concentration ($[Cl^-]$) that favors the movement of sodium and water into the lumen and promotes the lung liquid formation and the consequent pulmonary expansion (Olver & Strang, 1974; Olver *et al.*, 1981; Welsh *et al.*, 1982; Welsh, 1983; Dickson & Harding, 1987). In addition, inhibition of the apical ionic channels, such as CFTR, TMEM16A, voltage-sensitive chloride channel2 (ClC2) or the extracellular calcium receptor (CaR), induces key morphological defects in branching morphogenesis (Blaisdell *et al.*, 2004; Larson & Cohen, 2006; Finney *et al.*, 2008; Ousingsawat *et al.*, 2009; Rock *et al.*, 2009; Brennan *et al.*, 2016; Meyerholz *et al.*, 2018).

An emergent area, mechanotransduction, showed cells able to translate a mechanical stimulus, like pressure, into biochemical signaling. However, the mechanisms by which pressure is sensed in the lung have not yet been determined (Morrisey & Hogan, 2010). In fetal lung, smooth muscle cells are essential for peristaltic airway contractions, while the pulmonary neuroendocrine cells (PNECs)/ neuroepithelial bodies (NEBs) are indicated as chemo- and mechano-sensors, particularly during the perinatal period. Indeed, the peristaltic airway contractions generate not only the flow of intraluminal fluid but also the periodic distension and relaxation of the end buds essential for branching morphogenesis (Schittny *et al.*, 2000; Santos *et al.*, 2007; Kim *et al.*, 2015; Goodwin *et al.*, 2019). Oppositely, PNECs/NEBs are promotors of *in vivo* and *ex vivo* fetal lung growth (Sunday *et al.*, 1990; Santos *et al.*, 2006; Nunes *et al.*, 2008; Sakai *et al.*, 2014; Pereira-Terra *et al.*, 2015) and sensors for hypoxia, hypercapnia, acidosis, or airway stretch (reviewed in (Garg *et al.*, 2019)) with undefined functions in fetal lung development. A recent publication showed PIEZO2, a known mechanosensor (Nonomura *et al.*, 2017; Wang *et al.*, 2017; Zeng *et al.*, 2018) expressed in NEBs, indicating NEBs capable of sensing the mechanical stretch (Nonomura *et al.*, 2017). This study also reports PIEZO2 expressed in sensory neurons as important in the regulation of lung expansion and efficient neonatal respiration in a mechanism dependent on the central nervous system (Nonomura *et al.*, 2017). However, the inactivation of PIEZO2 in sensory neurons, but not in PNECs/NEBs, was essential for respiratory transition at birth (Nonomura *et al.*, 2017), maintaining the importance of stretch sensation by PNECs unclear.

PIEZO proteins, PIEZO1 and PIEZO2, are mechanically activated cation channels that form homomultimeric complexes sufficient to mediate mechanically induced currents (Coste *et al.*, 2010, 2012; Ge *et al.*, 2015). Previous work showed PIEZO1 as essential in the regulation of basal blood pressure and normal cellular volume in red blood cells in adulthood (Cahalan *et al.*, 2015; Zeng *et al.*, 2018), whereas

PIEZO2 mediated the sensory processes (Ranade *et al.*, 2014; Woo *et al.*, 2014; Feng *et al.*, 2018) and the respiratory physiology (Nonomura *et al.*, 2017).

In this context, to investigate the mechanotransduction signaling intrinsic to fetal lung growth, we explore both the neuroendocrine cells and the mechanoreceptors as intermediators of intraluminal fluid composition during branching morphogenesis.

Methods

Ethical approval

This study was carried out in strict accordance with FELASA guidelines (Benavides *et al.*, 2019) and European regulations (European Union Directive 86/609/EEC). All animal experiments were approved by the Life and Health Sciences Research Institute (ICVS), University of Minho, and by the Direção Geral de Alimentação e Veterinária (approval No. DGAV 021328).

Animals

Female Sprague–Dawley rats (225 g; Charles-River; Spain) were maintained in appropriate cages under controlled conditions and fed with commercial solid food. The rats were mated and checked daily for vaginal plug. The day of plugging was defined as embryonic day (E) 0.5 for time dating purposes. Embryos were dissected at either E13.5 or E17.5 and the embryonic lungs were removed for posterior analysis.

Lung explant cultures

Harvesting and dissection of E13.5 lungs were made in PBS under a dissection microscope (Leica MZFLIII, Switzerland). Lungs were then transferred to the nucleopore membranes (Cat No. TETP01300, Whatman, USA) and cultured in a complete medium [50% DMEM low glucose, 50% nutrient mixture F-12 (Gibco, USA) supplemented with 100 µg/mL glutamine (Cat. No 25030081, Gibco, USA), 100 units/mL penicillin-streptomycin, (Cat. No 15140122, Gibco, USA), 0.25 mg/mL l-ascorbic acid (Cat No. A4403, Sigma-Aldrich, USA) and 10% fetal bovine serum (FBS) (Cat No. 26140079, Gibco, USA)] (Gonçalves *et al.*, 2020). The fetal lung explants were incubated in a 5% CO2 incubator at 37°C for 96h, and the medium was replaced every 48h.

Lung fluid manipulation

Crescent Chloride concentration

According to *in vivo* (Olver *et al.*, 1981) and *ex vivo* (Nemeth *et al.*, 1998; Ma *et al.*, 2002; Brennan *et al.*, 2016) studies, 143mM Cl^- was defined as basal [Cl^-]. The manipulation of intraluminal [Cl^-] was achieved using three experimental concentrations: 5.8, 29, and 715mM Cl^-. Lungs were randomly assigned one of four experimental groups (n ≥ 12 per condition). After intraluminal injections at day 0 (D0) and D2, morphological and molecular dynamics were determined at D4.

To strictly manipulate the [Cl^-] maintaining the similar concentration of the remaining ions, the following chemical compounds were used: potassium chloride (KCl, Cat No. 7447-40-7, Merck, Germany), magnesium chloride ($MgCl_2$, Cat No. 7786-30-3, Merck, Germany), calcium chloride ($CaCl_2$, Cat No. C1016-100G, Sigma-Aldrich, USA), potassium D-Gluconate (Cat No. G8270-100G, Sigma-Aldrich, USA), MgSO4 (Cat No. M7506 Sigma-Aldrich, USA) and calcium D-gluconate (Cat No. C8231-100G, Sigma-Aldrich, USA). Specifically, KCl, $MgCl_2$, and $CaCl_2$ were used as donors of Cl^-, K^+, Mg^{2+}, and Ca^{2+}, while potassium D-gluconate, MgSO4, and calcium D-gluconate worked as replace compounds, as demonstrated in Supplementary Table S1a-b. Thus, the relative influence of the different chemical compounds for the lower and higher [Cl^-] were as follow (in mM, adapted from (Raimondo *et al.*, 2013)): 5.8mM Cl^-: KCl (5.711), $MgCl_2$ (0.049), $CaCl_2$ (0.041), D-glucose (10.000, Cat No. G8270-1KG, Sigma-Aldrich, USA), HEPES (5.000, Cat No. H3375-25G, Sigma-Aldrich, USA), potassium D-gluconate (698.290), $MgSO_4$ (5.950, Cat No. M7506-1KG-M, Sigma-Aldrich, USA), Calcium D-gluconate (4.960, Cat No. C8231-100G, Sigma-Aldrich, USA); 715mM Cl^-: KCl (704.000), $MgCl_2$ (6.000), $CaCl_2$ (5.000), D-glucose (10.000), HEPES (5.000) as shown in Supplementary Table S1a-b.

Chloride channel inhibitors

9-carboxylic acid (A9C, Cat No. A89405, Sigma-Aldrich, USA) (Valenzuela *et al.*, 2000; Al Khamici *et al.*, 2015), CFTRinh (Cat No. C2992, Sigma-Aldrich, USA) (Li *et al.*, 2007; Melis *et al.*, 2014) or CaCC (Cat No. SML0916, Sigma-Aldrich, USA) (Boedtkjer *et al.*, 2015; Nakazawa *et al.*, 2016) were dissolved in dimethyl sulfoxide (DMSO, Cat No. D8418, Sigma-Aldrich, USA) according to the manufacture's protocol guidelines. Lung explants were randomly assigned to one of four experimental groups: A9C (10μM), CFTRinh (5μM), CaCCinh (10μM), or matching volumes of DMSO for control. Lungs were randomly assigned one of four experimental groups (n ≥ 12 per condition).

Inhibitors and DMSO were diluted in a standard solution containing (in mM): sodium chloride (135.000, NaCl, Cat No. 7647-14-5, Merck, Germany), KCl (5.000), $MgCl_2$ (1.200), $CaCl_2$ (1.000), D-glucose

(10.000), HEPES (5.000) were used as vehicle according to the previously published work adapted from (Brennan *et al.*, 2016).

Intraluminal injections

Pulmonary tissues were punctured for intraluminal injections. For that, borosilicate glass capillaries (1.55 mm outer diameter, 1.15 mm inner diameter; HIRS9201590, VWR International, USA) were pulled using Flaming Brown Micropipette Puller (P500, Heat 545, Vel 13, Del 10; Model P-97, Sutter Instrument Co., USA). Lung explants were randomly selected and under the stereoscopic dissecting microscope (Olympus SZX16 stereomicroscope), the intraluminal injections were performed on day0 (D0) and day2 (D2). The pulled borosilicate glass capillary was filled with one of the experimental solutions marked with trypan blue (Cat No. T8154, Sigma-Aldrich, USA) and the capillary was then slowly inserted into the lumen. The presence of trypan blue in the lumen was indicative of successful assessment. Only the lung explants with effective injections at D0 and D2 and perfectly placed in the nucleopore membrane were considered for analysis.

PIEZO1/PIEZO2 inhibition

GsMTx4 (Cat No. ab141871, Abcam, UK), a selective PIEZO1/PIEZO2 inhibitor, was diluted in water and at the final concentration of 5µM, GsMTx4 were supplemented to the culture medium on the day of intraluminal injections, D0 and D2, following the previously published work (Gnanasambandam *et al.*, 2017; Wang *et al.*, 2017; Maneshi *et al.*, 2018). Lungs were randomly assigned one of four experimental groups ($n \geq 12$ per condition).

Morphometric analysis

The branching morphogenesis was monitored daily by photographing the explants. At D0 (0h) and D4 (96h) of culture, the branching of all lung explants was determined by counting the number of peripheral airway epithelial buds of the developing respiratory tree (Massoud *et al.*, 1993). For the morphometric analysis, the internal perimeter of the lung (epithelium) was assessed at D0 and D4 using Axion-Vision Rel 4.3 (Carl Zeiss GmbH, Germany). Lastly, explants were processed for immunofluorescence or western blot assay.

Immunofluorescence

For immunostaining, lungs at E17.5 and from the lung explant cultures at D4 were fixed in 4% paraformaldehyde for 2 hours or 15 minutes, respectively. Whole lungs and explants were then embedded in OCT (OCT compound, Cat No. 4582, Scigen, UK) sectioned (4μm) and placed on SuperFrost®Ultra Plus slides (11976299, Thermo Scientific, UK).

Double immunostained using a 3-day protocol were next performed (adapted from (Bajanca *et al.*, 2004; Lazarus *et al.*, 2011)). Slides were first boiled in 10mM citrate buffer (Cat No. AP-9003-125, Thermo Scientific, UK) for 20 minutes (*in vivo* samples) or 5 minutes (explant). Samples were blocked by incubation in 20% bovine serum albumin (Cat No. A3294, Sigma-Aldrich, USA) and 0.5% Triton X-100 (Cat No. 9036-19-5, Merck, Germany) for 4 hours followed by 36 hours of incubation with primary antibodies at room temperature (RT). Sections were then washed and incubated with the corresponding secondary antibodies for 12 hours in 1% BSA in PBS at RT. Finally, samples were washed in PBS1x, incubated with 4′,6-diamidino-2-phenylindole (DAPI, Cat No. D1306, Life Technologies, USA) for 1 minute at RT, and mounted in PermaFluor™ Aqueous Mounting Medium (Cat No. TA-006-FM, Life Technologies, USA). Visualization and image capture of immunofluorescence staining was performed using an Olympus Widefield Upright Microscope BX61 (Olympus Corporation, Japan).

The primary antibodies used were PGP9.5 (1:150, Cat No. ab72911, Abcam, UK), PIEZO1 (1:50, Cat No. NBP1-78537, Novus Biologicals, USA), and PIEZO2 (1:50, Cat No. NBP1-78624, Novus Biologicals, USA). Negative control reactions included the omission of the primary antibody. The secondary antibodies were: Alexa Fluor 647-conjugated donkey anti-rabbit IgG(H+L) (1:500, Cat No. A31573, Life Technologies, USA) and Alexa Fluor plus 488-conjugated goat anti-mouse IgG(H+L) (1:500, Cat No. A32723, Life Technologies, USA). Different and unrepeated *in vivo* samples or lung explants were randomly selected, n ≥ 4 per stage or condition/antibody for whole lungs and lung explants).

Western blot

Lungs explants were processed for Western blot analysis according to the previously described methods (Gonçalves *et al.*, 2020). In brief, 15 μg of protein were loaded onto 10% acrylamide mini gels, electrophoresed at 100 V at room temperature, and then transferred to nitrocellulose membranes (HybondTM-C Extra, GE Healthcare Life Sciences, UK). Blots were blocked in 5% bovine serum albumin and probed with primary antibodies to ghrelin (1:250, ON, 4°C; Cat No. sc10368, Santa Cruz Biotechnology Inc., USA), bombesin (1:250, ON, 4°C; Cat No. H00002922-MO3, Novus Biologicals, USA), PIEZO1 (1:250, ON, 4°C; Cat No. HPA047185, Sigma-Aldrich, USA), PIEZO2 (1:250, ON, 4°C; Cat No. HPA040616, Sigma-

Aldrich, USA), myosin light chain 2 (MLC2, 1:250; ON, 4°C; Cat No. #3672, Cell Signaling Technology Inc., USA), and alpha-smooth muscle actin (α-SMA, 1:500, ON, 4°C; Cat No. NBP2-33006, Novus Biologicals, USA) according to the manufacturer's instructions. For loading control, blots were probed with GAPDH (1:5000; Cat No. MAB5718, R&D system, USA). After this, membranes were incubated with the corresponding secondary antibodies, developed with Clarity West ECL substrate (Cat No. 1705060, Bio-Rad, USA), and the chemiluminescent signal was captured by the Chemidoc XRS (Bio-Rad, USA) (Gonçalves *et al.*, 2020).

Quantitative analysis was performed with Quantity One 4.6.5 1-D Analysis Software (Bio-Rad, USA). Three independent experiments were performed ($n \geq 4$ were used per antibody/condition).

Statistical Analysis

All quantitative data are presented as mean ± standard deviation (SD). One-way ANOVA was performed for the number of peripheral airway buds, epithelial perimeter, and protein expression levels on [Cl] (5.8, 29, 143, 715mM), and Cl^- channels inhibitors (SS, A9C, CFTRinh, CaCCinh). Two-way ANOVA was used in the analysis of both morphological (number of peripheral airway buds, epithelial perimeter) and the molecular (protein expression levels) effect after GsMTx4 exposure. The parametric test assumptions were previously verified, and an additional LSD test was used for post-test analysis. Statistical analysis was performed using the statistical software IBM SPSS Statistics 26.0. Statistical significance was confirmed at $p < {}^{\mu}0.05$, ${}^{\gamma}0.01$, ${}^{\beta}0.001$, and ${}^{\alpha}0.0001$.

Results

Intraluminal injection in *ex vivo* lung explant cultures.

To establish the intraluminal injections in *ex vivo* lung explant cultures, lung tissue was punctured using pulled borosilicate glass capillaries and, for the first time, effective intraluminal injections at D0 and D2 were performed as demonstrated in supplementary movie1 and movie2, respectively. Furthermore, dynamic luminal movements were observed at D4 (supplementary movie3) that recognized the existence of fetal lung liquid in *ex vivo* lung explant cultures.

Luminal chloride as a modulator of branching morphogenesis.

To study the role of intraluminal composition in branching morphogenesis, *ex vivo* lung explants were cultured for 4 days after injection of crescent [Cl]: 5.8, 29, 143, 715mM Cl^- or Cl^- channels inhibitors: SS, A9C, CFTRinh, CaCCinh.

Morphometric analysis revealed an opposite effect in branching morphogenesis after injection of 5.8 and 715mM Cl^-, indicated by the ratio of D4 and D0 in the number of peripheral airway buds (Figure 1a-b) and epithelial perimeter (Figure 1c). Specifically, when compared to basal [Cl^-], 5.8mM inhibits, whereas 715mM Cl^- stimulates both the number of peripheral airway buds (Figure 1b) and the epithelial perimeter (Figure 1c). Unexpectedly, injection of 29mM was unable to change branching morphogenesis at D4 (Figure 1a-c)

Regarding the Cl^- channels inhibitors, an important inhibitory effect in terms of the number of peripheral airway buds (Figure 1d-e) and epithelial perimeter (Figure 1f) were visualized after CFTRinh or CaCCinh injections when compared with SS, while unchanged lung growth was observed after A9C luminal injection (Figure 1d-f).

PIEZO1 and PIEZO2 are expressed in pulmonary neuroendocrine cells during branching morphogenesis.

To explore the molecular mechanism under branching morphogenesis and intraluminal composition, the spatial distribution of mechanosensors (PIEZO1 and PIEZO2), and neuroendocrine cell marker (PGP9.5) were determined in both *in vivo* and *ex vivo* branching morphogenesis. Immunofluorescence assay disclosed the colocalization of PIEZO1 and PIEZO2 with PGP9.5 at E17.5 (Figure 2a) and after intraluminal injection of SS or 143mM Cl^- in *ex vivo* lung explant cultures (Figure 2b). Regarding the [Cl^-] and Cl^- channels inhibitors, the similar expression profile observed for PIEZO1 and PIEZO2 in $PGP9.5^+$ cells at 5.8 and 715mM Cl^- (Figure 2c) contrast with the more restricted PIEZO1 and PIEZO2 pattern visualized in neuroendocrine cells after injection of CFTRinh or CaCCinh (Figure 2d).

Intraluminal chloride concentration regulates ghrelin, bombesin, PIEZO1, and PIEZO2, expression levels.

Since the PIEZO1 and PIEZO2 are expressed in neuroendocrine cells in branching morphogenesis, we then quantified by western blot the relative expression levels of receptors: PIEZO1, PIEZO2; and neuroendocrine products: ghrelin and bombesin, at the above-mentioned experimental conditions.

In comparison with 143mM Cl^-, 715mM was an inductor of ghrelin (Figure 3a-b), bombesin (Figure 3c), PIEZO1 (Figure 3d), and PIEZO2 (Figure 3e) expression, whereas 5.8mM Cl^- restrict inhibited the relative expression levels of ghrelin (Figure 3a-e). Unchanged molecular profile in terms of ghrelin (Figure 3b), bombesin (Figure 3c), PIEZO1 (Figure 3d), or PIEZO2 (Figure 3e) were detected analyzing 29 versus 143mM Cl^-.

Regarding the Cl^- channels inhibition, distinct effects on ghrelin (Fig. 3f-g), bombesin (Fig. 3h), PIEZO1 (Figure 3i), and PIEZO2 (Figure 3j) expression were visualized after inhibition of ClCs by A9C, CFTR by

CFTRinh, and CaCC by CaCCinh as demonstrated in Figure 3f-j. Specifically, compared with SS, the injection of CFTRinh or CaCCinh were inhibitors of ghrelin (Figure 3f-g), bombesin (Figure 3h), PIEZO1 (Figure 3i), and PIEZO2 (Figure 3j) expression, whereas no significant modifications in the protein expression levels were observed after A9C injection (Figure 3f-j).

PIEZO1 and PIEZO2 control branching morphogenesis.

To evaluate the functional role of PIEZO1 and PIEZO2 expression in branching morphogenesis, the culture medium was supplemented with GsMTX4, a known pharmacological inhibitor of PIEZO1 and PIEZO2, on the day of intraluminal injections, D0 and D2.

The morphologic analysis showed a similar number of peripheral airway buds and epithelial perimeter after simultaneously medium supplementation with GsMTx4 and intraluminal injection of 5.8, 143, or 715mM Cl^- (Figure 4a-c). Indeed, comparable branching morphogenesis was detected between 5.8mM Cl^- without GsMTx4 and 5.8, 143, or 715mM with GsMTx4 (Figure 4a-c). Concerning the Cl^- channels inhibition, the synchronous SS injection and PIEZO1/PIEZO2 downregulation triggered a relevant decrease in terms of the number of peripheral airway buds (Figure 4d-e). Oppositely, the decrease in branching morphogenesis induced by CFTR or CaCCs inhibitors versus SS without GsMTx4 was unchanged by PIEZO1/PIEZO2 inhibition (Figure 4d-f).

To better identify the PIEZO1/2 function in fetal lung growth, the relative expression levels of PIEZO1, PIEZO2, ghrelin, and bombesin were also evaluated at the aforementioned conditions. GsMTx4 treated-lung presented a decrease in PIEZO1 (Figure 5a-b), PIEZO2 (Figure 5c), ghrelin (Figure 5d), and bombesin (Figure 5e) expression at 143 and 715mM Cl^- when compared with the GsMTx4 untreated-lungs (Figure 5a-e). In contrast, unaffected expression levels of PIEZO1 (Figure 5a-b), PIEZO2 (Figure 5c), ghrelin (Figure 5d), and bombesin (Figure 5e) were visualized comparing the injection of 5.8mM Cl^- with and without GsMTx4.

Concerning the Cl^- channels inhibitors, we reported the GsMTx4 as an inhibitor of PIEZO1 (Figure 5f-g), PIEZO2 (Figure 5h) ghrelin (Figure 5i), and bombesin (Figure 5j) expression after intraluminal injection of SS. On the other hand, the simultaneous inhibition of PIEZO1/PIEZO2 and CFTR or CaCC injection had no additional effect on the relative expression levels of PIEZO1 (Figure 5f-g), PIEZO2 (Figure 5h), ghrelin (Figure 5i), or bombesin (Figure 5j).

The molecular effect of intraluminal injections in airway smooth muscle cells.

Previous work reported a morphological interaction between branching morphogenesis and peristaltic airway contractions. Thus, we then assessed the molecular profile of MLC2 and α-SMA^+ at the above-

mentioned experimental conditions (Figure 6a-c). Our findings revealed an opposite effect in the expression of MLC2 (Figure 6b) and α-SMA (Figure 6c) after injection of 5.8 or 715mM Cl^-. Indeed, when compared with 143mM Cl^-, 5.8 were exposed to be an inhibitor, while 715mM Cl^- promotes the expression of MLC2 (Figure 6b) and α-SMA (Figure 6c). Finally, the depletion of PIEZO1/PIEZO2 expression achieved by GsMTx4 medium supplementation had a similar decrease in terms of the relative expression levels of MLC2 (Figure 6b) and α-SMA (Figure 6c) at 143 and 715mM Cl^- observed at D4. No differences in the relative expression levels were visualized after injection of 5.8mM Cl^- with and without GsMTx4.

Regarding the Cl^- channel inhibitors, after the intraluminal injection of CFTRinh or CaCCinh versus SS, a significant inhibitory effect was visualized in terms of MLC2 (Figure 6d-e) and α-SMA (Figure 6f). In addition, the medium supplementation with GsMTx4 only decreased the relative expression levels of MLC2 (Figure 6e), and α-SMA (Figure 6f) previously observed after SS intraluminal. No additional effects in MLC2 (Figure 6e) or α-SMA (Figure 6f) were visualized after simultaneously GsMTX4 medium supplementation and intraluminal injections of CFTRinh or CaCCinh (Figure 6d-f).

Discussion

The fetal lung develops as a fluid-filled organ that maintains the lung in a constantly distended state, stimulating its growth and maturation (Alcorn *et al.*, 1977; Harding *et al.*, 1984; Hooper & Harding, 1995; Harding & Hooper, 1996). Unfortunately, the difficulty that it is capture or recapitulate these *in vivo* morphological dynamics in the lab compromise the study of the underlying mechanisms, particularly at early developmental stages. In this context, benefiting from the *ex vivo* lung explant cultures that maintain the *in vivo* physiologic architecture and the cellular interactions observed at pseudoglandular or branching stage (Massoud *et al.*, 1993; Yeganeh *et al.*, 2018), we established effective intraluminal injections at D0 and D2 for which the dynamic movements observed at D4 into the lumen indicate the existence of lung liquid in the *ex vivo* model and validate this as a valuable method for the study of lung fluid composition in branching morphogenesis.

On the strongly evidenced premise that the Cl^- movement under the epithelium is an inductor of Na^+ and water movements in the same direction (Olver & Strang, 1974; Olver *et al.*, 1981; Welsh *et al.*, 1982; Welsh, 1983), we manipulate the intraluminal lung fluid composition by injection of crescent [Cl^-] or Cl^- channel inhibitors, and then the branching morphogenesis was analyzed at D4. Our findings demonstrated the intraluminal [Cl^-] is able to regulate fetal lung growth. In fact, the increase of luminal [Cl^-] stimulates branching morphogenesis, whereas a significant decrease was observed after depletion of [Cl^-] at 5.8mM of Cl^-, CFTRinh or CaCCinh (Figure 7). Curiously, experiments in fetal sheep have demonstrated a direct link

between reduced distension due to fluid loss and lung hypoplasia. Conversely, tracheal obstruction in utero, leading to fluid accumulation and results in more rapid lung growth (Nardo *et al.*, 1998). These differences in pressure between the airway lumen and surrounding tissue are essential for normal airway development, with tension and mechanical stretch playing additional roles in cellular differentiation and airway growth (Badri *et al.*, 2008). Finally, the molecular inhibition of ionic channels, such as CFTR, ClC2, or CaR, critical for lung fluid secretion induces key defects *in vivo* and *ex vivo* branching morphogenesis (Blaisdell *et al.*, 2004; Larson & Cohen, 2006; Finney *et al.*, 2008; Brennan *et al.*, 2013, 2016; Meyerholz *et al.*, 2018; He *et al.*, 2020) that reinforce the value of our *ex vivo* model for the study of intraluminal fluid in fetal lung growth.

Our data detected PIEZO1 and PIEZO2 colocalized with PGP9.5, a molecular marker for PNECs/NEBs. Interestingly, PIEZO1 and PIEZO2 receptors are sensors for mechanical stretch, like pressure, with major roles in the regulation of blood pressure and respiratory function at birth, respectively (Coste *et al.*, 2010; Nonomura *et al.*, 2017; Zeng *et al.*, 2018). In contrast, PNECs/NEBs are described as airway sensors with little-understood functions (reviewed in (Garg *et al.*, 2019)). Literature also shows the secreted neuroendocrine products, ghrelin, and bombesin, as promotors of the *in vivo* and *ex vivo* fetal lung growth (Sunday *et al.*, 1990; Santos *et al.*, 2006; Nunes *et al.*, 2008; Sakai *et al.*, 2014; Pereira-Terra *et al.*, 2015). To further investigate these dynamics, neuroendocrine products (ghrelin, bombesin) and mechanoreceptors (PIEZO1 and PIEZO2) were quantified at the aforementioned conditions. We detected the intraluminal [Cl^-] as a modulator of ghrelin, bombesin, PIEZO1, and PIEZO2 expression in branching morphogenesis. Briefly, the decrease of luminal [Cl], 5.8mM Cl^-, was an inhibitor of ghrelin with no significant effects in the expression of the remaining markers (Figure 7). Surprisingly, 715mM Cl^- stimulated ghrelin, bombesin, PIEZO1, and PIEZO2 expression, whereas the luminal injection of CFTRinh or CaCCinh inhibited fetal lung growth and equally inhibited the four markers (Figure 7).

Dickson et al (Dickson & Harding, 1987) described the lung liquid as a regulator of fetal lung growth in a mechanism independent of the lung fluid secretion and indicated the lung as unable to respond to alterations in lung liquid volume (Dickson & Harding, 1987). Indeed, the decrease in pulmonary growth was related to reduced tracheal pressure and tracheal efflux rate in the fetal sheep model (Dickson & Harding, 1987). Now, our analysis demonstrated the molecular players (PIEZO1, PIEZO2, bombesin) overexpressed at 715mM Cl^- and unchanged at 5.8mM Cl^-, when compared with the basal [Cl^-], 143mM. As such, it is important to define the fundamental responses in fetal lung growth after PIEZO1/PIEZO2 inhibition. For that, we next inhibited the PIEZO1/PIEZO2 on the day of intraluminal injections by GsMTx4. We demonstrated a significant inhibition in terms of neuroendocrine products and branching morphogenesis after GsMTx4

medium supplementation. More importantly, these inhibitions were independent of the intraluminal [Cl^-]. In fact, apart for 5.8mM Cl^- where no significant differences between GsMTx4-treated and -untreated lungs were observed, the intraluminal injection of 143, 715mM Cl^- or SS with the synchronized inhibition of PIEZO1/PIEZO2 by GsMTx4 similarly decreased the morphological and molecular profiles. These findings indicate the PIEZO1 and PIEZO2 as major regulators of the mechanosensor pathway in branching morphogenesis. A recent publication showed PIEZO2 as regulator of pulmonary function in both neonates and adults (Nonomura *et al.*, 2017). Indeed, the global and sensory neuron-specific ablation of mechanically activated ion channel PIEZO2 causes respiratory distress and death in newborn mice, whereas the induced ablation of PIEZO2 in the sensory neuron of adult mice causes decreased neuronal responses to lung inflation, an impaired Hering-Breuer mechanoreflex (Nonomura *et al.*, 2017). In this context, our investigation suggests the PIEZO1/PIEZO2 expressed in PNECs/NEBs as sensors of branching morphogenesis in the fetal lung development.

Physiology also showed the movement of intraluminal fluid through epithelial tubules as a consequence of the peristaltic activity of fetal airway smooth muscle (ASM) that maintains positive pressure in the lumen area to keep the tubules in a distended state (Hooper & Harding, 1995). The formation of new airspaces during branching morphogenesis early in gestation is closely followed by the differentiation of mesenchymal cells into ASM cells. Evidenced by cellular expression of the contractile protein α-SMA as an early differentiation marker (Leslie *et al.*, 1990), ASM progenitor cells have been identified in both the proximal and distal lung mesenchyme (Mailleux *et al.*, 2005; Shan *et al.*, 2008). This differentiation of ASM simultaneous produce the MLC filaments in fetal lungs (Lowey & Trybus, 1995; Schittny *et al.*, 2000; Santos *et al.*, 2007; Kim *et al.*, 2015; Yu *et al.*, 2016; Goodwin *et al.*, 2019; Álvarez-Santos *et al.*, 2020). To determine the molecular effect of intraluminal Cl^- composition in airway smooth muscle cells, we evaluated α-SMA and MLC2 at the aforementioned experimental condition with and without GsMTx4. We observed the increase of [Cl^-] and branching morphogenesis related to the overexpression of MLC2 and α-SMA. Oppositely, the decrease in α-SMA and MLC2 were associated with reduced [Cl^-] and branching morphogenesis (Fig. 7). These results indicated the intraluminal composition and the neuroendocrine activation upstream of airway smooth muscle contraction and branching morphogenesis. Interestingly, the hypoplastic phenotype observed in CDH context was connected to decrease on α-SMA and MLC2 from pseudoglandular-to-canalicular (Santos *et al.*, 2007), whereas the tracheal occlusion in *in vivo* mouse model was inductor of α-SMA and MLC2 expression at later canalicular stage (Seaborn *et al.*, 2008), suggesting the PIEZO1/PIEZO2 pathway as a potential target for the treatment of fetal pulmonary hypoplasia.

Collectively, our findings offer a mechanistic basis for previous *in vivo* studies that report the excess of fluid drainage during fetal life or decrease of fluid pressure associated with lung hypoplasia with underbranched lungs (Moessinger *et al.*, 1986; Harding *et al.*, 1990; Copland & Post, 2004; Shi *et al.*, 2007; Wilson *et al.*, 2007; Jani *et al.*, 2009; Jani & Nicolaides, 2012; Gonçalves *et al.*, 2021). Here, we described key information on the specific pathway of action by which the intraluminal Cl^- composition regulates fetal lung growth. We demonstrate how the intraluminal [Cl^-] activate the PNECs/NEBs through PIEZO1/PIEZO2 mechanoreceptors that in turn regulate the expression of ghrelin, bombesin, α-SMA, and MLC2 in the fetal lung growth (Figure 7).

References

Al Khamici H, Brown LJ, Hossain KR, Hudson AL, Sinclair-Burton AA, Ng JP, Daniel EL, Hare JE, Cornell BA, Curmi PM, Davey MW & Valenzuela SM (2015). Members of the chloride intracellular ion channel protein family demonstrate glutaredoxin-like enzymatic activity. *PLoS One* **10,** e115699.

Alcorn D, Adamson TM, Lambert TF, Maloney JE, Ritchie BC & Robinson PM (1977). Morphological effects of chronic tracheal ligation and drainage in the fetal lamb lung. *J Anat* **123,** 649–660.

Ali K, Bendapudi P, Polubothu S, Andradi G, Ofuya M, Peacock J, Hickey A, Davenport M, Nicolaides K & Greenough A (2016). Congenital diaphragmatic hernia-influence of fetoscopic tracheal occlusion on outcomes and predictors of survival. *Eur J Pediatr* **175,** 1071–1076.

Álvarez-Santos MD, Álvarez-González M, Estrada-Soto S & Bazán-Perkins B (2020). Regulation of Myosin Light-Chain Phosphatase Activity to Generate Airway Smooth Muscle Hypercontractility. *Front Physiol* **11,** 701.

Badri KR, Zhou Y & Schuger L (2008). Embryological origin of airway smooth muscle. *Proc Am Thorac Soc* **5,** 4–10.

Bajanca F, Luz M, Duxson MJ & Thorsteinsdottir S (2004). Integrins in the mouse myotome: developmental changes and differences between the epaxial and hypaxial lineage. *Dev Dyn* **231,** 402–415.

Bardou O, Trinh NT & Brochiero E (2009). Molecular diversity and function of K+ channels in airway and alveolar epithelial cells. *Am J Physiol Lung Cell Mol Physiol* **296,** L145-55.

Benavides F, Rulicke T, Prins JB, Bussell J, Scavizzi F, Cinelli P, Herault Y & Wedekind D (2019). Genetic quality assurance and genetic monitoring of laboratory mice and rats: FELASA Working Group Report. *Lab Anim*23677219867719.

Blaisdell CJ, Morales MM, Andrade AC, Bamford P, Wasicko M & Welling P (2004). Inhibition of CLC-2 chloride channel expression interrupts expansion of fetal lung cysts. *Am J Physiol Lung Cell Mol Physiol* **286,** L420-6.

Boedtkjer DM, Kim S, Jensen AB, Matchkov VM & Andersson KE (2015). New selective inhibitors of calcium-activated chloride channels - T16A(inh) -A01, CaCC(inh) -A01 and MONNA - what do they inhibit? *Br J Pharmacol* **172,** 4158–4172.

Brennan SC, Finney BA, Lazarou M, Rosser AE, Scherf C, Adriaensen D, Kemp PJ & Riccardi D (2013). Fetal calcium regulates branching morphogenesis in the developing human and mouse lung: involvement of voltage-gated calcium channels. *PLoS One* **8,** e80294.

Brennan SC, Wilkinson WJ, Tseng HE, Finney B, Monk B, Dibble H, Quilliam S, Warburton D, Galietta LJ, Kemp PJ & Riccardi D (2016). The extracellular calcium-sensing receptor regulates human fetal lung development via CFTR. *Sci Rep* **6,** 21975.

Cahalan SM, Lukacs V, Ranade SS, Chien S, Bandell M & Patapoutian A (2015). Piezo1 links mechanical forces to red blood cell volume. *Elife*; DOI: 10.7554/eLife.07370.

Copland I & Post M (2004). Lung development and fetal lung growth. *Paediatr Respir Rev* **5 Suppl A,** S259-64.

Coste B, Mathur J, Schmidt M, Earley TJ, Ranade S, Petrus MJ, Dubin AE & Patapoutian A (2010). Piezo1 and Piezo2 are essential components of distinct mechanically activated cation channels. *Science* **330,** 55–60.

Coste B, Xiao B, Santos JS, Syeda R, Grandl J, Spencer KS, Kim SE, Schmidt M, Mathur J, Dubin AE, Montal M & Patapoutian A (2012). Piezo proteins are pore-forming subunits of mechanically activated channels. *Nature* **483,** 176–181.

Dickson KA & Harding R (1987). Restoration of lung liquid volume following its acute alteration in fetal sheep. *J Physiol* **385,** 531–543.

Feng J, Luo J, Yang P, Du J, Kim BS & Hu H (2018). Piezo2 channel-Merkel cell signaling modulates the conversion of touch to itch. *Science* **360,** 530–533.

Finney BA, del Moral PM, Wilkinson WJ, Cayzac S, Cole M, Warburton D, Kemp PJ & Riccardi D (2008). Regulation of mouse lung development by the extracellular calcium-sensing receptor, CaR. *J Physiol* **586,** 6007–6019.

Fletcher AJ, Edwards CM, Gardner DS, Fowden AL & Giussani DA (2000). Neuropeptide Y in the sheep fetus: effects of acute hypoxemia and dexamethasone during late gestation. *Endocrinology* **141,** 3976–3982.

Garg A, Sui P, Verheyden JM, Young LR & Sun X (2019). Consider the lung as a sensory organ: A tip from pulmonary neuroendocrine cells. *Curr Top Dev Biol* **132,** 67–89.

Ge J, Li W, Zhao Q, Li N, Chen M, Zhi P, Li R, Gao N, Xiao B & Yang M (2015). Architecture of the mammalian mechanosensitive Piezo1 channel. *Nature* **527,** 64–69.

Gillie DJ, Pace AJ, Coakley RJ, Koller BH & Barker PM (2001). Liquid and ion transport by fetal airway and lung epithelia of mice deficient in sodium-potassium-2-chloride transporter. *Am J Respir Cell Mol Biol* **25,** 14–20.

Gnanasambandam R, Ghatak C, Yasmann A, Nishizawa K, Sachs F, Ladokhin AS, Sukharev SI & Suchyna TM (2017). GsMTx4: Mechanism of Inhibiting Mechanosensitive Ion Channels. *Biophys J* **112,** 31–45.

Goncalves AN, Correia-Pinto J & Nogueira-Silva C (2019). Imagiological methods for prediction of fetal pulmonary hypoplasia: a systematic review. *J Matern Fetal Neonatal Med*1–10.

Gonçalves AN, Correia-Pinto J & Nogueira-Silva C (2020). ROBO2 signaling in lung development regulates SOX2/SOX9 balance, branching morphogenesis and is dysregulated in nitrofen-induced congenital diaphragmatic hernia. *Respiratory Research* **21,** 302.

Goodwin K, Mao S, Guyomar T, Miller E, Radisky DC, Košmrlj A & Nelson CM (2019). Smooth muscle differentiation shapes domain branches during mouse lung development. *Development*; DOI: 10.1242/dev.181172.

Harding R & Hooper SB (1996). Regulation of lung expansion and lung growth before birth. *J Appl Physiol (1985)* **81,** 209–224.

Harding R, Hooper SB & Dickson KA (1990). A mechanism leading to reduced lung expansion and lung hypoplasia in fetal sheep during oligohydramnios. *Am J Obstet Gynecol* **163,** 1904–1913.

Harding R, Pinkerton K & Plopper C (n.d.). The lung : development, aging and the environment.

Harding R, Sigger JN, Wickham PJ & Bocking AD (1984). The regulation of flow of pulmonary fluid in fetal sheep. *Respir Physiol* **57,** 47–59.

He M, Wu B, Ye W, Le DD, Sinclair AW, Padovano V, Chen Y, Li KX, Sit R, Tan M, Caplan MJ, Neff N, Jan YN, Darmanis S & Jan LY (2020). Chloride channels regulate differentiation and barrier functions of the mammalian airway. *Elife*; DOI: 10.7554/eLife.53085.

Hooper SB & Harding R (1995). Fetal lung liquid: a major determinant of the growth and functional development of the fetal lung. *Clin Exp Pharmacol Physiol* **22,** 235–247.

Jani JC, Benachi A, Nicolaides KH, Allegaert K, Gratacós E, Mazkereth R, Matis J, Tibboel D, Van Heijst A, Storme L, Rousseau V, Greenough A & Deprest JA (2009). Prenatal prediction of neonatal morbidity in survivors with congenital diaphragmatic hernia: a multicenter study. *Ultrasound Obstet Gynecol* **33,** 64–69.

Jani JC & Nicolaides KH (2012). Fetal surgery for severe congenital diaphragmatic hernia? *Ultrasound Obstet Gynecol* **39,** 7–9.

Jiménez JA, Eixarch E, DeKoninck P, Bennini JR, Devlieger R, Peralta CF, Gratacos E & Deprest J (2017). Balloon removal after fetoscopic endoluminal tracheal occlusion for congenital diaphragmatic hernia. *Am J Obstet Gynecol* **217,** 78.e1-78.e11.

Khan PA, Cloutier M & Piedboeuf B (2007). Tracheal occlusion: a review of obstructing fetal lungs to make them grow and mature. *Am J Med Genet C Semin Med Genet* **145c,** 125–138.

Khoshgoo N, Kholdebarin R, Pereira-Terra P, Mahood TH, Falk L, Day CA, Iwasiow BM, Zhu F, Mulhall D, Fraser C, Correia-Pinto J & Keijzer R (2019). Prenatal microRNA miR-200b Therapy Improves Nitrofen-induced Pulmonary Hypoplasia Associated With Congenital Diaphragmatic Hernia. *Ann Surg* **269,** 979–987.

Kim HY, Pang MF, Varner VD, Kojima L, Miller E, Radisky DC & Nelson CM (2015). Localized Smooth Muscle Differentiation Is Essential for Epithelial Bifurcation during Branching Morphogenesis of the Mammalian Lung. *Dev Cell* **34,** 719–726.

Larson JE & Cohen JC (2006). Improvement of pulmonary hypoplasia associated with congenital diaphragmatic hernia by in utero CFTR gene therapy. *Am J Physiol Lung Cell Mol Physiol* **291,** L4-10.

Lazarus A, Del-Moral PM, Ilovich O, Mishani E, Warburton D & Keshet E (2011). A perfusion-independent role of blood vessels in determining branching stereotypy of lung airways. *Development* **138,** 2359–2368.

Leslie KO, Mitchell JJ, Woodcock-Mitchell JL & Low RB (1990). Alpha smooth muscle actin expression in developing and adult human lung. *Differentiation* **44,** 143–149.

Li C, Krishnamurthy PC, Penmatsa H, Marrs KL, Wang XQ, Zaccolo M, Jalink K, Li M, Nelson DJ, Schuetz JD & Naren AP (2007). Spatiotemporal coupling of cAMP transporter to CFTR chloride channel function in the gut epithelia. *Cell* **131,** 940–951.

Lowey S & Trybus KM (1995). Role of skeletal and smooth muscle myosin light chains. *Biophys J* **68,** 120S-126S; discussion 126S-127S.

Ma T, Thiagarajah JR, Yang H, Sonawane ND, Folli C, Galietta LJ & Verkman AS (2002). Thiazolidinone CFTR inhibitor identified by high-throughput screening blocks cholera toxin-induced intestinal fluid secretion. *J Clin Invest* **110,** 1651–1658.

Mailleux AA, Kelly R, Veltmaat JM, De Langhe SP, Zaffran S, Thiery JP & Bellusci S (2005). Fgf10 expression identifies parabronchial smooth muscle cell progenitors and is required for their entry into the smooth muscle cell lineage. *Development* **132,** 2157–2166.

Maneshi MM, Ziegler L, Sachs F, Hua SZ & Gottlieb PA (2018). Enantiomeric Aβ peptides inhibit the fluid shear stress response of PIEZO1. *Sci Rep* **8,** 14267.

Massoud EA, Sekhon HS, Rotschild A, Puterman ML, Matsui R & Thurlbeck WM (1993). In vitro branching morphogenesis of the fetal rat lung. *Pediatr Pulmonol* **15,** 89–97.

Melis N, Tauc M, Cougnon M, Bendahhou S, Giuliano S, Rubera I & Duranton C (2014). Revisiting CFTR inhibition: a comparative study of CFTRinh -172 and GlyH-101 inhibitors. *Br J Pharmacol* **171,** 3716–3727.

Meyerholz DK, Stoltz DA, Gansemer ND, Ernst SE, Cook DP, Strub MD, LeClair EN, Barker CK, Adam RJ, Leidinger MR, Gibson-Corley KN, Karp PH, Welsh MJ & McCray Jr PB (2018). Lack of cystic fibrosis

transmembrane conductance regulator disrupts fetal airway development in pigs. *Lab Invest* **98,** 825–838.

Moessinger AC, Collins MH, Blanc WA, Rey HR & James LS (1986). Oligohydramnios-Induced Lung Hypoplasia: The Influence of Timing and Duration in Gestation. *Pediatric Research* **20,** 951–954.

Morrisey EE & Hogan BL (2010). Preparing for the first breath: genetic and cellular mechanisms in lung development. *Dev Cell* **18,** 8–23.

Nakazawa MS, Eisinger-Mathason TS, Sadri N, Ochocki JD, Gade TP, Amin RK & Simon MC (2016). Epigenetic re-expression of HIF-2alpha suppresses soft tissue sarcoma growth. *Nat Commun* **7,** 10539.

Nardo L, Hooper SB & Harding R (1998). Stimulation of lung growth by tracheal obstruction in fetal sheep: relation to luminal pressure and lung liquid volume. *Pediatr Res* **43,** 184–190.

Nemeth EF, Steffey ME, Hammerland LG, Hung BC, Van Wagenen BC, DelMar EG & Balandrin MF (1998). Calcimimetics with potent and selective activity on the parathyroid calcium receptor. *Proc Natl Acad Sci U S A* **95,** 4040–4045.

Nonomura K, Woo SH, Chang RB, Gillich A, Qiu Z, Francisco AG, Ranade SS, Liberles SD & Patapoutian A (2017). Piezo2 senses airway stretch and mediates lung inflation-induced apnoea. *Nature* **541,** 176–181.

Nunes S, Nogueira-Silva C, Dias E, Moura RS & Correia-Pinto J (2008). Ghrelin and obestatin: different role in fetal lung development? *Peptides* **29,** 2150–2158.

Olver RE, Schneeberger EE & Walters DV (1981). Epithelial solute permeability, ion transport and tight junction morphology in the developing lung of the fetal lamb. *J Physiol* **315,** 395–412.

Olver RE & Strang LB (1974). Ion fluxes across the pulmonary epithelium and the secretion of lung liquid in the foetal lamb. *J Physiol* **241,** 327–357.

Ousingsawat J, Martins JR, Schreiber R, Rock JR, Harfe BD & Kunzelmann K (2009). Loss of TMEM16A causes a defect in epithelial Ca2+-dependent chloride transport. *J Biol Chem* **284,** 28698–28703.

Pereira-Terra P, Moura RS, Nogueira-Silva C & Correia-Pinto J (2015). Neuroendocrine factors regulate retinoic acid receptors in normal and hypoplastic lung development. *J Physiol* **593,** 3301–3311.

Raimondo JV, Joyce B, Kay L, Schlagheck T, Newey SE, Srinivas S & Akerman CJ (2013). A genetically-encoded chloride and pH sensor for dissociating ion dynamics in the nervous system. *Front Cell Neurosci* **7,** 202.

Ranade SS, Woo SH, Dubin AE, Moshourab RA, Wetzel C, Petrus M, Mathur J, Bégay V, Coste B, Mainquist J, Wilson AJ, Francisco AG, Reddy K, Qiu Z, Wood JN, Lewin GR & Patapoutian A (2014). Piezo2 is the major transducer of mechanical forces for touch sensation in mice. *Nature* **516,** 121–125.

Rock JR, O'Neal WK, Gabriel SE, Randell SH, Harfe BD, Boucher RC & Grubb BR (2009). Transmembrane protein 16A (TMEM16A) is a Ca2+-regulated Cl- secretory channel in mouse airways. *J Biol Chem* **284,** 14875–14880.

Ruano R, Peiro JL, da Silva MM, Campos JA, Carreras E, Tannuri U & Zugaib M (2013). Early fetoscopic tracheal occlusion for extremely severe pulmonary hypoplasia in isolated congenital diaphragmatic hernia: preliminary results. *Ultrasound Obstet Gynecol* **42,** 70–76.

Sakai K, Kimura O, Furukawa T, Fumino S, Higuchi K, Wakao J, Kimura K, Aoi S, Masumoto K & Tajiri T (2014). Prenatal administration of neuropeptide bombesin promotes lung development in a rat model of nitrofen-induced congenital diaphragmatic hernia. *J Pediatr Surg* **49,** 1749–1752.

Santos M, Bastos P, Gonzaga S, Roriz JM, Baptista MJ, Nogueira-Silva C, Melo-Rocha G, Henriques-Coelho T, Roncon-Albuquerque Jr R, Leite-Moreira AF, De Krijger RR, Tibboel D, Rottier R & Correia-Pinto J (2006). Ghrelin expression in human and rat fetal lungs and the effect of ghrelin administration in nitrofen-induced congenital diaphragmatic hernia. *Pediatr Res* **59,** 531–537.

Santos M, Moura RS, Gonzaga S, Nogueira-Silva C, Ohlmeier S & Correia-Pinto J (2007). Embryonic essential myosin light chain regulates fetal lung development in rats. *Am J Respir Cell Mol Biol* **37,** 330–338.

Schittny JC, Miserocchi G & Sparrow MP (2000). Spontaneous peristaltic airway contractions propel lung liquid through the bronchial tree of intact and fetal lung explants. *Am J Respir Cell Mol Biol* **23,** 11–18.

Seaborn T, St-Amand J, Cloutier M, Tremblay MG, Maltais F, Dinel S, Moulin V, Khan PA & Piedboeuf B (2008). Identification of cellular processes that are rapidly modulated in response to tracheal occlusion within mice lungs. *Pediatr Res* **63,** 124–130.

Shan L, Subramaniam M, Emanuel RL, Degan S, Johnston P, Tefft D, Warburton D & Sunday ME (2008). Centrifugal migration of mesenchymal cells in embryonic lung. *Developmental Dynamics* **237,** 750–757.

Shi W, Bellusci S & Warburton D (2007). Lung development and adult lung diseases. *Chest* **132,** 651–656.

Sunday ME, Hua J, Dai HB, Nusrat A & Torday JS (1990). Bombesin increases fetal lung growth and maturation in utero and in organ culture. *Am J Respir Cell Mol Biol* **3,** 199–205.

Unbekandt M, del Moral PM, Sala FG, Bellusci S, Warburton D & Fleury V (2008). Tracheal occlusion increases the rate of epithelial branching of embryonic mouse lung via the FGF10-FGFR2b-Sprouty2 pathway. *Mech Dev* **125,** 314–324.

Valenzuela SM, Mazzanti M, Tonini R, Qiu MR, Warton K, Musgrove EA, Campbell TJ & Breit SN (2000). The nuclear chloride ion channel NCC27 is involved in regulation of the cell cycle. *J Physiol* **529 Pt 3,** 541–552.

Wang F, Knutson K, Alcaino C, Linden DR, Gibbons SJ, Kashyap P, Grover M, Oeckler R, Gottlieb PA, Li HJ, Leiter AB, Farrugia G & Beyder A (2017). Mechanosensitive ion channel Piezo2 is important for enterochromaffin cell response to mechanical forces. *J Physiol* **595,** 79–91.

Welsh MJ (1983). Evidence for basolateral membrane potassium conductance in canine tracheal epithelium. *Am J Physiol* **244,** C377-84.

Welsh MJ, Smith PL & Frizzell RA (1982). Chloride secretion by canine tracheal epithelium: II. The cellular electrical potential profile. *J Membr Biol* **70,** 227–238.

Wilson SM, Olver RE & Walters DV (2007). Developmental regulation of lumenal lung fluid and electrolyte transport. *Respir Physiol Neurobiol* **159,** 247–255.

Woo SH, Ranade S, Weyer AD, Dubin AE, Baba Y, Qiu Z, Petrus M, Miyamoto T, Reddy K, Lumpkin EA, Stucky CL & Patapoutian A (2014). Piezo2 is required for Merkel-cell mechanotransduction. *Nature* **509,** 622–626.

Yeganeh B, Bilodeau C & Post M (2018). Explant Culture for Studying Lung Development. *Methods Mol Biol* **1752,** 81–90.

Yu H, Chakravorty S, Song W & Ferenczi MA (2016). Phosphorylation of the regulatory light chain of myosin in striated muscle: methodological perspectives. *Eur Biophys J* **45,** 779–805.

Zeng WZ, Marshall KL, Min S, Daou I, Chapleau MW, Abboud FM, Liberles SD & Patapoutian A (2018). PIEZOs mediate neuronal sensing of blood pressure and the baroreceptor reflex. *Science* **362,** 464–467.

Additional information

Data availability statement

The authors declare that the data supporting the findings of the present study are available within the manuscript or from the corresponding author upon reasonable request.

Competing interests

The authors declare that they have no conflicts of interest.

Author contributions

ANG performed the research, analyzed the data, and wrote the paper; JCP designed the research, analyzed and interpreted the data; CNS designed the research, analyzed the data, and wrote the paper. All authors revise and approved the final version of the manuscript.

Acknowledgments

We are indebted to Goreti Pinto, Magda Carlos, and Alice Miranda for expert technical assistance. This work has been funded by National funds, through the Foundation for Science and Technology (FCT) – project UIDB/50026/2020; by the projects NORTE-01-0145-FEDER-000013 and NORTE-01-0145-FEDER-000023, supported by Norte Portugal Regional Operational Programme (NORTE 2020), under the PORTUGAL 2020 Partnership Agreement, through the European Regional Development Fund (ERDF); and by ICVS Scientific Microscopy Platform, member of the national infrastructure PPBI - Portuguese Platform of Bioimaging (PPBI-POCI-01-0145-FEDER-022122); This work was also funded by POCI-01-0145-FEDER-030881, financed by Fundos Europeus Estruturais e de Investimento (FEEI) and FCT. ANG was supported by FCT and the company José de Mello Saúde S.A. – 2CA Braga (reference PD/BDE/127829/2016). The funders had no role in study design, data collection, and analysis, decision to publish, or preparation of the manuscript.

Supporting information

Additional supporting information may be found online in the Supporting Information section at the end of the article.

Figure's legends

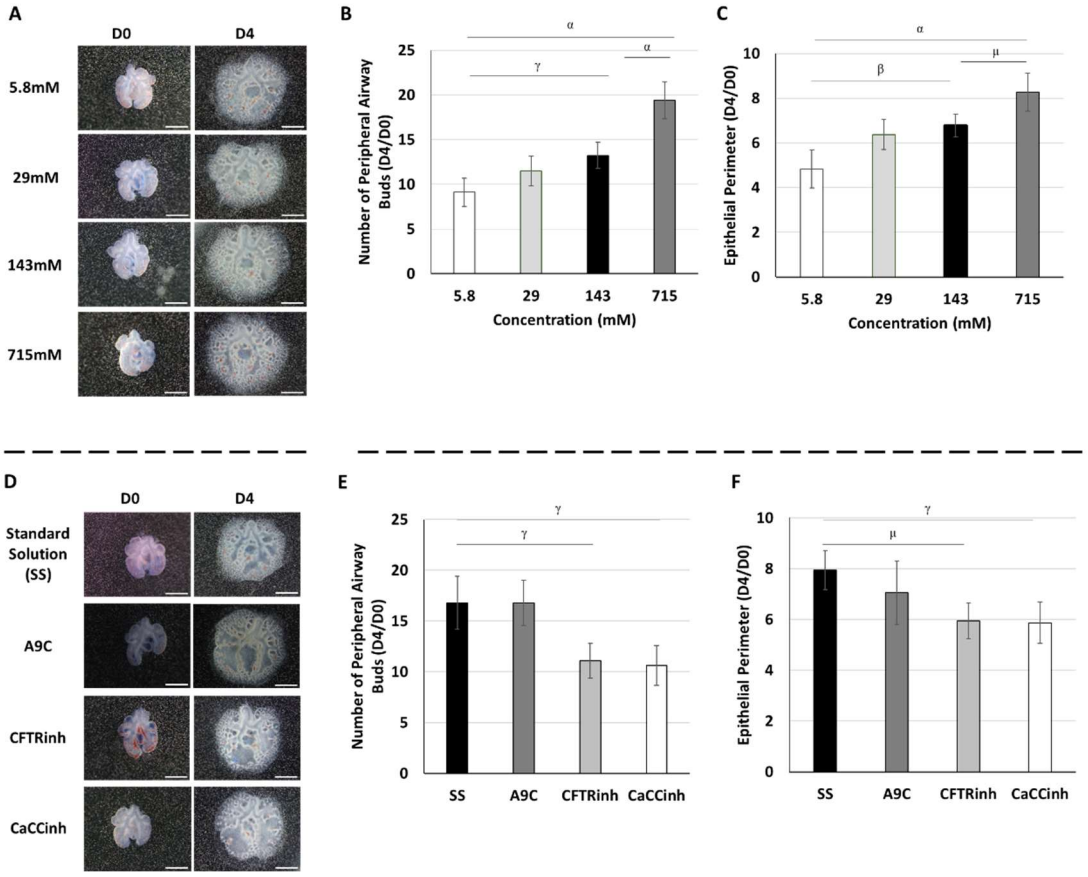

Figure 1 – Intraluminal chloride modulates branching morphogenesis. Upper panel: (A) represents lung explants at day0 and day4 after intraluminal injection of crescent chloride concentrations ([Cl-]): 5.8, 29, 143, and 715mM Cl^-, at day0 and day2. (B-C) Morphometric analysis of (B) number of peripheral airway buds and c epithelial perimeter at the different [Cl-]. Lower panel: (D) represents the fetal lung explants after intraluminal injection of distinct Cl^- channels inhibitors: anthracene-9-carboxylic acid (A9C) to Cl^- voltage-gated channel (ClC); cystic fibrosis transmembrane conductance regulator inhibitor172 (CFTRinh) to CFTR; and calcium-dependent Cl^- channel inhibitorA01 (CaCCinh) to CaCC. (E-F) Morphometric analysis of (E) number of peripheral airway buds and (F) epithelial perimeter. Lungs were randomly assigned one of eight experimental groups (n ≥ 12 per condition). Results are expressed as ratio of D4 and D0 (D4/D0) and presented as mean ±SD. Black rectangles define the control group. Scale bar, 1mm. p< $^{\alpha}0.0001$, $^{\beta}0.001$, $^{\gamma}0.01$, $^{\mu}0.05$.

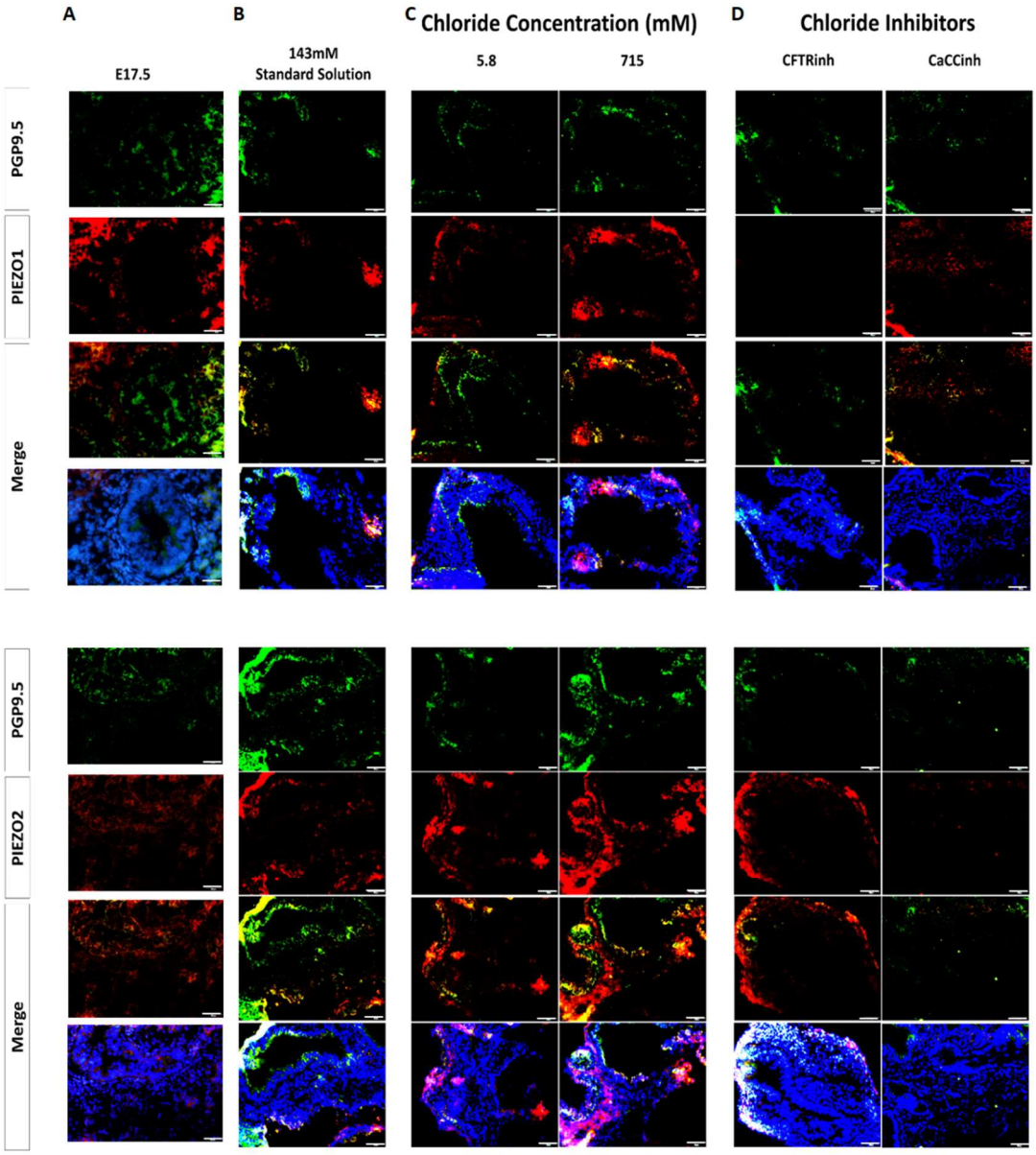

Figure 2 - Spatial distribution of PIEZO1 and PIEZO2 in *in vivo* and *ex vivo* branching morphogenesis. Representative examples of immunofluorescence assay for PIEZO1, PIEZO2, and PGP9.5 staining at (*A*) embryonic day (E)17.5; and after intraluminal injections of (*B*) 143mM Cl^- or standard solution (SS); (*C*) crescent chloride concentrations ([Cl^-]): 5.8 and 715mM Cl^-; and (*D*) Cl^- channels inhibitors: anthracene-9-carboxylic acid (A9C) to Cl^- voltage-gated channel (ClC); cystic fibrosis transmembrane conductance regulator inhibitor172 (CFTRinh) to CFTR; and calcium-dependent Cl^- channel inhibitorA01 (CaCCinh) to CaCCs. 143mM Cl^- and standard solution (SS) represent the control condition for [Cl^-] and Cl^- channels inhibitors, respectively. n ≥ 4 per stage or condition/antibody for whole lungs and lung explants Scale bar 50µm.

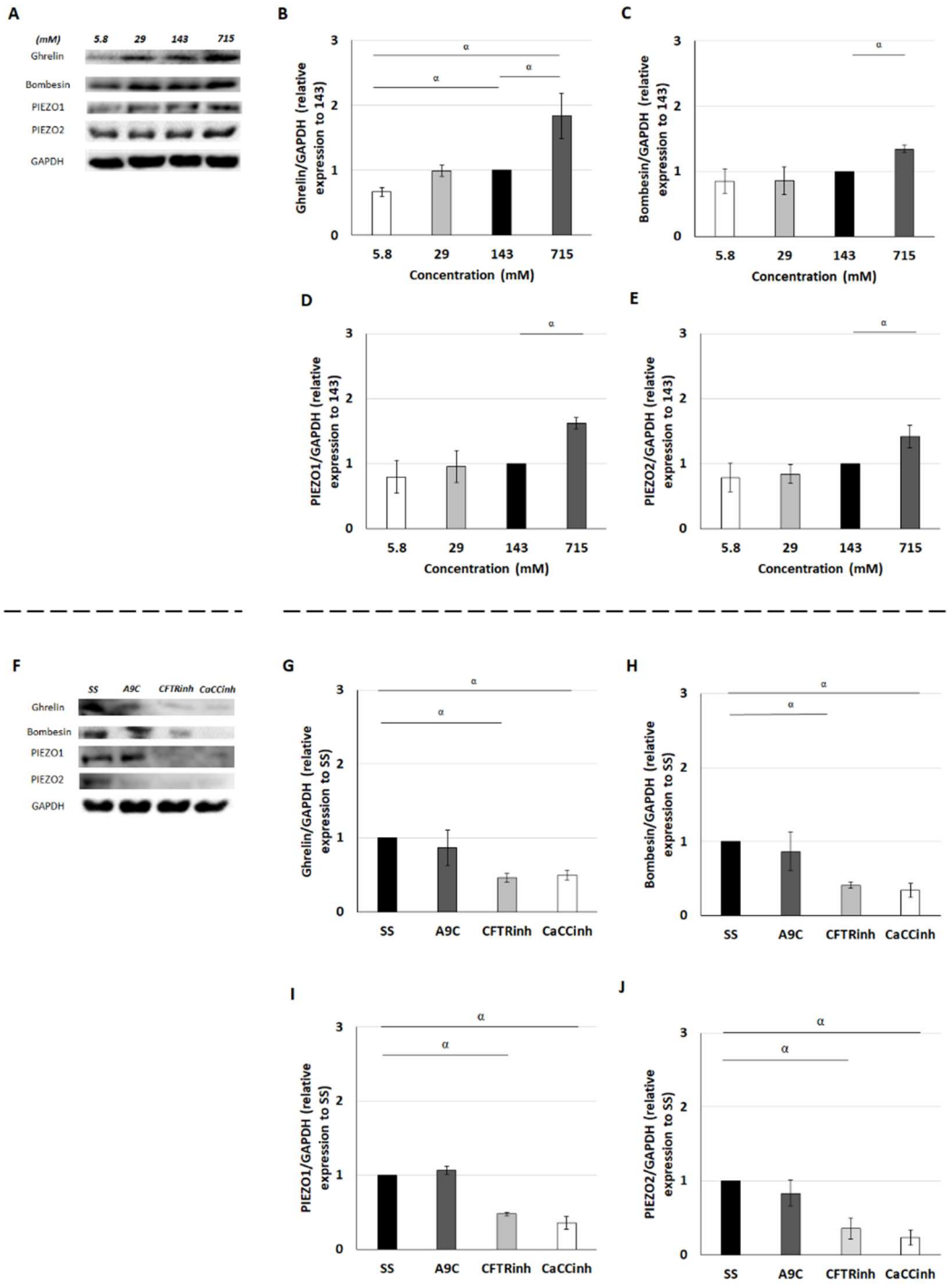

Figure 3 - Intraluminal chloride modulates the expression of ghrelin, bombesin, PIEZO1, and PIEZO2. (*A-E*) Upper panel represents the main effects of the crescent chloride concentrations ([Cl⁻]). (*A*) Examples of representative blots are shown. (*B-E*) Relative expression levels of (*B*) ghrelin, (*C*) bombesin, (*D*) PIEZO1, and (*E*) PIEZO2. (*F-J*) Lower panel shows the molecular effect of intraluminal Cl^- channels inhibition by anthracene-9-carboxylic acid (A9C) to Cl^- voltage-gated channel (ClCs); cystic fibrosis transmembrane conductance regulator inhibitor172 (CFTRinh) to CFTR and calcium-dependent Cl^- channel inhibitor A01 (CaCCinh) to CaCCs. (*F*) Examples of representative blots are shown. (*G-J*) Protein expression levels for (*G*)

ghrelin, (*H*) bombesin, (*I*) PIEZO1, and (*J*) PIEZO2. Black rectangles define the control group. Each lane represents a pooled tissue sample, and relative expression levels are determined against GAPDH. n ≥ 4 were used per antibody/condition. Results are presented as mean±SD. Symbols indicate the main effects and non-redundant interactions of the one-way ANOVA. $p < {}^{\alpha}0.0001$.

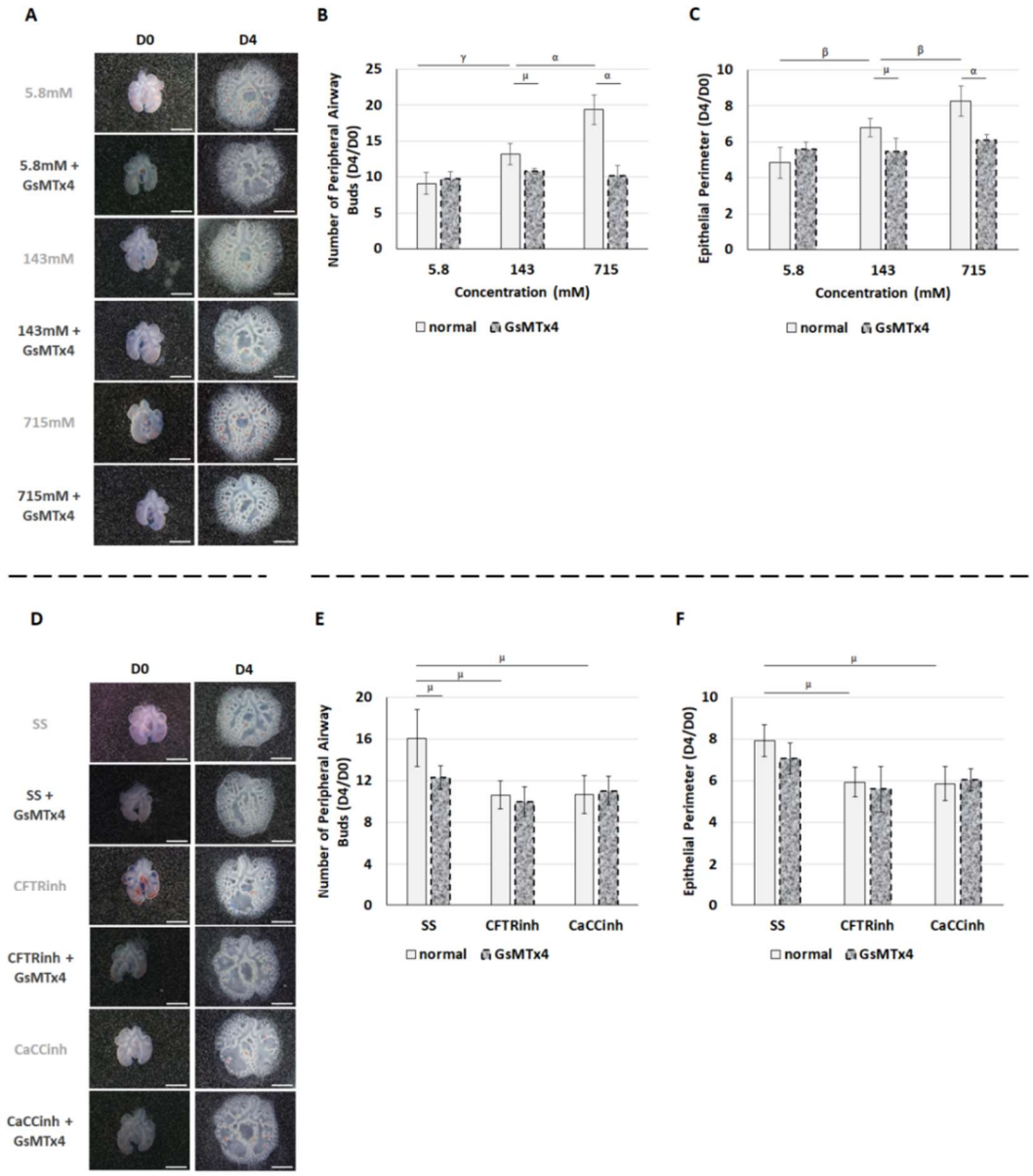

Figure 4 - GsMTx4, a PIEZO1/2 inhibitor, abolishes the effect of Cl^- intraluminal manipulation and decreases the branching morphogenesis. (*A-C*) Upper panel represents the main cumulative effect of intraluminal injection of crescent chloride concentrations ([Cl]) 5.8, 143, or 715mM Cl^- and the medium supplementation with GsMTx4 at day0 (D0) and day2 (D2). (*A*) Represents lung explants at D0 and D4 for the crescent [Cl]. (*B-C*) Morphometric analysis of (*B*) peripheral airway buds and (*C*) epithelial perimeter. (*D-F*) Lower panel shows the additional effect of PIEZO1/2 inhibition after intraluminal injection of Cl^- channels inhibitors: cystic fibrosis transmembrane conductance regulator inhibitor172 (CFTRinh) to CFTR; and calcium-dependent Cl^- channel inhibitor A01 (CaCCinh) to CaCCs. (d) represents the fetal lung explants at D0 and D4 for the distinct Cl^- channels inhibitors. (*E-F*) Morphometric analysis of (*E*) peripheral airway buds and (*F*) epithelial perimeter. 143mM Cl^- and standard solution (SS) identified the control condition for [Cl] and Cl^- channels inhibitors, respectively. White and dotted rectangles represent the medium *(continues on the next page)*

(continuation of the previous page) supplementation with and without GsMTx4, respectively. n ≥ 4 were used per antibody/condition. Results are expressed as ratio of D4 and D0 (D4/D0) and presented as mean±SD. Symbols indicate the main effects and non-redundant interactions of the two-way ANOVA. p< $^{\alpha}$0.0001, $^{\beta}$0.001, $^{\gamma}$0.01, $^{\mu}$0.05.

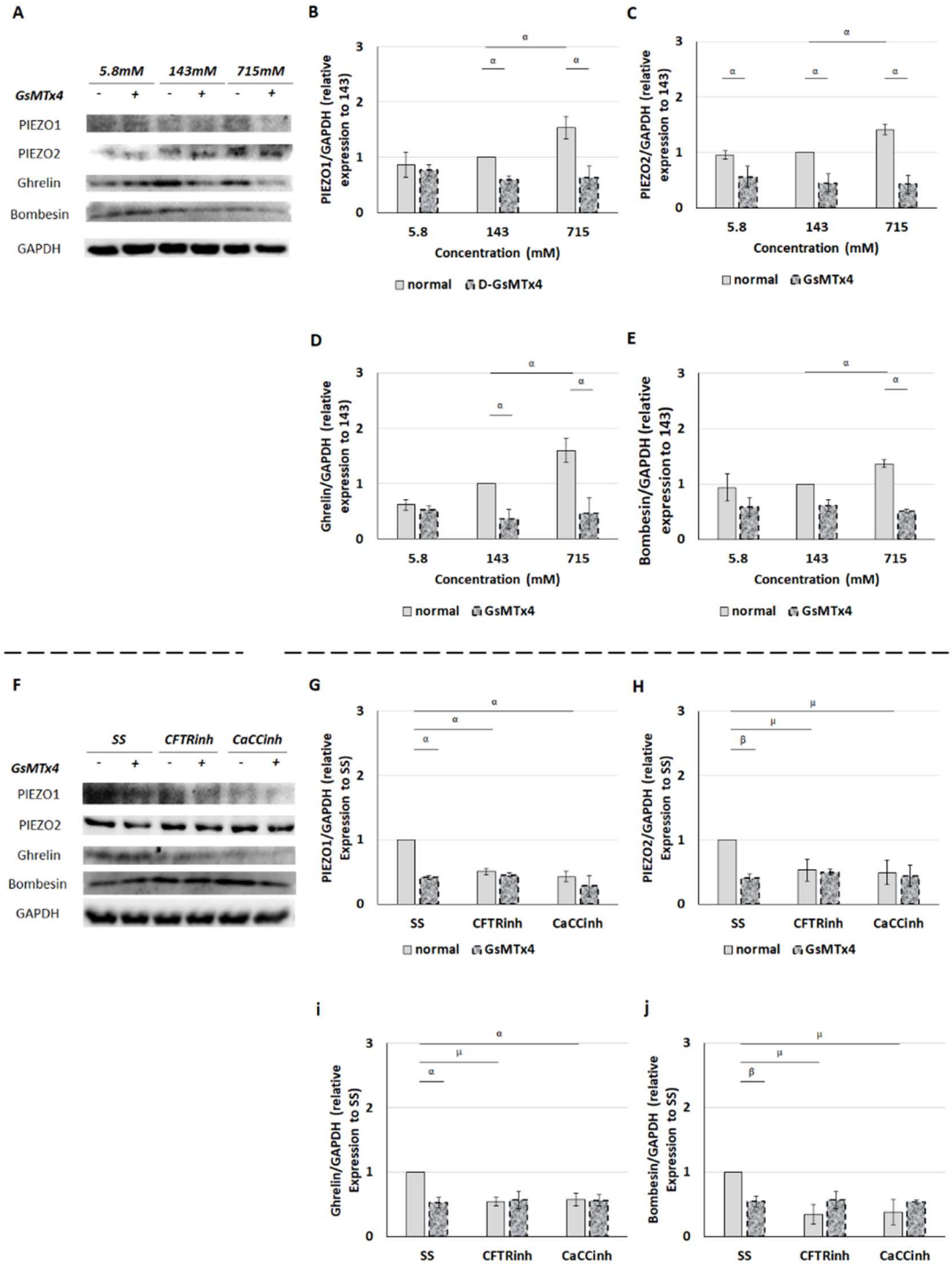

Figure 5 – Decrease of PIEZO1 and PIEZO2 expression removes the molecular dynamics triggered by intraluminal chloride concentration. (*A-E*) Upper panel represents the main cumulative effect of intraluminal chloride concentration ([Cl-]) and medium supplementation with (dotted rectangles) and without (white rectangles) GsMTx4. (*A*) Examples of representative blots are shown. (*B-E*) Protein expression levels for (*B*) PIEZO1, (*C*) PIEZO2, (*D*) ghrelin and e bombesin are indicated. (*F-J*) Lower panel shows the additional effect of GsMTx4 after intraluminal injection of Cl- channels inhibitors: cystic fibrosis transmembrane conductance regulator inhibitor172 (CFTRinh) to CFTR; and *(continues on the next page)*

(continuation of the previous page) calcium-dependent Cl^- channel inhibitor A01 (CaCCinh) to CaCCs. (*F*) Examples of blots are shown. (G-J) Relative expression levels of (G) PIEZO1, (H) PIEZO2, (I) ghrelin, and (J) bombesin. 143mM Cl- and standard solution (SS) represents the control condition for [Cl-] and Cl- channels inhibitors, respectively. White and dotted rectangles represent the medium supplementation with and without GsMTx4, respectively. $n \geq 4$ were used per antibody/condition. Results are presented as mean±SD. Symbols indicate main effects and non-redundant interactions of the two-way ANOVA. $p < {}^{\alpha}0.0001$.

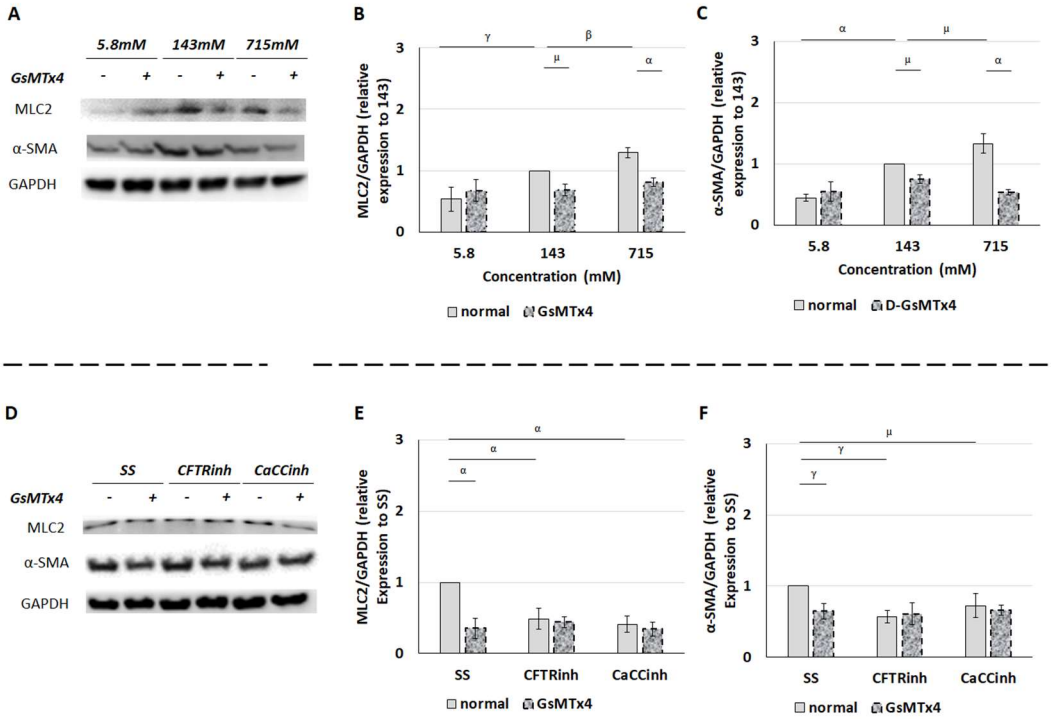

Figure 6 - Molecular effect of intraluminal chloride and GsMTx4 in smooth muscle cells. (*A-C*) The upper panel represents the main cumulative effect of intraluminal chloride concentration ([Cl^-]) and medium supplementation with and without GsMTx4. (*A*) Examples of representative blots are shown. (*B-C*) Protein expression levels for (*B*) myosin light chain 2 (MLC2), and (*C*) alpha-smooth muscle actin (α-SMA) are quantified. (*D-F*) Lower panel shows the additional effect of PIEZO1/2 inhibition after intraluminal injection of Cl^- channels inhibitors: cystic fibrosis transmembrane conductance regulator inhibitor172 (CFTRinh) to CFTR and; calcium-dependent Cl^- channel inhibitor A01 (CaCCinh) to CaCCs. (*D*) Examples of representative blots are shown. (*E-F*) Relative expression levels of (*E*) myosin light chain 2 (MLC2), and (*F*) alpha-smooth muscle actin are showed. 143mM Cl^- and standard solution (SS) represents the control condition for [Cl^-] and Cl^- channels inhibitors, respectively. White and dotted rectangles represent the medium supplementation with and without GsMTx4, respectively. Each lane represents a pooled tissue sample, and the relative expression levels were determined against GAPDH. n ≥ 4 were used per antibody/condition. Results are presented as mean±SD. Symbols indicate the main effects and non-redundant interactions of the two-way ANOVA. $p < {}^{\alpha}0.0001$, ${}^{\beta}0.001$, ${}^{\gamma}0.01$, ${}^{\mu}0.05$.

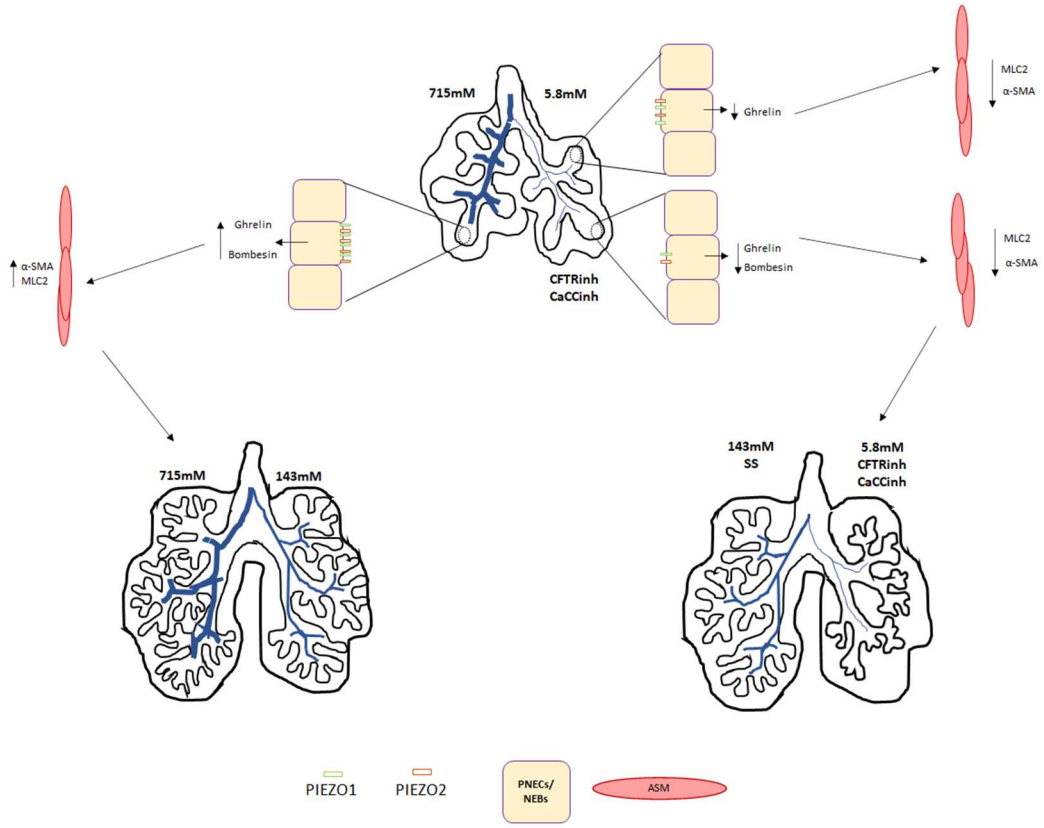

Figure 7 – Schematic representation of the role of intraluminal chloride concentrations in fetal branching morphogenesis. α-SMA, alpha-smooth muscle actin; CaCCinh calcium-dependent Cl- channel inhibitorA01; CFTRinh, cystic fibrosis transmembrane conductance regulator inhibitor172; MLC2, myosin light chain 2; SS, standard solution.

Supplementary information

Table S1. Summary of chemical compounds in the injected solution used for manipulation of the intraluminal fluid. (a) show the chemical concentration by compound for standard solution (SS) and crescent chloride concentrations, [Cl]: 5.8, 29, 143, and 715mM. (b) demonstrates the ionic composition in terms of chloride (Cl^-), potassium (K^+), magnesium ($Mg2^+$) and calcium ($Ca2^+$) in SS, 5.8, 29, 143 and 715mM Cl

a

	Standard Solution (SS, mM)	Chloride Concentration (mM)			
	143	*5.8*	*29*	*143*	*715*
NaCl	135,000				
KCl	5,000	5,711	28,55	140,800	704,000
MgCl2	1,200	0,049	0,24	1,200	6,000
CaCl2	1,000	0,041	0,203	1,000	5,000
D-glucose	10,000	10,000	10,000	10,000	10,000
HEPES	5,000	5,000	5,000	5,000	5,000
potassium D-gluconate		698,29	675,45	563,200	
MgSO4		5,95	5,76	4,800	
Calcium D-gluconate H2O		4,96	4,797	4,000	

b

	Standard Solution (SS, mM)	Chloride Concentration (mM)			
	143	*5.8*	*29*	*143*	*715*
Cl-	142,200	5,801	28,993	143,000	715,000
K+	5,000	704,001	704,000	704,000	704,000
Mg2+	1,200	5,999	6,000	6,000	6,000
Ca2+	1,000	5,001	5,000	5,000	5,000

Movie1. Intraluminal injection at day0 (D0).

Movie 2. Intraluminal injection at day2 (D2).

Movie 3. Dynamic intraluminal fluid at day4 (D4).

Chapter 6 – General discussion

Research regarding the prediction of FLH and the mechanisms underlying normal and hypoplastic fetal lung development are two sides of the same coin. If prediction is critical for familiar counseling and neonatal assistance, the understanding of causality between morphology and the molecular/cellular pathways allows us the development of new therapeutic strategies to improve pulmonary growth/maturation during fetal life.

In this thesis, we first analyzed the value of available noninvasive methods, 2D- and 3D-US and MRI, in the prediction of lethal pulmonary hypoplasia before birth (Chapter 2). Regarding the molecular/cellular mechanisms, epithelial cell markers were evaluated in normal and hypoplastic fetal lungs (Chapter 3 and 4). ROBO was assessed in the context of branching morphogenesis, and it was described as a regulator of SOX2 versus SOX9 molecular profile. Spatiotemporal distribution and the relative expression levels of receptors (ROBO1 and ROBO2) and epithelial progenitors (SOX2 and SOX9) were also compared in normal and hypoplastic lungs from embryonic-to-saccular stages (Chapter 3). We then extended our studies to investigate the impact of lung fluid composition, namely chloride concentration ($[Cl^-]$), in branching morphogenesis, and the potential of *ex vivo* lung explant cultures to study lung fluid composition in fetal branching morphogenesis (Chapter 5).

In light of the major findings achieved throughout this thesis, the particular aspects of undifferentiated and differentiated epithelial cells in nitrofen-induced CDH rat model and the relative contribution of ROBO in branching morphogenesis are discussed. Furthermore, intraluminal Cl^- in the modulation of *ex vivo* branching morphogenesis through PIEZO1/PIEZO2 is debated under the mechanotransduction value. Finally, a general discussion of how these findings can contribute to the body of knowledge in (ab)normal fetal lung development and in the improvement of fetal lung growth after tracheal occlusion will be provided.

6.1. Imagiological methods predict lethal pulmonary hypoplasia before birth

Secondary for multiple disorders with intra or extrathoracic causes, FLH is evaluated in terms of neonatal respiratory function. Respiratory function depends on the overall epithelial cell surface that correlates with fetal lung volume, making reasonable the use of imagiological methods to detect macroscopic hypoplastic lungs. Subsequently, focusing on two fundamental topics: 1) detect general gaps regarding the clinical experimental design; and 2) describe the more predictive method for lethal FLH, our systematic review compares published articles that assessed the predictive capacity of 2D-, 3D-US, or MRI to recognize lethal FLH secondary to general diseases, PPROM or CDH.

Our systematic review indicated the US as valuable method to detect lethal pulmonary hypoplasia. We reveal discrepant statistical values for similar US methods, for which data normalization for uncomplicated pregnancies and medical centers were constant factors of superior predictive values (Gonçalves et al 2021). Comparing the 2D and 3D-US, our research identified 3D-fetal lung volume to body weight ratio (3D-FLB) and 2D-lung area (LA) with similar predictive capacities of lethal FLH in groups with 0% survival. In contrast, an unchanged accuracy for 3D-US with the progressive decrease on 2D-US correlates with the decrease in disease severity degree (Gonçalves et al 2021). These differences are easily explained in the light of the individual specification by method and their association with neonatal respiratory function. In fact, since the pulmonary function depends on the overall alveolar surface area that correlates with lung volume, the virtual organ computer-aided analysis technique (VOCAL) that constructs a 3D lung from a sequence of 6 sections of each lung around a fixed axis, each after a 30° rotation from the previous one (Strizek et al 2015) is an obviously better predictor than the 2D measurements. Interestingly, Gerards et al (Geralds et al 2008) compare the 2D and 3D-US in prediction of lethal FLH in general diseases, renal anomalies, and skeletal and neuromuscular malformations and also report 3D as better predictor than 2D-US. However, the precise analysis of the results showed improvements in 2D- and 3D-US accuracies after disease segregation according with their etiology. This discussion is relevant considering the typical equipment's available in medical centers. In fact, the better (observed-to-expect total fetal lung volume) and the used (2D-o/e-LHR) method to predict FLH in CDH fetuses corroborate this descrepacy.

Our results also detected increased predictive values after disease segregation according to etiology. These improvements are understandable considering the multiple factors, e.g. severity degree, gestational age at insult and duration, gestational age at delivery, or additional abnormalities, that not only define the intra and extrathoracic causes of FLH but also distinguish the effects on fetal lung growth or maturation. Indeed, the comparison of fetal lung growth observed in PPROM as CDH easily illustrates these differences, with the lung growing bilaterally and symmetrically in PPROM (Cavoretto 2012), whereas in CDH the maximum compression of the contralateral lung occurs laterally rather than longitudinally. Subsequently, Jozan et al (Jozan et al 2018) described total o/e-LHR adjusted for prematurity and persistent oligohydramnios as useful to detect lethal FLH in pre-viable PPROM (Jozan et al 2018). However, the reported statistical value is lower than the described by 2D-(chest area-heart area)x100/chest area in prediction of FLH, secondary to PPROM (Gonçalves et al 2021). Concomitant with these observations, clinical studies also report additional elements for estimation of neonatal respiratory function. For instance, lung volume, femur length to abdominal circumference ratio, chest circumference to abdominal circumference ratio, and the presence or absence of polyhydramnios in skeletal dysplasia (Milks et al 2017);

the secondary persistent pulmonary hypertension in CDH; and the gestational age at rupture of membranes and latency period in PPROM, are all important predictive factors of respiratory function at birth that genuinely depends on etiology (Soylu et al 2010, Toukam et al 2019, Winn et al 2000).

Since an immature pulmonary system may not oxygenate, another predictive method for the neonatal outcome is fetal lung maturation (Johnson et al 2019, Yarbrough et al 2014). Biochemical tests that measure the concentration of particular components of pulmonary surfactant are traditionally used to estimate pulmonary maturation. In contrast, a recent publication describes the ability of fetal lung maturation tests as poor (approximately 20-50%) in the prediction of immature lungs and suggests the discontinuity of these tests (Johnson et al 2019). Meanwhile, the US has long been proposed as a noninvasive alternative to amniocentesis in the prediction of fetal lung maturity. Generally, these studies showed a good correlation with neonatal respiratory morbidity, but the diagnostic accuracy was insufficient for clinical use. Over recent years, image resolution of fetal US and computer image processing has evolved immensely, allowing the development of quantitative texture analysis. As such, Palacio et al (Palacio et al 2017) described the echo texture analysis as an indirect approach to estimate the neonatal respiratory function. This method extracts information from medical images and quantifies tissue changes not visible to the human eye, whereas uses an indirect approach to estimate lung maturity (Blitz et al 2021, Palacio et al 2017). Authors show a decrease in fetal lung heterogeneity US imaging when applied to pregnancies at high risk for hypoplasia and suggest this image-processing technique as helpful for the improvement of risk stratification and treatment approaches for pulmonary hypoplasia (Blitz et al 2021).

In conclusion, our observations recommend restrict studies for disease groups with increasing severity degrees and correlating prenatal FLH, survival at birth, and the need for neonatal respiratory support. The use of quantitative texture analysis must also be considered as an additional method to estimate FLH.

6.2. Altered epithelial cell profile in induced-CDH lungs

The recognized alterations in hypoplastic lungs detected by quantitative texture analysis (Blitz et al 2021, Palacio et al 2017) reinforce the study of the cellular dynamics by pulmonary structure and developmental stage to qualify the tissue heterogeneity in hypoplasia. In CDH lungs, the arrested branching morphogenesis at early and reduced airways with alveoli notably thicker at later developmental phases are the major indicators of neonatal respiratory failure.

In this Ph.D. thesis, the spatiotemporal distribution of SOX2/SOX9 allowed us to demonstrate the proximodistal patterning to be altered in the nitrofen-induced CDH rat model, for which the unexpected $SOX2^{+}$ cells in primordia of bronchiole at pseudoglandular and alveolar duct at saccular stage were evident

(Table 1) (Gonçalves et al 2020). Furthermore, the downregulation (near zero) of SOX2 in BADJ at canalicular and saccular stages indicated a diffuse transition from conducting to respiratory airways (Table 1) (Gonçalves et al 2020). Conversely, the more relevant alterations in SOX9 expression occurred at later developmental stages, with SOX9 overexpressed in proximal and downregulated in distal airways (Table 1). Literature shows SOX2 and $SOX9^{+}$ cells as upstream targets for bronchiolar and alveolar lineages that later differentiate and form the conducting (allows the continuous passageway of the air) and respiratory (where gas exchange takes place) airways. Given the fundamental role of these epithelial cell types in both fetal lung development and future pulmonary function, we decide to go further and reveal the spatiotemporal dynamics and the relative expression levels of the distinct epithelial cell markers in CDH-induced versus normal fetal lungs (Gonçalves et al *submitted*). Importantly, the reported markers: FOXJ1, CCSP, CGRP, and SP-C identified ciliated, clara, PNECs/NEBs, and AT2 profiles, respectively, when expressed in differentiated epithelial tissues. Conversely, when expressed in undifferentiated epithelium recognize the cellular progenitor capacity to give rise to the above-mentioned epithelial cell types.

Table 2 - Summary of the major findings about epithelial cell makers in hypoplastic versus normal fetal lungs at pseudoglandular, canalicular and saccular stages. Nitrofen-induced congenital diaphragmatic hernia (CDH) rat model was used for the study of epithelial cell profiles in hypoplastic lungs. SRY-related HMG BOX 2 (SOX2) identified proximal and SOX9 distal epithelial progenitor cells, whereas forkhead box protein J1 (FOXJ1), clara cell secretory protein (CCSP), calcitonin gene-related peptide (CGRP), and surfactant protein-C (SP-C) recognized ciliated, clara, pulmonary neuroendocrine cells/ neuroepithelial bodies, and alveolar type 2 profiles, respectively. Spatiotemporal distribution was quantified by pulmonary structure and developmental stage in the hypoplastic versus normal fetal lungs. up and down represent the up and downregulated proteins, respectively, in induced-CDH versus normal lungs. Black rectangles evidence the more relevant losses or gains of expression. BADJ: bronchioalveolar duct junction; E: embryonic day; NE: not expressed. (Gonçalves et al 2020, Gonçalves et al *submitted*).

	Pseudoglandular E17.5		Canalicular E19.5			Saccular E21.5			
	Bronchi	Primordia for bronchiole	Bronchi	Terminal Bronchiole	BADJ	Bronchi	Terminal Bronchiole	BADJ	Alveolar Duct
SOX2	=	new	=	up	near zero	up	up	near zero	new
SOX9	up	up	up	up	up	up	up	=	down
FOXJ1	up	up	up	up	new	=	up	new	=
CCSP	=	=	down	=	up	up	=	up	=
CGRP	up	up	up	up	NE	up	up	NE	NE
SP-C	up	=	up	up	up	=	=	up	up

We have reported aberrant expressions for FOXJ1, CGRP, CCSP, and SP-C by pulmonary structure and developmental stage after CDH induction (Table 1). These findings arose from the overexpression of FOXJ1 and CGRP in bronchi and primordia of bronchiole at pseudoglandular; and the increased expression of CGRP in bronchi; FOXJ1 and CGRP in terminal bronchiole; and CCSP and SP-C in BADJ at both canalicular and saccular stages in induced CDH-lungs (Table 1) (Gonçalves et al *submitted*). Previous work regarding the mechanisms controlling the epithelial cell differentiation indicated a preferable formation of PNECs/NEBs instead of clara cells at the canalicular stage in nitrofen-induced CDH rat model (Makanga et al 2013, Santos et al 2007, Sivakumar & Frank 2019). Now, our results by developmental stage and pulmonary structure evidenced a peculiar spatiotemporal distribution for SOX2 and FOXJ1 in induced-CDH lungs. In fact, at the same pulmonary structure (BADJ) and developmental stages (E19.5 and E21.5), we

showed SOX2 to be downregulated (near zero), whereas FOXJ1 was unexpectedly expressed (Gonçalves et al 2020, Gonçalves et al *submitted*). Interestingly, SOX2 is a progenitor marker of the bronchiolar lineage that gives rise to ciliated, clara, or PNECs, while FOXJ1 that identifies the ciliated cell profile regulates the basal body docking, cilia formation, and motility (Vladar & Mitchell 2016, You et al 2004). As such, our findings linked the induced CDH-lungs with a diffuse transition from conducting to respiratory airways, while demonstrate a preferable expression of FOXJ1, SP-C, and CCSP in the bronchioalveolar transition zone (Gonçalves et al *submitted*). BADJ is formed at the canalicular stage (Barre et al 2016, Barre et al 2014) and demarcates airway-fated epithelial cells from alveolar-fated epithelial cells that work as stem cell niches in adult lung regeneration (Kuo & Krasnow 2015, Liu et al 2019).

At the saccular stage, morphological studies in induced-CDH lung identify arrested airway branching with very narrow air spaces that contrast with the normal terminal sac observed in healthy lungs. These observations make obvious the increased interest in fetal pulmonary maturation in CDH lungs. As such, multiple studies have demonstrated a general impairment on surfactant production and secretion, evidenced by the low levels of phosphatidylcholine, and the factors involved in stimulating the maturation of surfactant lipids, such as PTHrP, ADRP, Thy1, and RA in the nitrofen-induced CDH rat model, whereas the inhibitor of surfactant phospholipid synthesis, TNFα, was overexpressed (Carroll et al 2002, Doi et al 2010, Friedmacher et al 2014a, Friedmacher et al 2014c, Gosemann et al 2012, Nakazawa et al 2007, Shima et al 1999). Now, at E21.5, we described CCSP and CGRP in bronchi; FOXJ1 and CGRP in terminal bronchiole; CCSP and SP-C in BADJ; and SP-C in the alveolar duct as the major overexpressed markers by pulmonary structure in induced-CDH lungs. We also identified a significant absence of the differentiated profile in terms of ciliated cells in bronchi at E21.5 that suggest an undifferentiated epithelium in CDH lungs (Gonçalves et al *submitted*).

Since the primordial function of SOX2 and SOX9 in fetal lung development is defined the proximodistal patterning at branching morphogenesis and differentiate into bronchiolar and alveolar lineages at canalicular and saccular stages, we intend to further contribute to the body of knowledge with the analysis of potential upstream targets that define SOX2 versus SOX9 molecular profiles. Interestingly, during the development of CNS (Borrell et al 2012), mammary gland (Ballard et al 2015, Harburg et al 2014, Macias et al 2011), and pancreas (Escot et al 2018), ROBO/SLIT signaling regulates the epithelial progenitor cell profile. In fetal lungs, genome-wide studies in CDH versus normal lungs indicated ROBO/SLIT signaling as potential therapeutic target for CDH. More relevant, *Robo1/2* knockout-mice induce a delay in diaphragm formation, whereas the absence of *Robo1* impairs the neonatal respiratory function (Domyan et al 2013, Nakamura et al 2020, Xian et al 2001). In this context, we hypothesize a molecular function for ROBO1 and/or ROBO2

in fetal lung development, and particularly in branching morphogenesis. Our experimental research established unaffected branching morphogenesis after ROBO1 inhibition that decreases the expression of BMP4 and promotes SOX2. In contrast, the decrease on ROBO2 expression stimulates fetal lung growth through activation of BMP4 and β-Catenin that in turn promote SOX9 instead of SOX2 molecular profiles. Together, these observations suggest ROBO1/2 as molecular intervenient of SOX9 versus SOX2 expression in a mechanism dependent of BMP4 and β-Catenin (Gonçalves et al 2020). Concomitant with these findings, bibliography showed the molecular differentiation of SOX2 and SOX9 as dependent on BMP4 and β-Catenin, in which the progressive decrease in BMP4 and β-Catenin expression promote the SOX2 expression at the proximal airways, whereas the high levels of BMP4, β-Catenin, and FGF10 at the distal tip of the lungs stimulates the SOX9 expression at pseudoglandular stage (Hashimoto et al 2012, Mucenski et al 2005, Mucenski et al 2003, Shu et al 2005, Volckaert et al 2013). Furthermore, in the adjacent literature, the molecular regulators of SOX2/SOX9 profiles (WNT, FGF, or BMP) have been confusedly reported in induced-CDH lungs with undefined conclusions (Doi & Puri 2009, Gosemann et al 2013, Makanga et al 2013, Takahashi et al 2013, Takahashi et al 2017, Takayasu et al 2007a). In part, these observations are explained by the limited information that can be taken from the protein quantification in the whole lung, once the assessed markers work as a proximodistal patterning. Indeed, when we are looking for formation of the conducting and respiratory airways, the molecular and cellular analysis by pulmonary structure could be relevant since distinct mechanisms can be at work. As such, we postulate the ROBO1 or ROBO2 expression to be damaged at pseudoglandular-to-saccular phases in induced-CDH lungs.

Our *in vivo* observations showed an opposite effect on ROBO1 and ROBO2 expression at pseudoglandular and saccular stages in a pulmonary structure-dependent manner. For instance, the overexpression of ROBO1 with the downregulation of ROBO2 identified the terminal bronchiole at saccular stage, whereas the inversive effect was observed in bronchi and primordia of bronchiole at pseudoglandular and in BADJ at saccular stages (Gonçalves et al 2020). Regarding our *in vivo* and *ex vivo* findings, we revealed the overexpression of ROBO2 in lung hypoplasia, while the significant decrease in ROBO2 expression promotes the *ex vivo* branching morphogenesis that indicates a concordant role for ROBO2 in *in vivo* and *ex vivo* branching morphogenesis. On the other hand, there is similar inhibition of ROBO1 and overexpression of ROBO2 and SOX9 in bronchi and primordia of bronchiole with loss of $SOX2^{+}$cells only in primordia of bronchiole in experimental-CDH (Gonçalves et al 2020). This contrasts with the consistent opposite effect on SOX2 and SOX9 expression triggered by ROBO2 inhibition in *ex vivo* branching morphogenesis, providing evidence of the complexity of the *in vivo* model. Collectively, our observations

report an upstream target, ROBO2, that forms SOX9 instead of SOX2^{+} cells at branching morphogenesis, whose expression is damaged in nitrofen-induced CDH lungs.

In conclusion, the molecular analysis of the epithelial cell profile along the fetal lung development identified the proximodistal patterning to be damage in induced-CDH lungs, for which the relevant findings in terms of SOX2 and FOXJ1 expression were particularly relevant in BADJ with indication of a diffuse transition from conducting to respiratory airways. In addition, the undifferentiated profile of ciliated cells in bronchi at saccular stage makes reasonable the assumption of an undifferentiated epithelium in induced-CDH lungs. Finally, the described effect of ROBO2 in branching morphogenesis through SOX2/SOX9 molecular profile and the significative differences in terms of expression and spatiotemporal distribution for receptors (ROBO1 and ROBO2) and epithelial progenitor cell markers (SOX2 and SOX9) reinforce the opened question concerning the differentiated or undifferentiated tissues in hypoplastic fetal lungs.

6.3. Intraluminal lung fluid composition modulates fetal lung growth

During the fetal life, the future airways are filled with a liquid (fetal lung liquid) that is secreted by the lungs. This luminal liquid maintains the lung in a constantly distended state, stimulating its growth and maturation. In fact, clinical and experimental evidence demonstrated the increase in lung fluid volume as promotor of intraluminal pressure, lung expansion, and growth (Fletcher et al 2000, Jiménez et al 2017, Khan et al 2007, Unbekandt et al 2008, Wilson et al 2007). This evidence allowed the development of FETO, which is currently under clinical investigation to be applied in the treatment of the more severe cases of FLH, secondary to CDH (Ali et al 2016, Jiménez et al 2017, Khoshgoo et al 2019, Ruano et al 2013). FETO impairs the *in vivo* tracheal efflux that increases intraluminal lung fluid volume and stimulates lung growth. In addition, the prenatal removal of the balloon is recommended before birth since facilitates delivery and allows the AT2 cell maturation, surfactant production, and improves neonatal survival (Flageole et al 1998, Jiménez et al 2017, Tsao & Johnson 2020). These *in vivo* observations indicate a sustained development of the lung under FETO therapy and expose the underlying mechanisms as an urgent topic of research. However, the difficulty that is capture or recapitulates these *in vivo* morphological dynamics in the lab harms the study of fetal lung expansion, particularly at earlier developmental stages.

In this Ph.D. thesis, we performed effective injections into lung lumen at D0 and D2, for which the visualized movements in intraluminal lung fluid at D4 validate the presence of lung fluid in *ex vivo* lung explant cultures. Subsequently, we postulate this *ex vivo* model as useful for the study of the effects of lung fluid composition in branching morphogenesis (Gonçalves et al *in revision*). Importantly, lung explant culture is a validated model used in the study of branching morphogenesis since maintain the *in vivo* physiologic

architecture and the cellular interactions observed at pseudoglandular stage (Yeganeh et al 2018). In addition, electrophysiology and *in vivo* studies showed Cl^- movement under the epithelium as an inductor of Na^+ and water movement in the same direction that produces the fetal lung fluid (Olver et al 1981, Olver & Strang 1974, Welsh 1983, Welsh et al 1982). Experimental evidence regarding the lung fluid composition in sheep and mice allowed us to fix 143mM Cl^- as basal concentration and establish the remaining experimental [Cl^-] as follows, 5.8, 29, and 715mM Cl^-. We have demonstrated that higher [Cl^-], 715mM, induce branching morphogenesis, whist it was inhibited by lower, 5.8mM [Cl^-]. Furthermore, the injected Cl^- channels inhibitors, CFTRinh and CaCCinh, equally decrease branching morphogenesis, whereas no significant alterations were detected after injection of anthracene-9-carboxylic acid (A9C, inhibitor of ClCs) (Gonçalves et al *in revision*). Interestingly, the ClC family, CaCC, and CFTR are all expressed in fluid-secreting fetal epithelial cells with functions in fetal lung development. Indeed, inhibition of ionic channels, i.e. CFTR, ClC2, or extracellular calcium receptor (CaR), decrease the fetal lung morphogenesis (Blaisdell et al 2004, Brennan et al 2013, Brennan et al 2016, Finney et al 2008, He et al 2020, Meyerholz et al 2018), whereas the *in utero* gene transfer of CFTR improve the fetal lung development in the nitrofen-induced CDH rat model (Larson & Cohen 2006). Furthermore, the molecular profile of a CDH and CDH+TO lung showed other ionic channels (ENaC, or CLC2,3) and cotransporters (NKCC) to be downregulated in CDH and overexpressed in CDH+TO, supporting a functional role of these molecules in fetal lung development (Seaborn et al 2008, Sozo et al 2006, Vuckovic et al 2013, reviewed in Wallace et al 2014). Together, our findings showed the intraluminal [Cl^-] as a modulator of fetal lung growth. As consequence, our next interest was to reveal the mechanisms triggered by lung fluid composition in the regulation of fetal lung growth.

An emergent area, mechanotransduction, meaning the conversion of mechanical stimuli into biochemical signaling has highlighted our understanding of the molecular mechanisms involved in many biological processes. In fetal lungs, PNECs/NEBs are chemo- and mechano-sensors, for which the secreted products, ghrelin, bombesin, or serotonin, regulate the *in vivo* and *ex vivo* lung growth in both normal and hypoplastic lungs (Nunes et al 2008, Pereira-Terra et al 2015, Sakai et al 2014, Santos et al 2006, Sunday et al 1990). In addition, Pan et al 2006 showed mechanical stretch as an inductor of serotonin release from cultured PNECs, exposed to sinusoidal cyclic stretch (Pan et al 2006). Unfortunately, the true value of this mechanosensory capacity in fetal lungs remains almost undetermined. As such, we postulate the intraluminal lung fluid able to active the PNECs/NEBs in the *ex vivo* branching morphogenesis. Our investigation demonstrates the secreted neuroendocrine products, ghrelin, and bombesin, overexpressed at 715mM [Cl^-], while they were downregulated after the injection of CaCCinh or CFTRinh. Conversely, the injection of 5.8mM [Cl^-] only decreases the ghrelin expression (Gonçalves et al *in revision*). These results

seem to be in line with the morphological dynamics observed after *in vivo* lung fluid manipulation, in which the increase in lung fluid volume stimulates fetal lung expansion, whereas their decrease impairs fetal lung growth. This study also reports the increased pulmonary growth as dependent upon increased tracheal pressure and rapid efflux of liquid from the trachea, while the significant decrease in fetal lung size was supported by reduced tracheal pressure, near cessation of tracheal efflux rate, and unchanged lung fluid secretion rate (Dickson & Harding 1987).

To further explore these morphological dynamics and detect the molecular sensor in fetal lung growth, we analyzed the PIEZO1 and PIEZO2 receptors. We showed a similar co-localization between PIEZO1, PIEZO2, and PGP9.5 (a marker for PNECs/NEBs) expressed in *in vivo* pseudoglandular stage (E17.5) and in *ex vivo* lung explant cultures at D4, after injection of 143mM [Cl^-]. Concerning the injection of the remaining intraluminal [Cl^-] and Cl^- channels inhibitors, we described the increase on intraluminal [Cl^-], 715mM [Cl^-], able to stimulate PIEZO1/PIEZO2 expression, whereas it was inhibited by CaCCinh or CFTRinh intraluminal injections, (Gonçalves et al *in revision*). PIEZO1/PIEZO2 are mechanically activated cation channels that sense and respond to mechanical stimuli in the modulation of multiple physiologic functions, e.g. vascular development, sensory transduction, or respiratory physiology at birth or thereafter (Alcaino et al 2018, Cahalan et al 2015, Coste et al 2012, Feng et al 2018, Maneshi et al 2018, Nonomura et al 2017, Ranade et al 2014b, Wang et al 2017, Woo et al 2014, Zeng et al 2018). Interestingly, a recent publication showed PIEZO2 expressed in NEBs at term with, however, an undefined role since the neonatal respiratory function was mediated by PIEZO2 expressed in global and sensory neurons (Nonomura et al 2017). As such, we then hypothesize the intraluminal pressure as an activator of PIEZO1/PIEZO2 that in turn stimulates the production of neuroendocrine factors. Our complementary work regarding the simultaneous intraluminal lung fluid manipulation and PIEZO1/PIEZO2 inhibition demonstrated a significant decrease in ghrelin and bombesin expression as well as in branching morphogenesis. This effect was independent of the injected intraluminal solution, crescent [Cl^-] or Cl^- inhibitors, that reinforce the role of PIEZO1/PIEZO2 in *ex vivo* branching morphogenesis (Gonçalves et al *in revision*).

It is well known among lung developmental biologists that spontaneous phasic contraction of fetal ASM is critical for normal branching morphogenesis by regulating the ASM differentiation and intraluminal fluid movement. In fact, the periodic distension and relaxation of the end buds of the lung are generated by the peristaltic activity of fetal ASM contraction under the movement of intraluminal fluid. More relevant, the fetal lung growth is concentrated at these end buds with stretch and the early differentiation of ASM cells as modulators of branching morphogenesis (reviewed in Lam et al 2019). Since our molecular, cellular, and morphological research showed a significant effect of intraluminal pressure in branching morphogenesis, we

intend to go further and analyze key molecular markers (myosin light chain 2, MLC2, and α-SMA) of ASM cells and explore this potential interdependency. Importantly, MLC2 and α-SMA are restricted expressed in ASM cells in the developing lung, in which the expression of contractile protein α-SMA and the smooth muscle actin filaments recognize the airway smooth muscle progenitor cells that later promote the movement of lung fluid from proximal to the distal tip of the lung (Bokka et al 2015, Jesudason 2009, Jesudason et al 2006, Schittny 2017, Schittny et al 2000). We demonstrate a similar effect in MLC2 and α-SMA expression after intraluminal manipulation of [Cl^-]. For instance, the increase of [Cl^-] stimulate MLC2 and α-SMA expression in the promotion of branching morphogenesis, whereas the significant decrease in fetal lung growth after depletion of [Cl^-] relates with decrease in MLC2 and α-SMA expression. In addition, the simultaneous PIEZO1/PIEZO2 inhibition and the intraluminal injection of crescent [Cl^-] or Cl^- channels inhibitors, shows an unaltered inhibitory effect on MLC2 and α-SMA expression as well as in branching morphogenesis (Gonçalves et al *in revision*). These results indicate the intraluminal composition and the neuroendocrine activation upstream of airway smooth muscle contraction and branching morphogenesis. Interestingly, the hypoplastic phenotype observed in CDH context was connected to decrease on α-SMA and MLC2 from pseudoglandular-to-canalicular (Santos *et al.*, 2007), whereas the tracheal occlusion in *in vivo* mouse model was inductor of α-SMA and MLC2 expression at later canalicular stage (Seaborn *et al.*, 2008) that suggests the PIEZO1/PIEZO2 pathway as a potential target for the treatment of fetal pulmonary hypoplasia.

Collectively, we demonstrated that injections of high [Cl^-] enhanced lung branching and upregulated the expression of PIEZO1, PIEZO2, ghrelin, bombesin, MLC2, and α-SMA. In concordance, injections of diverse Cl^- channel inhibitors had the opposite effect on lung branching and protein expression. Finally, we further demonstrated, through pharmacological inhibition experiments, that these effects require PIEZO and Cl^- channel activation.

Chapter 7 – General conclusion

Having in mind the overall aim of the present Ph.D. thesis to provide novel insights regarding the prediction and (patho)physiology in (ab)normal fetal lung development, the main conclusions are listed below.

Overall, the work indicates US methods useful for lethal pulmonary hypoplasia prediction and suggests specific studies by disease type and severity degree to improve the US predictive value. Concerning fetal lung development, we characterize the hypoplastic lung and demonstrate a significant impairment on proximodistal patterning from pseudoglandular-to-saccular stages in induced-CDH lungs. In addition, the disrupted expression of CCSP, SP-C, CGRP, and the unexpectedly $FOXJ1^{+}$ cells in BADJ describe a diffuse transition from conducting to respiratory airways at canalicular and saccular phases after CDH-induction. Conversely, the decreased differentiated profile of ciliated cells in bronchi at term opens the possibility for an undifferentiated epithelial tissue in hypoplasia. Finally, we demonstrate the decrease in ROBO2 expression as stimulator of *ex vivo* branching morphogenesis through SOX9 instead of SOX2 expression, indicating ROBO2 as upstream target of SOX9/SOX2 profile with functions in hypoplasia. The *in vivo* experiments identify the spatiotemporal distribution of ROBO2 to be dysregulated from pseudoglandular-to-saccular stages in induced-CDH lungs.

Regarding the study of the mechanisms underlying fetal lung growth, we describe an *ex vivo* model that allows the molecular analysis of lung fluid composition in branching morphogenesis. We show that increasing the intraluminal [Cl^{-}] in cultured developing rat lung explants leads to increased branching morphogenesis and expression of neuroendocrine products, PIEZO channels, and smooth muscle markers. We further demonstrate, through pharmacological inhibition experiments that these effects require PIEZO and Cl^{-} channel activation, indicating the PIEZO1/PIEZO2 pathway as a potential target to increase the *in vivo* fetal lung growth.

Despite all the new findings in (ab)normal fetal lung morphogenesis reported in this thesis, the current more relevant questions are those for one we remain unanswered. In fact, albeit our investigation characterizes an induced-CDH lung in terms of epithelial cell profile and identified a mechanism that promotes fetal lung growth/expansion under intraluminal lung fluid manipulation, these research points are far to be complete. Indeed, understanding the more relevant *in vivo* differences and similarities in hypoplastic lungs with distinct etiologies and neonatal outcomes are fundamental questions to predict and treat FLH. In addition, the use of biomarkers to detect the fetal lung capacity to grow and maturate or the description of new therapeutic targets to improve fetal lung development remains a fascinating and current topic of research. Crucial for that are the basic mechanisms that explain fetal lung growth or maturation since not only improve our understanding of the abnormal fetal lung development but also open new opportunities for

the treatment of FLH. In this context, we consider the interdependency between clinical and experimental research as the key future points of investigation.

Chapter 8 – References

Abler LL, Mansour SL, Sun X. 2009. Conditional gene inactivation reveals roles for Fgf10 and Fgfr2 in establishing a normal pattern of epithelial branching in the mouse lung. *Dev Dyn* 238: 1999-2013

Alcaino C, Knutson KR, Treichel AJ, Yildiz G, Strege PR, et al. 2018. A population of gut epithelial enterochromaffin cells is mechanosensitive and requires Piezo2 to convert force into serotonin release. *Proc Natl Acad Sci U S A* 115: E7632-e41

Alcorn D, Adamson TM, Lambert TF, Maloney JE, Ritchie BC, Robinson PM. 1977. Morphological effects of chronic tracheal ligation and drainage in the fetal lamb lung. *J Anat* 123: 649-60

Alfanso LF, Arnaiz A, Alvarez FJ, Qi B, Diez-Pardo JA, et al. 1996. Lung hypoplasia and surfactant system immaturity induced in the fetal rat by prenatal exposure to nitrofen. *Biol Neonate* 69: 94-100

Alfaraj MA, Shah PS, Bohn D, Pantazi S, O'Brien K, et al. 2011. Congenital diaphragmatic hernia: lung-to-head ratio and lung volume for prediction of outcome. *Am J Obstet Gynecol* 205: 43.e1-8

Alfonso LF, Vilanova J, Aldazabal P, Lopez de Torre B, Tovar JA. 1993. Lung growth and maturation in the rat model of experimentally induced congenital diaphragmatic hernia. *Eur J Pediatr Surg* 3: 6-11

Ali K, Bendapudi P, Polubothu S, Andradi G, Ofuya M, et al. 2016. Congenital diaphragmatic hernia-influence of fetoscopic tracheal occlusion on outcomes and predictors of survival. *Eur J Pediatr* 175: 1071-6

Alper SL. 2017. Genetic Diseases of PIEZO1 and PIEZO2 Dysfunction. *Curr Top Membr* 79: 97-134

Ameis D, Khoshgoo N, Keijzer R. 2017. Abnormal lung development in congenital diaphragmatic hernia. *Semin Pediatr Surg* 26: 123-28

Amy RW, Bowes D, Burri PH, Haines J, Thurlbeck WM. 1977. Postnatal growth of the mouse lung. *J Anat* 124: 131-51

Andrae J, Gouveia L, He L, Betsholtz C. 2014. Characterization of platelet-derived growth factor-A expression in mouse tissues using a lacZ knock-in approach. *PLoS One* 9: e105477

Araujo Júnior E, De Oliveira PS, Nardozza LM, Simioni C, Rolo LC, et al. 2010. Fetal lung volume in fetuses with urinary tract malformations: comparison by 2D-, 3D-sonography and magnetic resonance imaging. *J Matern Fetal Neonatal Med* 23: 60-8

Arbi M, Pefani DE, Kyrousi C, Lalioti ME, Kalogeropoulou A, et al. 2016. GemC1 controls multiciliogenesis in the airway epithelium. *EMBO Rep* 17: 400-13

Arora R, Metzger RJ, Papaioannou VE. 2012. Multiple roles and interactions of Tbx4 and Tbx5 in development of the respiratory system. *PLoS Genet* 8: e1002866

Askenazi SS, Perlman M. 1979. Pulmonary hypoplasia: lung weight and radial alveolar count as criteria of diagnosis. *Arch Dis Child* 54: 614-8

Ballard MS, Zhu A, Iwai N, Stensrud M, Mapps A, et al. 2015. Mammary Stem Cell Self-Renewal Is Regulated by Slit2/Robo1 Signaling through SNAI1 and mINSC. *Cell Rep* 13: 290-301

Baptista MJ, Melo-Rocha G, Pedrosa C, Gonzaga S, Teles A, et al. 2005. Antenatal vitamin A administration attenuates lung hypoplasia by interfering with early instead of late determinants of lung underdevelopment in congenital diaphragmatic hernia. *J Pediatr Surg* 40: 658-65

Bardou O, Trinh NT, Brochiero E. 2009. Molecular diversity and function of K+ channels in airway and alveolar epithelial cells. *Am J Physiol Lung Cell Mol Physiol* 296: L145-55

Barkauskas CE, Cronce MJ, Rackley CR, Bowie EJ, Keene DR, et al. 2013. Type 2 alveolar cells are stem cells in adult lung. *J Clin Invest* 123: 3025-36

Barre SF, Haberthur D, Cremona TP, Stampanoni M, Schittny JC. 2016. The total number of acini remains constant throughout postnatal rat lung development. *Am J Physiol Lung Cell Mol Physiol* 311: L1082-l89

Barre SF, Haberthur D, Stampanoni M, Schittny JC. 2014. Efficient estimation of the total number of acini in adult rat lung. *Physiol Rep* 2: e12063

Barros CA, Rezende Gde C, Araujo Júnior E, Tonni G, Pereira AK. 2016. Prediction of lethal pulmonary hypoplasia by means fetal lung volume in skeletal dysplasias: a three-dimensional ultrasound assessment. *J Matern Fetal Neonatal Med* 29: 1725-30

Beck V, Lewi P, Gucciardo L, Devlieger R. 2012. Preterm prelabor rupture of membranes and fetal survival after minimally invasive fetal surgery: a systematic review of the literature. *Fetal Diagn Ther* 31: 1-9

Bellusci S, Furuta Y, Rush MG, Henderson R, Winnier G, Hogan BL. 1997. Involvement of Sonic hedgehog (Shh) in mouse embryonic lung growth and morphogenesis. *Development* 124: 53-63

Benjamin JT, Gaston DC, Halloran BA, Schnapp LM, Zent R, Prince LS. 2009. The role of integrin $\alpha 8\beta 1$ in fetal lung morphogenesis and injury. *Developmental Biology* 335: 407-17

Berend N, Rynell AC, Ward HE. 1991. Structure of a human pulmonary acinus. *Thorax* 46: 117-21

Berger TM, Hirsch E, Djonov V, Schittny JC. 2003. Loss of beta1-integrin-deficient cells during the development of endoderm-derived epithelia. *Anat Embryol* 207: 283-8

Bernhard W. 2016. Lung surfactant: Function and composition in the context of development and respiratory physiology. *Ann Anat* 208: 146-50

Blaisdell CJ, Morales MM, Andrade AC, Bamford P, Wasicko M, Welling P. 2004. Inhibition of CLC-2 chloride channel expression interrupts expansion of fetal lung cysts. *Am J Physiol Lung Cell Mol Physiol* 286: L420-6

Blitz MJ, Ghorayeb SR, Solmonovich R, Glykos S, Jauhari A, et al. 2021. Fetal Lung Echo Texture in Pregnancies at Risk for Pulmonary Hypoplasia. *J Ultrasound Med* 40: 805-10

Blockus H, Chédotal A. 2016. Slit-Robo signaling. *Development* 143: 3037-44

Boers JE, Ambergen AW, Thunnissen FB. 1999. Number and proliferation of clara cells in normal human airway epithelium. *Am J Respir Crit Care Med* 159: 1585-91

Bohnhorst B, Peter C. 2020. Pediatric Respiratory Physiology In *Pediatric Surgery: General Principles and Newborn Surgery*, ed. P Puri, pp. 181-200. Berlin, Heidelberg: Springer Berlin Heidelberg

Bokka KK, Jesudason EC, Warburton D, Lubkin SR. 2015. Morphogenetic implications of peristaltic fluid-tissue dynamics in the embryonic lung. *J Theor Biol* 382: 378-85

Borges M, Linnoila RI, van de Velde HJ, Chen H, Nelkin BD, et al. 1997. An achaete-scute homologue essential for neuroendocrine differentiation in the lung. *Nature* 386: 852-5

Borrell V, Cardenas A, Ciceri G, Galceran J, Flames N, et al. 2012. Slit/Robo signaling modulates the proliferation of central nervous system progenitors. *Neuron* 76: 338-52

Boström H, Gritli-Linde A, Betsholtz C. 2002. PDGF-A/PDGF alpha-receptor signaling is required for lung growth and the formation of alveoli but not for early lung branching morphogenesis. *Dev Dyn* 223: 155-62

Boström H, Willetts K, Pekny M, Levéen P, Lindahl P, et al. 1996. PDGF-A Signaling Is a Critical Event in Lung Alveolar Myofibroblast Development and Alveogenesis. *Cell* 85: 863-73

Boucherat O, Benachi A, Barlier-Mur AM, Franco-Montoya ML, Martinovic J, et al. 2007. Decreased lung fibroblast growth factor 18 and elastin in human congenital diaphragmatic hernia and animal models. *Am J Respir Crit Care Med* 175: 1066-77

Bratu I, Flageole H, Laberge JM, Chen MF, Piedboeuf B. 2001. Pulmonary structural maturation and pulmonary artery remodeling after reversible fetal ovine tracheal occlusion in diaphragmatic hernia. *J Pediatr Surg* 36: 739-44

Brennan SC, Finney BA, Lazarou M, Rosser AE, Scherf C, et al. 2013. Fetal calcium regulates branching morphogenesis in the developing human and mouse lung: involvement of voltage-gated calcium channels. *PLoS One* 8: e80294

Brennan SC, Wilkinson WJ, Tseng HE, Finney B, Monk B, et al. 2016. The extracellular calcium-sensing receptor regulates human fetal lung development via CFTR. *Sci Rep* 6: 21975

Briceño-Pérez C, Reyna-Villasmil E, Vigil-De-Gracia P. 2019. Antenatal corticosteroid therapy: Historical and scientific basis to improve preterm birth management. *European Journal of Obstetrics & Gynecology and Reproductive Biology* 234: 32-37

Brose K, Bland KS, Wang KH, Arnott D, Henzel W, et al. 1999. Slit proteins bind Robo receptors and have an evolutionarily conserved role in repulsive axon guidance. *Cell* 96: 795-806

Brouns I, Adriaensen D, Burnstock G, Timmermans JP. 2000. Intraepithelial vagal sensory nerve terminals in rat pulmonary neuroepithelial bodies express P2X(3) receptors. *Am J Respir Cell Mol Biol* 23: 52-61

Burgos CM, Frenckner B, Luco M, Harting MT, Lally PA, Lally KP. 2019. Prenatally versus postnatally diagnosed congenital diaphragmatic hernia - Side, stage, and outcome. *J Pediatr Surg* 54: 651-55

Burgos CM, Pearson EG, Davey M, Riley J, Jia H, et al. 2016. Improved pulmonary function in the nitrofen model of congenital diaphragmatic hernia following prenatal maternal dexamethasone and/or sildenafil. *Pediatr Res* 80: 577-85

Burri PH. 1984. Fetal and postnatal development of the lung. *Annu Rev Physiol* 46: 617-28

Burri PH. 2006. Structural aspects of postnatal lung development - alveolar formation and growth. *Biol Neonate* 89: 313-22

Burri PH, Dbaly J, Weibel ER. 1974. The postnatal growth of the rat lung. I. Morphometry. *Anat Rec* 178: 711-30

Cahalan SM, Lukacs V, Ranade SS, Chien S, Bandell M, Patapoutian A. 2015. Piezo1 links mechanical forces to red blood cell volume. *Elife* 4: e07370

Campbell EP, Quigley IK, Kintner C. 2016. Foxn4 promotes gene expression required for the formation of multiple motile cilia. *Development* 143: 4654-64

Candilera V, Bouchè C, Schleef J, Pederiva F. 2016. Lung growth factors in the amniotic fluid of normal pregnancies and with congenital diaphragmatic hernia. *J Matern Fetal Neonatal Med* 29: 2104-8

Cardoso WV, Lu J. 2006. Regulation of early lung morphogenesis: questions, facts and controversies. *Development* 133: 1611-24

Carroll JL, Jr., McCoy DM, McGowan SE, Salome RG, Ryan AJ, Mallampalli RK. 2002. Pulmonary-specific expression of tumor necrosis factor-alpha alters surfactant lipid metabolism. *Am J Physiol Lung Cell Mol Physiol* 282: L735-42

Cavoretto P. 2012. Prediction of pulmonary hypoplasia in mid-trimester preterm prelabor rupture of membranes: research or clinical practice? *Ultrasound Obstet Gynecol* 39: 489-94

Chandrasekharan PK, Rawat M, Madappa R, Rothstein DH, Lakshminrusimha S. 2017. Congenital Diaphragmatic hernia - a review. *Matern Health Neonatol Perinatol* 3: 6

Chang DR, Martinez Alanis D, Miller RK, Ji H, Akiyama H, et al. 2013. Lung epithelial branching program antagonizes alveolar differentiation. *Proc Natl Acad Sci U S A* 110: 18042-51

Chao CM, El Agha E, Tiozzo C, Minoo P, Bellusci S. 2015. A breath of fresh air on the mesenchyme: impact of impaired mesenchymal development on the pathogenesis of bronchopulmonary dysplasia. *Front Med* 2: 27

Chapin CJ, Ertsey R, Yoshizawa J, Hara A, Sbragia L, et al. 2005. Congenital diaphragmatic hernia, tracheal occlusion, thyroid transcription factor-1, and fetal pulmonary epithelial maturation. *Am J Physiol Lung Cell Mol Physiol* 289: L44-L52

Chen CM, Chou HC, Wang LF, Lang YD. 2008. Experimental oligohydramnios decreases collagen in hypoplastic fetal rat lungs. *Exp Biol Med* 233: 1334-40

Chen CM, Chou HC, Wang LF, Lang YD, Yeh CY. 2007a. Retinoic acid fails to reverse oligohydramnios-induced pulmonary hypoplasia in fetal rats. *Pediatr Res* 62: 553-8

Chen CM, Chou HC, Wang LF, Yeh TF. 2013. Effects of maternal retinoic acid administration on lung angiogenesis in oligohydramnios-exposed fetal rats. *Pediatr Neonatol* 54: 88-94

Chen CM, Wang LF, Chou HC, Lang YD. 2007b. Oligohydramnios decreases platelet-derived growth factor expression in fetal rat lungs. *Neonatology* 92: 187-93

Chen F, Desai TJ, Qian J, Niederreither K, Lu J, Cardoso WV. 2007c. Inhibition of Tgf beta signaling by endogenous retinoic acid is essential for primary lung bud induction. *Development* 134: 2969-79

Chiu PP. 2014. New Insights into Congenital Diaphragmatic Hernia - A Surgeon's Introduction to CDH Animal Models. *Front Pediatr* 2: 36

Cho SJ, George CL, Snyder JM, Acarregui MJ. 2005. Retinoic acid and erythropoietin maintain alveolar development in mice treated with an angiogenesis inhibitor. *Am J Respir Cell Mol Biol* 33: 622-8

Cho T, Chan W, Cutz E. 1989. Distribution and frequency of neuro-epithelial bodies in post-natal rabbit lung: quantitative study with monoclonal antibody against serotonin. *Cell Tissue Res* 255: 353-62

Cilley RE, Zgleszewski SE, Chinoy MR. 2000. Fetal lung development: airway pressure enhances the expression of developmental genes. *J Pediatr Surg* 35: 113-8

Cock ML, Joyce BJ, Hooper SB, Wallace MJ, Gagnon R, et al. 2004. Pulmonary elastin synthesis and deposition in developing and mature sheep: effects of intrauterine growth restriction. *Exp Lung Res* 30: 405-18

Copland IB, Post M. 2007. Stretch-activated signaling pathways responsible for early response gene expression in fetal lung epithelial cells. *J Cell Physiol* 210: 133-43

Corey DP, Hudspeth AJ. 1979. Response latency of vertebrate hair cells. *Biophys J* 26: 499-506

Cornett B, Snowball J, Varisco BM, Lang R, Whitsett J, Sinner D. 2013. Wntless is required for peripheral lung differentiation and pulmonary vascular development. *Dev Biol* 379: 38-52

Coste B, Mathur J, Schmidt M, Earley TJ, Ranade S, et al. 2010. Piezo1 and Piezo2 are essential components of distinct mechanically activated cation channels. *Science* 330: 55-60

Coste B, Xiao B, Santos JS, Syeda R, Grandl J, et al. 2012. Piezo proteins are pore-forming subunits of mechanically activated channels. *Nature* 483: 176-81

Costlow RD, Manson JM. 1981. The heart and diaphragm: target organs in the neonatal death induced by nitrofen (2,4-dichlorophenyl-p-nitrophenyl ether). *Toxicology* 20: 209-27

Cotten CM. 2017. Pulmonary hypoplasia. *Semin Fetal Neonatal Med* 22: 250-55

Coughlin MA, Werner NL, Gajarski R, Gadepalli S, Hirschl R, et al. 2016. Prenatally diagnosed severe CDH: mortality and morbidity remain high. *J Pediatr Surg* 51: 1091-5

Cutz E, Speirs V, Yeger H, Newman C, Wang D, Perrin DG. 1993. Cell biology of pulmonary neuroepithelial bodies-validation of an in vitro model. I. Effects of hypoxia and Ca2+ ionophore on serotonin content and exocytosis of dense core vesicles. *Anat Rec* 236: 41-52

Daniel E, Barlow HR, Sutton GI, Gu X, Htike Y, et al. 2020. Cyp26b1 is an essential regulator of distal airway epithelial differentiation during lung development. *Development* 147: dev181560

Dawes GS, Fox HE, Leduc BM, Liggins GC, Richards RT. 1972. Respiratory movements and rapid eye movement sleep in the foetal lamb. *J Physiol* 220: 119-43

De Arcangelis A, Mark M, Kreidberg J, Sorokin L, Georges-Labouesse E. 1999. Synergistic activities of alpha3 and alpha6 integrins are required during apical ectodermal ridge formation and organogenesis in the mouse. *Development* 126: 3957-68

De Bellard ME, Rao Y, Bronner-Fraser M. 2003. Dual function of Slit2 in repulsion and enhanced migration of trunk, but not vagal, neural crest cells. *J Cell Biol* 162: 269-79

De Paepe ME, Friedman RM, Gundogan F, Pinar H. 2005. Postmortem lung weight/body weight standards for term and preterm infants. *Pediatr Pulmonol* 40: 445-8

De Paepe ME, Johnson BD, Papadakis K, Luks FI. 1999. Lung growth response after tracheal occlusion in fetal rabbits is gestational age-dependent. *Am J Respir Cell Mol Biol* 21: 65-76

De Paepe ME, Johnson BD, Papadakis K, Sueishi K, Luks FI. 1998. Temporal pattern of accelerated lung growth after tracheal occlusion in the fetal rabbit. *Am J Pathol* 152: 179-90

deMello DE, Sawyer D, Galvin N, Reid LM. 1997. Early fetal development of lung vasculature. *Am J Respir Cell Mol Biol* 16: 568-81

Deprest J, Gratacos E, Nicolaides KH. 2004. Fetoscopic tracheal occlusion (FETO) for severe congenital diaphragmatic hernia: evolution of a technique and preliminary results. *Ultrasound Obstet Gynecol* 24: 121-6

Deprest J, Jani J, Van Schoubroeck D, Cannie M, Gallot D, et al. 2006. Current consequences of prenatal diagnosis of congenital diaphragmatic hernia. *J Pediatr Surg* 41: 423-30

Desai TJ, Brownfield DG, Krasnow MA. 2014. Alveolar progenitor and stem cells in lung development, renewal and cancer. *Nature* 507: 190-4

Dhillon GS, Maskatia SA, Loar RW, Colquitt JL, Mehollin-Ray AR, et al. 2018. The impact of fetal endoscopic tracheal occlusion in isolated left-sided congenital diaphragmatic hernia on left-sided cardiac dimensions. *Prenat Diagn* 38: 812-20

Dickson KA, Harding R. 1987. Restoration of lung liquid volume following its acute alteration in fetal sheep. *J Physiol* 385: 531-43

Didon L, Zwick RK, Chao IW, Walters MS, Wang R, et al. 2013. RFX3 modulation of FOXJ1 regulation of cilia genes in the human airway epithelium. *Respir Res* 14: 70

Dingemann J, Doi T, Ruttenstock E, Puri P. 2010. Abnormal platelet-derived growth factor signaling accounting for lung hypoplasia in experimental congenital diaphragmatic hernia. *J Pediatr Surg* 45: 1989-94

Doi T, Lukosiūte A, Ruttenstock E, Dingemann J, Puri P. 2010. Disturbance of parathyroid hormone-related protein signaling in the nitrofen-induced hypoplastic lung. *Pediatr Surg Int* 26: 45-50

Doi T, Puri P. 2009. Up-regulation of Wnt5a gene expression in the nitrofen-induced hypoplastic lung. *J Pediatr Surg* 44: 2302-6

Domyan ET, Branchfield K, Gibson DA, Naiche LA, Lewandoski M, et al. 2013. Roundabout receptors are critical for foregut separation from the body wall. *Dev Cell* 24: 52-63

Donahoe PK, Longoni M, High FA. 2016. Polygenic Causes of Congenital Diaphragmatic Hernia Produce Common Lung Pathologies. *Am J Pathol* 186: 2532-43

Doné E, Gucciardo L, Van Mieghem T, Jani J, Cannie M, et al. 2008. Prenatal diagnosis, prediction of outcome and in utero therapy of isolated congenital diaphragmatic hernia. *Prenat Diagn* 28: 581-91

Du Y, Guo M, Whitsett JA, Xu Y. 2015. 'LungGENS': a web-based tool for mapping single-cell gene expression in the developing lung. *Thorax* 70: 1092-4

Du Y, Kitzmiller JA, Sridharan A, Perl AK, Bridges JP, et al. 2017. Lung Gene Expression Analysis (LGEA): an integrative web portal for comprehensive gene expression data analysis in lung development. *Thorax* 72: 481-84

Eastwood MP, Russo FM, Toelen J, Deprest J. 2015. Medical interventions to reverse pulmonary hypoplasia in the animal model of congenital diaphragmatic hernia: A systematic review. *Pediatr Pulmonol* 50: 820-38

Eblaghie MC, Reedy M, Oliver T, Mishina Y, Hogan BL. 2006. Evidence that autocrine signaling through Bmpr1a regulates the proliferation, survival and morphogenetic behavior of distal lung epithelial cells. *Dev Biol* 291: 67-82

Edmonds RD, Silva IV, Guggino WB, Butler RB, Zeitlin PL, Blaisdell CJ. 2002. ClC-5: ontogeny of an alternative chloride channel in respiratory epithelia. *Am J Physiol Lung Cell Mol Physiol* 282: L501-7

El Agha E, Bellusci S. 2014. Walking along the Fibroblast Growth Factor 10 Route: A Key Pathway to Understand the Control and Regulation of Epithelial and Mesenchymal Cell-Lineage Formation during Lung Development and Repair after Injury. *Scientifica* 2014: 538379

El Agha E, Herold S, Al Alam D, Quantius J, MacKenzie B, et al. 2014. Fgf10-positive cells represent a progenitor cell population during lung development and postnatally. *Development* 141: 296-306

Emanuel RL, Torday JS, Mu Q, Asokananthan N, Sikorski KA, Sunday ME. 1999. Bombesin-like peptides and receptors in normal fetal baboon lung: roles in lung growth and maturation. *Am J Physiol* 277: L1003-17

Engels AC, Brady PD, Kammoun M, Finalet Ferreiro J, DeKoninck P, et al. 2016. Pulmonary transcriptome analysis in the surgically induced rabbit model of diaphragmatic hernia treated with fetal tracheal occlusion. *Dis Model Mech* 9: 221-8

Epaud R, Aubey F, Xu J, Chaker Z, Clemessy M, et al. 2012. Knockout of insulin-like growth factor-1 receptor impairs distal lung morphogenesis. *PLoS One* 7: e48071

Escot S, Willnow D, Naumann H, Di Francescantonio S, Spagnoli FM. 2018. Robo signalling controls pancreatic progenitor identity by regulating Tead transcription factors. *Nat Commun* 9: 5082

Feng J, Luo J, Yang P, Du J, Kim BS, Hu H. 2018. Piezo2 channel-Merkel cell signaling modulates the conversion of touch to itch. *Science* 360: 530-33

Fernandes-Silva H, Araújo-Silva H, Correia-Pinto J, Moura RS. 2020. Retinoic Acid: A Key Regulator of Lung Development. *Biomolecules* 10: 152

Fernandes-Silva H, Vaz-Cunha P, Barbosa VB, Silva-Gonçalves C, Correia-Pinto J, Moura RS. 2017. Retinoic acid regulates avian lung branching through a molecular network. *Cell Mol Life Sci* 74: 4599-619

Fewell JE, Johnson P. 1983. Upper airway dynamics during breathing and during apnoea in fetal lambs. *J Physiol* 339: 495-504

Filby CE, Hooper SB, Sozo F, Zahra VA, Flecknoe SJ, Wallace MJ. 2006. VDUP1: a potential mediator of expansion-induced lung growth and epithelial cell differentiation in the ovine fetus. *Am J Physiol Lung Cell Mol Physio* 290: L250-L58

Finney BA, del Moral PM, Wilkinson WJ, Cayzac S, Cole M, et al. 2008. Regulation of mouse lung development by the extracellular calcium-sensing receptor, CaR. *J Physiol* 586: 6007-19

Flageole H, Evrard VA, Piedboeuf B, Laberge JM, Lerut TE, Deprest JA. 1998. The plug-unplug sequence: an important step to achieve type II pneumocyte maturation in the fetal lamb model. *J Pediatr Surg* 33: 299-303

Flake AW, Crombleholme TM, Johnson MP, Howell LJ, Adzick NS. 2000. Treatment of severe congenital diaphragmatic hernia by fetal tracheal occlusion: clinical experience with fifteen cases. *Am J Obstet Gynecol* 183: 1059-66

Fleck S, Bautista G, Keating SM, Lee TH, Keller RL, et al. 2013. Fetal production of growth factors and inflammatory mediators predicts pulmonary hypertension in congenital diaphragmatic hernia. *Pediatr Res* 74: 290-8

Flecknoe S, Harding R, Maritz G, Hooper SB. 2000. Increased lung expansion alters the proportions of type I and type II alveolar epithelial cells in fetal sheep. *Am J Physiol Lung Cell Mol Physiol* 278: L1180-5

Fletcher AJ, Edwards CM, Gardner DS, Fowden AL, Giussani DA. 2000. Neuropeptide Y in the sheep fetus: effects of acute hypoxemia and dexamethasone during late gestation. *Endocrinology* 141: 3976-82

Florez-Paz D, Bali KK, Kuner R, Gomis A. 2016. A critical role for Piezo2 channels in the mechanotransduction of mouse proprioceptive neurons. *Sci Rep* 6: 25923

Fong K, Ohlsson A, Zalev A. 1988. Fetal thoracic circumference: a prospective cross-sectional study with real-time ultrasound. *Am J Obstet Gynecol* 158: 1154-60

Fox ZD, Jiang G, Ho KKY, Walker KA, Liu AP, Kunisaki SM. 2018. Fetal lung transcriptome patterns in an ex vivo compression model of diaphragmatic hernia. *J Surg Res* 231: 411-20

Frank DB, Peng T, Zepp JA, Snitow M, Vincent TL, et al. 2016. Emergence of a Wave of Wnt Signaling that Regulates Lung Alveologenesis by Controlling Epithelial Self-Renewal and Differentiation. *Cell Rep* 17: 2312-25

Frank DB, Penkala IJ, Zepp JA, Sivakumar A, Linares-Saldana R, et al. 2019. Early lineage specification defines alveolar epithelial ontogeny in the murine lung. *Proc Natl Acad Sci U S A* 116: 4362-71

Friedmacher F, Fujiwara N, Hofmann AD, Takahashi H, Alvarez LA, et al. 2014a. Prenatal retinoic acid increases lipofibroblast expression in hypoplastic rat lungs with experimental congenital diaphragmatic hernia. *J Pediatr Surg* 49: 876-81

Friedmacher F, Fujiwara N, Hofmann AD, Takahashi H, Gosemann JH, Puri P. 2014b. Evidence for decreased lipofibroblast expression in hypoplastic rat lungs with congenital diaphragmatic hernia. *Pediatr Surg Int* 30: 1023-9

Friedmacher F, Hofmann AD, Takahashi H, Takahashi T, Gosemann JH, Puri P. 2014c. Disruption of THY-1 signaling in alveolar lipofibroblasts in experimentally induced congenital diaphragmatic hernia. *Pediatr Surg Int* 30: 129-35

Gallot D, Coste K, Jani J, Roubliova X, Marceau G, et al. 2008. Effects of maternal retinoic acid administration in a congenital diaphragmatic hernia rabbit model. *Pediatr Pulmonol* 43: 594-603

Garg A, Sui P, Verheyden JM, Young LR, Sun X. 2019. Consider the lung as a sensory organ: A tip from pulmonary neuroendocrine cells. *Curr Top Dev Biol* 132: 67-89

Gerards FA, Twisk JW, Fetter WP, Wijnaendts LC, Van Vugt JM. 2007. Two- or three-dimensional ultrasonography to predict pulmonary hypoplasia in pregnancies complicated by preterm premature rupture of the membranes. *Prenat Diagn* 27: 216-21

Gerards FA, Twisk JW, Fetter WP, Wijnaendts LC, van Vugt JM. 2008. Predicting pulmonary hypoplasia with 2- or 3-dimensional ultrasonography in complicated pregnancies. *Am J Obstet Gynecol* 198: 140.e1-6

Gillie DJ, Pace AJ, Coakley RJ, Koller BH, Barker PM. 2001. Liquid and ion transport by fetal airway and lung epithelia of mice deficient in sodium-potassium-2-chloride transporter. *Am J Respir Cell Mol Biol* 25: 14-20

Giovannone D, Reyes M, Reyes R, Correa L, Martinez D, et al. 2012. Slits affect the timely migration of neural crest cells via Robo receptor. *Dev Dyn* 241: 1274-88

Gontan C, de Munck A, Vermeij M, Grosveld F, Tibboel D, Rottier R. 2008. Sox2 is important for two crucial processes in lung development: branching morphogenesis and epithelial cell differentiation. *Dev Biol* 317: 296-309

Gonçalves AN, Correia-Pinto J, Nogueira-Silva C. 2020. ROBO2 signaling in lung development regulates SOX2/SOX9 balance, branching morphogenesis and is dysregulated in nitrofen-induced congenital diaphragmatic hernia. *Respiratory Research* 21: 302

Gonçalves AN, Correia-Pinto J, Nogueira-Silva C. 2021. Imagiological methods for prediction of fetal pulmonary hypoplasia: a systematic review. *J Matern Fetal Neonatal Med* 34: 1459-68

Goodwin K, Mao S, Guyomar T, Miller E, Radisky DC, et al. 2019. Smooth muscle differentiation shapes domain branches during mouse lung development. *Development* 146: dev181172

Gosemann JH, Doi T, Kutasy B, Friedmacher F, Dingemann J, Puri P. 2012. Alterations of peroxisome proliferator-activated receptor γ and monocyte chemoattractant protein 1 gene expression in the nitrofen-induced hypoplastic lung. *J Pediatr Surg* 47: 847-51

Gosemann JH, Friedmacher F, Fujiwara N, Alvarez LA, Corcionivoschi N, Puri P. 2013. Disruption of the bone morphogenetic protein receptor 2 pathway in nitrofen-induced congenital diaphragmatic hernia. *Birth Defects Res B Dev Reprod Toxicol* 98: 304-9

Goss AM, Morrisey EE. 2010. Wnt signaling and specification of the respiratory endoderm. *Cell Cycle* 90, 10-1

Grieshammer U, Le M, Plump AS, Wang F, Tessier-Lavigne M, Martin GR. 2004. SLIT2-mediated ROBO2 signaling restricts kidney induction to a single site. *Dev Cell* 6: 709-17

Grindley JC, Bellusci S, Perkins D, Hogan BL. 1997. Evidence for the involvement of the Gli gene family in embryonic mouse lung development. *Dev Biol* 188: 337-48

Grivell RM, Andersen C, Dodd JM. 2015. Prenatal interventions for congenital diaphragmatic hernia for improving outcomes. *Cochrane Database Syst Rev* 11: Cd008925

Guha A, Vasconcelos M, Cai Y, Yoneda M, Hinds A, et al. 2012. Neuroepithelial body microenvironment is a niche for a distinct subset of Clara-like precursors in the developing airways. *Proc Natl Acad Sci U S A* 109: 12592-7

Guo M, Bao EL, Wagner M, Whitsett JA, Xu Y. 2017. SLICE: determining cell differentiation and lineage based on single cell entropy. *Nucleic Acids Res* 45: e54

Guo M, Du Y, Gokey JJ, Ray S, Bell SM, et al. 2019. Single cell RNA analysis identifies cellular heterogeneity and adaptive responses of the lung at birth. *Nat Commun* 10: 37

Guo M, Wang H, Potter SS, Whitsett JA, Xu Y. 2015. SINCERA: A Pipeline for Single-Cell RNA-Seq Profiling Analysis. *PLoS Comput Biol* 11: e1004575

Guo M, Xu Y. 2018. Single-Cell Transcriptome Analysis Using SINCERA Pipeline. *Methods Mol Biol* 1751: 209-22

Guseh JS, Bores SA, Stanger BZ, Zhou Q, Anderson WJ, et al. 2009. Notch signaling promotes airway mucous metaplasia and inhibits alveolar development. *Development* 136: 1751-9

Haidar A, Ryder TA, Wigglesworth JS. 1991. Failure of elastin development in hypoplastic lungs associated with oligohydramnios: an electronmicroscopic study. *Histopathology* 18: 471-3

Harburg G, Compton J, Liu W, Iwai N, Zada S, et al. 2014. SLIT/ROBO2 signaling promotes mammary stem cell senescence by inhibiting Wnt signaling. *Stem Cell Reports* 3: 385-93

Harding R, Hooper SB. 1996. Regulation of lung expansion and lung growth before birth. *J Appl Physiol* 81: 209-24

Harding R, Hooper SB, Han VK. 1993. Abolition of fetal breathing movements by spinal cord transection leads to reductions in fetal lung liquid volume, lung growth, and IGF-II gene expression. *Pediatr Res* 34: 148-53

Harding R, Sigger JN, Wickham PJ, Bocking AD. 1984. The regulation of flow of pulmonary fluid in fetal sheep. *Respir Physiol* 57: 47-59

Harper J. 1996. Human Embryology and Teratology. Second Edition. By Ronan O'Rahilly and Fabiola Muller. *Annals of Human Genetics* 60: 533-33

Harrison MR, Adzick NS, Flake AW, VanderWall KJ, Bealer JF, et al. 1996. Correction of congenital diaphragmatic hernia in utero VIII: Response of the hypoplastic lung to tracheal occlusion. *J Pediatr Surg* 31: 1339-48

Harrison MR, Albanese CT, Hawgood SB, Farmer DL, Farrell JA, et al. 2001. Fetoscopic temporary tracheal occlusion by means of detachable balloon for congenital diaphragmatic hernia. *Am J Obstet Gynecol* 185: 730-3

Harrison MR, Keller RL, Hawgood SB, Kitterman JA, Sandberg PL, et al. 2003. A Randomized Trial of Fetal Endoscopic Tracheal Occlusion for Severe Fetal Congenital Diaphragmatic Hernia. *N Engl J Med* 349: 1916-24

Harrison MR, Mychaliska GB, Albanese CT, Jennings RW, Farrell JA, et al. 1998. Correction of congenital diaphragmatic hernia in utero IX: fetuses with poor prognosis (liver herniation and low lung-to-head ratio) can be saved by fetoscopic temporary tracheal occlusion. *J Pediatr Surg* 33: 1017-22

Hashimoto S, Chen H, Que J, Brockway BL, Drake JA, et al. 2012. β-Catenin-SOX2 signaling regulates the fate of developing airway epithelium. *J Cell Sci* 125: 932-42

Havrilak JA, Melton KR, Shannon JM. 2017. Endothelial cells are not required for specification of respiratory progenitors. *Dev Biol* 427: 93-105

He M, Wu B, Ye W, Le DD, Sinclair AW, et al. 2020. Chloride channels regulate differentiation and barrier functions of the mammalian airway. *Elife* 9: e53085

Hedrick HL, Danzer E, Merchant A, Bebbington MW, Zhao H, et al. 2007. Liver position and lung-to-head ratio for prediction of extracorporeal membrane oxygenation and survival in isolated left congenital diaphragmatic hernia. *Am J Obstet Gynecol* 197: 422.e1-4

Hislop AA, Wigglesworth JS, Desai R. 1986. Alveolar development in the human fetus and infant. *Early Hum Dev* 13: 1-11

Hooper SB, Han VK, Harding R. 1993. Changes in lung expansion alter pulmonary DNA synthesis and IGF-II gene expression in fetal sheep. *Am J Physiol* 265: L403-9

Hooper SB, Harding R. 1995. Fetal lung liquid: a major determinant of the growth and functional development of the fetal lung. *Clin Exp Pharmacol Physiol* 22: 235-47

Hrycaj SM, Dye BR, Baker NC, Larsen BM, Burke AC, et al. 2015. Hox5 Genes Regulate the Wnt2/2b-Bmp4-Signaling Axis during Lung Development. *Cell Rep* 12: 903-12

Huminiecki L, Gorn M, Suchting S, Poulsom R, Bicknell R. 2002. Magic roundabout is a new member of the roundabout receptor family that is endothelial specific and expressed at sites of active angiogenesis. *Genomics* 79: 547-52

Ikeda R, Cha M, Ling J, Jia Z, Coyle D, Gu JG. 2014. Merkel cells transduce and encode tactile stimuli to drive Aβ-afferent impulses. *Cell* 157: 664-75

Ito T, Udaka N, Yazawa T, Okudela K, Hayashi H, et al. 2000. Basic helix-loop-helix transcription factors regulate the neuroendocrine differentiation of fetal mouse pulmonary epithelium. *Development* 127: 3913-21

Jacobs IJ, Ku WY, Que J. 2012. Genetic and cellular mechanisms regulating anterior foregut and esophageal development. *Dev Biol* 369: 54-64

Jani J, Keller RL, Benachi A, Nicolaides KH, Favre R, et al. 2006. Prenatal prediction of survival in isolated left-sided diaphragmatic hernia. *Ultrasound Obstet Gynecol* 27: 18-22

Jani JC, Benachi A, Nicolaides KH, Allegaert K, Gratacós E, et al. 2009. Prenatal prediction of neonatal morbidity in survivors with congenital diaphragmatic hernia: a multicenter study. *Ultrasound Obstet Gynecol* 33: 64-9

Jesudason EC. 2009. Airway smooth muscle: an architect of the lung? *Thorax* 64: 541-5

Jesudason EC, Smith NP, Connell MG, Spiller DG, White MR, et al. 2005. Developing rat lung has a sided pacemaker region for morphogenesis-related airway peristalsis. *Am J Respir Cell Mol Biol* 32: 118-27

Jesudason EC, Smith NP, Connell MG, Spiller DG, White MR, et al. 2006. Peristalsis of airway smooth muscle is developmentally regulated and uncoupled from hypoplastic lung growth. *Am J Physiol Lung Cell Mol Physiol* 291: L559-65

Ji CM, Plopper CG, Pinkerton KE. 1995. Clara cell heterogeneity in differentiation: correlation with proliferation, ultrastructural composition, and cell position in the rat bronchiole. *Am J Respir Cell Mol Biol* 13: 144-51

Jiménez JA, Eixarch E, DeKoninck P, Bennini JR, Devlieger R, et al. 2017. Balloon removal after fetoscopic endoluminal tracheal occlusion for congenital diaphragmatic hernia. *Am J Obstet Gynecol* 217: 78.e1-11

Johnson LM, Johnson C, Karger AB. 2019. End of the line for fetal lung maturity testing. *Clin Biochem* 71: 74-76

Joyce BJ, Wallace MJ, Pierce RA, Harding R, Hooper SB. 2003. Sustained changes in lung expansion alter tropoelastin mRNA levels and elastin content in fetal sheep lungs. *Am J Physiol Lung Cell Mol Physiol* 284: L643-L49

Jozan C, Huissoud C, Labaune JM, Fichez A, Sesques A, Cortet M. 2018. Contribution of ultrasound pulmonary ratio in pre-viable premature ruptures of membranes. *Gynecol Obstet Fertil Senol* 46: 78-85

Kanai M, Kitano Y, von Allmen D, Davies P, Adzick NS, Flake AW. 2001. Fetal tracheal occlusion in the rat model of nitrofen-induced congenital diaphragmatic hernia: tracheal occlusion reverses the arterial structural abnormality. *J Pediatr Surg* 36: 839-45

Kashyap A, DeKoninck P, Crossley K, Thio M, Polglase G, et al. 2018. Antenatal Medical Therapies to Improve Lung Development in Congenital Diaphragmatic Hernia. *Am J Perinatol* 35: 823-36

Kashyap AJ, Dekoninck PLJ, Rodgers KA, Thio M, McGillick EV, et al. 2019. Antenatal sildenafil treatment improves neonatal pulmonary hemodynamics and gas exchange in lambs with diaphragmatic hernia. *Ultrasound Obstet Gynecol* 54: 506-16

Keramidaris E, Hooper SB, Harding R. 1996. Effect of gestational age on the increase in fetal lung growth following tracheal obstruction. *Exp Lung Res* 22: 283-98

Khan PA, Cloutier M, Piedboeuf B. 2007. Tracheal occlusion: a review of obstructing fetal lungs to make them grow and mature. *Am J Med Genet C Semin Med Genet* 145c: 125-38

Khoshgoo N, Kholdebarin R, Pereira-Terra P, Mahood TH, Falk L, et al. 2019. Prenatal microRNA miR-200b Therapy Improves Nitrofen-induced Pulmonary Hypoplasia Associated With Congenital Diaphragmatic Hernia. *Ann Surg* 269: 979-87

Kidd T, Bland KS, Goodman CS. 1999. Slit is the midline repellent for the robo receptor in *Drosophila*. *Cell* 96: 785-94

Kidd T, Brose K, Mitchell KJ, Fetter RD, Tessier-Lavigne M, et al. 1998. Roundabout controls axon crossing of the CNS midline and defines a novel subfamily of evolutionarily conserved guidance receptors. *Cell* 92: 205-15

Kilbride HW, Yeast J, Thibeault DW. 1996. Defining limits of survival: lethal pulmonary hypoplasia after midtrimester premature rupture of membranes. *Am J Obstet Gynecol* 175: 675-81

Kim HY, Pang MF, Varner VD, Kojima L, Miller E, et al. 2015. Localized Smooth Muscle Differentiation Is Essential for Epithelial Bifurcation during Branching Morphogenesis of the Mammalian Lung. *Dev Cell* 34: 719-26

Kimura S, Hara Y, Pineau T, Fernandez-Salguero P, Fox CH, et al. 1996. The T/ebp null mouse: thyroid-specific enhancer-binding protein is essential for the organogenesis of the thyroid, lung, ventral forebrain, and pituitary. *Genes Dev* 10: 60-9

King KA, Torday JS, Sunday ME. 1995. Bombesin and [Leu8]phyllolitorin promote fetal mouse lung branching morphogenesis via a receptor-mediated mechanism. *Proc Natl Acad Sci U S A* 92: 4357-61

King SK, Alfaraj M, Gaiteiro R, O'Brien K, Moraes T, et al. 2016. Congenital diaphragmatic hernia: Observed/expected lung-to-head ratio as a predictor of long-term morbidity. *J Pediatr Surg* 51: 699-702

Kiver V, Boos V, Thomas A, Henrich W, Weichert A. 2018. Perinatal outcomes after previable preterm premature rupture of membranes before 24 weeks of gestation. *Journal of Perinatal Medicine* 46: 555-65

Kluth D, Kangah R, Reich P, Tenbrinck R, Tibboel D, Lambrecht W. 1990. Nitrofen-induced diaphragmatic hernias in rats: an animal model. *J Pediatr Surg* 25: 850-4

Knox WF, Barson AJ. 1986. Pulmonary hypoplasia in a regional perinatal unit. *Early Hum Dev* 14: 33-42

Kovler ML, Jelin EB. 2019. Fetal intervention for congenital diaphragmatic hernia. *Semin Pediatr Surg* 28: 150818

Kreidberg JA, Donovan MJ, Goldstein SL, Rennke H, Shepherd K, et al. 1996. Alpha 3 beta 1 integrin has a crucial role in kidney and lung organogenesis. *Development* 122: 3537-47

Kuo CS, Krasnow MA. 2015. Formation of a Neurosensory Organ by Epithelial Cell Slithering. *Cell* 163: 394-405

Lally KP, Bagolan P, Hosie S, Lally PA, Stewart M, et al. 2006. Corticosteroids for fetuses with congenital diaphragmatic hernia: can we show benefit? *J Pediatr Surg* 41: 668-74;

Lam M, Lamanna E, Bourke JE. 2019. Regulation of Airway Smooth Muscle Contraction in Health and Disease. *Adv Exp Med Biol* 1124: 381-422

Lamb FS, Graeff RW, Clayton GH, Smith RL, Schutte BC, McCray PB, Jr. 2001. Ontogeny of CLCN3 chloride channel gene expression in human pulmonary epithelium. *Am J Respir Cell Mol Biol* 24: 376-81

Langston C, Kida K, Reed M, Thurlbeck WM. 1984. Human lung growth in late gestation and in the neonate. *Am Rev Respir Dis* 129: 607-13

Larson JE, Cohen JC. 2006. Improvement of pulmonary hypoplasia associated with congenital diaphragmatic hernia by in utero CFTR gene therapy. *Am J Physiol Lung Cell Mol Physiol* 291: L4-10

Lau M, Masood A, Yi M, Belcastro R, Li J, Tanswell AK. 2011. Long-term failure of alveologenesis after an early short-term exposure to a PDGF-receptor antagonist. *Am J Physiol Lung Cell Mol Physiol* 300: L534-47

Laudy JA, Wladimiroff JW. 2000. The fetal lung. 2: Pulmonary hypoplasia. *Ultrasound Obstet Gynecol* 16: 482-94

Lauria MR, Gonik B, Romero R. 1995. Pulmonary hypoplasia: pathogenesis, diagnosis, and antenatal prediction. *Obstet Gynecol* 86: 466-75

Lauweryns JM, Cokelaere J, Theunynck P. 1973. Serotonin producing neuroepithelial bodies in rabbit respiratory mucosa. *Science* 180: 410-3

Leslie KO, Mitchell JJ, Woodcock-Mitchell JL, Low RB. 1990. Alpha smooth muscle actin expression in developing and adult human lung. *Differentiation* 44: 143-9

Lewis NA, Holm BA, Rossman J, Swartz D, Glick PL. 2011. Late administration of antenatal vitamin A promotes pulmonary structural maturation and improves ventilation in the lamb model of congenital diaphragmatic hernia. *Pediatr Surg Int* 27: 119-24

Li A, Ma S, Smith SM, Lee MK, Fischer A, et al. 2016. Mesodermal ALK5 controls lung myofibroblast versus lipofibroblast cell fate. *BMC Biol* 14: 19

Li C, Li M, Li S, Xing Y, Yang CY, et al. 2015. Progenitors of secondary crest myofibroblasts are developmentally committed in early lung mesoderm. *Stem Cells* 33: 999-1012

Li J, Hou B, Tumova S, Muraki K, Bruns A, et al. 2014. Piezo1 integration of vascular architecture with physiological force. *Nature* 515: 279-82

Li J, Hoyle GW. 2001. Overexpression of PDGF-A in the lung epithelium of transgenic mice produces a lethal phenotype associated with hyperplasia of mesenchymal cells. *Dev Biol* 239: 338-49

Li J, Wang Z, Chu Q, Jiang K, Tang N. 2018. The Strength of Mechanical Forces Determines the Differentiation of Alveolar Epithelial Cells. *Dev Cell* 44: 297-312.e5

Liebeskind A, Srinivasan S, Kaetzel D, Bruce M. 2000. Retinoic acid stimulates immature lung fibroblast growth via a PDGF-mediated autocrine mechanism. *Am J Physiol Lung Cell Mol Physiol* 279: L81-90

Lin C, Yao E, Zhang K, Jiang X, Croll S, et al. 2017. YAP is essential for mechanical force production and epithelial cell proliferation during lung branching morphogenesis. *Elife* 6: e21130

Lin H, Wang Y, Xiong Z, Tang Y, Liu W. 2007. Effect of antenatal tetrandrine administration on endothelin-1 and epidermal growth factor levels in the lungs of rats with experimental diaphragmatic hernia. *Journal of Pediatric Surgery* 42: 1644-51

Lindahl P, Karlsson L, Hellström M, Gebre-Medhin S, Willetts K, et al. 1997. Alveogenesis failure in PDGF-A-deficient mice is coupled to lack of distal spreading of alveolar smooth muscle cell progenitors during lung development. *Development* 124: 3943-53

Lines A, Nardo L, Phillips ID, Possmayer F, Hooper SB. 1999. Alterations in lung expansion affect surfactant protein A, B, and C mRNA levels in fetal sheep. *Am J Physiol* 276: L239-45

Liu J, Zhang L, Wang D, Shen H, Jiang M, et al. 2003. Congenital diaphragmatic hernia, kidney agenesis and cardiac defects associated with Slit3-deficiency in mice. *Mech Dev* 120: 1059-70

Liu J-P, Baker J, Perkins AS, Robertson EJ, Efstratiadis A. 1993. Mice carrying null mutations of the genes encoding insulin-like growth factor I (Igf-1) and type 1 IGF receptor (Igf1r). *Cell* 75: 59-72

Liu M, Liu J, Buch S, Tanswell AK, Post M. 1995a. Antisense oligonucleotides for PDGF-B and its receptor inhibit mechanical strain-induced fetal lung cell growth. *Am J Physiol* 269: L178-L84

Liu M, Qin Y, Liu J, Tanswell AK, Post M. 1996. Mechanical Strain Induces pp60src Activation and Translocation to Cytoskeleton in Fetal Rat Lung Cells. *J Biol Chem* 271: 7066-71

Liu M, Xu J, Liu J, Kraw ME, Tanswell AK, Post M. 1995b. Mechanical strain-enhanced fetal lung cell proliferation is mediated by phospholipase C and D and protein kinase C. *Am J Physiol* 268: L729-L38

Liu M, Xu J, Souza P, Tanswell B, Tanswell AK, Post M. 1995c. The effect of mechanical strain on fetal rat lung cell proliferation: comparison of two- and three-dimensional culture systems. *In Vitro Cell Dev Biol Anim* 31: 858-66

Liu M, Xu J, Tanswell AK, Post M. 1994. Inhibition of mechanical strain-induced fetal rat lung cell proliferation by gadolinium, a stretch-activated channel blocker. *J Cell Physiol* 161: 501-07

Liu Q, Liu K, Cui G, Huang X, Yao S, et al. 2019. Lung regeneration by multipotent stem cells residing at the bronchioalveolar-duct junction. *Nat Genet* 51: 728-38

Longoni M, High FA, Russell MK, Kashani A, Tracy AA, et al. 2014. Molecular pathogenesis of congenital diaphragmatic hernia revealed by exome sequencing, developmental data, and bioinformatics. *Proc Natl Acad Sci U S A* 111: 12450-5

Losada A, Tovar JA, Xia HM, Diez-Pardo JA, Santisteban P. 2000. Down-regulation of thyroid transcription factor-1 gene expression in fetal lung hypoplasia is restored by glucocorticoids. *Endocrinology* 141: 2166-73

Lovric G, Mokso R, Arcadu F, Vogiatzis Oikonomidis I, Schittny JC, et al. 2017. Tomographic in vivo microscopy for the study of lung physiology at the alveolar level. *Sci Rep* 7: 12545

Luks FI, Wild YK, Piasecki GJ, De Paepe ME. 2000. Short-term tracheal occlusion corrects pulmonary vascular anomalies in the fetal lamb with diaphragmatic hernia. *Surgery* 128: 266-72

Lundström A, Gallio M, Englund C, Steneberg P, Hemphälä J, et al. 2004. Vilse, a conserved Rac/Cdc42 GAP mediating Robo repulsion in tracheal cells and axons. *Genes Dev* 18: 2161-71

Luong C, Rey-Perra J, Vadivel A, Gilmour G, Sauve Y, et al. 2011. Antenatal sildenafil treatment attenuates pulmonary hypertension in experimental congenital diaphragmatic hernia. *Circulation* 123: 2120-31

Lü J, Qian J, Izvolsky KI, Cardoso WV. 2004. Global analysis of genes differentially expressed in branching and non-branching regions of the mouse embryonic lung. *Dev Biol* 273: 418-35

Macias H, Moran A, Samara Y, Moreno M, Compton JE, et al. 2011. SLIT/ROBO1 signaling suppresses mammary branching morphogenesis by limiting basal cell number. *Dev Cell* 20: 827-40

Mailleux AA, Kelly R, Veltmaat JM, De Langhe SP, Zaffran S, et al. 2005. Fgf10 expression identifies parabronchial smooth muscle cell progenitors and is required for their entry into the smooth muscle cell lineage. *Development* 132: 2157-66

Makanga M, Dewachter C, Maruyama H, Vuckovic A, Rondelet B, et al. 2013. Downregulated bone morphogenetic protein signaling in nitrofen-induced congenital diaphragmatic hernia. *Pediatr Surg Int* 29: 823-34

Maksimovic S, Nakatani M, Baba Y, Nelson AM, Marshall KL, et al. 2014. Epidermal Merkel cells are mechanosensory cells that tune mammalian touch receptors. *Nature* 509: 617-21

Maltais F, Seaborn T, Guay S, Piedboeuf B. 2003. In vivo tracheal occlusion in fetal mice induces rapid lung development without affecting surfactant protein C expression. *Am J Physiol Lung Cell Mol Physiol* 284: L622-32

Maneshi MM, Ziegler L, Sachs F, Hua SZ, Gottlieb PA. 2018. Enantiomeric Aβ peptides inhibit the fluid shear stress response of PIEZO1. *Sci Rep* 8: 14267

Mantilla CB, Fahim MA, Brandenburg JE, Sieck GC. 2017. Chapter 68 - Functional Development of Respiratory Muscles In *Fetal and Neonatal Physiology (Fifth Edition)*, ed. RA Polin, SH Abman, DH Rowitch, WE Benitz, WW Fox, pp. 692-705.e3: Elsevier

Manuck TA, Varner MW. 2014. Neonatal and early childhood outcomes following early vs later preterm premature rupture of membranes. *Am J Obstet Gynecol* 211: 308.e1-6

Marshall CB, Mays DJ, Beeler JS, Rosenbluth JM, Boyd KL, et al. 2016. p73 Is Required for Multiciliogenesis and Regulates the Foxj1-Associated Gene Network. *Cell Rep* 14: 2289-300

Massaro GD, Singh G, Mason R, Plopper CG, Malkinson AM, Gail DB. 1994. Biology of the Clara cell. *Am J Physiol* 266: L101-L06

McDougall ARA, Hooper SB, Zahra VA, Cole TJ, Lo CY, et al. 2013. Trop2 regulates motility and lamellipodia formation in cultured fetal lung fibroblasts. *Am J Physiol Lung Cell Mol Physiol* 305: L508-L21

McDougall ARA, Hooper SB, Zahra VA, Sozo F, Lo CY, et al. 2011. The oncogene Trop2 regulates fetal lung cell proliferation. *Am J Physiol Lung Cell Mol Physiol* 301: L478-L89

McGowan SE, Harvey CS, Jackson SK. 1995. Retinoids, retinoic acid receptors, and cytoplasmic retinoid binding proteins in perinatal rat lung fibroblasts. *Am J Physiol* 269: L463-72

Mehler K, Beck BB, Kaul I, Rahimi G, Hoppe B, Kribs A. 2011. Respiratory and general outcome in neonates with renal oligohydramnios- a single-centre experience. *Nephrol Dial Transplant* 26: 3514-22

Mehollin-Ray AR, Cassady CI, Cass DL, Olutoye OO. 2012. Fetal MR imaging of congenital diaphragmatic hernia. *Radiographics* 32: 1067-84

Mendelsohn C, Lohnes D, Décimo D, Lufkin T, LeMeur M, et al. 1994. Function of the retinoic acid receptors (RARs) during development (II). Multiple abnormalities at various stages of organogenesis in RAR double mutants. *Development* 120: 2749-71

Mesas Burgos C, Hammarqvist-Vejde J, Frenckner B, Conner P. 2016. Differences in Outcomes in Prenatally Diagnosed Congenital Diaphragmatic Hernia Compared to Postnatal Detection: A Single-Center Experience. *Fetal Diagn Ther* 39: 241-7

Metzger RJ, Klein OD, Martin GR, Krasnow MA. 2008. The branching programme of mouse lung development. *Nature* 453: 745-50

Meyerholz DK, Stoltz DA, Gansemer ND, Ernst SE, Cook DP, et al. 2018. Lack of cystic fibrosis transmembrane conductance regulator disrupts fetal airway development in pigs. *Lab Invest* 98: 825-38

Mileto A, Itani M, Katz DS, Siebert JR, Dighe MK, et al. 2018. Fetal Urinary Tract Anomalies: Review of Pathophysiology, Imaging, and Management. *AJR Am J Roentgenol* 210: 1010-21

Milks KS, Hill LM, Hosseinzadeh K. 2017. Evaluating skeletal dysplasias on prenatal ultrasound: an emphasis on predicting lethality. *Pediatr Radiol* 47: 134-45

Miller AA, Hooper SB, Harding R. 1993. Role of fetal breathing movements in control of fetal lung distension. *J Appl Physiol* 75: 2711-7

Mižíková I, Morty RE. 2015. The Extracellular Matrix in Bronchopulmonary Dysplasia: Target and Source. *Front Med* 2: 91

Moessinger AC, Bassi GA, Ballantyne G, Collins MH, James LS, Blanc WA. 1983. Experimental production of pulmonary hypoplasia following amniocentesis and oligohydramnios. *Early Hum Dev* 8: 343-50

Moessinger AC, Santiago A, Paneth NS, Rey HR, Blanc WA, Driscoll JM, Jr. 1989. Time-trends in necropsy prevalence and birth prevalence of lung hypoplasia. *Paediatr Perinat Epidemiol* 3: 421-31

Moiseenko A, Kheirollahi V, Chao CM, Ahmadvand N, Quantius J, et al. 2017. Origin and characterization of alpha smooth muscle actin-positive cells during murine lung development. *Stem Cells* 35: 1566-78

Montalva L, Zani A. 2019. Assessment of the nitrofen model of congenital diaphragmatic hernia and of the dysregulated factors involved in pulmonary hypoplasia. *Pediatr Surg Int* 35: 41-61

Montedonico S, Nakazawa N, Puri P. 2008a. Congenital diaphragmatic hernia and retinoids: searching for an etiology. *Pediatr Surg Int* 24: 755-61

Montedonico S, Sugimoto K, Felle P, Bannigan J, Puri P. 2008b. Prenatal treatment with retinoic acid promotes pulmonary alveologenesis in the nitrofen model of congenital diaphragmatic hernia. *J Pediatr Surg* 43: 500-7

Morimoto M, Liu Z, Cheng HT, Winters N, Bader D, Kopan R. 2010. Canonical Notch signaling in the developing lung is required for determination of arterial smooth muscle cells and selection of Clara versus ciliated cell fate. *J Cell Sci* 123: 213-24

Morimoto M, Nishinakamura R, Saga Y, Kopan R. 2012. Different assemblies of Notch receptors coordinate the distribution of the major bronchial Clara, ciliated and neuroendocrine cells. *Development* 139: 4365-73

Morrisey EE, Cardoso WV, Lane RH, Rabinovitch M, Abman SH, et al. 2013. Molecular determinants of lung development. *Ann Am Thorac Soc* 10: S12-6

Morrisey EE, Hogan BL. 2010. Preparing for the first breath: genetic and cellular mechanisms in lung development. *Dev Cell* 18: 8-23

Morton SU, Brodsky D. 2016. Fetal Physiology and the Transition to Extrauterine Life. *Clin Perinatol* 43: 395-407

Mous DS, Kool HM, Buscop-van Kempen MJ, Koning AH, Dzyubachyk O, et al. 2016. Clinically relevant timing of antenatal sildenafil treatment reduces pulmonary vascular remodeling in congenital diaphragmatic hernia. *Am J Physiol Lung Cell Mol Physiol* 311: L734-l42

Mucenski ML, Nation JM, Thitoff AR, Besnard V, Xu Y, et al. 2005. β-Catenin regulates differentiation of respiratory epithelial cells in vivo. *Am J Physiol Lung Cell Mol Physiol* 289: L971-L79

Mucenski ML, Wert SE, Nation JM, Loudy DE, Huelsken J, et al. 2003. beta-Catenin is required for specification of proximal/distal cell fate during lung morphogenesis. *J Biol Chem* 278: 40231-8

Muratore CS, Nguyen HT, Ziegler MM, Wilson JM. 2000. Stretch-induced upregulation of VEGF gene expression in murine pulmonary culture: a role for angiogenesis in lung development. *J Pediatr Surg* 35: 906-12

Mychaliska GB, Officer SM, Heintz CK, Starcher BC, Pierce RA. 2004. Pulmonary elastin expression is decreased in the nitrofen-induced rat model of congenital diaphragmatic hernia. *J Pediatr Surg* 39: 666-71

Nakamura H, Doi T, Puri P, Friedmacher F. 2020. Transgenic animal models of congenital diaphragmatic hernia: a comprehensive overview of candidate genes and signaling pathways. *Pediatr Surg Int* 36: 991-97

Nakamura Y, Fukuda S, Hashimoto T. 1990. Pulmonary elastic fibers in normal human development and in pathological conditions. *Pediatr Pathol* 10: 689-706

Nakazawa N, Montedonico S, Takayasu H, Paradisi F, Puri P. 2007. Disturbance of retinol transportation causes nitrofen-induced hypoplastic lung. *J Pediatr Surg* 42: 345-9

Nardo L, Hooper SB, Harding R. 1998. Stimulation of lung growth by tracheal obstruction in fetal sheep: relation to luminal pressure and lung liquid volume. *Pediatr Res* 43: 184-90

Nardo L, Maritz G, Harding R, Hooper SB. 2000. Changes in lung structure and cellular division induced by tracheal obstruction in fetal sheep. *Exp Lung Res* 26: 105-19

Nawapun K, Eastwood MP, Diaz-Cobos D, Jimenez J, Aertsen M, et al. 2015. In vivo evidence by magnetic resonance volumetry of a gestational age dependent response to tracheal occlusion for congenital diaphragmatic hernia. *Prenatal Diagnosis* 35: 1048-56

Nelson CM, Gleghorn JP, Pang MF, Jaslove JM, Goodwin K, et al. 2017. Microfluidic chest cavities reveal that transmural pressure controls the rate of lung development. *Development* 144: 4328-35

Nelson SM, Hajivassiliou CA, Haddock G, Cameron AD, Robertson L, et al. 2005. Rescue of the hypoplastic lung by prenatal cyclical strain. *Am J Respir Crit Care Med* 171: 1395-402

Nemajerova A, Kramer D, Siller SS, Herr C, Shomroni O, et al. 2016. TAp73 is a central transcriptional regulator of airway multiciliogenesis. *Genes Dev* 30: 1300-12

Nguyen TM, Jimenez J, Rendin LE, Müller C, Westergren-Thorsson G, et al. 2019. The proportion of alveolar type 1 cells decreases in murine hypoplastic congenital diaphragmatic hernia lungs. *PLoS One* 14: e0214793

Nicola T, Hagood JS, James ML, Macewen MW, Williams TA, et al. 2009. Loss of Thy-1 inhibits alveolar development in the newborn mouse lung. *Am J Physiol Lung Cell Mol Physiol* 296: L738-50

Noble BR, Babiuk RP, Clugston RD, Underhill TM, Sun H, et al. 2007. Mechanisms of action of the congenital diaphragmatic hernia-inducing teratogen nitrofen. *Am J Physiol Lung Cell Mol Physiol* 293: L1079-87

Nobuhara KK, DiFiore JW, Ibla JC, Siddiqui AM, Ferretti ML, et al. 1998. Insulin-like growth factor-I gene expression in three models of accelerated lung growth. *J Pediatr Surg* 33: 1057-60

Noguchi M, Sumiyama K, Morimoto M. 2015. Directed Migration of Pulmonary Neuroendocrine Cells toward Airway Branches Organizes the Stereotypic Location of Neuroepithelial Bodies. *Cell Rep* 13: 2679-86

Nonomura K, Woo SH, Chang RB, Gillich A, Qiu Z, et al. 2017. Piezo2 senses airway stretch and mediates lung inflation-induced apnoea. *Nature* 541: 176-81

North AJ, Moya FR, Mysore MR, Thomas VL, Wells LB, et al. 1995. Pulmonary endothelial nitric oxide synthase gene expression is decreased in a rat model of congenital diaphragmatic hernia. *Am J Respir Cell Mol Biol* 13: 676-82

Nunes S, Nogueira-Silva C, Dias E, Moura RS, Correia-Pinto J. 2008. Ghrelin and obestatin: different role in fetal lung development? *Peptides* 29: 2150-8

Olmeda B, Martínez-Calle M, Pérez-Gil J. 2017. Pulmonary surfactant metabolism in the alveolar airspace: Biogenesis, extracellular conversions, recycling. *Ann Anat* 209: 78-92

Oluyomi-Obi T, Kuret V, Puligandla P, Lodha A, Lee-Robertson H, et al. 2017. Antenatal predictors of outcome in prenatally diagnosed congenital diaphragmatic hernia (CDH). *J Pediatr Surg* 52: 881-88

Olver RE, Schneeberger EE, Walters DV. 1981. Epithelial solute permeability, ion transport and tight junction morphology in the developing lung of the fetal lamb. *J Physiol* 315: 395-412

Olver RE, Strang LB. 1974. Ion fluxes across the pulmonary epithelium and the secretion of lung liquid in the foetal lamb. *J Physiol* 241: 327-57

Oshiro T, Asato Y, Sakanashi M, Ohta T, Sugahara K. 2005. Differential effects of vitamin A on fetal lung growth and diaphragmatic formation in nitrofen-induced rat model. *Pulm Pharmacol Ther* 18: 155-64

Palacio M, Bonet-Carne E, Cobo T, Perez-Moreno A, Sabrià J, et al. 2017. Prediction of neonatal respiratory morbidity by quantitative ultrasound lung texture analysis: a multicenter study. *Am J Obstet Gynecol* 217: 196.e1-96.e14

Pan H, Deutsch GH, Wert SE. 2019. Comprehensive anatomic ontologies for lung development: A comparison of alveolar formation and maturation within mouse and human lung. *J Biomed Semantics* 10: 18

Pan J, Copland I, Post M, Yeger H, Cutz E. 2006. Mechanical stretch-induced serotonin release from pulmonary neuroendocrine cells: implications for lung development. *Am J Physiol Lung Cell Mol Physiol* 290: L185-93

Pandya HC, Innes J, Hodge R, Bustani P, Silverman M, Kotecha S. 2006. Spontaneous contraction of pseudoglandular-stage human airspaces is associated with the presence of smooth muscle-alpha-actin and smooth muscle-specific myosin heavy chain in recently differentiated fetal human airway smooth muscle. *Biol Neonate* 89: 211-9

Papadakis K, De Paepe ME, Tackett LD, Piasecki GJ, Luks FI. 1998. Temporary tracheal occlusion causes catch-up lung maturation in a fetal model of diaphragmatic hernia. *J Pediatr Surg* 33: 1030-7

Park WY, Miranda B, Lebeche D, Hashimoto G, Cardoso WV. 1998. FGF-10 is a chemotactic factor for distal epithelial buds during lung development. *Dev Biol* 201: 125-34

Peralta CF, Jani JC, Van Schoubroeck D, Nicolaides KH, Deprest JA. 2008. Fetal lung volume after endoscopic tracheal occlusion in the prediction of postnatal outcome. *Am J Obstet Gynecol* 198: 60.e1-5

Peralta CF, Kazan-Tannus JF, Bunduki V, Santos EM, de Castro CC, et al. 2006. Evaluation of the agreement between 3-dimensional ultrasonography and magnetic resonance imaging for fetal lung volume measurement. *J Ultrasound Med* 25: 461-7

Pereira-Terra P, Moura RS, Nogueira-Silva C, Correia-Pinto J. 2015. Neuroendocrine factors regulate retinoic acid receptors in normal and hypoplastic lung development. *J Physiol* 593: 3301-11

Perrone EE, Deprest JA. 2021. Fetal endoscopic tracheal occlusion for congenital diaphragmatic hernia: a narrative review of the history, current practice, and future directions. *Transl Pediatr* 10: 1448-60

Plopper CG, Hyde DM. 2015. Chapter 7 - Epithelial Cells of the Bronchiole In *Comparative Biology of the Normal Lung (Second Edition)*, ed. RA Parent, pp. 83-92. San Diego: Academic Press

Plosa EJ, Young LR, Gulleman PM, Polosukhin VV, Zaynagetdinov R, et al. 2014. Epithelial β1 integrin is required for lung branching morphogenesis and alveolarization. *Development* 141: 4751-62

Post LC, Ternet M, Hogan BL. 2000. Notch/Delta expression in the developing mouse lung. *Mech Dev* 98: 95-8

Probyn ME, Wallace MJ, Hooper SB. 2000. Effect of increased lung expansion on lung growth and development near midgestation in fetal sheep. *Pediatr Res* 47: 806-12

Quigley IK, Kintner C. 2017. Rfx2 Stabilizes Foxj1 Binding at Chromatin Loops to Enable Multiciliated Cell Gene Expression. *PLoS Genet* 13: e1006538

Ranade SS, Qiu Z, Woo SH, Hur SS, Murthy SE, et al. 2014a. Piezo1, a mechanically activated ion channel, is required for vascular development in mice. *Proc Natl Acad Sci U S A* 111: 10347-52

Ranade SS, Woo SH, Dubin AE, Moshourab RA, Wetzel C, et al. 2014b. Piezo2 is the major transducer of mechanical forces for touch sensation in mice. *Nature* 516: 121-5

Rankin SA, Han L, McCracken KW, Kenny AP, Anglin CT, et al. 2016. A Retinoic Acid-Hedgehog Cascade Coordinates Mesoderm-Inducing Signals and Endoderm Competence during Lung Specification. *Cell Rep* 16: 66-78

Rawlins EL, Okubo T, Xue Y, Brass DM, Auten RL, et al. 2009. The role of Scgb1a1+ Clara cells in the long-term maintenance and repair of lung airway, but not alveolar, epithelium. *Cell Stem Cell* 4: 525-34

Rawlins EL, Ostrowski LE, Randell SH, Hogan BL. 2007. Lung development and repair: contribution of the ciliated lineage. *Proc Natl Acad Sci U S A* 104: 410-7

Retailleau K, Duprat F, Arhatte M, Ranade SS, Peyronnet R, et al. 2015. Piezo1 in Smooth Muscle Cells Is Involved in Hypertension-Dependent Arterial Remodeling. *Cell Rep* 13: 1161-71

Reynolds SD, Malkinson AM. 2010. Clara cell: progenitor for the bronchiolar epithelium. *Int J Biochem Cell Biol* 42: 1-4

Reynolds SD, Pinkerton KE, Mariassy AT. 2015. Chapter 6 - Epithelial Cells of Trachea and Bronchi In *Comparative Biology of the Normal Lung (Second Edition)*, ed. RA Parent, pp. 61-81. San Diego: Academic Press

Rhee J, Buchan T, Zukerberg L, Lilien J, Balsamo J. 2007. Cables links Robo-bound Abl kinase to N-cadherin-bound beta-catenin to mediate Slit-induced modulation of adhesion and transcription. *Nat Cell Biol* 9: 883-92

Rhee J, Mahfooz NS, Arregui C, Lilien J, Balsamo J, VanBerkum MF. 2002. Activation of the repulsive receptor Roundabout inhibits N-cadherin-mediated cell adhesion. *Nat Cell Biol* 4: 798-805

Riveline D, Zamir E, Balaban NQ, Schwarz US, Ishizaki T, et al. 2001. Focal contacts as mechanosensors: externally applied local mechanical force induces growth of focal contacts by an mDia1-dependent and ROCK-independent mechanism. *J Cell Biol* 153: 1175-86

Rock JR, Hogan BL. 2010. Developmental biology. Branching takes nerve. *Science* 329: 1610-1

Rock JR, Hogan BL. 2011. Epithelial progenitor cells in lung development, maintenance, repair, and disease. *Annu Rev Cell Dev Biol* 27: 493-512

Rockich BE, Hrycaj SM, Shih HP, Nagy MS, Ferguson MA, et al. 2013. Sox9 plays multiple roles in the lung epithelium during branching morphogenesis. *Proc Natl Acad Sci U S A* 110: E4456-64

Rodríguez-Castillo JA, Pérez DB, Ntokou A, Seeger W, Morty RE, Ahlbrecht K. 2018. Understanding alveolarization to induce lung regeneration. *Respir Res* 19: 148

Rothberg JM, Hartley DA, Walther Z, Artavanis-Tsakonas S. 1988. slit: an EGF-homologous locus of D. melanogaster involved in the development of the embryonic central nervous system. *Cell* 55: 1047-59

Ruano R, Duarte SA, Pimenta EJ, Takashi E, da Silva MM, et al. 2011. Comparison between fetal endoscopic tracheal occlusion using a 1.0-mm fetoscope and prenatal expectant management in severe congenital diaphragmatic hernia. *Fetal Diagn Ther* 29: 64-70

Ruano R, Lazar DA, Cass DL, Zamora IJ, Lee TC, et al. 2014. Fetal lung volume and quantification of liver herniation by magnetic resonance imaging in isolated congenital diaphragmatic hernia. *Ultrasound Obstet Gynecol* 43: 662-9

Ruano R, Peiro JL, da Silva MM, Campos JA, Carreras E, et al. 2013. Early fetoscopic tracheal occlusion for extremely severe pulmonary hypoplasia in isolated congenital diaphragmatic hernia: preliminary results. *Ultrasound Obstet Gynecol* 42: 70-6

Ruano R, Takashi E, da Silva MM, Campos JA, Tannuri U, Zugaib M. 2012a. Prediction and probability of neonatal outcome in isolated congenital diaphragmatic hernia using multiple ultrasound parameters. *Ultrasound Obstet Gynecol* 39: 42-9

Ruano R, Yoshisaki CT, da Silva MM, Ceccon ME, Grasi MS, et al. 2012b. A randomized controlled trial of fetal endoscopic tracheal occlusion versus postnatal management of severe isolated congenital diaphragmatic hernia. *Ultrasound Obstet Gynecol* 39: 20-7

Russell MK, Longoni M, Wells J, Maalouf FI, Tracy AA, et al. 2012. Congenital diaphragmatic hernia candidate genes derived from embryonic transcriptomes. *Proc Natl Acad Sci U S A* 109: 2978-83

Russo FM, De Bie F, Hodges R, Flake A, Deprest J. 2019. Sildenafil for Antenatal Treatment of Congenital Diaphragmatic Hernia: From Bench to Bedside. *Curr Pharm Des* 25: 601-08

Sakai K, Kimura O, Furukawa T, Fumino S, Higuchi K, et al. 2014. Prenatal administration of neuropeptide bombesin promotes lung development in a rat model of nitrofen-induced congenital diaphragmatic hernia. *J Pediatr Surg* 49: 1749-52

Sanchez-Esteban J, Tsai S-W, Sang J, Qin J, Torday JS, Rubin LP. 1998. Effects of Mechanical Forces on Lung-Specific Gene Expression. *Am J Med Sci* 316: 200-04

Sanchez-Esteban J, Wang Y, Filardo EJ, Rubin LP, Ingber DE. 2006. Integrins $\beta 1$, $\alpha 6$, and $\alpha 3$ contribute to mechanical strain-induced differentiation of fetal lung type II epithelial cells via distinct mechanisms. *Am J Physiol Lung Cell Mol Physiol* 290: L343-L50

Santos M, Bastos P, Gonzaga S, Roriz JM, Baptista MJ, et al. 2006. Ghrelin expression in human and rat fetal lungs and the effect of ghrelin administration in nitrofen-induced congenital diaphragmatic hernia. *Pediatr Res* 59: 531-7

Santos M, Nogueira-Silva C, Baptista MJ, Soares-Fernandes J, Moura RS, Correia-Pinto J. 2007. Pulmonary epithelial cell differentiation in the nitrofen-induced congenital diaphragmatic hernia. *J Pediatr Surg* 42: 1231-7

Sanz-López E, Maderuelo E, Peláez D, Chimenti P, Lorente R, et al. 2013. Changes in the expression of vascular endothelial growth factor after fetal tracheal occlusion in an experimental model of congenital diaphragmatic hernia. *Crit Care Res Pract* 2013: 958078

Schittny JC. 2017. Development of the lung. *Cell Tissue Res* 367: 427-44

Schittny JC, Miserocchi G, Sparrow MP. 2000. Spontaneous peristaltic airway contractions propel lung liquid through the bronchial tree of intact and fetal lung explants. *Am J Respir Cell Mol Biol* 23: 11-8

Schmidt AF, Gonçalves FLL, Regis AC, Gallindo RM, Sbragia L. 2012. Prenatal retinoic acid improves lung vascularization and VEGF expression in CDH rat. *Am J Obstet Gynecol* 207: 76.e25-76.e32

Schulze PC, De Keulenaer GW, Yoshioka J, Kassik KA, Lee RT. 2002. Vitamin D3-upregulated protein-1 (VDUP-1) regulates redox-dependent vascular smooth muscle cell proliferation through interaction with thioredoxin. *Circ Res* 91: 689-95

Seaborn T, St-Amand J, Cloutier M, Tremblay MG, Maltais F, et al. 2008. Identification of cellular processes that are rapidly modulated in response to tracheal occlusion within mice lungs. *Pediatr Res* 63: 124-30

Serra R, Moses HL. 1995. pRb is necessary for inhibition of N-myc expression by TGF-beta 1 in embryonic lung organ cultures. *Development* 121: 3057-66

Shan L, Aster JC, Sklar J, Sunday ME. 2007. Notch-1 regulates pulmonary neuroendocrine cell differentiation in cell lines and in transgenic mice. *Am J Physiol Lung Cell Mol Physiol* 292: L500-9

Shan L, Subramaniam M, Emanuel RL, Degan S, Johnston P, et al. 2008. Centrifugal migration of mesenchymal cells in embryonic lung. *Dev Dyn* 237: 750-57

Shanmugam H, Brunelli L, Botto LD, Krikov S, Feldkamp ML. 2017. Epidemiology and Prognosis of Congenital Diaphragmatic Hernia: A Population-Based Cohort Study in Utah. *Birth Defects Res* 109: 1451-59

Shiau CE, Bronner-Fraser M. 2009. N-cadherin acts in concert with Slit1-Robo2 signaling in regulating aggregation of placode-derived cranial sensory neurons. *Development* 136: 4155-64

Shima H, Ohshiro K, Taira Y, Miyazaki E, Oue T, Puri P. 1999. Antenatal dexamethasone suppresses tumor necrosis factor-alpha expression in hypoplastic lung in nitrofen-induced diaphragmatic hernia in rats. *Pediatr Res* 46: 633-7

Shu W, Guttentag S, Wang Z, Andl T, Ballard P, et al. 2005. Wnt/beta-catenin signaling acts upstream of N-myc, BMP4, and FGF signaling to regulate proximal-distal patterning in the lung. *Dev Biol* 283: 226-39

Silbert O, Wang Y, Maciejewski BS, Lee HS, Shaw SK, Sanchez-Esteban J. 2008. Roles of RhoA and Rac1 on actin remodeling and cell alignment and differentiation in fetal type II epithelial cells exposed to cyclic mechanical stretch. *Exp Lung Res* 34: 663-80

Silva D, Venihaki M, Guo W-H, Lopez MF. 2006. Igf2 Deficiency Results in Delayed Lung Development at the End of Gestation. *Endocrinology* 147: 5584-91

Sivakumar A, Frank DB. 2019. Paradigms That Define Lung Epithelial Progenitor Cell Fate in Development and Regeneration. *Curr Stem Cell Rep* 5: 133-44

Snoek KG, Peters NCJ, van Rosmalen J, van Heijst AFJ, Eggink AJ, et al. 2017. The validity of the observed-to-expected lung-to-head ratio in congenital diaphragmatic hernia in an era of standardized neonatal treatment; a multicenter study. *Prenat Diagn* 37: 658-65

Soylu H, Jefferies A, Diambomba Y, Windrim R, Shah PS. 2010. Rupture of membranes before the age of viability and birth after the age of viability: comparison of outcomes in a matched cohort study. *J Perinatol* 30: 645-9

Sozo F, Hooper SB, Wallace MJ. 2007. Thrombospondin-1 expression and localization in the developing ovine lung. *J Physiol* 584: 625-35

Sozo F, Wallace MJ, Zahra VA, Filby CE, Hooper SB. 2006. Gene expression profiling during increased fetal lung expansion identifies genes likely to regulate development of the distal airways. *Physiol Genomics* 24: 105-13

Sparrow MP, Warwick SP, Mitchell HW. 1994. Foetal airway motor tone in prenatal lung development of the pig. *Eur Respir J* 7: 1416-24

Spiro JE, Konrad M, Rieger-Fackeldey E, Masjosthusmann K, Amler S, et al. 2015. Renal oligo- and anhydramnios: cause, course and outcome-a single-center study. *Arch Gynecol Obstet* 292: 327-36

Strizek B, Cos Sanchez T, Khalifé J, Jani J, Cannie M. 2015. Impact of operator experience on the variability of fetal lung volume estimation by 3D-ultrasound (VOCAL) and magnetic resonance imaging in fetuses with congenital diaphragmatic hernia. *J Matern Fetal Neonatal Med* 28: 858-64

Stubbs JL, Vladar EK, Axelrod JD, Kintner C. 2012. Multicilin promotes centriole assembly and ciliogenesis during multiciliate cell differentiation. *Nat Cell Biol* 14: 140-7

Stupnikov MR, Yang Y, Mori M, Lu J, Cardoso WV. 2019. Jagged and Delta-like ligands control distinct events during airway progenitor cell differentiation. *Elife* 8: e50487

Style CC, Olutoye OO, Belfort MA, Ayres NA, Cruz SM, et al. 2019. Fetal endoscopic tracheal occlusion reduces pulmonary hypertension in severe congenital diaphragmatic hernia. *Ultrasound Obstet Gynecol* 54: 752-58

Suarez CJ, Dintzis SM, Frevert CW. 2012. Chapter 9 - Respiratory In *Comparative Anatomy and Histology (Second Edition)*, ed. PM Treuting, SM Dintzis, pp. 121-34. San Diego: Academic Press

Sunday ME, Hua J, Dai HB, Nusrat A, Torday JS. 1990. Bombesin increases fetal lung growth and maturation in utero and in organ culture. *Am J Respir Cell Mol Biol* 3: 199-205

Swarr DT, Morrisey EE. 2015. Lung endoderm morphogenesis: gasping for form and function. *Annu Rev Cell Dev Biol* 31: 553-73

Taira Y, Oue T, Shima H, Miyazaki E, Puri P. 1999. Increased tropoelastin and procollagen expression in the lung of nitrofen-induced diaphragmatic hernia in rats. *J Pediatr Surg* 34: 715-9

Takahashi H, Friedmacher F, Fujiwara N, Hofmann A, Kutasy B, et al. 2013. Pulmonary FGF-18 gene expression is downregulated during the canalicular-saccular stages in nitrofen-induced hypoplastic lungs. *Pediatr Surg Int* 29: 1199-203

Takahashi T, Friedmacher F, Zimmer J, Puri P. 2017. Expression of T-box transcription factors 2, 4 and 5 is decreased in the branching airway mesenchyme of nitrofen-induced hypoplastic lungs. *Pediatr Surg Int* 33: 139-43

Takayasu H, Nakazawa N, Montedonico S, Puri P. 2007a. Down-regulation of Wnt signal pathway in nitrofen-induced hypoplastic lung. *J Pediatr Surg* 42: 426-30

Takayasu H, Nakazawa N, Montedonico S, Puri P. 2007b. Reduced expression of aquaporin 5 water channel in nitrofen-induced hypoplastic lung with congenital diaphragmatic hernia rat model. *J Pediatr Surg* 42: 415-9

Takayasu H, Nakazawa N, Montedonico S, Sugimoto K, Sato H, Puri P. 2007c. Impaired alveolar epithelial cell differentiation in the hypoplastic lung in nitrofen-induced congenital diaphragmatic hernia. *Pediatr Surg Int* 23: 405-10

Tan CMJ, Lewandowski AJ. 2020. The Transitional Heart: From Early Embryonic and Fetal Development to Neonatal Life. *Fetal Diagn Ther* 47: 373-86

Tchirikov M, Schlabritz-Loutsevitch N, Maher J, Buchmann J, Naberezhnev Y, et al. 2017. Mid-trimester preterm premature rupture of membranes (PPROM): etiology, diagnosis, classification, international recommendations of treatment options and outcome. *J Perinat Med* 46: 465-88

Tenbrinck R, Tibboel D, Gaillard JL, Kluth D, Bos AP, et al. 1990. Experimentally induced congenital diaphragmatic hernia in rats. *J Pediatr Surg* 25: 426-9

Teramoto H, Guarino N, Puri P. 2001. Altered gene level expression of thyroid hormone receptors alpha-1 and beta-1 in the lung of nitrofen-induced diaphragmatic hernia. *J Pediatr Surg* 36: 1675-8

Thibeault DW, Haney B. 1998. Lung volume, pulmonary vasculature, and factors affecting survival in congenital diaphragmatic hernia. *Pediatrics* 101: 289-95

Thurlbeck WM. 1975. Postnatal growth and development of the lung. *Am Rev Respir Dis* 111: 803-44

Thurlbeck WM. 1992. Prematurity and the developing lung. *Clin Perinatol* 19: 497-519

Thébaud B, Tibboel D, Rambaud C, Mercier J-C, Bourbon JR, et al. 1999. Vitamin A decreases the incidence and severity of nitrofen-induced congenital diaphragmatic hernia in rats. *Am J Physiol* 277: L423-L29

Tisekar OR, AK AK. Hypoplastic Lung Disease. [Updated 2021 Feb 8]. In: StatPearls [Internet]. Treasure Island (FL): StatPearls Publishing; 2021 Jan-. Available from: https://www.ncbi.nlm.nih.gov/books/NBK562139/

Tompkins DH, Besnard V, Lange AW, Keiser AR, Wert SE, et al. 2011. Sox2 activates cell proliferation and differentiation in the respiratory epithelium. *Am J Respir Cell Mol Biol* 45: 101-10

Tompkins DH, Besnard V, Lange AW, Wert SE, Keiser AR, et al. 2009. Sox2 is required for maintenance and differentiation of bronchiolar Clara, ciliated, and goblet cells. *PLoS One* 4: e8248

Torday JS, Rehan VK. 2002. Stretch-stimulated surfactant synthesis is coordinated by the paracrine actions of PTHrP and leptin. *Am J Physiol Lung Cell Mol Physiol* 283: L130-5

Torday JS, Sun H, Wang L, Torres E, Sunday ME, Rubin LP. 2002. Leptin mediates the parathyroid hormone-related protein paracrine stimulation of fetal lung maturation. *Am J Physiol Lung Cell Mol Physiol* 282: L405-10

Toskala E, Smiley-Jewell SM, Wong VJ, King D, Plopper CG. 2005. Temporal and spatial distribution of ciliogenesis in the tracheobronchial airways of mice. *Am J Physiol Lung Cell Mol Physiol* 289: L454-9

Toukam ME, Luisin M, Chevreau J, Lanta-Delmas S, Gondry J, Tourneux P. 2019. A predictive neonatal mortality score for women with premature rupture of membranes after 22-27 weeks of gestation. *J Matern Fetal Neonatal Med* 32: 258-64

Treutlein B, Brownfield DG, Wu AR, Neff NF, Mantalas GL, et al. 2014. Reconstructing lineage hierarchies of the distal lung epithelium using single-cell RNA-seq. *Nature* 509: 371-5

Triebwasser JE, Treadwell MC. 2017. Prenatal prediction of pulmonary hypoplasia. *Semin Fetal Neonatal Med* 2: 245-9

Tsao K, Johnson A. 2020. Fetal tracheal occlusion for congenital diaphragmatic hernia. *Semin Perinatol* 44: 151164

Tsao PN, Vasconcelos M, Izvolsky KI, Qian J, Lu J, Cardoso WV. 2009. Notch signaling controls the balance of ciliated and secretory cell fates in developing airways. *Development* 136: 2297-307

Tschanz SA, Salm LA, Roth-Kleiner M, Barré SF, Burri PH, Schittny JC. 2014. Rat lungs show a biphasic formation of new alveoli during postnatal development. *J Appl Physiol (1985)* 117: 89-95

Unbekandt M, del Moral PM, Sala FG, Bellusci S, Warburton D, Fleury V. 2008. Tracheal occlusion increases the rate of epithelial branching of embryonic mouse lung via the FGF10-FGFR2b-Sprouty2 pathway. *Mech Dev* 125: 314-24

Utsuki T, Hashizume K, Iwamori M. 2001. Impaired spreading of surfactant phospholipids in the lungs of newborn rats with pulmonary hypoplasia as a model of congenital diaphragmatic hernia induced by nitrofen. *Biochim Biophys Acta* 1531: 90-8

Van der Veeken L, Russo FM, De Catte L, Gratacos E, Benachi A, et al. 2018. Fetoscopic endoluminal tracheal occlusion and reestablishment of fetal airways for congenital diaphragmatic hernia. *Gynecol Surg* 15: 9

van Loenhout RB, Tibboel D, Post M, Keijzer R. 2009. Congenital diaphragmatic hernia: comparison of animal models and relevance to the human situation. *Neonatology* 96: 137-49

van Teeffelen AS, van der Ham DP, Oei SG, Porath MM, Willekes C, Mol BW. 2010. The accuracy of clinical parameters in the prediction of perinatal pulmonary hypoplasia secondary to midtrimester prelabour rupture of fetal membranes: a meta-analysis. *Eur J Obstet Gynecol Reprod Biol* 148: 3-12

van Teeffelen AS, Van Der Heijden J, Oei SG, Porath MM, Willekes C, et al. 2012. Accuracy of imaging parameters in the prediction of lethal pulmonary hypoplasia secondary to mid-trimester prelabor rupture of fetal membranes: a systematic review and meta-analysis. *Ultrasound Obstet Gynecol* 39: 495-9

Van Tuyl M, Blommaart P, Keijzer R, Wert SE, Ruijter J, et al. 2003. Pulmonary surfactant protein A, B, and C mRNA and protein expression in the nitrofen-induced congenital diaphragmatic hernia rat model. *Pediatr Res* 54: 641-52

Vergani P, Andreani M, Greco M, Farina G, Fedeli T, Cuttin S. 2010. Two- or three-dimensional ultrasonography: which is the best predictor of pulmonary hypoplasia? *Prenat Diagn* 30: 834-8

Vladar EK, Mitchell BJ. 2016. It's a family act: the geminin triplets take center stage in motile ciliogenesis. *Embo j* 35: 904-6

Volckaert T, Campbell A, Dill E, Li C, Minoo P, De Langhe S. 2013. Localized Fgf10 expression is not required for lung branching morphogenesis but prevents differentiation of epithelial progenitors. *Development* 140: 3731-42

Volckaert T, De Langhe SP. 2015. Wnt and FGF mediated epithelial-mesenchymal crosstalk during lung development. *Dev Dyn* 244: 342-66

Vuckovic A, Herber-Jonat S, Flemmer AW, Roubliova XI, Jani JC. 2013. Alveolarization genes modulated by fetal tracheal occlusion in the rabbit model for congenital diaphragmatic hernia: a randomized study. *PLoS One* 8: e69210

Wallace MJ, Hooper SB, Harding R. 2017. Chapter 63 - Physiologic Mechanisms of Normal and Altered Lung Growth Before and After Birth In *Fetal and Neonatal Physiology (Fifth Edition)*, ed. RA Polin, SH Abman, DH Rowitch, WE Benitz, WW Fox, pp. 646-57.e4: Elsevier

Wallace MJ, Hooper SB, McDougall ARA. 2014. Chapter 8 - Physical, Endocrine, and Growth Factors in Lung Development In *The Lung (Second Edition)*, ed. R Harding, KE Pinkerton, pp. 157-81. Boston: Academic Press

Wang F, Knutson K, Alcaino C, Linden DR, Gibbons SJ, et al. 2017. Mechanosensitive ion channel Piezo2 is important for enterochromaffin cell response to mechanical forces. *J Physiol* 595: 79-91

Wang S, Chennupati R, Kaur H, Iring A, Wettschureck N, Offermanns S. 2016a. Endothelial cation channel PIEZO1 controls blood pressure by mediating flow-induced ATP release. *J Clin Invest* 126: 4527-36

Wang X, Wang Y, Snitow ME, Stewart KM, Li S, et al. 2016b. Expression of histone deacetylase 3 instructs alveolar type I cell differentiation by regulating a Wnt signaling niche in the lung. *Dev Biol* 414: 161-9

Wang Y, Frank DB, Morley MP, Zhou S, Wang X, et al. 2016c. HDAC3-Dependent Epigenetic Pathway Controls Lung Alveolar Epithelial Cell Remodeling and Spreading via miR-17-92 and TGF-β Signaling Regulation. *Dev Cell* 36: 303-15

Wang Y, Huang Z, Nayak PS, Matthews BD, Warburton D, et al. 2013. Strain-induced Differentiation of Fetal Type II Epithelial Cells Is Mediated via the Integrin $\alpha 6\beta 1$-ADAM17/Tumor Necrosis Factor-α-converting Enzyme (TACE) Signaling Pathway. *J Biol Chem* 288: 25646-57

Wang Y, Maciejewski BS, Lee N, Silbert O, McKnight NL, et al. 2006. Strain-induced fetal type II epithelial cell differentiation is mediated via cAMP-PKA-dependent signaling pathway. *Am J Physiol Lung Cell Mol Physiol* 291: L820-L27

Wang Y, Maciejewski BS, Soto-Reyes D, Lee H-S, Warburton D, Sanchez-Esteban J. 2009. Mechanical stretch promotes fetal type II epithelial cell differentiation via shedding of HB-EGF and TGF-α. *J Physiol* 587: 1739-53

Wataganara T, Ebrashy A, Aliyu LD, Moreira de Sa RA, Pooh R, et al. 2016. Fetal magnetic resonance imaging and ultrasound. *J Perinat Med* 44: 533-42

Weaver KN, Johnson J, Kline-Fath B, Zhang X, Lim FY, et al. 2014. Predictive value of fetal lung volume in prenatally diagnosed skeletal dysplasia. *Prenat Diagn* 34: 1326-31

Weaver M, Batts L, Hogan BL. 2003. Tissue interactions pattern the mesenchyme of the embryonic mouse lung. *Dev Biol* 258: 169-84

Weaver M, Dunn NR, Hogan BL. 2000. Bmp4 and Fgf10 play opposing roles during lung bud morphogenesis. *Development* 127: 2695-704

Weaver M, Yingling JM, Dunn NR, Bellusci S, Hogan BL. 1999. Bmp signaling regulates proximal-distal differentiation of endoderm in mouse lung development. *Development* 126: 4005-15

Weibel ER. 1971. The mystery of "non-nucleated plates" in the alveolar epithelium of the lung explained. *Acta Anat* 78: 425-43

Weibel ER. 2015. On the tricks alveolar epithelial cells play to make a good lung. *Am J Respir Crit Care Med* 191: 504-13

Welsh MJ. 1983. Evidence for basolateral membrane potassium conductance in canine tracheal epithelium. *Am J Physiol* 244: C377-84

Welsh MJ, Smith PL, Frizzell RA. 1982. Chloride secretion by canine tracheal epithelium: II. The cellular electrical potential profile. *J Membr Biol* 70: 227-38

Whitsett JA, Alenghat T. 2015. Respiratory epithelial cells orchestrate pulmonary innate immunity. *Nat Immunol* 16: 27-35

Whitsett JA, Kalin TV, Xu Y, Kalinichenko VV. 2019. Building and Regenerating the Lung Cell by Cell. *Physiol Rev* 99: 513-54

Whitsett JA, Wert SE, Weaver TE. 2015. Diseases of pulmonary surfactant homeostasis. *Annu Rev Pathol* 10: 371-93

Wigglesworth JS, Desai R. 1981. Use of DNA estimation for growth assessment in normal and hypoplastic fetal lungs. *Arch Dis Child* 56: 601-5

Wild YK, Piasecki GJ, De Paepe ME, Luks FI. 2000. Short-term tracheal occlusion in fetal lambs with diaphragmatic hernia improves lung function, even in the absence of lung growth. *J Pediatr Surg* 35: 775-9

Wilson SM, Olver RE, Walters DV. 2007. Developmental regulation of lumenal lung fluid and electrolyte transport. *Respir Physiol Neurobiol* 159: 247-55

Winn HN, Chen M, Amon E, Leet TL, Shumway JB, Mostello D. 2000. Neonatal pulmonary hypoplasia and perinatal mortality in patients with midtrimester rupture of amniotic membranes-a critical analysis. *Am J Obstet Gynecol* 182: 1638-44

Woo SH, Lukacs V, de Nooij JC, Zaytseva D, Criddle CR, et al. 2015. Piezo2 is the principal mechanotransduction channel for proprioception. *Nat Neurosci* 18: 1756-62

Woo SH, Ranade S, Weyer AD, Dubin AE, Baba Y, et al. 2014. Piezo2 is required for Merkel-cell mechanotransduction. *Nature* 509: 622-6

Wu J, Ge X, Verbeken EK, Gratacós E, Yesildaglar N, Deprest JA. 2002. Pulmonary effects of in utero tracheal occlusion are dependent on gestational age in a rabbit model of diaphragmatic hernia. *J Pediatr Surg* 37: 11-7

Wynn J, Yu L, Chung WK. 2014. Genetic causes of congenital diaphragmatic hernia. *Semin Fetal Neonatal Med* 19: 324-30

Wynne K, Rowe C, Delbridge M, Watkins B, Brown K, et al. 2020. Antenatal corticosteroid administration for foetal lung maturation. *F1000Res* 9: 219

Xian J, Clark KJ, Fordham R, Pannell R, Rabbitts TH, Rabbitts PH. 2001. Inadequate lung development and bronchial hyperplasia in mice with a targeted deletion in the Dutt1/Robo1 gene. *Proc Natl Acad Sci U S A* 98: 15062-6

Yamamoto M, Wilting J, Abe H, Murakami G, Rodríguez-Vázquez JF, Abe SI. 2018. Development of the pulmonary pleura with special reference to the lung surface morphology: a study using human fetuses. *Anat Cell Biol* 51: 150-57

Yang J, Chen J. 2014. Developmental programs of lung epithelial progenitors: a balanced progenitor model. *Wiley Interdiscip Rev Dev Biol* 3: 331-47

Yang J, Hernandez BJ, Martinez Alanis D, Narvaez del Pilar O, Vila-Ellis L, et al. 2016. The development and plasticity of alveolar type 1 cells. *Development* 143: 54-65

Yang W, Carmichael SL, Harris JA, Shaw GM. 2006. Epidemiologic characteristics of congenital diaphragmatic hernia among 2.5 million california births, 1989–1997. *Birth Defects Res A Clin Mol Teratol* 76: 170-74

Yarbrough ML, Grenache DG, Gronowski AM. 2014. Fetal lung maturity testing: the end of an era. *Biomark Med* 8: 509-15

Ye BQ, Geng ZH, Ma L, Geng JG. 2010. Slit2 regulates attractive eosinophil and repulsive neutrophil chemotaxis through differential srGAP1 expression during lung inflammation. *J Immunol* 185: 6294-305

Yeganeh B, Bilodeau C, Post M. 2018. Explant Culture for Studying Lung Development. *Methods Mol Biol* 1752: 81-90

Yi L, Domyan ET, Lewandoski M, Sun X. 2009. Fibroblast growth factor 9 signaling inhibits airway smooth muscle differentiation in mouse lung. *Dev Dyn* 238: 123-37

Yoshizawa J, Chapin CJ, Sbragia L, Ertsey R, Gutierrez JA, et al. 2003. Tracheal occlusion stimulates cell cycle progression and type I cell differentiation in lungs of fetal rats. Am J *Physiol Lung Cell Mol Physiol* 285: L344-L53

You Y, Huang T, Richer EJ, Schmidt JE, Zabner J, et al. 2004. Role of f-box factor foxj1 in differentiation of ciliated airway epithelial cells. *Am J Physiol Lung Cell Mol Physiol* 286: L650-7

Young RE, Jones MK, Hines EA, Li R, Luo Y, et al. 2020. Smooth Muscle Differentiation Is Essential for Airway Size, Tracheal Cartilage Segmentation, but Dispensable for Epithelial Branching. Dev Cell 53: 73-85.e5

Yuan W, Rao Y, Babiuk RP, Greer JJ, Wu JY, Ornitz DM. 2003. A genetic model for a central (septum transversum) congenital diaphragmatic hernia in mice lacking Slit3. *Proc Natl Acad Sci U S A* 100: 5217-22

Zeltner TB, Caduff JH, Gehr P, Pfenninger J, Burri PH. 1987. The postnatal development and growth of the human lung. I. Morphometry. *Respir Physiol* 67: 247-67

Zeng WZ, Marshall KL, Min S, Daou I, Chapleau MW, et al. 2018. PIEZOs mediate neuronal sensing of blood pressure and the baroreceptor reflex. *Science* 362: 464-67

Zhang S, Loch AJ, Radtke F, Egan SE, Xu K. 2013. Jagged1 is the major regulator of Notch-dependent cell fate in proximal airways. *Dev Dyn* 242: 678-86

Zhang Y, Jiang M, Kim E, Lin S, Liu K, et al. 2017. Development and stem cells of the esophagus. *Semin Cell Dev Biol* 66: 25-35

Zhou F, Narasimhan V, Shboul M, Chong YL, Reversade B, Roy S. 2017. Gmnc Is a Master Regulator of the Multiciliated Cell Differentiation Program. *Curr Biol* 27: 305-07

Annex A

RE: Request permission - Full article

Academic UK Non Rightslink <permissionrequest@tandf.co.uk>
Thu 2021-07-01 09:59
To: Ana Cristina Nunes Gonçalves <id6528@alunos.uminho.pt>

Dear Ana Gonçalves

Ana N. Gonçalves, Jorge Correia-Pinto & Cristina Nogueira-Silva (2021) Imagiological methods for prediction of fetal pulmonary hypoplasia: a systematic review, The Journal of Maternal-Fetal & Neonatal Medicine, 34:9, 1459-1468, DOI: 10.1080/14767058.2019.1636029
Thank you for your correspondence requesting permission to reproduce your **authors accepted manuscript** from our Journal in your thesis and to be posted in the university's repository – University of Minho.

We will be pleased to grant permission to reproduce your '**Accepted Manuscript**' on the sole condition that you acknowledge the original source of publication.

This is an '**Accepted Manuscript**' of an article published by Taylor & Francis Group in The Journal of Maternal-Fetal & Neonatal Medicine,2019 , available online: https://www.tandfonline.com/doi/full/10.1080/14767058.2019.1636029
Please note: This **does not allow** the use of the **Version of Record (VoR)** to be posted online, however you may include the VoR as an Appendix to the printed version of your thesis.
(VoR is the final, definitive, citable version of your paper, which has been copyedited, typeset, had metadata applied, and has been allocated a DOI (Digital Object Identifier). This is the published version (PDF) on Taylor & Francis Online.

Using a DOI to link to the VoR on Taylor & Francis Online means that downloads, Altmetric data, and citations can be tracked and collated – data you can use to assess the impact of your work.

This permission does not cover any third party copyrighted work which may appear in the material requested.

Sharing your work - https://authorservices.taylorandfrancis.com/sharing-your-work/

Please do not hesitate to let me know if I can be of futher assistance.

Yours sincerely

Karin Beesley - Permissions Administrator, Journals
Taylor & Francis Group
4 Park Square, Milton Park, Abingdon, Oxon, OX14 4RN, UK
permissionrequest@tandf.co.uk
+44 (0)20 80520699
www.tandfonline.com
Taylor & Francis Group is a trading name of Informa UK Limited, registered in England under no. 1072954

Information Classification: General

From: Ana Cristina Nunes Gonçalves <id6528@alunos.uminho.pt>
Sent: 30 June 2021 17:06
To: Academic UK Non Rightslink <permissionrequest@tandf.co.uk>
Cc: Cristina Isabel Nogueira Silva <cristinasilva@med.uminho.pt>; Jorge Manuel Nunes Correia Pinto <jcp@med.uminho.pt>
Subject: Request permission - Full article

Dear Sir or Madam Permissions Manager,

Annex B

RE: Request permission - Full article

Leslie Lansman <leslie.lansman@springernature.com>
Wed 2021-07-14 14:06

To: Ana Cristina Nunes Gonçalves <id6528@alunos.uminho.pt>
Cc: Cristina Isabel Nogueira Silva <cristinasilva@med.uminho.pt>; Jorge Manuel Nunes Correia Pinto <jcp@med.uminho.pt>

Dear Ana,
Thank you for your recent Springer Nature permissions enquiry. Please follow the guidelines below.
To obtain your permission, please locate the article that contains the content you wish to reuse on link.springer.com or nature.com. At the bottom of the article page, you will find the 'Reprints and Permissions' link. Clicking on it will take you to our RightsLink service where you may input the details of your request and receive your copyright licence. Be sure to select 'reuse in a disseration/thesis' as your type of use.
During the process, you will need to set up an account with RightsLink. Please note, this step may be required regardless of whether your permission is gratis or not. You will be able to use your RightsLink account in the future to request (and to pay for) permissions from Springer Nature and from other participating publishers. RightsLink will also email you confirmation that your permission has been granted, in the form of a link to a printable licence.

Kind Regards,
Leslie

From: Ana Cristina Nunes Gonçalves <id6528@alunos.uminho.pt>
Sent: 30 June 2021 17:10
To: Journalpermissions <journalpermissions@springernature.com>
Cc: Cristina Isabel Nogueira Silva <cristinasilva@med.uminho.pt>; Jorge Manuel Nunes Correia Pinto <jcp@med.uminho.pt>
Subject: Request permission - Full article

[External - Use Caution]

Dear Sir or Madam Permissions Manager,

I, Ana Gonçalves, am writing this email to require authorization to include the paper entitle "*ROBO2 signaling in lung development regulates SOX2/SOX9 balance, branching morphogenesis and is dysregulated in nitrofen-induced congenital diaphragmatic hernia*" published on "*Respiratory Research*" in my PhD thesis that I will submit to evaluation at the University of Minho.

Please, be aware that my PhD thesis will be confidential for the next three years and the above-mentioned paper is essential for defense.

If you have any additional questions or requirements, please feel free to contact me via email for any further clarification needed.

Sincerely,

Ana Gonçalves (MSc),
PhD student in Applied Health Sciences
Surgical Sciences Research Domain
Life and Health Sciences Research Institute (ICVS)
School of Medicine
University of Minho
and
ICVS/3B`s - PT Government Associate Laboratory, Braga/Guimarães, Portugal

---

As instructed, on the article page: https://respiratory-research.biomedcentral.com/articles/10.1186/s12931-020-01568-w, we click on "*Reprints and Permissions*" and the opened window in *RightsLink* indicate that it is an open-access article distributed under the terms of the Creative Commins CC BY license, which permits unrestricted use, distribution, and reproduction in any medium since the original work is properly cited. As such, it is not required to obtain permission to reuse this article.